

University of Cambridge

Department of Applied Mathematics
and Theoretical Physics

arXiv:1502.04503v1 [astro-ph.CO] 16 Feb 2015

Astrophysical Tests of Modified Gravity

Jeremy Aaron Sakstein

This thesis is submitted to the University of Cambridge

for the degree of Doctor of Philosophy



Downing College

Cambridge, United Kingdom

March 2014

Ph.D. Dissertation, March 2014

Jeremy Aaron Sakstein

Department of Applied Mathematics and Theoretical Physics

&

Downing College

University of Cambridge, United Kingdom

Abstract

Einstein's theory of general relativity has been the accepted theory of gravity for nearly a century but how well have we really tested it? The laws of gravity have been probed in our solar system to extremely high precision using several different tests and general relativity has passed each one with flying colours. Despite this, there are still some mysteries it cannot account for, one of which being the recently discovered acceleration of the universe and this has prompted a theoretical study of modified theories of gravity that can self-accelerate on large scales. Indeed, the next decade will be an exciting era where several satellites will probe the structure of gravity on cosmological scales and put these theoretical predictions to the test. Despite this, one must still worry about the behaviour of gravity on smaller scales and the vast majority of these theories are rendered cosmologically uninteresting when confronted with solar system tests of gravity. This has motivated the study of theories that differ from general relativity on large scales but include screening mechanisms which act to hide any modifications in our own solar system. This then presents the problem of being able to distinguish these theories from general relativity. In the last few years, astrophysical scales have emerged as a new and novel way of probing these theories. These scales encompass the mildly non-linear regime between galactic and cosmological scales where the astrophysical objects have not yet joined the Hubble flow. For this reason, the screening mechanism is active but not overly efficient and novel effects may be present. Furthermore, these tests do not require a large

sample of galaxies and hence do not require dedicated surveys; instead they can piggyback on other experiments.

This thesis explores a class of theories of screened modified gravity which are scalar-tensor theories where the field is conformally coupled to matter via the metric and includes chameleon and symmetron models as well as those that screen using the environment-dependent Damour-Polyakov effect. The thesis is split into two parts.

The first is aimed at searching for new and novel astrophysical probes and using them to place new constraints on the model parameters. In particular, we derive the equations governing hydrodynamics in the presence of an external gravitational field that includes the modifications of general relativity. Using this, we derive the equations governing the equilibrium structure of stars and show that unscreened stars are brighter and hotter than their screened counterparts owing to the larger nuclear burning rate in the core needed to combat the additional inward force. These theories have the property that the laws of gravity are different in unscreened galaxies from our own. This means that the inferred distance to an unscreened galaxy using a stellar effect that depends on the law gravity will not agree with a measurement using a different method that is insensitive gravitational physics. We exploit this property by comparing the distances inferred using pulsating Cepheid variable stars, tip of the red giant branch stars and water masers to place new constraints on the model parameters that are three orders of magnitude stronger than those previously reported. Finally, we perturb the equations of modified gravity hydrodynamics to first order and derive the equations governing the oscillations of stars about their equilibrium structure. By solving these equations we show that unscreened stars are more stable to small perturbations than screened stars. Furthermore, we find that the oscillation period is far shorter than was previously estimated and this means that the current constraints can potentially be improved using previous data-sets. We discuss these new results in light of current and future astrophysical tests of modified gravity.

The final part of this thesis is dedicated to the search for supersymmetric completions of modified theories of gravity. There have been recent investigations into the quantum stability

of these models and there is evidence that they may suffer from quantum instabilities. Supersymmetric theories enjoy powerful non-renormalisation theories that may help to avoid these issues. For this reason, we construct a framework for embedding these models into global supersymmetry and investigate the new features this introduces. We show how supersymmetry is broken at a scale set by the ambient density and that, with the exception of no-scale models, supergravity corrections already constrain the model parameters to levels where it is not possible to probe the theories with astrophysics or laboratory experiments. Next, we construct a class of supersymmetric chameleon models and investigate their cosmology. In particular, we find that they are indistinguishable from the ΛCDM model at the background level but that they may show deviations in the cold dark matter power spectrum that can be probed using upcoming experiments. Finally, we introduce a novel mechanism where a cosmological constant in the form of a Fayet-Illiopoulos term can appear at late times and investigate the constraints this imposes on the model parameter space.

Contents

Abstract **3**

1 Introduction **3**

1.1 Conventions 9

1.2 General Relativity 11

1.3 Cosmological Solutions of General Relativity 13

1.3.1 The Standard Cosmological Model 16

1.3.2 The ΛCDM Model 18

1.4 Dark Energy 21

1.4.1 A Simple Example: Quintessence 22

1.5 Stellar Structure in General Relativity 24

1.5.1 The Equations of Stellar Structure 24

1.5.2 Lane-Emden Models 25

1.6 Supersymmetry 28

1.6.1 Foundations of Supersymmetry 28

1.6.2 Global Supersymmetry 31

1.6.3 Supergravity 33

2 Modified Gravity **35**

2.1 Screening Mechanisms . . . 41
2.2 Conformal Scalar-Tensor Theories . . . 44
2.2.1 The Chameleon Effect . . . 48
2.2.2 $f(R)$ Theories . . . 49
2.2.3 The Symmetron Mechanism . . . 52
2.2.4 The Environment-Dependent Damour-Polyakov Effect . . . 55
2.2.5 The Screening Mechanism . . . 60
2.2.6 Current Constraints . . . 66
2.2.7 Identification of Unscreened Galaxies . . . 70
2.2.8 Cosmological Behaviour . . . 72
2.3 The Vainshtein Mechanism . . . 75
2.3.1 Galileon Theories of Gravity . . . 76

3 Equilibrium Stellar Structure in Modified Gravity 81
3.1 Modified Gravity Hydrodynamics . . . 83
3.1.1 Equilibrium Structure . . . 87
3.2 Lane-Emden Stars . . . 88
3.3 Main-Sequence Stars . . . 91
3.3.1 Scaling Relations . . . 91
3.3.2 The Eddington Standard Model . . . 94
3.3.3 Effects on the Galactic Properties . . . 99
3.4 Numerical Modelling of Stars in Modified Gravity . . . 103

4 Distance Indicator Constraints on Modified Gravity 107
4.1 Distance Indicators as Probes of Modified Gravity . . . 107
4.1.1 Cepheid Variable Stars . . . 109
4.1.2 Tip of The Red Giant Branch Stars . . . 112
4.1.3 Water Masers . . . 113

4.2 Distance Indicators in Modified Gravity . . . 116
4.2.1 Tip of the Red Giant Branch Stars in Modified Gravity . . . 117
4.2.2 Cepheid Distances in Modified Gravity . . . 119
4.3 Distance Indicator Constraints on Modified Gravity . . . 124
4.3.1 Comparison of Water Maser and TRGB distances . . . 124
4.3.2 Comparison of Cepheid and TRGB distances . . . 126
4.4 Summary of Main Results . . . 131

5 Stellar Oscillations in Modified Gravity 133
5.1 Modified Gravity Hydrodynamics: Linear Perturbation Theory . . . 137
5.2 Properties of the Modified Linear Adiabatic Wave Equation . . . 142
5.2.1 Boundary Conditions . . . 143
5.2.2 Sturm-Liouville Nature of the Equation . . . 143
5.2.3 Scaling Behaviour of the Eigenfrequencies . . . 144
5.3 Stellar Stability . . . 146
5.4 Numerical Results . . . 149
5.4.1 Perturbations of Lane-Emden Models . . . 150
5.4.2 Perturbations of MESA Models . . . 162
5.5 Summary of Main Results . . . 165

6 Supersymmetric Models of Modified Gravity 169
6.1 The Framework . . . 173
6.2 Supersymmetric Features . . . 174
6.2.1 Environment-Dependent Supersymmetry Breaking . . . 175
6.2.2 Absence of Observational Signatures . . . 175

7 Phenomenology of Supersymmetric Chameleons 183
7.1 Supersymmetric Chameleon Models . . . 185
7.1.1 Supergravity Corrections and Screening . . . 190

7.2 Cosmology . . . 191
7.2.1 Background Cosmology . . . 192
7.2.2 A Late-time Cosmological Constant . . . 193
7.2.3 The Model Parameter Space . . . 195
7.2.4 Constraints on the Parameter Space . . . 199
7.3 Linear Perturbations . . . 202
7.3.1 $z_\infty < 0$ . . . 205
7.3.2 $z_\infty > 0$ . . . 207
7.4 Other Models . . . 211
7.5 Summary of Main Results . . . 212

8 Discussion and Conclusions **217**
8.1 Problems Addressed in this Thesis . . . 217
8.2 Summary of Original Results . . . 219
8.2.1 Astrophysical Tests of Conformal Scalar-Tensor Theories . . . 219
8.2.2 Supersymmetric Completions of Conformal-Scalar Tensor Theories . . . 223
8.3 Outlook . . . 224

A Weyl Rescalings of the Metric **253**
A.1 Transformation of the Ricci Scalar . . . 253
A.2 The Energy-Momentum Tensor . . . 255

B Cepheid and TRGB Data **257**

C Numerical Methods **261**
C.1 MESA . . . 261
C.1.1 The Architecture of MESA . . . 261
C.1.2 Implementation of Modified Gravity . . . 264
C.2 Numerical Methods for Solving the MLAWE . . . 265

C.2.1 First-Order form of the MLAWE . . . 265
C.2.2 Lane-Emden Form . . . 266
C.2.3 MESA form . . . 267

D Modified Bessel Equations 269
D.1 Generalised Modified Bessel Equations . . . 269
D.2 Second Kind Power Series Expansions for the Power Spectra . . . 271

E The Global Potential for Supersymmetric Chameleon Models 273
E.1 Minimisation of the Global Potential . . . 273

F Corrections to the Effective Potential for Supersymmetric Chameleon Models 277
F.1 Late Time Importance of the Corrections . . . 277
F.1.1 Mass Scales . . . 278
F.2 The Quadratic Correction . . . 279
F.3 The Quartic Correction . . . 280
F.4 Simultaneous Corrections . . . 281

List of Figures

2.1 The chameleon effective potential (solid line) for small and large densities. The blue dashed lines show the contribution from the potential and the red dotted lines show the contribution from the coupling. 49

2.2 The symmetron effective potential for small and large densities. 53

2.3 The field profile in the screened and unscreened scenarios. 61

2.4 The general field profile for a partially unscreened object. 62

3.1 The ratio of the stellar luminosity of a partially screened star in $f(R)$ chameleon gravity compared with one that is completely screened as a function of stellar mass M. $L_{\rm std}$ is the luminosity of a completely screened (general relativity) star. From top to bottom: $\chi_0 = (10^{-4}, 10^{-5}, 5\times10^{-6}, 10^{-6})$. 100

3.2 The Hertsprung-Russell diagram for stars of one solar mass with initial metallicity $Z = 0.02$. The black line shows the tracks for stars in general relativity while the red, blue and green tracks correspond to stars in modified gravity with $\chi_0 = 10^{-7}, 10^{-6}$ and 5×10^{-6} respectively. The radius and age at the point where the central hydrogen mass fraction has fallen to 0.5, 0.1 and 10^{-5} is shown for each star except the $\chi_0 = 10^{-7}$ case. 106

4.1 The evolution of Cepheid stars in the HR diagram. The instability strip shown in the black lines is taken from [114]. 111

4.2 Masing gas orbiting the central black hole (labelled BH) at a distance D from an observer. Figure reproduced from [115]. 115

4.3 An illustration of the accretion disc and water masers in NGC 4258; the black dots show the position of individual masers. This figure has been adapted from [119]. 116

4.4 The rotation curve for NGC 4258. This figure has been adapted from [116]. . . 117

4.5 The radial profile of $1 + \Delta G/G$. We have indicated the core radius for the $\chi_0 = 10^{-5}$ model. Note that since we are using the rescaled radius $x \equiv r/R$ the core radius does not necessarily occur at fixed x for different χ_0. Numerically, we find that the core radius is largely insensitive to the value of χ_0. 120

4.6 The normalised Epstein function $f(x)$ with $x \equiv r/R$. The function was reconstructed by interpolating the data in [120]. 122

4.7 The radial profile of $1 + \Delta G/G$ as a function of $x \equiv r/R$ for a $6M_\odot$ star at the blue edge of the instability strip. Different values of χ_0 are indicated and $\alpha = 1/3$ in each case. 123

4.8 The period-luminosity relation for the galaxies in our sample; the black and red points denote screened and unscreened galaxies respectively. *Left panel*: we show all the Cepheids observed along with the reported error bars. *Right panel*: the mean period and dispersion within bins in absolute magnitude of size 0.5. . 128

4.9 *Left panel:* A comparison of distances measured using the Cepheid period-luminosity relation and TRGB luminosities. The black and red points show galaxies from the screened and unscreened sub-samples respectively. *Right panel:* $\Delta d/d$, the fractional difference between Cepheid and TRGB distances, as a function of TRGB distance. The shaded region in the right panel shows the 68% confidence region around our best fit to the unscreened sample (red line). The best fit to the screened sample is shown by the dashed black line. Both sub-samples are consistent with the general relativity expectation of zero deviation. The dotted and dashed green lines show two possible predictions of chameleon theories with $\alpha = 1$, $\chi_0 = 4 \times 10^{-7}$ and $\alpha = 1/3$, $\chi_0 = 1 \times 10^{-6}$, which corresponds to $f(R)$ gravity. 129

4.10 The excluded region in the χ_0–α plane for chameleon models. The boundaries of the shaded regions show the upper limits at 68% and 95% confidence level. The black arrow shows the previous constraint, $\chi_0 \leq 10^{-4}$, coming from cosmological and cluster constraints, which was obtained for $f(R)$ theories with $\alpha = 1/3$. 130

5.1 The fractional change in the stellar pulsation period as a function of $\log_{10}\chi_0$ when only the change to the equilibrium structure is considered (case 1). The red squares correspond to eigenfrequencies of the LAWE whereas the blue circles show the approximation (5.54). The green dashed line shows the ratio for a fully unscreened star and the black dashed line shows a ratio of 1, corresponding to a general relativity star. The magenta line shows the fully-unscreened value of $\sqrt{\frac{G}{\langle G\rangle}} = (1+\alpha)^{-\frac{1}{2}}$. 156

5.2 The fractional change in the stellar pulsation period as a function of $\log_{10}\chi_0$ when both the effects of the modified equilibrium structure and modified perturbation equation are considered (case 2). The red squares correspond to eigenfrequencies of the MLAWE whereas the blue circles show the approximation (5.54). The green dashed line shows the ratio for a fully unscreened star and the black dashed line shows a ratio of 1, corresponding to a general relativity star. The magenta line shows the fully-unscreened value of $\sqrt{\frac{G}{\langle G\rangle}} = (1+\alpha)^{-\frac{1}{2}}$. 157

5.3 The fractional change in the stellar pulsation period as a function of $\log_{10}\chi_0$ for case 1 (blue circles) and case 2 (red squares). The black dashed line shows the general relativity ratio of 1 and the red and blue lines show the fully-unscreened ratio for the full simulation and the one including only the modified equilibrium structure respectively. 159

5.4 The ratio of the modified gravity to general relativity eigenfrequencies as a function of $\log_{10}\chi_0$ when $\Gamma_{1,0} \approx 1.2333$. The black dotted line shows the general relativity ratio of 1 and the green dotted line shows the ratio for a fully unscreened star. 160

5.5 The critical value of $\Gamma_{1,0}$ as a function of $\log_{10}\chi_0$. The blue circles show the critical values when the modifications to the equilibrium structure are ignored and the red squares show the critical values when the full MLAWE is solved. The black dashed line shows the general relativity value of $4/3$ and the magenta line shows the fully unscreened value when we ignore the modified equilibrium structure. The green line shows the fully unscreened value found by solving the full MLAWE. 161

7.1 The effective potential. 188

7.2 The various regions in the z_∞–log(x) plane with $n = \delta = 2$, $\mu = 10^3$ TeV and $\mathscr{G} = 10^{-2}$. The yellow region shows the parameter range where the corrections are negligible. The magenta region shows the ranges where the quadratic correction is important, the dark blue region where both corrections are important. The grey region corresponds to parameters where the model deviates from ΛCDM at the level of linear perturbations. 200

7.3 The various regions in the log(μ)–log(x) plane with $n = \delta = 2$, $z_\infty = 5$ and $\mathscr{G} = 10^{-2}$. The yellow region shows the parameter range where the corrections are negligible. The magenta region shows the ranges where the quadratic correction is important and the dark blue region where both corrections are important. The red region corresponds to models where a cosmological constant is generated after last scattering and are therefore excluded and the green region corresponds to models where $\phi_{\rm min} < \Delta$ and a cosmological constant is only generated at some time in the future. The grey region corresponds to parameters where the model deviates from ΛCDM at the level of linear perturbations. 214

7.4 The various regions in the log($\mathscr{G}$)-log(x) plane with $n = \delta = 2$, $z_\infty = 5$ TeV and $\mu = 10^3$ TeV. The yellow region shows the parameter range where the corrections are negligible. The magenta region shows the ranges where the quadratic correction is important and the dark blue region where both corrections are important. The red region corresponds to models where a cosmological constant is generated after last scattering and are therefore excluded and the green region corresponds to models where $\phi_{\rm min} < \Delta$ and a cosmological constant is only generated at some time in the future. The grey region corresponds to parameters where the model deviates from ΛCDM at the level of linear perturbations. 215

7.5 The deviation from the ΛCDM power spectrum when a cosmological constant is present, with $\delta = n = 2$, $x = 5 \times 10^{-7}$ and $z_\infty = 5$. In red we show the exact power spectrum deviation. The linearised deviation found using equation (7.56) is shown in green. Smaller values of x result in smaller deviations. 216

C.1 The cell structure of stars in MESA and the cell assignments of various stellar quantities. Figure reproduced from [108]. The variables shown that are relevant for this thesis are the temperature T, the density ρ the mass m enclosed by radius r and the luminosity L. $\mathrm{d}m_k$ refers to the mass enclosed within cell k and $\mathrm{d}\bar{m}_k$ is the average mass enclosed in cells k and $k-1$. The reader is referred to [108] for the details of the other quantities shown. 263

List of Tables

1.1 Abbreviations used throughout this thesis. 10

1.2 The Planck best fit cosmological parameters, taken from [60]. 19

1.3 Representations of the superpoincaré group that will be useful later on. In each case $\mu = 0, 1, 2, 3$, labels space-time components and $\alpha = 1, 2$ labels spinorial components. 30

2.1 The screening status of different collapsed objects in the universe given the constraint $\chi_0 < 10^{-6}$. We do not include linear and non-linear cosmological scales since there is no unequivocal equivalent of the Newtonian potential with which to compare χ_0 (see the discussion above). Post-main-sequence stars located in dwarf galaxies in clusters or in galaxies with any other morphology are blanket screened by their host galaxy. 70

3.1 The luminosity enhancement in unscreened relative to screened dwarf galaxies as a function of χ_0. All values were computed using the fitting formulae (3.43) and equation (3.46) in (3.47) taking $\alpha = 1/3$. 102

4.1 Change in the inferred distance using the TRGB indicator for $f(R)$ chameleon models for a $1.5M_\odot$ stellar model. 125

4.2 Change in inferred distance due to the change in the Cepheid periods for different modified gravity parameters. In each case the quantities were computed using $6M_\odot$ stellar models with initial metallicity $Z = 0.004$. 127

4.3 Best fit values for $\Delta d/d$ and uncertainty σ in the fractional difference between Cepheid and TRGB distances for the screened and unscreened sub-samples. Our estimated σ includes systematic errors. The number of galaxies N in each sub-sample is given as is the reduced χ^2. 128

5.1 The change in the period of Cepheid pulsations due to modified gravity effects. . 163

5.2 The change in the inferred Cepheid distance due to modified gravity. In each case $\Delta d/d$ was found using the perturbed period-luminosity relation 5.55. . . . 164

5.3 The lower bounds on χ_0 and α that could potentially be placed if one were to use the same procedure and data-sets as [89] using the full MLAWE instead of the approximation. 165

B.1 The galaxies used in the period-luminosity relation and their references. The second column labelled N gives the number of Cepheids observed in each galaxy. Names that end with * are galaxies with unacceptably large dispersion in period-luminosity relation. 258

B.2 Cepheid and TRGB based distances to the galaxies used in the comparison. The final column gives the screening for $\phi = 4 \times 10^{-7}$ as follows: 0: Unscreened, 1: environmentally screened, 2: self-screened. 259

An Englishman's self-assurance is founded on his being a citizen of the best organised state in the world and on the fact that, as an Englishman, he always knows what to do, and that whatever he does as an Englishman is unquestionably correct.

Leo Tolstoy, *War and Peace*

Were the succession of stars endless, then the background of the sky would present us a uniform luminosity, like that displayed by the Galaxy — since there could be absolutely no point, in all that background, at which would not exist a star. The only mode, therefore, in which, under such a state of affairs, we could comprehend the voids which our telescopes find in innumerable directions, would be by supposing the distance of the invisible background so immense that no ray from it has yet been able to reach us at all.

Edgar Allen Poe

1 Introduction

Physics has always been an experimentally driven science. Whenever a new and unaccountable phenomena has been observed in nature there are two possible explanations: either there is new, previously unknown physics or the current theory is not as complete as we believe. In 1854 Hermann von Helmholtz proposed that the energy source powering the Sun was its own gravitational contraction. This presented a problem since this time-scale for this process is of the order of millions of years yet there was geological evidence at the time that the Earth is older than this. It was not until 1938 that Hans Bethe provided the solution in the form of new physics. Using the theory of nuclear physics he was able to show that nuclear reactions in the Sun's core could provide the relevant energy and the correct lifetime. Similarly, by 1846 astronomers had discovered several irregularities in the orbit of Uranus compared to the prediction found using Newtonian gravity. Urbain Le Verrier inferred that there must be another planet orbiting further than Uranus if the current laws of gravity were correct at this distance. Neptune was indeed discovered in 1846, another instance of new physics. By 1859, a similar problem had arisen with Mercury, its orbit was precessing and this could not be accounted for by either the finite extent of the Sun or perturbations due to any known planets. After his success with Neptune, Le Verrier again inferred the existence of a new planet orbiting closer to the Sun: Vulcan. This time however, no such planet could be found and new physics was

not the answer. It was not until the advent of general relativity that the solution was found. In some sense, general relativity is a modified theory of Newtonian gravity. In non-relativistic and low-density environments it reproduces the predictions of Newton's laws but away from this regime its predictions are drastically different.

It has been nearly 100 years since Einstein first published his theory of general relativity [1]. Since then, it has been remarkably successful at predicting and explaining all known phenomena in the solar system from the perihelion of Mercury to the bending of light by the Sun. So much so that modern experiments[1] constrain any other theory to be indistinguishable on solar system scales. The radius of the Earth differs from the size of the observable universe by 18 orders of magnitude and the density differs by 41 and so it is natural to ask: is the structure of gravity the same across all of these scales?

Indeed, there are several reasons why this question is well-motivated. It is well-known that general relativity is not a renormalisable quantum field theory, which suggests that it may require ultra-violet (UV) modifications. These would be indistinguishable from general relativity on cosmological and solar system scales but could show drastic differences in the strong-field regime[2]. There are also hints that the structure of gravity may be different in the infra-red (IR). The recent discovery that the universe is accelerating [3,4] is one of the biggest unsolved problems in modern physics. One possible explanation (see [5,6] for reviews) is that gravity is altered on cosmological scales such that it allows for self-accelerating solutions. For this reason, infra-red modifications of gravity have received a renewed interest in the last few years.

We are living in an age of precision cosmology and the standard cosmological model predicated on a cosmological constant and dark matter is the best-fit to the cosmic microwave background (CMB) as measured by Planck [7]. Inherent in this analysis is the assumption that density perturbations evolve according to general relativity. When this assumption is relaxed

[1] See [2] for a review of experimental tests of general relativity.

[2] One may näively think that we have already probed this regime in the form of binary pulsars. In fact, whereas neutron stars themselves are highly relativistic, the Newtonian potential GM/Rc^2 of binary pulsar systems lie in the range 10^{-5}–10^{-4} and so these systems only probe the post-Newtonian structure of gravity.

and the theory of gravity is allowed to vary in conjunction with the cosmology the current cosmological data constrains the theory with far less precision than solar system tests [8].

The situation will change drastically in the next decade or so with a series of ambitious programs aimed at probing the structure of gravity on new scales. Lensing missions such as Euclid [9] will measure the redshift-distance relation and baryon acoustic oscillation (BAO) scale out to redshift 2 and will hence probe dark energy over much of the period where it has dominated the expansion of the universe. Imaging surveys such as the *Large Synoptic Survey Telescope* (LSST) [10] and the *Dark Energy Survey* (DES) [11] will provide galaxy clustering, supernova and lensing data that can be combined to constrain the dark energy equation of state and distinguish dark energy from modified gravity. LSST will also provide optical data pertaining to variable stars in the nearby universe which can be used to constrain certain modified gravity models directly. The *Wide-Field Infra-red Survey Telescope* (WFIRST) [12] will provide near-infra-red data on galactic properties and stellar populations which can be useful in placing astrophysical constraints on certain modified theories of gravity. Finally, gravitational wave detectors such as the Advanced Laser Interferometer Gravitational-Wave Observatory (Advanced-LIGO) [13] and eLISA [14] will probe black hole and neutron star mergers and in-spirals and will thus provide a window into the strong-field regime of gravity.

One may wonder how such drastic deviations from general relativity are compatible with the solar system tests that have stood the test of time for nearly a century. Indeed, general relativity (and a cosmological constant) is the unique Lorentz-invariant theory of a massless spin-2 particle [15] and any modification necessarily introduces new degrees of freedom. In the absence of any symmetry, we would then generically expect these to couple to matter with order-one strength, which gives rise to additional or *fifth*- forces. In general, these forces are present at both the Newtonian and post-Newtonian level and hence must be fine-tuned to be negligible in order to be compatible with the solar system bounds. This generally renders them cosmologically uninteresting[3].

[3]The same is not necessarily true in the strong-field regime which can show interesting effects such as spontaneous scalarisation [16].

Many theories of modified gravity do indeed fall at this first hurdle but in the last 10 years or so a new and interesting class of theories which include *screening mechanisms* have emerged. Screening mechanisms allow for order-one (or larger) deviations from general relativity on large, galactic or cosmological scales whilst *screening* these modifications on smaller scales so that they satisfy the current solar system bounds. They thus represent both viable and interesting modifications of general relativity and it is this class of theory that this thesis is concerned with.

Screened modified gravity generally falls into two classes. The chameleon [17, 18] effect, the symmetron mechanism [19] and the environment-dependent Damour-Polyakov effect (EDDP) [20] all screen by suppressing the scalar charge to mass ratio of dense objects and the Vainshtein mechanism [21] screens by suppressing the scalar-gradients sourced by dense objects[4]. This thesis investigates several aspects of the first class[5], which are referred to collectively as chameleon-like theories when necessary.

These mechanisms all rely on dense environments to screen any fifth-forces. In particular, our own galaxy must be screened and so one must generally look for new and novel probes in more under-dense environments such as dwarf galaxies, inter-galactic scales and the cosmological background and to date, experimental tests of chameleon-like theories have either focused on laboratory experiments [31–40] or cosmological probes[6] [28, 42–55]. In the last few years, astrophysical effects have emerged as a new and novel probe of these theories. Astrophysical tests probe scales between the Milky Way and the Hubble flow and provide smoking-gun signals. This regime is mildly non-linear so that some degree of screening is present but not so much as to destroy all observable consequences. Cosmology on the other hand only probes the linear regime and so any deviations from general relativity are degenerate with other theories of dark energy and modified gravity. Fully non-linear scales show only minimal deviations from general relativity. Thus, astrophysical tests have the potential to

[4] We do not consider theories that screen linearly [22, 23] in this thesis.
[5] Reviews of different classes of screened modified gravity can be found in [24–30].
[6] Recently, binary pulsar tests have also been considered [41].

constrain these theories to levels unattainable using other methods.

The first part of this thesis is dedicated to finding new and novel astrophysical probes of chameleon-like theories and using current data to place new constraints. In particular, we investigate the structure and evolution of stars in chameleon-like theories of gravity, first using a simple, semi-analytic method and then by implementing the modified equations of stellar structure into an existing stellar structure code that is precise enough to allow a comparison with observational data. Subsequently, we do just this; by examining the effects on tip of the red giant branch stars we obtain a new and independent constraint that the Milky way is self-screening[7] and by examining the properties of Cepheid stars we place new constraints on the model parameters two orders of magnitude stronger than the previous bounds. At the time of writing, these are currently the strongest constraints in the literature.

Going beyond equilibrium, we derive the equations governing hydrodynamics in the presence of modified gravity and perturb them to first-order to find the new equations governing the radial oscillations of stars about their equilibrium configurations. We identify two new effects: the period of oscillations is shorter than one might näively expect using previous approximations and stars are more stable in modified gravity. Next, we solve the modified equations numerically using both semi-analytic convective models and realistic Cepheid models and investigate the size of these effects. We show that the Cepheid oscillation period can be up to three times shorter than previously predicted and therefore that the current constraints can be improved using the same data-sets. Finally, we estimate the possible improvement and discuss the results in light of future and upcoming astrophysical tests of gravity.

The remainder of this thesis is dedicated to the search for supersymmetric completions of chameleon-like theories. Recently, the quantum stability of chameleon theories have come into question after it has emerged that certain models suffer from strong-coupling issues [56] and that it is difficult to evolve them through the cosmological era of radiation domination [57]. One might hope to circumvent these issues by imposing some sort of symmetry that protects

[7] This had previously been debated in the field.

the structure of the theory. Unfortunately, this is not possible since any Lie symmetry would imply that any fields in the system are Goldstone bosons with a technically-natural light mass. This is incompatible with the screening mechanism. The exception is supersymmetry, which transfers this property to a Goldstone fermion instead.

An investigation into possible supersymmetric completions is therefore worthwhile, both to avoid these issues and to aid in the search for an ultra-violet completion. We will present a framework for embedding chameleon-like theories into global supersymmetry[8] and investigate the new features that arise. At finite density, supersymmetry is broken at a scale that depends on the ambient density and not the TeV scale associated with supersymmetry breaking in the observable sector. We prove a general no-go theorem showing that when supergravity corrections are accounted for, the model-independent parameters are already so constrained that it is not possible to probe the theories with laboratory or astrophysical tests[9] and that only the background cosmology and linear perturbations can show deviations from general relativity. For this reason, we construct a class of supersymmetric chameleon models and investigate their cosmological behaviour. Like all chameleon-like models, these ultimately require a cosmological constant to account for the observed acceleration of the universe [58][10]. Unlike regular models, the introduction of a cosmological constant at the level of the action breaks supersymmetry and is forbidden. Hence, we next introduce a mechanism where a small cosmological constant can be generated at late times in the form of a Fayet-Illiopoulos (FI) term and explore the associated parameter space. Finally, we prove a general no-go theorem showing that, with the exception of no-scale models, which, to date, have been unsuccessful at incorporating the chameleon mechanism, every object in the universe is self-screened and the theory's predictions are identical to those of general relativity in all environments.

This thesis is organised as follows: The rest of this chapter presents some background material. A basic introduction to the salient features of general relativity, cosmology, dark energy,

[8] Such a bottom-up approach is sensible for low-energy infra-red modifications of general relativity such as these.

[9] The exception to this are no-scale models, which we discuss thoroughly.

[10] Technically, these models do not satisfy the authors assumptions, however the conclusions are the same.

stellar structure and supersymmetry is given. This is by no means a comprehensive review and only the aspects relevant to the original work presented in this thesis are included, often without derivation. In chapter 2 we give a detailed description of modified gravity with screening mechanisms, focussing on chameleon-like models since these are the main focus of this thesis. In chapters 3, 4 and 5 we turn our attention to astrophysical probes of chameleon-like models. In chapter 3 we present the equations of modified gravity hydrodynamics and use them to derive and solve the new equations governing equilibrium stellar structure both analytically and numerically. We then discuss potential observational probes using the new features we will discern. In chapter 4 we will use distance indicator measurements to place new constraints on the model-independent parameters appearing in these theories, which at the time of writing are the strongest in the literature by two orders of magnitude. In chapter 5 we perturb the equations of modified gravity hydrodynamics to first order and obtain the new equations governing the radial, adiabatic oscillations of stars. We find that stars are more stable in modified theories of gravity than general relativity and furthermore that the oscillation period is far shorter than has previously been estimated. We discuss these results in the context of current and upcoming astrophysical tests of modified gravity. Next, we change focus and investigate supersymmetric theories of chameleon-like models in chapters 6 and 7. In chapter 6 we present a general framework for embedding these models into global supersymmetry and discuss the new features that this construction predicts. In chapter 7 we present a class of supersymmetric chameleon models and investigate their cosmology. We conclude in chapter 8 with a discussion of the future of astrophysical probes of modified gravity in light of the results presented here and discuss the prospects for finding viable supersymmetric completions.

1.1 Conventions

Throughout this thesis we will use the metric convention $\eta_{\mu\nu} = \text{diag}(-,+,+,+)$ for the Minkowski metric and will use the same signature convention when dealing with curved space-

Abbreviation	Expression
AGB	asymptotic giant branch
CDM	cold dark matter
CGS	centimeter-grams-seconds
CMB	cosmic microwave background
EDDP	environment-dependent Damour-Polyakov effect
FI	Fayet-Illiopoulos
FLRW	Friedman-Lemaître-Robertson-Walker
LAWE	linear adiabatic wave equation
LOS	line of sight
MLAWE	modified linear adiabatic wave equation
PNLF	planetary nebula luminosity function
TRGB	tip of the red giant branch
VEV	vacuum expectation value

Table 1.1: Abbreviations used throughout this thesis.

times. Greek letters refer to four-dimensional Lorentzian coordinates when used as indices and Roman letters likewise for three-dimensional Euclidean coordinates. When describing identical theories of gravity in different frames the Jordan frame quantities are distinguished from their Einstein frame counterparts using tildes, for example, the Jordan frame metric is $\tilde{g}_{\mu\nu}$. ∇ denotes a covariant derivative and ∂ a partial derivative. We will work in units where $\hbar = c = 1$. The Planck mass is ${M_{\rm pl}}^2 = 1/8\pi G$. We will often use abbreviations for cumbersome expressions and, for convenience, a complete list is given in table 1.1.

1.2 General Relativity

Before discussing any modified theory of gravity one must first discuss general relativity. This is governed by the Einstein-Hilbert action action[11]

$$S_{\rm EH} = \int \mathrm{d}^4x\sqrt{-g}\,\frac{{M_{\rm pl}}^2}{2}R + S_{\rm m}[g_{\mu\nu};\psi_{\rm i}], \tag{1.1}$$

where $\psi_{\rm i}$ represent the various matter fields. Varying this with respect to the metric yields the Einstein field equations

$$G_{\mu\nu} = 8\pi G T_{\mu\nu}, \tag{1.2}$$

where $T_{\mu\nu}$ is the energy-momentum tensor for matter and the Einstein tensor $G_{\mu\nu} = R_{\mu\nu} + 1/2Rg_{\mu\nu}$ with $R_{\mu\nu}$ and R the Ricci tensor and scalar respectively. In this theory of gravity, the energy-momentum tensor is conserved, $\nabla_\mu T^{\mu\nu} = 0$ and this implies that particles move on geodesics of the metric. To see this, one can consider the energy-momentum tensor for a pressureless fluid of density ρ:

$$T^{\mu\nu} = \rho u^\mu u^\nu, \tag{1.3}$$

where $u^\mu = x'^\mu$ is the 4-velocity and a dash denotes a derivative with respect to the affine parameter λ. The conservation of the energy-momentum tensor then implies that (recall $\nabla_\mu(\rho u^\mu) = 0$)

$$u^\mu\nabla_\mu u^\nu = u^\mu(\partial_\mu u^\nu + \Gamma^\nu_{\mu\alpha}u^\alpha) = x''^\nu + \Gamma^\nu_{\mu\alpha}x'^\alpha x'^\mu = 0, \tag{1.4}$$

which is the geodesic equation. This can also be found by extremising the action for a point particle

$$S = -m\int \mathrm{d}s, \tag{1.5}$$

where m is the mass of the particle and $s = \sqrt{-g_{\mu\nu}x'^\mu x'^\nu}$ is the proper time. One may then find the non-relativistic limit of this theory by considering perturbations about Minkowski

[11] Up to boundary terms that are not relevant for this thesis.

space-time in the *conformal Newtonian gauge*

$$\mathrm{d}s^2 = -(1+2\Phi)\,\mathrm{d}t^2 + (1-2\Psi)\,\mathrm{d}x^2, \tag{1.6}$$

where the metric potentials are time-independent. Using this metric along with the non-relativistic condition $\mathrm{d}x^i/\mathrm{d}x^0 = v/c \ll 1$ in the geodesic equation (1.4) we find that the particles evolve according to

$$\ddot{\mathbf{x}} = -\nabla\Phi, \tag{1.7}$$

where a dot denotes a derivative with respect to the time coordinate. Equation (1.7) is simply Newton's second law with Φ identified with the Newtonian potential Φ_N. Using the Einstein equations (1.2) with a non-relativistic density source $T^{\mu\nu} = \mathrm{diag}(\rho, P, P, P)$ such that $P \ll \rho c^2$ we find the Poisson equation

$$\nabla^2\Phi_\mathrm{N} = 4\pi G\rho. \tag{1.8}$$

One can then see that general relativity reproduces Newton's law of gravitation exactly in the non-relativistic limit.

We have already mentioned that one can augment the Einstein-Hilbert action (1.1) to include a cosmological constant Λ without introducing new degrees of freedom. In this case, the action is

$$S_\mathrm{EH} = \int \mathrm{d}^4x\,\sqrt{-g}\,\frac{{M_\mathrm{pl}}^2}{2}(R-2\Lambda) + S_\mathrm{m}[g_{\mu\nu};\psi_\mathrm{i}], \tag{1.9}$$

which yields the modified equation

$$G_{\mu\nu} = 8\pi G T_{\mu\nu} - \Lambda g_{\mu\nu}. \tag{1.10}$$

In the Newtonian limit, the effective Newtonian potential is

$$\Phi_\mathrm{N} = \Phi_\mathrm{N}^{\Lambda=0} - \frac{1}{6}\Lambda r^2 \tag{1.11}$$

corresponding to a repulsive force. Current measurements [7] indicate that $\Lambda/{M_{\rm pl}}^2 \sim \mathcal{O}(10^{-120})$ and so one generally has $|\Phi_{\rm N}^{\Lambda=0}| \gg |\Lambda r^2|$. The exception to this is the largest scales since outside any matter distribution one generically has $|\Phi_{\rm N}^{\Lambda=0}| \propto r^{-1}$. This term is then only relevant on cosmological scales. One can then see that the addition of a cosmological constant to the Einstein-Hilbert action represents an infra-red modification of general relativity.

1.3 Cosmological Solutions of General Relativity

In this section we will briefly review some aspects of cosmology as predicted by general relativity. This is a rich and vast subject and a full account would be both lengthy and beyond the scope of this thesis. We will hence include only those features that are directly related to the original work presented later.

The standard cosmological model is predicated on the observation that on large scales, the universe is spatially homogeneous and isotropic. This is known as the *cosmological principle*, and the most general space-time compatible with its assumptions is the Friedmann-Lemaître-Robertson-Walker (FLRW) metric

$$\mathrm{d}s^2 = -\,\mathrm{d}t^2 + a^2(t)\left[\frac{\mathrm{d}x^2}{1-\kappa x^2} + x^2\,\mathrm{d}\Omega_2^2\right], \tag{1.12}$$

where $\mathrm{d}\Omega_2$ is the line element on a 2-sphere, x is the co-moving radial coordinate and $a(t)$ is the scale factor of the universe and is the only dynamical degree of freedom. Its dynamics depend both on the matter content of the universe and the theory of gravity. When it is non-constant, the metric describes an expanding universe and physical distances are given by

$$\mathrm{d}r = a(t)\,\mathrm{d}x. \tag{1.13}$$

We are free to choose the normalisation of a and in this thesis we will always choose a normalisation such that its value today $a_0 = 1$. κ is the spatial curvature of the universe; if it

is identically zero then the universe is spatially flat, if it is greater than zero the universe is spatially a 3-sphere and if it is negative the universe is a 3-hyperboloid.

Before specifying a theory of gravity there are some theory-independent quantities that can be defined. The Hubble parameter is

$$H(t) = \frac{\dot{a}}{a}, \tag{1.14}$$

where a dot denotes a derivative with respect to coordinate time t. Unlike $a(t)$ this is a physical observable and a useful quantity is its present day value H_0.This is often parametrised using the dimensionless number h as $H_0 = 100h$ km s^{-1} Mpc^{-1}. Another useful quantity is the redshift

$$1 + z = \frac{\lambda_o}{\lambda_e}, \tag{1.15}$$

where λ_e is the wavelength of light emitted by some source and λ_o is the wavelength observed at the present time. Using the FLRW metric (1.12) one can show that

$$a(t) = \frac{1}{1+z}. \tag{1.16}$$

Finally, one needs to define the notion of distance in an expanding universe. The instantaneous distance is not useful since it is unobservable and may even refer to space-like separated points. Instead, we shall work with the *luminosity distance*. When we look out into the sky and observe we see photons moving on radial null geodesics emitted at some redshift z and observed at $z = 0$. These have been red-shifted and diluted by the expansion of the universe and have also had their path length altered from the static case. Using the FLRW metric (1.12), the co-moving distance between us and the point at which the light was emitted is[12]

$$x(z) = \int_0^z \frac{\mathrm{d}z}{H(z)}. \tag{1.17}$$

Now in Minkowski space, the flux F at radius r is simply the luminosity per unit area and so

[12]We have set $\kappa = 0$ here because, as we shall see later on, observational evidence indicates that the universe is very close to flat.

one has

$$F = \frac{L}{4\pi r^2}, \tag{1.18}$$

where L is the bolometric luminosity of the source and F is the observed flux. Generalising this to an expanding space-time we define the luminosity distance via

$$d_L{}^2 = \frac{L}{4\pi F}. \tag{1.19}$$

The luminosity is not directly observable and instead we must infer it using known principles such as standard candles. There is an added complication in an expanding space-time that the observed flux integrated over a sphere of radius $4\pi r^2$ is not equal to the luminosity. This is because the radiation we observe at some wavelength λ_o has been redshifted by the expansion of the universe from its emitted value λ_e, therefore diluting its energy content. Furthermore, the time-period over which we observe is longer than the period over which the light was emitted owing to the increased wavelength. Ultimately, these two effects are due to the non-conservation of the photon number and energy density in an expanding space-time. Using equation (1.15) and the fact that the energy of a single photon is proportional to the inverse of its wavelength, we have

$$\frac{\Delta E_e}{\Delta E_o} = \frac{\lambda_o}{\lambda_e} = 1 + z, \tag{1.20}$$

where E_o and E_e are the observed and emitted photon energies respectively. Since the speed of light is constant[13], the time-period for one wave-cycle is proportional to the wavelength and so

$$\frac{\Delta t_o}{\Delta t_e} = 1 + z. \tag{1.21}$$

The observed flux is then related to the luminosity of the source by

$$F = \frac{L}{4\pi x^2 (1+z)^2} \tag{1.22}$$

[13] Or rather, ignoring effects from regions of finite permittivity or permeability between us and the source.

$$d_L = \sqrt{\frac{L_{\text{emitted}}}{4\pi F}} = (1+z)x(z) = (1+z)\int_0^z \frac{\mathrm{d}z}{H(z)} \tag{1.23}$$

using equation (1.17). This result is independent of the theory of gravity, however $H(z)$ is not and so any measured luminosity distance is sensitive to the theory of gravity for a fixed matter content.

1.3.1 The Standard Cosmological Model

Using the FLRW metric (1.12) in the Einstein field equations (1.2) will yield the equations governing the dynamics of $H(t)$ but first we must specify an energy-momentum tensor. The standard cosmological model takes the universe to consist of a non-interacting multi-component perfect fluid with energy-momentum tensor

$$T^{\mu\nu} = (\rho + P)u^\mu u^\nu + P g^{\mu\nu} = \text{diag}\left(\rho, P, P, P\right), \tag{1.24}$$

where u^μ is again the 4-velocity, ρ is the total energy density and P is the total pressure. Using this in the Einstein equation (with a cosmological constant) (1.10), one arrives at the Friedmann equations

$$H^2 = \frac{8\pi G}{3}\rho - \frac{\kappa}{a^2} + \frac{\Lambda}{3} \tag{1.25}$$

$$\frac{\ddot{a}}{a} = -\frac{4\pi G}{3}\left(\rho + 3P\right). \tag{1.26}$$

In general relativity, different types of matter do not exchange energy so that the energy-momentum tensor for each species is covariantly conserved independently ($\nabla_\mu T_{\text{i}}^{\mu\nu} = 0$). This leads to the continuity equation for each species:

$$\dot{\rho}_{\text{i}} + 3H\left(\rho_{\text{i}} + P_{\text{i}}\right) = 0. \tag{1.27}$$

The system of equations (1.25)–(1.27) does not close and one must specify an equation of state relating the pressure to the density. This is usually taken to be of the form

$$P_{\mathrm{i}} = w_{\mathrm{i}}\rho_{\mathrm{i}} \tag{1.28}$$

where $w_{\mathrm{i}} = 0$ for non-relativistic matter, $1/3$ for radiation and -1 for a cosmological constant and is referred to as the *equation of state parameter* or simply the *equation of state*. Solving the continuity equation for an arbitrary equation of state one finds

$$\rho_{\mathrm{i}} = \begin{cases} \frac{\rho_0}{a^{3(1+w)}} & w_{\mathrm{i}} \neq -1 \\ \rho_0 & w_{\mathrm{i}} = -1 \end{cases}, \tag{1.29}$$

where ρ_0 is the present day density and is equal to ${M_{\mathrm{pl}}}^2\Lambda$ for a cosmological constant. One may then define the *density parameter* for species i:

$$\Omega_{\mathrm{i}} = \frac{\rho_{\mathrm{i}}}{3H_0^2{M_{\mathrm{pl}}}^2} \quad w_{\mathrm{i}} \neq -1. \tag{1.30}$$

The cosmological constant requires a special treatment so we define $\Omega_\Lambda \equiv \Lambda/3H^2$ and we define $\Omega_\kappa = -\kappa/a^2H^2$. The Friedmann equation (1.25) is then

$$\sum_{\mathrm{i}} \Omega_{\mathrm{i}} + \Omega_\Lambda + \Omega_\kappa = 1. \tag{1.31}$$

If we then define $\Omega = \sum_{\mathrm{i}} \Omega_{\mathrm{i}} + \Omega_\Lambda$ we can set $\Omega_\kappa = 0$ in (1.31) to find

$$\Omega = \sum_{\mathrm{i}} \Omega_{\mathrm{i}} + \Omega_\Lambda = 1, \tag{1.32}$$

which implies

$$\sum_{\mathrm{i}} \rho_{\mathrm{i}} + \rho_\Lambda = 3H^2{M_{\mathrm{pl}}}^2 \tag{1.33}$$

This is an important equation, it tells us that if the universe is spatially flat then the total density is constrained to be equal to the *critical density* $\rho_c = 3{M_{pl}}^2 H^2$. Moreover, equations (1.32) and (1.33) hold at all times. In a spatially flat universe $\Omega_i(t)$ is then a measure of the fraction that species i contributes to the total density. Current observational experiments (see [7] for example) indicate that Ω_κ is indeed very close to zero and so from here on we will work with a spatially flat universe[14].

1.3.2 The ΛCDM Model

Background Cosmology

The Λ-Cold Dark Matter (ΛCDM) model is the Planck best fit [7] model to several different cosmological observables and is a model of the late-time universe well after big bang nucleosynthesis (BBN). It describes a spatially flat universe composed of baryons, cold dark matter (CDM), radiation and a cosmological constant. Including these components and using the solution to the continuity equation (1.29), we can write the Friedmann equation (1.25) in the form

$$H^2 = H_0^2 \left(\frac{\Omega_c^0 + \Omega_b^0}{a^3} + \frac{\Omega_\gamma}{a^4} + \Omega_\Lambda \right), \tag{1.34}$$

where c refers to cold dark matter, b to baryons and γ to radiation. Since $a(t)$ is a monotonically increasing function of time, the various terms come to dominate at different times resulting in different epochs where different species dominate. The details of the very early universe are unimportant for this thesis and so we assume that the universe exits from inflation (or some other early universe process) with a scale-invariant power spectrum and leave the processes of reheating and preheating unspecified. At this time, a is very small and the radiation term dominates leading to a radiation dominated era. As the scale factor grows, the

[14] Technically this is only correct for general relativity since the result is derived from a Bayesian fit to the CMB data and assuming general relativity. The theories considered later all behave like general relativity at early times and outside the horizon. Furthermore, null geodesics are unaffected by the theories we will study and so we expect this observation to be largely independent of our theory of gravity. That being said, there are minor second-order effects when the radiation fluid is tightly coupled to the baryons since the equations governing non-relativistic perturbations are altered [59].

Parameter	Planck best-fit value
$\Omega_b^0 h^2$	0.022
$\Omega_c^0 h^2$	0.12
Ω_γ^0	$\mathcal{O}(10^{-5})$
Ω_Λ^0	0.68
H_0	68.14 km s^{-1} Mpc^{-1}

Table 1.2: The Planck best fit cosmological parameters, taken from [60].

baryons and dark matter come to dominate leading to a matter dominated era that begins at a redshift $z \sim 1000$. Finally, as these dilute and the scale factor continues to grow, only the cosmological constant is left and this dominates the subsequent evolution of the universe. The solutions of equation (1.34) deep in each of these eras so that the other terms can truly be neglected are

$$a(t) = \begin{cases} \left(\frac{t}{t_0}\right)^{\frac{2}{3}} & \text{matter domination} \\ \left(\frac{t}{t_0}\right)^{\frac{1}{2}} & \text{radiation domination} \\ e^{\frac{\Lambda}{3}t} & \Lambda \text{ domination} \end{cases}, \tag{1.35}$$

where t_0 is the time today (i.e. the age of the universe). The *Planck* best fit parameters are shown in table 1.2. The values of Ω_Λ^0 and Ω_c^0 are of the same order of magnitude and so we are currently living in the transition period between matter and cosmological constant domination. The mystery of why we observe during this small transition time and not any other has been dubbed the *coincidence problem* and we will have nothing to say about it in this thesis.

Linear Perturbations

So far we have only looked at the background cosmology but many interesting cosmological probes including the CMB arise due to departures from the homogeneous and isotropic background in the form of linear perturbations. Linear perturbation theory in general relativity and

cosmology is a broad and interesting subject and a full treatment is well beyond the scope of this thesis. Here we will only focus on the evolution of perturbations to the cold dark matter density deep inside the horizon since we will investigate this for chameleon-like models in chapter 7.

Throughout this thesis we will work in the *conformal Newtonian gauge*, in which the perturbed form of the flat FLRW metric (1.12) is fully specified by the two potentials Φ and Ψ[15]

$$ds^2 = -(1+2\Phi)\,dt^2 + a(t)^2(1-2\Psi)\,dx^2. \tag{1.36}$$

We also need to specify the perturbations to the cold dark matter energy-momentum tensor. For our purposes, it will be enough to specify the perturbation to the 00-component only, which is the density perturbation $\delta\rho$ in this gauge. This choice completely fixes all the gauge degrees of freedom and there is no residual gauge redundancy provided the potentials decay to zero at spatial infinity. We define the linear density contrast Δ_c via

$$\Delta_c(x) \equiv \frac{\delta\rho_c}{\bar{\rho}_c}, \tag{1.37}$$

where barred quantities refer to unperturbed, background quantities. This is defined in position space but in practice it is useful to Fourier-transform the spatial part and so we define

$$\Delta_c = \int \frac{d^3\mathbf{k}}{(2\pi)^3}\delta_c(\mathbf{k},t)e^{i\mathbf{k}\cdot\mathbf{x}}. \tag{1.38}$$

Since the theory is both translationally and rotationally invariant[16] we generally have $\delta_c = \delta_c(t,k)$. Physically, a given k-mode corresponds to the wave number of a perturbation of proper wavelength λ:

$$k = \frac{2\pi a}{\lambda}. \tag{1.39}$$

[15] Note that these are different metric perturbations from those defined in equation (1.6).
[16] We will not deal with theories where this is not the case in this thesis.

Upon solving the perturbed Einstein and energy conservation equations, one finds that the linear density contrast evolves according to

$$\ddot{\delta}_{\mathrm{c}} + 2H\dot{\delta}_{\mathrm{c}} - 4\pi G\bar{\rho}_{\mathrm{c}}\delta_{\mathrm{c}} = 0. \tag{1.40}$$

Eliminating the factor of $G\bar{\rho}_{\mathrm{c}}$ using the Friedmann equation (1.25) we have

$$\ddot{\delta}_{\mathrm{c}} + 2H\dot{\delta}_{\mathrm{c}} - \frac{3}{2}H^2\frac{\bar{\rho}_{\mathrm{c}}}{\bar{\rho}_{\mathrm{c}} + \bar{\rho}_{\gamma}}\delta_{\mathrm{c}} = 0, \tag{1.41}$$

where we have neglected the contribution from the baryons and the cosmological constant. During matter domination when $\bar{\rho}_{\mathrm{c}} \gg \bar{\rho}_{\gamma}$ the growing solution is

$$\delta_{\mathrm{c}} \propto t^n; \quad n = -\frac{1}{6} + \frac{1}{2}\sqrt{\frac{1}{9} + \frac{8}{3}\Omega_{\mathrm{c}}^0}\,. \tag{1.42}$$

Now Δ_{c} and δ_{c} are not physical observables since δ_{c} is a gauge-dependent quantity and so we need to relate it to something we can physically measure in order to extract the model predictions. The relevant quantity is the two-point correlation function or *power spectrum* defined via

$$\langle \delta_{\mathrm{c}}(t,\mathbf{k})\delta_{\mathrm{c}}^*(t,\mathbf{k}')\rangle = \frac{2\pi^2}{k^3}P_{\delta_{\mathrm{c}}\delta_{\mathrm{c}}{}^*}(k)\delta^{(3)}\left(\mathbf{k}-\mathbf{k}'\right). \tag{1.43}$$

For brevity, we will often denote $P_{\delta_{\mathrm{c}}\delta_{\mathrm{c}}{}^*}(k)$ by $P(k)$.

1.4 Dark Energy

We have already alluded to the presence of dark energy in the universe in the previous section where we included a cosmological constant in our model of the universe and noted that ΛCDM is currently the best-fit to the cosmological data. Equation (1.35) shows that the universe expands exponentially when the cosmological constant dominates. Indeed, if one takes the second Friedmann equation (1.26) and sets every component except Λ equal to zero we have

$\ddot{a} > 0$ so that the universe is accelerating. This acceleration seems counter-intuitive. Gravity dominates the evolution of the universe on large scales and this is an attractive force between all matter and so surely the universe should be decelerating? The acceleration is due to the fact that $w_\Lambda = -1$ so that the pressure of the cosmological constant is negative. This behaviour is not unique to the cosmological constant. Indeed, examination of equation (1.26) shows that any fluid satisfying

$$w < -\frac{1}{3} \tag{1.44}$$

will accelerate if it dominates the universe's expansion. In 1998, two teams [3, 4] published the luminosity distance measured from supernovae distances estimates and found that a flat universe composed only of matter and radiation could not fit the data well; a component with $w \approx -1$ is needed. The universe is indeed accelerating. Since then there have been many independent experiments using cosmological probes such as weak lensing, baryon acoustic oscillations and the integrated Sachs-Wolfe effect that all point to the need for dark energy and a full review may be found in [5]. The most compelling evidence by far comes from the temperature-temperature power spectrum of the CMB including the effects of lensing [61][17]. The Planck limits on w vary depending on the model assumed [60] but there is a large region around $w = -1$ that is not excluded and so the underlying mechanism driving this acceleration is far from clear. The mysterious component causing this acceleration has been dubbed *dark energy*. Its physical origin is one of the biggest unsolved problems in modern physics.

1.4.1 A Simple Example: Quintessence

Quintessence models are an attempt to promote the cosmological constant to a dynamical field. The simplest models have a canonically normalised scalar field slowly rolling down a

[17] The power spectrum alone does not determine Ω_m and Ω_Λ uniquely; their values are degenerate with H_0. Including the effects of lensing breaks this degeneracy.

potential $V(\phi)$ and are described by the action:

$$S = \int \mathrm{d}^4x\sqrt{-g}\left[\frac{{M_{\mathrm{pl}}}^2}{2}R - \frac{1}{2}\nabla_\mu\phi\nabla^\mu\phi - V(\phi)\right] + S_{\mathrm{m}}[g_{\mu\nu};\psi_{\mathrm{i}}]. \tag{1.45}$$

Note that the field is *minimally coupled* to gravity in the sense that there are no direct couplings to any curvature tensors or to the matter degrees of freedom. The (conserved) energy-momentum tensor for the field is

$$T^{\mu\nu} = \nabla^\mu\phi\nabla^\nu\phi - g^{\mu\nu}\left[\frac{1}{2}\nabla_\mu\phi\nabla^\mu\phi + V(\phi)\right], \tag{1.46}$$

from which one can obtain the energy density

$$\rho = T^{00} = \frac{1}{2}\dot{\phi}^2 + V(\phi) \tag{1.47}$$

and the pressure

$$P = T^{|ii|} = \frac{1}{2}\dot{\phi}^2 - V(\phi), \tag{1.48}$$

where the use of $|ii|$ notation indicates that we are not summing over repeated indices. The equation of state is then

$$w_\phi = \frac{\dot{\phi}^2 - 2V(\phi)}{\dot{\phi}^2 + 2V(\phi)}. \tag{1.49}$$

One can see that when $V(\phi) \gg \dot{\phi}^2$ we have $w_\phi \approx -1$ and so provided that the field is slowly-rolling, this model mimics the effects of a cosmological constant. In practice, these models suffer from fine-tuning problems since one needs to tune the initial conditions and the parameters in the potential in order to reproduce the measured values of the equation of state and the energy density in dark energy. Furthermore, if one wishes to address the coincidence problem then one must fine-tune further so that field starts to dominate the energy density of the universe around the current epoch. More complicated models attempt to address these issues by looking for late-time attractors that give a dark energy dominated universe no matter

the initial conditions. Some also exhibit *scaling solutions* where the dark energy tracks the evolution of the dominant fluid component and remains sub-dominant until some mechanism causes it to deviate from this solution and quickly dominate the universe. We will not be concerned with these models here and the interested reader is referred to [5] and references therein.

1.5 Stellar Structure in General Relativity

Part of this thesis is concerned with the structure and evolution of stars in modified gravity and so in this section we will change direction and briefly discuss the structure of stars in general relativity. We will see in chapter 2 that the theories studied in this thesis only show novel effects in non-relativistic stars and so we will limit our discussion to these.

1.5.1 The Equations of Stellar Structure

The equilibrium structure of non-relativistic stars are described by the stellar structure equations. In chapter 3 we will derive them[18] formally from modified gravity hydrodynamics and so here we shall simply present them and discuss their solutions.

By equilibrium, we refer to hydrostatic equilibrium where a star maintains a spherical shape with constant radius and supports itself against gravitational collapse by balancing the inward force with an outward pressure gradient. This is described by the *hydrostatic equilibrium equation*

$$\frac{\mathrm{d}P}{\mathrm{d}r} = -\frac{GM(r)\rho(r)}{r^2}, \tag{1.50}$$

where r is the radial coordinate (with the centre of the star at $r = 0$), $P(r)$ is the pressure and $\rho(r)$ is the density. $M(r)$ is the mass enclosed within radius r. If the radius is R then the total stellar mass is $M \equiv M(R)$. Since the start is spherically symmetric the mass is related to the

[18] In fact, we will derive them for modified theories of gravity but the general relativity equations can be obtained in a straightforward manner by setting the additional terms to zero.

density via the continuity equation,

$$\frac{\mathrm{d}M}{\mathrm{d}r} = 4\pi r^2 \rho. \tag{1.51}$$

Photon propagation in the interior of the star is described by the radiative transfer equation,

$$\frac{\mathrm{d}T}{\mathrm{d}r} = -\frac{3}{4a}\frac{\kappa(r)}{T^3}\frac{\rho(r)L(r)}{4\pi r^2}, \tag{1.52}$$

where $L(r)$ and $T(r)$ are the luminosity and temperature respectively at coordinate r. The quantity κ is known as the *opacity* and represents the cross section for radiation absorption per unit mass; it is generally a function of the temperature and density. Finally, if energy is generated — by nuclear (or possibly other) processes — at a rate $\epsilon(r)$ per unit volume then the luminosity gradient is determined by the energy generation equation,

$$\frac{\mathrm{d}L}{\mathrm{d}r} = 4\pi r^2 \rho \epsilon(r). \tag{1.53}$$

Taken by themselves, these equations do not close and one must specify the equations of state relating P, ρ, κ and ϵ, which are themselves determined by further equations involving energy transfer and nuclear burning networks.

One can see that the stellar structure equations include aspects of nuclear, atomic, thermal and gravitational physics and are hence perfect laboratories for testing fundamental physics.

1.5.2 Lane-Emden Models

The equations of stellar structure are incredibly complicated and in order to achieve realistic models one must couple them to a complete set of atmosphere models, nuclear burning networks and opacity tables. It is often necessary to include effects such as convection and mass-loss. In practice, this requires complicated numerical codes if one wishes to find models that are realistic enough to compare to data. If one is only interested in the gross physical

features then there are some simple approximations that one can make. In this thesis we will be interested in the effects of changing the theory of gravity whilst leaving the other stellar physics unaltered[19]. A particularly useful class of simple models for investigating the effects of gravity are *Lane-Emden* models. Lane-Emden models make the simplifying assumption that the star can be described as a barotropic fluid with a *polytropic* equation of state

$$P = K\rho^{\gamma}, \tag{1.54}$$

where K is a constant and γ is known as the *adiabatic index*. Main-sequence stars are well described by $\gamma = 4/3$ [62] whereas convective regions in post-main-sequence stars such as red giants are well approximated by $\gamma = 5/3$ [63]. In practice, it is more convenient to work with the polytropic index n defined by

$$\gamma = \frac{n+1}{n} \tag{1.55}$$

so that $\gamma = 4/3$ corresponds to $n = 3$ and $\gamma = 5/3$ corresponds to $n = 1.5$. Using this assumption, the hydrostatic equilibrium equation and the continuity equation do not depend on temperature and so are decoupled from the radiative transfer and energy generation equations and this allows us to solve the first two for the structure of the star independent of the energy source or opacity profile. This is why these models are good for investigating the effects of changing the theory of gravity. These are two coupled first-order differential equations and so we require two boundary conditions at the centre of the star. The central pressure P_c is arbitrary and we take this to be one boundary condition. The central density ρ_c is then fixed by equation (1.54). The second boundary condition comes from the assumption of spherical symmetry, which requires that the pressure (or equivalently the density) is a smooth function

[19]This is not to say that the other physics is unaltered. Indeed, we will see in the coming chapters that changing the theory of gravity will result in changes to the non-gravitational features such as the luminosity and the temperature. The important difference is that the physical theory governing these features has not been altered and the new phenomena exhibited are the response to the change in the gravitational theory.

of r and so its derivative must vanish at $r = 0$. The problem is then reduced to that of solving for the pressure as a function of the radial position.

The stellar structure equations are self-similar and so we can work with both a dimensionless coordinate and a dimensionless pressure. We begin by defining the Lane-Emden coordinate[20]

$$y = r/r_c, \tag{1.56}$$

where

$$r_c^2 \equiv \frac{(n+1)P_c}{4\pi G\rho_c^2}. \tag{1.57}$$

Next, we define the dimensionless pressure variable θ via

$$P(y) = P_c\theta^{n+1}(y); \quad \rho(y) = \rho_c\theta^n(y). \tag{1.58}$$

Substituting the equation of state (1.54) into the hydrostatic equilibrium equation (1.50) we can differentiate once and eliminate $\mathrm{d}M(r)/\mathrm{d}r$ using equation (1.51) in order to find the Lane-Emden equation

$$\frac{1}{y^2}\frac{\mathrm{d}}{\mathrm{d}y}\left(y^2\frac{\mathrm{d}\theta}{\mathrm{d}y}\right) = -\theta^n \tag{1.59}$$

with boundary conditions $\theta(0) = 1$ ($P(0) = P_c$) and $\mathrm{d}\theta/\mathrm{d}y(0) = 0$ ($\mathrm{d}P/\mathrm{d}r(0) = 0$). The Lane-Emden equation can then be solved numerically for any value of n for the function $\theta(y)$, which fully specifies the structure of the star for a given P_c and ρ_c (or equivalently K). The definition of the stellar radius is slightly ambiguous. In reality, one observes light emitted from the photosphere, which is defined as the surface at which the optical depth falls to 2/3. Stars that are simple enough to be well-described by Lane-Emden models have radii that are well approximated by the condition that the pressure falls to zero at the stellar radius and so we have $R = r_c y_R$ where y_R is defined by $\theta(y_R) = 0$[21]. Finally, one can integrate equation (1.51)

[20] Note that this is typically called ξ in the literature. Later on we will use ξ to refer to the Fourier transform of the radial perturbation when studying stellar oscillations and so here we use y instead.

[21] One must be careful because the solution of the Lane-Emden equation does not go to zero at finite y when $n > 4$ and so one needs to choose the radius according to some prescription set by the problem. This will not

to find the mass of the star:

$$M = \int_0^{y_R} 4\pi r_c^3 \rho_c y^2 \theta^n \, \mathrm{d}y = -4\pi r_c^3 \rho_c y_R^2 \left.\frac{\mathrm{d}\theta}{\mathrm{d}y}\right|_{y=y_R} = 4\pi r_c^3 \rho_c \omega_R \tag{1.60}$$

where we have used the Lane-Emden equation (1.59) and have defined

$$\omega_R \equiv y_R^2 \left.\frac{\mathrm{d}\theta}{\mathrm{d}y}\right|_{y=y_R} \tag{1.61}$$

for later convenience.

One can see that the solutions of the Lane-Emden equation are enough to fully determine the structure and mass of a polytropic star given any choice of central pressure and density. We will return to the Lane-Emden equation in chapter 3 where we will derive and investigate its generalisation in modified theories of gravity.

1.6 Supersymmetry

In chapters 6 and 7 we will study supersymmetric models of modified gravity. A comprehensive treatment of supersymmetry starting from first principles is far beyond the scope of this thesis and the interested reader is referred to review articles such as [64] and references therein. Here we will only present the salient features — often without proof — necessary for the understanding of the construction of the models presented later on. We will always work within an $\mathcal{N} = 1$ framework.

1.6.1 Foundations of Supersymmetry

Supersymmetry is a space-time symmetry that extends the Poincaré group ISO(1, 3), which acts on the space-time coordinates x^μ, to the superpoincaré group, which acts on the coor-

be a problem for the work presented in this thesis since we will only investigate the cases $n = 3$ and $n = 1.5$, however this is a problem for isothermal core models that have $n = \infty$.

dinates $\{x^\mu, \theta^\alpha, \bar{\theta}^{\dot{\alpha}}\}$[22] with $\alpha = \dot{\alpha} = 1, 2$. Here, θ^α and $\bar{\theta}^{\dot{\alpha}} \equiv (\theta^\alpha)^\dagger$ are anti-commuting two-component spinors[23]. In addition to the usual generators of the Poincaré group, the Lie algebra of the superpoincaré group includes four new generators $\{Q_\alpha, \bar{Q}_{\dot{\alpha}}\}$. The total momentum $C_1 \equiv P_\mu P^\mu$ (where P^μ is the generator of translations) is still a Casimir of the superpoincaré group but the Pauli-Ljubanski vector $W_\mu = 1/2\epsilon_{\mu\nu\rho\sigma}P^\nu M^{\rho\sigma}$, where $M^{\mu\nu}$ is the generator of Lorentz transformations, is not. If the representation is massless then the second Casimir operator is zero. In this case we can choose to label states in each representation by their helicity given by the eigenvalue λ of J_3 but this will vary between different states. The Casimir operator for massive representations is a combination of P^μ, $M^{\nu\sigma}$, Q_α and $\bar{Q}_{\dot{\alpha}}$ and is given by $C_2 \equiv Y_\mu Y^\mu$ where Y_μ is known as the *super spin*. It satisfies the same commutation relations as the generators of SU(2) and hence states are labelled by the eigenvalue y of Y^2. Its precise definition is not important in what follows. Representations of the superpoincaré group are therefore classified by their mass m such that $P_\mu P^\mu = -m^2$ and either their helicity if the representation is massless or the eigenvalue of Y^2 if not. Unlike the Poincaré group, given a starting value for the helicity λ ($J_3|\lambda>=\lambda|\lambda>$) or the superspin y ($C_2|y>=y(y+1)|y>$), the rest of the states in the representation have different helicities or spins and so any representation of the superpoincaré group has a fixed particle content. This is because the total spin J^2 and helicity J_3 do not commute with the other generators of the superpoincaré group. Each representation is referred to as a *multiplet* and in table 1.3 we list some multiplets that we will encounter in chapters 6 and 7. Note that the number of fermionic degrees of freedom is equal to the number of bosonic degrees of freedom. There is a general theorem proving that this is the case for any representation of the supersymmetry algebra. Furthermore, when supersymmetry is unbroken the masses of each species are identical. There is a particularly simple method for constructing $\mathcal{N} = 1$ Lagrangians by packaging the fields in different multiplets into *superfields* defined on superspace which are hence functions of $\{x^\mu, \theta^\alpha, \bar{\theta}^{\dot{\alpha}}\}$. For

[22] Extended supersymmetry introduces more spinorial dimensions.

[23] Our convention will be such that contractions of spinors are defined as follows: $\psi\chi = \psi^\alpha\chi_\alpha$ and $\bar{\psi}\bar{\chi} = \bar{\psi}_{\dot{\alpha}}\bar{\chi}^{\dot{\alpha}}$, where contractions are performed with the anti-symmetric epsilon symbol $\epsilon_{\alpha\beta}$ and $\epsilon_{\dot{\alpha}\dot{\beta}}$ where $\epsilon_{12} = \epsilon_{\dot{1}\dot{2}} = -1$.

Multiplet	Field Content
massless chiral	massless scalar ϕ & massless Majorana fermion ψ_α
massive chiral	massive scalar ϕ & massive Majorana fermion ψ_α
massless vector	massless vector V_μ & massless Majorana fermion λ_α
gravity	massless graviton $g_{\mu\nu}$ & gravitino $\psi_{\mu\alpha}$

Table 1.3: Representations of the superpoincaré group that will be useful later on. In each case $\mu = 0, 1, 2, 3$, labels space-time components and $\alpha = 1, 2$ labels spinorial components.

the massless and massive chiral multiplet, the scalar and fermion are packaged into *chiral superfields*:

$$\Phi(y) = \phi(y) + \sqrt{2}\theta\psi(y) + \theta\theta F(y), \tag{1.62}$$

where $y^\mu = x^\mu + i\theta\sigma^\mu\bar{\theta}$ and $\sigma^\mu = (\mathbb{I}_2, \sigma^i)$, where σ^i are the Pauli matrices that generate SU(2)[24]. The field F is unusual in that it has mass dimension 2. At the level of the action, it is an auxiliary field that is eliminated using the equations of motion in order to find the complete equations of motion. We will not elaborate on the co-ordinate y^μ here since we will not present the technical derivation of any of the results below. It is introduced here purely for notational convenience and the interested reader is referred to [64]. The massless vector multiplet can be described by a vector superfield $V = V^\dagger$

$$V(x) = \theta\sigma^\mu\bar{\theta}V_\mu(x) + (\theta\theta)\,\bar{\theta}\bar{\lambda}(x) + \left(\bar{\theta}\bar{\theta}\right)\theta\lambda(x) + \frac{1}{2}(\theta\theta)\left(\bar{\theta}\bar{\theta}\right)D(x), \tag{1.63}$$

where $D(x)$ is another auxiliary field that is eliminated to produce the equations of motion. We do not write down the superfield corresponding to the gravity multiplet since there are several, all of which correspond to geometric tensors on superspace. A complete treatment of this can be found in [65]. These are all the tools that we require in order to construct supersymmetric Lagrangians. We will briefly indicate how this is done below.

[24] In the context of supersymmetry σ^μ has the index structure $\sigma^\mu_{\alpha\dot{\alpha}}$.

1.6.2 Global Supersymmetry

Global supersymmetry refers to actions where the supersymmetry transformations are a symmetry of the action and not a gauge redundancy i.e. the transformations act on each point in superspace in exactly the same manner. Globally supersymmetric actions for a U(1) Abelian vector multiplet interacting with i chiral multiplets are fully specified by two functions[25]: the Kähler potential $K(\Phi_i, \Phi_j^\dagger, V_j)$ and the superpotential $W(\Phi_i)$. Note that the Kähler potential depends on both Φ and its complex adjoint whereas the superpotential is holomorphic. Rather than write down the action in full, we will simply state how each of these functions act to specify the kinetic functions for the scalar, the fermion masses and the scalar potential.

The Kähler potential sets the kinetic term for the scalars. It is useful to define the *Kähler metric*

$$K_{ij} = \left.\frac{\partial^2 K}{\partial \Phi_i \partial \Phi_j}\right|_{\Phi=\phi, V=0}, \tag{1.64}$$

whose inverse is K^{ij}. The kinetic term for the scalars is then

$$\frac{\mathscr{L}_{\text{kin}}}{\sqrt{-g}} \supset K_{ij} \nabla_\mu \phi_i \nabla^\mu \phi_j^*. \tag{1.65}$$

For a single chiral superfield Φ, the field will only be canonically normalised if $K(\Phi, \Phi^\dagger) = \Phi\Phi^\dagger$. The superpotential sets the mass of the fermions:

$$M_{ij} = \frac{\partial^2 W}{\partial \Phi^i \partial \Phi^j}, \tag{1.66}$$

where M_{ij} is the fermion mass-matrix[26]. A combination of the Kähler potential and the superpotential sets the scalar potential for ϕ_i. There are two terms contributing to the scalar potential. The first is the *F-term* potential, so-called because it is found by eliminating the

[25] Technically one also requires a kinetic term for the vector superfield and this is accompanied by a third gauge-kinetic function. In this thesis we will only consider vector fields whose kinetic terms are canonical and so this will not be relevant.

[26] The reader may worry that this can be complex according to (1.66). Since the fermions are described by Majorana spinors this is perfectly acceptable and the true masses are given by the eigenvalues of $M^2 = M^\dagger M$.

auxiliary field F from the equations of motion. This is given by

$$V_{\mathrm{F}} = K^{ij} \left. \frac{\partial W}{\partial \Phi_i} \frac{\partial W^\dagger}{\partial \Phi^\dagger} \right|_{\Phi=\phi, \Phi^\dagger=\phi^*} . \tag{1.67}$$

The second term comes from eliminating the auxiliary field D from the equations of motion and is hence known as the *D-term* potential. In this thesis, we will only be interested in U(1) gauge theories, in which case the D-term potential is

$$V_{\mathrm{D}} = \frac{1}{8} \left(\xi + \sum_j q_j \left| \varphi_j \right|^2 \right), \tag{1.68}$$

where $\{\varphi_j\}$ are the subset of the scalar fields that transform under the U(1) symmetry with charge q_j. Here we have assumed that there is a single vector multiplet coupled to an arbitrary number of chiral multiplets; the generalisation to several multiplets is straightforward. We have also included a Fayet-Illiopoulos term ξ. This term is only allowed if the gauge symmetry for the vector is U(1). The extension to multiple vector fields and non-Abelian symmetry groups is straightforward. We will not present the general formula here since we will have no need of it in this thesis.

The supersymmetry algebra is so constraining that only when $V = V_{\mathrm{F}} + V_{\mathrm{D}} = 0$ is supersymmetry unbroken. Since these two terms can be non-zero independently, there are two methods of breaking supersymmetry. The first is F-term supersymmetry breaking where

$$F_i = -\frac{\partial W}{\partial \Phi_i} \neq 0 \tag{1.69}$$

and D-term breaking, where

$$D = \xi + \sum_j q_j \left| \varphi_j \right|^2 \neq 0. \tag{1.70}$$

1.6.3 Supergravity

The introduction of any Lorentz-invariant spin-2 field mandates that the theory is invariant under local diffeomorphisms in order for the graviton to propagate the two degrees of freedom imposed by Lorentz symmetry. When one introduces the gravity multiplet, one is then forced to introduce diffeomorphism invariance on the entire superspace i.e. one must promote global supersymmetry to general superspace co-ordinate transformations so that supersymmetry is now a gauge redundancy. This greatly complicates the Lagrangian and, in particular, the F-term scalar potential is different from (1.67). A full construction of $\mathcal{N} = 1$ supergravity can be found in [65]; here we will only write down the F-term scalar potential and discuss the relevant new features that arise from gauging the theory. Defining

$$D_i W \equiv \frac{\partial W}{\partial \Phi_i} + \frac{W}{{M_{\rm pl}}^2}\frac{\partial K}{\partial \Phi_i}, \tag{1.71}$$

which has the physical interpretation as the covariant derivative on the manifold defined by the Kähler metric, the scalar potential in supergravity is

$$V_{\rm F} = e^{\frac{K}{{M_{\rm pl}}^2}}\left(K^{ij} D_i W (D_j W)^\dagger - 3\frac{|W|^2}{{M_{\rm pl}}^2}\right). \tag{1.72}$$

One can see that the global supersymmetry formula (1.67) is recovered in the limit $M_{\rm pl} \to \infty$[27]. The D-term potential is left unaltered. Unlike global supersymmetry, the scalar potential can be non-zero and still preserve supersymmetry. The strict condition for F-term supersymmetry breaking is

$$\langle F_i \rangle = -e^{\frac{K}{2{M_{\rm pl}}^2}} D_i \Phi = 0 \; \forall i. \tag{1.73}$$

In global supersymmetry the F-term is given by equation (1.69). In supergravity we have an extra term $-3|W|^2/{M_{\rm pl}}^2$ in the potential and so one can have a negative scalar potential and still preserve supersymmetry. A positive scalar potential always breaks supersymmetry since

[27] The correct limit is $m_{3/2}/M_{\rm pl} \to 0$ ($m_{3/2}$ is the gravitino mass) since $M_{\rm pl}$ is a dimensionless quantity. This distinction is relevant if supergravity is broken.

equation (1.72) is only positive if at least one $F_i \neq 0$. Note also that $V_{\mathrm{F}} = 0$ does not necessarily imply that supersymmetry is preserved since this will only be true if $W = 0$ at the minimum. Kähler potentials where $V_{\mathrm{F}} = 0$ at the minimum are known as *no-scale* potentials. The simplest example for a single chiral superfield is

$$K(\Phi, \Phi^\dagger) = -n{M_{\mathrm{pl}}}^2 \ln\left(\frac{\Phi + \Phi^\dagger}{{M_{\mathrm{pl}}}^2}\right). \tag{1.74}$$

$n = 3$ models are known as *pure no-scale* models[28] and we will refer to $n \neq 3$ as *no-scale type* models. Finally, we note that the gravitino mass is not arbitrary in this theory but is given by[29]

$$m_{3/2}^2 = \frac{|W|^2}{{M_{\mathrm{pl}}}^4} e^{\frac{K}{{M_{\mathrm{pl}}}^2}}. \tag{1.75}$$

[28] This is because $n = 3$ models give $V_{\mathrm{F}} = 0$ provided that one chooses the superpotential correctly.

[29] Note that the gauging of the supersymmetry algebra means that a non-zero gravitino mass does not imply that supersymmetry is broken.

The absence of evidence is not the evidence of absence.

Donald Rumsfeld

2

Modified Gravity

Before discussing any particular theory, the first question to address is *what exactly constitutes a modified theory of gravity?* We have already mentioned in the introduction that general relativity is the unique Lorentz invariant theory of a massless spin-2 particle so perhaps we should define modified gravity as any theory containing more than one spin-2 degree of freedom? Such a theory has already been presented in the form of Quintessence (1.45), which includes another scalar degree of freedom minimally coupled to gravity. The problem with this definition is that it is ambiguous whether this is indeed a modification of gravity or whether we should consider the scalar as a matter component that interacts with gravity according to general relativity. One point of view is that gravity is modified on large scales because including this scalar modifies the expansion history (and other cosmological properties) when the same FLRW metric is used to describe cosmology. On the other hand, this modification can equivalently be interpreted as adding another fluid to the matter content of the universe with a variable equation of state with the underlying cosmological dynamics being governed by general relativity. This issue is purely philosophical and has no absolute resolution. In this work we will not consider this theory a modification for the following reason: suppose we were to look at the non-relativistic limit of the geodesic equation (1.4) for matter moving in this theory. The energy-momentum tensor of the individual matter species are still covariantly

conserved and so we obtain the same Newtonian force law that we found for general relativity. The difference here is that the scalar profile could in principle modify the Newtonian potential of a given source compared to what would have been obtained if it were absent. Since there is no coupling of the field to the curvature the scalar field has a spatially homogeneous source. In this case the field value on all scales is its cosmologically rolling value[1]. This can at most modify the Newtonian potential by a time-dependent contribution and hence does not affect the dynamics in the Newtonian limit. It is important to stress that this is simply an aesthetic choice for what constitutes a modified theory of gravity and that one generally expects deviations from the motion described by general relativity at the post-Newtonian level and beyond[2]. We will see presently that this is a well motivated choice for this thesis since it deals with astrophysical effects of theories of gravity that do modify the Newtonian force law.

As an example of a theory that does alter the Newtonian limit consider the non-minimally coupled action

$$S = \int \mathrm{d}^4x\sqrt{\tilde{g}}\left[\frac{{M_{\rm pl}}^2}{2}\Omega^2(\phi)\tilde{R} - \frac{1}{2}k^2(\phi)\tilde{\nabla}_\mu\phi\tilde{\nabla}^\mu\phi - \Omega^4(\phi)V(\phi)\right] + S_{\rm m}[\tilde{g}_{\mu\nu};\psi_{\rm i}] \qquad (2.1)$$

with

$$k^2(\phi) = \Omega^2\left[1 - \frac{3}{2}\left(\frac{\partial\ln\Omega^2}{\partial\phi}\right)^2\right]. \qquad (2.2)$$

At first glance, this looks like a trivial generalisation of the quintessence case with the potential redefined and a non-canonical kinetic term for the field. The field is not present in the matter action and so matter follows geodesics $\tilde{g}_{\mu\nu}$ but are these geodesics necessarily the same as those found in general relativity? To answer this question, we will perform the same non-relativistic analysis using the same metric perturbations as (1.6). Since the geodesic equation

[1] In this case it is the boundary conditions at infinity that ensure that the field is spatially homogeneous but time-dependent.

[2] The absence of any coupling of the field to matter means that one can think of this scalar as a new source of matter that back-reacts on the space-time given by the appropriate vacuum solution of general relativity. This gives rise to different geodesics at any order beyond the Newtonian limit and hence alters the post-Newtonian motion. Given this interpretation, we will not consider these theories as modifications of general relativity.

is the same we again find

$$\ddot{\mathbf{x}} = -\nabla\Phi_{\mathrm{N}}, \tag{2.3}$$

However, this time the Poisson equation is sourced by both the density and the scalar:

$$\nabla^2\Phi_{\mathrm{N}} = \frac{1}{\Omega^2}\left[4\pi G\rho + \frac{1}{4{M_{\mathrm{pl}}}^2}k^2\nabla_i\phi\nabla^i\phi + \frac{1}{2{M_{\mathrm{pl}}}^2}\Omega^4 V + \frac{1}{2{M_{\mathrm{pl}}}^2}\nabla^2\Omega^2\right]. \tag{2.4}$$

Now in the case of quintessence we had $k = \Omega = 1$ and so the only modification is the potential term, which is $\ll G\rho$[3] and so we indeed find that the Newtonian limit is unaltered. Of course, one must find the scalar field's equation of motion in order to solve the system, which in our case is

$$\frac{1}{\Omega^2}\Box\phi + \frac{1}{M_{\mathrm{pl}}\Omega^4}\frac{\mathrm{d}\Omega^2}{\mathrm{d}\phi}\nabla_i\phi\nabla^i\phi = \frac{\mathrm{d}V}{\mathrm{d}\phi} - \frac{M_{\mathrm{pl}}}{\Omega^4}\frac{\mathrm{d}\ln\Omega^2}{\mathrm{d}\phi}4\pi G\rho. \tag{2.5}$$

Unlike the case of quintessence, the non-minimal coupling term $\Omega^2 R$ in the action (2.1) has resulted in an inhomogeneous source term for the scalar field and hence we expect an inhomogeneous solution. In this case, the new Poisson equation (2.4) contains an extra source apart from the density and in general the solution for the Newtonian potential sourced by the same density profile will be different if one uses general relativity or this theory to describe the dynamics of gravity. For this reason, it is sensible to consider theories such as these modified theories of gravity and we will do so from here on. Before leaving this example we will briefly show how theories such as these can be interpreted as including additional scalars coupled to matter.

So far, we have worked in the *Jordan frame* where the scalar is non-minimally coupled to gravity and matter is coupled only to the *Jordan frame metric* $\tilde{g}_{\mu\nu}$. It is possible to restore minimal coupling and diagonalise the kinetic term for the graviton using the field redefinition

$$g_{\mu\nu} = \Omega^2(\phi)\tilde{g}_{\mu\nu} \tag{2.6}$$

[3] If this is not the case then the model gives rise to an unacceptable cosmology where the onset of dark energy domination happens at very early times.

known as a *Weyl rescaling*. After this transformation (see appendix A for the transformation laws of various geometric quantities, including the Ricci scalar, under this transformation) the action takes the form

$$S = \int \mathrm{d}^4x\sqrt{g}\left[\frac{{M_{\mathrm{pl}}}^2}{2}R - \frac{1}{2}\nabla_\mu\phi\nabla^\mu\phi - V(\phi)\right] + S_{\mathrm{m}}\left[\Omega^{-2}g_{\mu\nu};\psi_{\mathrm{i}}\right]. \tag{2.7}$$

This is known as the *Einstein frame* and $g_{\mu\nu}$ the *Einstein frame metric*. In this frame the gravitational action looks almost like general relativity with a minimally coupled scalar[4], the difference being that ϕ is now coupled directly to matter through the function Ω. This direct coupling has the effect that the energy-momentum tensor defined using this metric, $T^{\mu\nu}_{\mathrm{m}} = 2/\sqrt{-g}\,\delta S_{\mathrm{m}}/\delta g_{\mu\nu}$ for matter is not conserved in this frame:

$$\nabla_\mu T^{\mu\nu}_{\mathrm{m}} = \frac{\mathrm{d}\ln\Omega}{\mathrm{d}\phi}T_{\mathrm{m}}\nabla^\mu\phi, \tag{2.8}$$

where $T_{\mathrm{m}} = g_{\mu\nu}T^{\mu\nu}_{\mathrm{m}}$ is the trace of the energy-momentum tensor (see appendix A for a derivation of this formula). According to equation (1.4), this non-conservation implies that matter does not move on geodesics of $g_{\mu\nu}$ and so if one were to take the non-relativistic limit of the modified equation one would find extra terms in the Newtonian force law proportional to the gradient of the scalar. In this frame, the Poisson equation is identical to that found in general relativity[5] and it is the force law that is altered. This additional term thus represents a new or *fifth*-force. The two frames are completely equivalent and so the only difference between the two lies in how one interprets the resultant dynamics. Any debate as to which frame is more "fundamental" is purely philosophical. That being said, the Einstein frame may be more convenient if one wishes to study the quantum properties of gravity since the kinetic term for the graviton is canonical in this frame.

This thesis is primarily concerned with the non-relativistic and cosmological dynamics of

[4] note the factor $k(\phi)$ was chosen such that ϕ is canonically normalised in this frame.

[5] Provided one interprets the density as coming from both the scalar and the matter, we will return to this point shortly.

modified theories of gravity and not the strong field regime. For this reason, we will consider any theory containing a graviton and additional degrees of freedom non-minimally coupled to matter a modified theory of gravity. In particular, this choice means that we do not consider quintessence to be a modified theory of gravity. The example presented above in equation (2.7) is considered a modified theory of gravity on account of the function $\Omega(\phi)$ appearing in the matter action.

So far we have only presented a discussion of modified theories of gravity in terms of theories which can be written as general relativity with a non-minimal coupling of a single scalar to matter. In terms of Weinberg's theorem [15], this corresponds to allowing more than one degree of freedom but there are other ways to violate this. One method is to simply drop the requirement of Lorentz invariance, which leads to interesting theories such as Einstein-Aether theory [66] and Hořava-Lifshitz gravity [67]. Another is to add multiple scalar fields or other particles such as vectors. A third alternative is to look at other curvature invariants such as torsion, the Weyl tensor or higher-derivative terms such as $R_{\mu\nu}R^{\mu\nu}$. These modifications typically introduce Ostrogradsky ghost degrees of freedom and so their stability must be considered very carefully. One can avoid these problems by asking what is the most general theory describing a scalar and a massless graviton such that the equations of motion are second order so that there are no ghosts? The answer was written down by Horndeski in 1974 [68] and a derivation using modern methods was presented in [69]. Another approach is to abandon the requirement that gravity is described by a massless spin-2 particle. The simplest alternative is to allow it to have a mass. The linear theory for Lorentz invariant massive spin-2 particle, the Fierz-Pauli action, has been known since 1939 [70] however any attempts to generalise it to non-linear orders resulted in the introduction of an additional degree of freedom beyond the five mandated by Lorentz invariance. This extra mode is always a ghost [71] and so the theory seemed doomed. Very recently, de-Rham, Gabadadze and Tolley [72] have constructed the most general action where this ghost does not appear at any order in perturbation theory and since then a substantial amount of work on the subject has appeared (see [73] for a review).

Massive gravity and its generalisations can provide a technically natural solution to the cosmological constant problem and screen the modifications on small scales using the Vainshtein mechanism. This thesis is primarily concerned with testing the chameleon mechanism and so we will not investigate it in detail here. The Vainshtein mechanism is more efficient at screening than the chameleon mechanism and these nice properties certainly motivate a search for new observational signatures. More exotic models of modified gravity such as non-local modifications (see e.g. [74]) and higher-dimensional generalisations, for example, brane-world and Kaluza-Klein models, have also been considered.

The few models mentioned above are just a small fraction of the models that have been studied and the literature is overflowing with a plethora of models with more appearing daily (see [6] for a recent 312 page review). The challenge then is to decide which theories are viable alternatives to general relativity. Clearly any viable alternative must be compatible with all current data on all scales from compact objects to the laboratory to the solar system to cluster scales and cosmology[6]. Presently, there are many theories which can achieve this (for example, $f(R)$ theories can always have their parameters tuned such that the cosmological expansion history mimics ΛCDM). In this thesis, we are interested in infra-red modifications that may be able to resolve the dark energy problem and many of these theories fail at the first hurdle: in order to produce interesting effects on cosmological scales the additional degrees of freedom need to have masses of order the Hubble parameter. This implies that they mediate a long-range force of order 10^4 Mpc and such a force range violates laboratory bounds of a few microns [76].

One may then think that we have failed before we have started but this is not the case. As alluded to in chapter 1, it is possible to construct theories with screening mechanisms. These can circumvent this issue by changing the strength of the fifth-force relative to the Newtonian one in dense environments. Exactly how this is achieved will be the subject of the next section.

[6] See [75] for a discussion on the cosmological distinguishability of interacting dark energy and modified gravity models.

2.1 Screening Mechanisms

From here on we will specialise to the case of a single scalar field ϕ coupled to matter. In particular, we will focus on the Einstein frame coupling

$$\frac{\mathscr{L}}{\sqrt{-g}} \supset C(\phi)T_{\rm m}, \tag{2.9}$$

where $T^{\mu\nu}_{\rm m} = 2/\sqrt{-g}\,\delta S_{\rm m}/\delta g_{\mu\nu}$ is the (non-conserved) energy-momentum tensor for matter and $T_{\rm m}$ is its trace. Furthermore, we define the *coupling* $\beta(\phi)$ via

$$\beta(\phi) \equiv M_{\rm pl}\frac{{\rm d}C(\phi)}{{\rm d}\phi}. \tag{2.10}$$

This non-minimal coupling of the scalar to the energy-momentum tensor means that it is not conserved in this frame and instead one has (see appendix A for the derivation of this formula)

$$\nabla_\mu T^{\mu\nu} = \frac{\beta(\phi)}{M_{\rm pl}}T_{\rm m}\nabla^\nu\phi. \tag{2.11}$$

Now we showed in equation (1.4) that a point particle with $T^{\mu\nu}_{\rm m} = \rho_{\rm m}u^\mu u^\nu$ gives the geodesic equation for the left hand side of this expression (multiplied by the density, which cancelled in (1.4) since the entire expression was equal to zero). Furthermore, in equation (1.7) we showed that the non-relativistic limit of the geodesic equation resulted in Newton's second law. This is unchanged in this case and so all the effects of the non-conservation of the energy-momentum tensor manifest as a deviation from the geodesic equation. Particles do not follow geodesics of the metric in the Einstein frame. The non-relativistic limit of the left hand side of equation (2.11) was calculated in equation (1.7) and is equal to $\rho_{\rm m}(\ddot{\mathbf{x}} + \nabla\Phi_{\rm N})$. Therefore, the non-relativistic limit of the right hand side gives the fifth-force. In the non-relativistic limit we

have $T_{\rm m} = -\rho_{\rm m}$[7] and so cancelling the factors of $\rho_{\rm m}$ we find the fifth-force per unit mass

$$F_\phi = -\frac{\beta(\phi)}{M_{\rm pl}}\nabla\phi. \tag{2.12}$$

All known screening mechanisms can be classified by subsets of the general Lagrangian expanded in the field perturbation $\phi = \bar{\phi} + \delta\phi$ in the Einstein frame:

$$\frac{\mathscr{L}}{\sqrt{-g}} \supset -\frac{1}{2}Z^2(\bar{\phi})\nabla_\mu\delta\phi\nabla^\mu\delta\phi - m^2_{\rm eff}(\bar{\phi})\delta\phi^2 + \beta(\bar{\phi})\frac{\delta\phi}{M_{\rm pl}}T_{\rm m} + \cdots, \tag{2.13}$$

where the dots denote higher-order terms not relevant for this discussion. Here the wave-function normalisation $Z(\bar{\phi})$, the effective mass $m_{\rm eff}(\bar{\phi})$ and the coupling to the trace of the energy momentum tensor $\beta(\bar{\phi})$ are all field-dependent and can vary as a function of position. It is this positional dependence that allows for the existence of screening mechanisms. If we can somehow arrange for the local value of the field to be such that the fifth-force (2.12) is rendered negligible compared with the Newtonian one then we will not be able to detect it and the force is screened. There are several ways this can be achieved: firstly, if the wave-function normalisation $Z(\bar{\phi})$ is different from unity then the canonically normalised field is $\delta\phi/Z(\bar{\phi})$. If $Z(\bar{\phi})$ is large enough in dense environments such that the effective coupling to matter, $\beta(\bar{\phi})/Z(\bar{\phi}) \ll 1$ then the fifth-force (2.12) will be negligible. This is the method employed by the Vainshtein mechanism [21]. If the effective mass of the perturbation at solar system densities is large enough that the force range $\lambda = m^{-1}_{\rm eff}$ is smaller than a few microns then the theory will satisfy all laboratory bounds and the force is again screened. In the language of equation (2.12), this corresponds to suppressing field gradients and is employed by the chameleon mechanism [17, 18]. Finally, if the coupling $\beta(\bar{\phi})$ is small enough in dense environments so that the fifth-force is negligible compared with the Newtonian force then the fifth-force is again screened. This method is utilised by the symmetron [19] mechanism and

[7] Here we interpret $\rho_{\rm m}$ as the energy density in matter. The reader should be aware that since the scalar is coupled to matter directly this interpretation is not always clear-cut. We will see below that the theories this thesis is concerned with do not have this ambiguity.

the environment-dependent Damour-Polyakov effect [20].

The Vainshtein mechanism screens in a very different manner to chameleon-like models. This thesis is primarily concerned with the latter class of theories and so below we will describe their properties in detail. The chameleon mechanism, the symmetron effect and the EDDP all arise from a general scalar-tensor theory where the scalar is conformally coupled to matter through the metric and we will refer to these as *conformal scalar tensor theories*. First, we present the general framework and describe the salient new features that are not present in general relativity. We then give detailed examples of each screening mechanism and present a model-independent description of the screening mechanism. In particular, we will derive the criteria for an object to be self-screening and will show how any mechanism can be parametrised by two model-independent parameters: one controlling how efficient an object is at screening itself and another that sets the strength of the fifth-force relative to the Newtonian force in unscreened objects. Next, we discuss the current observational constraints on the model-independent parameters and present a screening map of galaxies in the nearby universe that will be useful for the astrophysical tests presented in chapters 3, 4 and 5. Finally, we discuss the cosmological dynamics of the scalar, which will be useful for the discussion in chapters 6 and 7. At the end of the chapter we will provide a short introduction to the Vainshtein mechanism using Galileon theories as an example. Many of the results in this thesis apply equally to Vainshtein screened theories and so it will be enlightening to discuss the differences between the two screening mechanisms. The Vainshtein mechanism is more efficient at screening than chameleon-like theories. For this reason, whereas it is often the case that the formulae presented apply to both mechanisms, in practice only chameleon-like theories show novel effects once we specialise to collapsed astrophysical objects. We will always begin by presenting the most general equations and will unambiguously indicate where we have specialised to chameleon-like theories.

2.2 Conformal Scalar-Tensor Theories

Our starting point is the Einstein frame action for a scalar field coupled to matter via the *coupling function* $A(\phi)$

$$S = \int \mathrm{d}^4x\sqrt{-g}\left[\frac{{M_{\rm pl}}^2}{2}R - \frac{1}{2}k^2(\phi)\nabla_\mu\phi\nabla^\mu\phi - V(\phi)\right] + S_{\rm m}[A^2(\phi)g_{\mu\nu};\psi_{\rm i}], \tag{2.14}$$

where $\psi_{\rm i}$ represent the various matter fields and we have allowed for the fact that the field may not be canonically normalised by including the factor $k(\phi)$. One may instead work in the Jordan frame (see appendix A for the transformation laws of various geometric quantities under Weyl rescalings)

$$S = \int \mathrm{d}^4x\sqrt{-\tilde{g}}\left[\frac{{M_{\rm pl}}^2}{2A^2(\phi)}\tilde{R} - \frac{1}{2}\left[\frac{k^2(\phi)}{A^2(\phi)} - 6\left(\frac{A'(\phi)}{A}\right)^2\right]\tilde{\nabla}_\mu\phi\tilde{\nabla}^\mu\phi - \frac{V(\phi)}{A^4(\phi)}\right] + S_{\rm m}[\tilde{g}_{\mu\nu};\psi_{\rm i}]. \tag{2.15}$$

Whereas the choice of frame is irrelevant, one should note that specifying the functional form of the (so far) free functions in one frame will yield an inequivalent theory to the same choice made in a different frame. For example, the Jordan frame potential with $V(\phi)$ defined in the Einstein frame is $\tilde{V}(\phi) = V(\phi)/A^4(\phi)$, however, we could just as easily fix the Jordan frame potential to some specified function $\tilde{V}(\phi)$, in which case the Einstein frame potential is $V(\phi) = A^4(\phi)\tilde{V}(\phi)$. The same is true of the normalisation of the field. We could arbitrarily decide to have a canonical kinetic term in either the Jordan or Einstein frame, in which case the other frame will pick up a non-canonical factor multiplying the kinetic term. The choice of normalisation in one frame then represents a different theory to the same choice in the other frame[8]. This arbitrariness is simply a matter of definition. In what follows we will work in the Einstein frame wherever possible[9], both because it is more transparent and it is easier to discern the physics when applied to astrophysical systems. A full account of screening in the

[8] Of course two theories are equivalent if a consistent normalisation and scalar potential is used in both frames.

[9] The issue of frame definitions will be important when we discuss $f(R)$ theories and the environment-dependent dilaton and we will have no choice other than to define the theory in the Jordan frame and find the Einstein frame action using a Weyl rescaling.

Jordan frame can be found in [24], Appendix C. We will set the wavefunction normalisation in this frame equal to unity. Given a choice of potential, coupling function and wavefunction normalisation, one can always work with the canonically normalised field $\mathrm{d}\varphi = k(\phi)\mathrm{d}\phi$ and re-write these functions in terms of the new field. For this reason, we can make this choice without loss of generality. The one exception to this is the case where the fundamental theory is defined using a factor $k(\phi)$ such that $\varphi(\phi)$ cannot be found analytically and one is forced to retain it in the analysis as is the case with the environment-dependent dilation. In cases such as these we will clearly indicate that $k(\phi) \neq 1$ and discuss the modifications to the standard results thoroughly.

Varying the action (2.14) with respect to the field (note we have set $k(\phi = 1)$ as discussed above) gives the equation of motion

$$\Box\phi = -\frac{\mathrm{d}V(\phi)}{\mathrm{d}\phi} + \frac{A'(\phi)}{A(\phi)}T_{\mathrm{m}}. \tag{2.16}$$

This can be derived from the effective Lagrangian

$$\frac{\mathscr{L}}{\sqrt{g}} \supset -V(\phi) + T\ln A \tag{2.17}$$

and hence is exactly the type of theory described in section (2.1) with $C(\phi) = \ln A$. The fifth-force in this theory is then given by equation (2.12) with

$$\beta(\phi) = M_{\mathrm{pl}}\frac{\mathrm{d}\ln A}{\mathrm{d}\phi}. \tag{2.18}$$

In order to have gravitational strength fifth-forces that are screened locally one typically has $\beta(\phi) \sim \mathscr{O}(1)$ or greater when an object is unscreened. Theories without screening mechanisms typically need to impose $\beta(\phi) \ll 1$ in order to be compatible with current observations. Using the fact that $T_{\mathrm{m}} = -\rho_{\mathrm{m}}$ for non-relativistic matter, equation (2.17) defines and effective

potential

$$V_{\rm eff}(\phi) \equiv V(\phi) + \rho_{\rm m} \ln A(\phi). \tag{2.19}$$

In fact, this definition is not so useful because the density $\rho_{\rm m}$ is not conserved on account of equation (2.11). In any theory of gravity such as this, the conserved density is the Jordan frame density found using $\tilde{T}^{\mu\nu}_{\rm m} = A^{-6} T^{\mu\nu}_{\rm m}$. In this case one has $\tilde{\rho}_{\rm m} = -\tilde{g}_{\mu\nu}\tilde{T}^{\mu\nu} = A^4\rho_{\rm m}$. It is this density that results when one integrates over microphysical distribution functions, the Einstein frame density contains interactions with the scalar and the true properties of objects, such as their mass, can only be found once the scalar interactions have been accounted for. In general, an interpretation in terms of an effective potential would then require frame mixing, however, we will see later that theories with screening mechanisms have the property that

$$A(\phi) = 1 + \mathcal{O}\left(\beta(\phi)\frac{\phi}{M_{\rm pl}}\right). \tag{2.20}$$

$A(\phi)$ never differs too significantly from 1 since we require $\phi \ll M_{\rm pl}$ in order to have a sensible infra-red modification of gravity and this allows us to define a conserved density in the Einstein frame. Consider the 0-component of equation (2.11) with a non-relativistic source $T^{\mu\nu}_{\rm m} = \left(\rho_{\rm m}, 0, 0, 0\right)$. We have

$$\dot{\rho}_{\rm m} + \Gamma^{\mu}_{\mu 0}\rho_{\rm m} + \Gamma^{0}_{00}\rho_{\rm m} = \frac{A'(\phi)}{A(\phi)}\frac{\dot{\phi}}{M_{\rm pl}}\rho_{\rm m}. \tag{2.21}$$

Defining the conserved density $\rho_{\rm m} = A(\phi)\rho$ this reduces to

$$\dot{\rho} + \Gamma^{\mu}_{\mu 0}\rho + \Gamma^{0}_{00}\rho = 0, \tag{2.22}$$

which is the continuity equation for a conserved non-relativistic density ρ ($= A^3\tilde{\rho}_{\rm m}$ in the Jordan frame). From here on we will use ρ as the density of non-relativistic matter, both in cosmology and astrophysics, however we stress that while it is conserved, it does not correspond to the trace of any conserved energy-momentum tensor describing the translational invariance

of the theory in any frame[10]. Later in the chapter we will see that $\beta(\phi)\phi/M_{\rm pl} \leq 10^{-6}$ and so quantities such as mass defined by integrating over this density do not differ significantly from those found using the Jordan frame density by virtue of equation (2.20). For this reason, it does not matter which density we use to define the density of an object such as a non-relativistic star; the choice of the conserved density is made for calculational convenience and is more intuitive than a non-conserved quantity. Using this definition of the density, equation (2.16) can be written

$$\Box\phi = -\frac{\mathrm{d}V(\phi)}{\mathrm{d}\phi} - \rho\frac{\mathrm{d}A(\phi)}{\mathrm{d}\phi}, \tag{2.23}$$

which allows for a definition of the effective potential in terms of the conserved density[11]:

$$V_{\rm eff} = V(\phi) + \rho(A(\phi) - 1). \tag{2.24}$$

It is the density-dependence in the effective potential that allows these theories to screen. In particular, if the effective potential has a minimum whose position depends on the density then the field will move to different positions in field space as a function of the local density. If we then choose the functions $A(\phi)$ and $V(\phi)$ such that the mass of the field in high density regions is large enough to evade laboratory bounds or the coupling $\beta(\phi) \ll 1$ then the theory will screen. The first of these methods is employed by the chameleon effect [17, 18] and the latter by the symmetron mechanism [19] and the environment-dependent Damour-Polyakov effect (EDDP) [20][12]. We will briefly review how all three mechanisms work using simple examples before presenting a model-independent description of how they can screen a spherical object.

[10] One may define the tensor $\mathcal{T}^{\mu\nu} = A^5\tilde{T}^{\mu\nu}_{\rm m}$, whose trace corresponds to ρ, however it does not correspond to a physical energy-momentum tensor and so we will not use it here.

[11] Note that the effective potential is often defined as $V_{\rm eff} = V + \rho A$ in the literature. Since $V_{\rm eff}$ is not a fundamental quantity but is instead inferred from the equation of motion it is only defined up to an arbitrary field-independent function. We have chosen to define it with the factor of $(A(\phi) - 1)$ in order to keep track of the energy density in the field and the matter separately. This definition does not impact the field dynamics but is important when describing the cosmological dynamics, which we will investigate later, because the effective potential (and not its derivative) appears in the Friedmann equation. For this reason, we have chosen to use this definition throughout this thesis in the interest of consistency.

[12] Including generalised symmetrons and dilatons [28].

2.2.1 The Chameleon Effect

First introduced by [18], the simplest example of models exhibiting the chameleon effect are those with run-away potentials and exponentially increasing coupling functions

$$V(\phi) = \frac{M^{4+n}}{\phi^n}; \quad A(\phi) = e^{\beta(\phi)\frac{\phi}{M_{\rm pl}}}, \tag{2.25}$$

the simplest case being that of constant $\beta(\phi) \equiv \beta$. We shall use this case as an example. These models have a minimum at

$$\phi_{\rm min} = \left(\frac{nM_{\rm pl}}{\beta\rho}\right)^{\frac{1}{n+1}} M^{\frac{n+4}{n+1}} \tag{2.26}$$

and so the field is pushed to smaller values in denser environments. The effective mass of oscillations about the minimum is

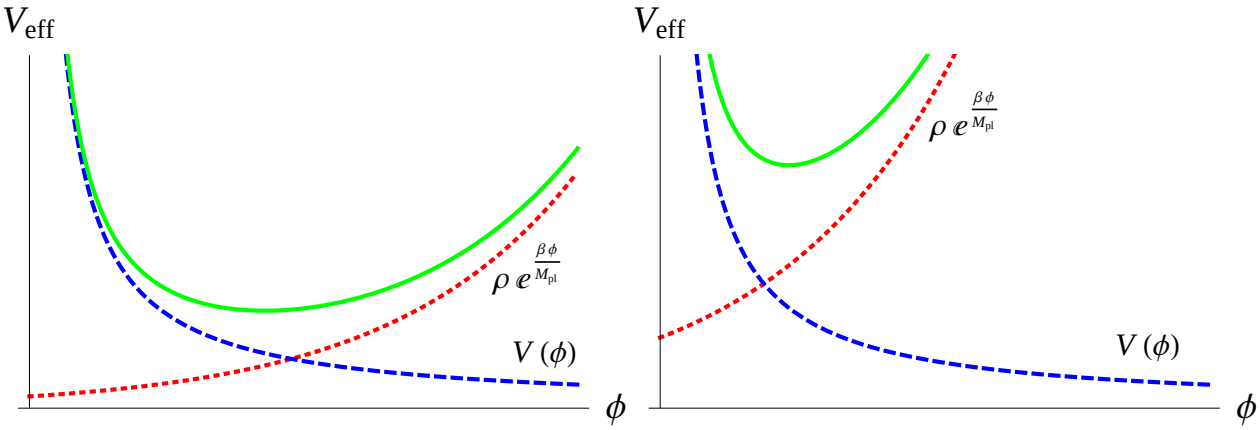
$$m^2_{\rm eff} = V'' + \rho A''(\phi) \tag{2.27}$$

$$\approx \frac{n(n+1)}{M^{\frac{n+4}{n+2}}} \left(\frac{\beta\rho}{M_{\rm pl}}\right)^{\frac{n+2}{n+1}} \tag{2.28}$$

and so one can see that this mass is larger in denser environments. This is shown in figure 2.1 where we plot the effective potential. Figure 2.1(a) shows this for low densities and figure 2.1(b) for high densities. One can see by eye that the potential near the minimum in 2.1(a) is far shallower than the potential near the minimum in 2.1(b).

This is how the chameleon mechanism screens. In high density environments, the field is pushed to smaller values where the potential is steeper and the effective mass is larger. Provided the parameters are chosen such that the Compton wavelength of the chameleon on Earth is less than a few microns, the fifth-force will evade all current bounds.

The class of models (2.25) are just the simplest and more complicated variants have indeed been studied. Any model where the field is pushed to smaller values where the mass is larger will screen and these include power law potentials [32], field-dependent couplings [77] and even supersymmetric models [78–81]. Laboratory tests probe the parameter space of each



(a) Smallρ (b) Largeρ

Figure 2.1: The chameleon effective potential (solid line) for small and large densities. The blue dashed lines show the contribution from the potential and the red dotted lines show the contribution from the coupling.

model on a model by model basis whereas astrophysical tests probe model-independent combinations of these parameters that can be mapped to any specific model. Since this thesis is focused on astrophysical tests, we will not present a complete list of models here.

2.2.2 $f(R)$ Theories

One popular theory of modified gravity is the $f(R)$ class of models where the Einstein-Hilbert term in the action is generalised to an arbitrary function of the Ricci scalar:

$$S = \int \mathrm{d}^4x\sqrt{-\tilde{g}}\,\frac{{M_{\rm pl}}^2}{2}f(R) + S_{\rm m}[\tilde{g}_{\mu\nu};\psi_{\rm i}], \tag{2.29}$$

where the Ricci scalar is computed using $\tilde{g}_{\mu\nu}$. It is well-known that these theories are equivalent to scalar-tensor theories and here we will follow the derivation of [82][13]. We begin by defining the scalar field ϕ via

$$f'(R) = e^{-\frac{2\phi}{\sqrt{6}M_{\rm pl}}}, \tag{2.30}$$

[13]One could instead use a Lagrange multiplier to find the equivalent Jordan frame action and proceed from there. The two approaches yield identical results and we have chosen to follow this alternate derivation in order to make contact with the chameleon literature.

where a prime denotes a derivative with respect to R. We can invert this relation to find

$$f(R) = \int f'(R)\,\mathrm{d}R = \int e^{-\frac{2\phi}{\sqrt{6}M_{\rm pl}}}\frac{\mathrm{d}R}{\mathrm{d}\Phi}\,\mathrm{d}\phi = -\frac{2\phi}{\sqrt{6}M_{\rm pl}}R + \frac{2}{\sqrt{6}M_{\rm pl}}\int e^{-\frac{2\phi}{\sqrt{6}M_{\rm pl}}}R\,\mathrm{d}R. \tag{2.31}$$

Using the definition of ϕ (2.30), we have

$$\frac{\mathrm{d}\Phi}{\mathrm{d}R} = -\frac{\sqrt{6}M_{\rm pl}}{2}\frac{f''(R)}{f'(R)} \tag{2.32}$$

and the last integral is

$$\frac{2}{\sqrt{6}M_{\rm pl}}\int e^{-\frac{2\phi}{\sqrt{6}M_{\rm pl}}}R\,\mathrm{d}R = -\int Rf''\,\mathrm{d}R = -(Rf' - f). \tag{2.33}$$

The action can then be written as a scalar-tensor theory of the form

$$S = \int \mathrm{d}^4x\sqrt{-\tilde{g}}\left[\frac{{M_{\rm pl}}^2 e^{-\frac{2\phi}{\sqrt{6}M_{\rm pl}}}R}{2} - \tilde{V}(\phi)\right] + S_{\rm m}[\tilde{g}_{\mu\nu};\psi_{\rm i}], \tag{2.34}$$

where using $\phi = \phi(R)$ the Jordan frame scalar potential is

$$\tilde{V}(\phi) = \frac{{M_{\rm pl}}^2\left(Rf'(R) - f(R)\right)}{2}. \tag{2.35}$$

Equation (2.34) is precisely of the form (2.15) with no kinetic term for the scalar and so we can find the equivalent Einstein frame formulation by performing a Weyl rescaling of the metric with

$$A(\phi) = e^{\frac{2\phi}{\sqrt{6}M_{\rm pl}}}. \tag{2.36}$$

The transformation of the Ricci scalar under this rescaling can be found in appendix A equation (A.7) and the square root of the determinant transforms as $\sqrt{-\tilde{g}} = A^4(\phi)\sqrt{-g} =$

$f^{-2}(R)\sqrt{-g}$. Performing this rescaling, we find the Einstein frame action

$$S = \int \mathrm{d}^4x\sqrt{-g}\left[\frac{{M_{\rm pl}}^2}{2}R - \frac{1}{2}\nabla_\mu\phi\nabla^\mu\phi - V(\phi)\right] + S_{\rm m}[A^2(\phi)g_{\mu\nu};\psi_{\rm i}], \tag{2.37}$$

where the scalar potential

$$V(\phi) = \frac{{M_{\rm pl}}^2(Rf'(R) - f(R))}{2f'(R)^2}. \tag{2.38}$$

Note that the factor of $1/\sqrt{6}$ was chosen so that the field is canonically normalised in this frame. Equation (2.37) is a conformal scalar-tensor theory with a coupling function given by (2.36). This is a chameleon coupling with constant $\beta(\phi) = 1/\sqrt{6}$. The theory is not yet a chameleon because one must choose a potential that will give rise to the chameleon mechanism such as a run-away potential. One well-studied example of this is the model of Hu and Sawicki [44]

$$f(R) = -m^2\frac{c_1\left(R/m^2\right)^n}{1 + c_2\left(R/m^2\right)^n} \tag{2.39}$$

which is often studied in the context of N-body simulations (see, for example, [47] and references therein). One generally tunes the values of c_1 and c_2 so that $c_1/c_2 = 6\Omega_{\rm m}/\Omega_\Lambda$ in order to yield an identical expansion history to the ΛCDM model. $m^2 \equiv 8\pi G\tilde{\rho}/3$ is also fixed leaving n and a choice of either c_1 or c_2 as free parameters. In fact, it is not necessary to use the scalar field formulation of the theory in order to understand the screening mechanism. Instead of interpreting the modified gravity effects as a fifth-force augmenting the Newtonian force, the effective value of G felt by non-relativistic matter is $4/3G_{\rm N}$ where $G_{\rm N}$ is the measured value of G in the solar system. This would then immediately violate solar system bounds, except that the Poisson equation (1.8) contains another source proportional to the Ricci scalar in addition to the density. Consider an object of mass M and radius R. When the new term is negligible the solution is $\Phi_{\rm N} = GM/R$ outside the object and so the effective value of G is really $4/3$ times as large as predicted by general relativity. In this case the object is unscreened. When the new term is comparable to the density term one finds that the effective mass found by integrating

the Poisson equation is $M_{\rm eff} \approx 3/4M$ so that the force-law is identical to general relativity and the object is screened. We will shortly present the general screening mechanism for a conformal scalar-tensor theory, which includes $f(R)$ theories but is more general and encapsulates any screening mechanism using two model-independent parameters. For this reason we will always work with this more general framework but will often refer to $f(R)$ theories owing to their ubiquity.

2.2.3 The Symmetron Mechanism

In contrast to chameleon models, symmetrons have a light mass in all environments and instead work by moving $\beta(\phi)$ to small values when the density is large. They are defined by a $\mathbb{Z}_2$ symmetry breaking potential and a quadratic coupling function:

$$V(\phi) = -\frac{1}{2}\mu^2\phi^2 + \frac{\lambda}{4}\phi^4; \quad A(\phi) = 1 + \frac{\phi^2}{2M^2} \tag{2.40}$$

so that the effective potential is

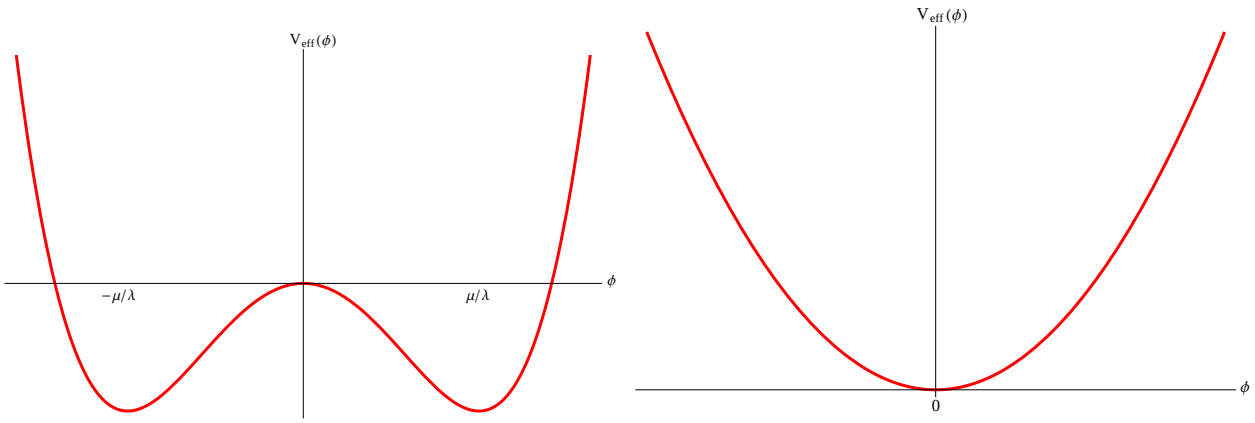
$$V_{\rm eff} = \frac{\mu^2}{2}\left(\frac{\rho}{M^2\mu^2} - 1\right)\phi^2 + \frac{\lambda}{4}\phi^4, \tag{2.41}$$

which is invariant under the $\mathbb{Z}_2$ symmetry $\phi \to -\phi$. The shape of this potential then depends on the local density. When $\rho > M\mu$ the coefficient of the quadratic term is positive and the minimum lies at $\phi = 0$ so that symmetry is unbroken. Conversely, when $\rho \ll M\mu$ the minimum lies at

$$\phi \approx \pm\frac{\mu}{\sqrt{\lambda}} \tag{2.42}$$

and the symmetry is broken. This is shown in figure 2.2. Calculating the coupling, we find

$$\beta(\phi) \approx \frac{\phi M_{\rm pl}}{M^2} \tag{2.43}$$



(a) $\rho \ll M\mu$ (b) $\rho > M\mu$

Figure 2.2: The symmetron effective potential for small and large densities.

and so $\beta(\phi) \approx 0$ in the symmetry unbroken phase and

$$\beta(\phi) \approx \frac{\mu M_{\rm pl}}{\sqrt{\lambda} M^2} \tag{2.44}$$

in the broken phase. This immediately reveals how the symmetron screens: in small density environments the symmetry is broken and the field sits at one of the two minima leading to a non-negligible fifth-force. In high density environments the symmetry is restored and the field moves rapidly to zero in order to minimise the new effective potential, at which point $\beta(\phi) = 0$ and the fifth-force is absent. Of course, one must choose the parameters such that the symmetry is restored in densities corresponding to the solar system if fifth-forces are to be absent locally. Cosmologically, we are interested in theories where the phase transition

happens in the recent past[14] and so it is common to set[15]

$$\mu^2 M^2 \sim \rho_0 \sim H_0^2 {M_{\rm pl}}^2. \tag{2.45}$$

We are also interested in modifications of gravity that are comparable with the Newtonian force when unscreened[16] and so we set $\beta(\phi) \sim 1$ in equation (2.44):

$$\frac{H_0 {M_{\rm pl}}^2}{\sqrt{\lambda} M^3} \sim 1 \tag{2.46}$$

where we have used equation (2.45). We will see later that current constraints impose $M < 10^{-3} M_{\rm pl}$, in which case we find [46]

$$\lambda \sim \frac{H_0^2 {M_{\rm pl}}^4}{M^6} \geq 10^{-96}, \tag{2.47}$$

where the equality is satisfied when M assumes its largest possible value. Assuming the bounds from local tests of gravity are saturated, the mass of the field in the unbroken phase is

$$m_{\rm eff} \approx \sqrt{2}\mu \sim 10^4 H_0 \sim \mathcal{O}({\rm Mpc}^{-1}). \tag{2.48}$$

Hence, the symmetron mediates a force with a range (Compton wavelength) $\lambda_{\rm C} = m_{\rm eff}^{-1} \leq$ Mpc. Since the matter coupling is irrelevant at late times — when the cosmic density is well below the critical density for the phase transition — the symmetron behaves a quintessence field rolling down its scalar potential $V(\phi)$. Dark energy driven by quintessence-type models

[14] More specifically, we are interested in theories where the phase transition occurs around the present epoch so that the appearance of modified gravity coincides with the onset of dark energy domination. One may then hope that it is a possible explanation for the cosmic acceleration and the coincidence problem. It is now known that it is not [58].

[15] One may wonder what happens if we drop this requirement and push the phase transition to earlier times. In fact, we require the theory to screen in the dark matter halo of the milky way, which corresponds to a density of $10^6 \rho_0$ and so the phase transition could not have occurred at redshifts greater than 10^2. This leaves a little leeway for moving the transition but not so much that there are any new features compared with the standard case. Ultimately, the field rolls to its new minimum very quickly and remains there throughout the subsequent cosmic evolution [46, 83].

[16] Again, this is an arbitrary choice and there is nothing precluding force enhancements much larger than this.

requires the mass at the minimum be of order Hubble in order to achieve slow-roll [5] so that the Compton wavelength is $H_0^{-1} \sim \mathcal{O}(10^4\text{Mpc})$. Hence, the requirement (2.48) means that the symmetron force is too short-ranged to account for the cosmic acceleration.

The key element behind this screening mechanism was the second order phase transition and so one may wonder if more general models described by potentials and coupling functions of the form

$$V(\phi) = -\left(\frac{\phi}{\phi_n}\right)^n + \left(\frac{\phi}{\phi_m}\right)^m; \quad A(\phi) = 1 + \frac{\phi^n}{M^n} \tag{2.49}$$

with $m > n > 2$ can be constructed. Provided that both m and n are even, the effective potential will be even and will indeed exhibit a second order phase transition when the density is below some threshold and can indeed screen fifth-forces locally in the same manner as all of the other mechanisms. Such models go by the name *generalised symmetrons* and were discovered using a tomographic reverse-engineering of the potential and coupling function from a generalised form for the cosmological evolution of the coupling for symmetrons [28]. Since then, they have received little attention and their only other mention in the literature is in the form of a no-go theorem precluding them from being realised within supersymmetric models [80].

2.2.4 The Environment-Dependent Damour-Polyakov Effect

Historically, this screening mechanism was discovered in the context of the environment-dependent dilaton [20] and subsequently generalised to what have become known as *generalised dilatons* [28,51]. This is, in some sense, a misnomer because the underlying mechanism has little to do with whether the particle is a dilaton or not and is more transparent in the general framework. For this reason, here we will construct the mechanism from the bottom-up and then specialise to the case of the dilaton. Generalised dilatons are not easily written down in terms of potentials and coupling functions and are instead reconstructed tomographically [51]. Since we will have no need for Tomography in this thesis we will not discuss them

here and simply remark that they are specific choices for the coupling functions and potentials described in the general case below.

We have already noted that the force is screened in dense environments when

$$\beta(\phi) = M_{\rm pl}\frac{\mathrm{d}\ln A}{\mathrm{d}\phi} = \frac{M_{\rm pl}}{A(\phi)}\frac{\mathrm{d}A(\phi)}{\mathrm{d}\phi} = 0. \tag{2.50}$$

The symmetron mechanism described in subsection 2.2.3 has $\beta(\phi) \propto \phi$ and used a phase transition to push ϕ to zero in dense environments. Another way of moving $\beta(\phi)$ to zero is to utilise the last relation in equation (2.50) and somehow set $\mathrm{d}A/\mathrm{d}\phi$ to zero in dense environments. This is tantamount to minimising the function $A(\phi)$. Consider then the effective potential in the Einstein frame

$$V_{\rm eff} = V(\phi) + (\rho A(\phi) - 1) = A^n(\phi)\tilde{V}(\phi) + \rho(A(\phi) - 1), \tag{2.51}$$

where we demand that $A(\phi)$ has a minimum. Minimising this, one has

$$\beta(\phi_{\rm min}) = -\frac{M_{\rm pl}\tilde{V}'(\phi_{\rm min})}{n\tilde{V}(\phi_{\rm min}) + \rho}, \tag{2.52}$$

where, by virtue of (2.20), we have set $A(\phi) \approx 1$. In the limit $\rho \gg \tilde{V}(\phi_{\rm min})$, minimising the effective potential is identical to minimising the coupling function and screening the fifth-force. This screening by minimising the coupling function in dense environments is the environment-dependent Damour-Polyakov effect[17].

Now one may wonder why we have bothered to introduce the factor of A^n in the potential. Surely if we leave it arbitrary then at high enough densities minimising the effective potential is equivalent to minimising $A(\phi)$ and so the theory should screen. The problem with this statement is what does one mean by the term *high enough density*? Omitting the factor of A^n,

[17]This is named after a similar mechanism introduced by Damour and Polyakov [84] where the cosmological evolution of a scalar conformally coupled to matter minimises the coupling function and suppresses fifth-forces.

the relevant equation for the minimum is (again setting $A(\phi) \approx 1$)

$$\beta(\phi_{\rm min}) = -\frac{M_{\rm pl} V'(\phi_{\rm min})}{\rho} \tag{2.53}$$

and so the condition for screening is then $\rho \to \infty$. Without the A^n term we need to go to infinite densities in order to realise the screening mechanisms and this limit is ill-defined in conformal scalar-tensor theories (see [85, 86] for a discussion on this). Whilst potentials of this form may look contrived in the Einstein frame, they have a very natural interpretation in terms of fundamental theories where the potential is defined in the Jordan frame. We have already argued in section 2.2 that a potential $\tilde{V}(\phi)$ defined in the Jordan frame is described by the potential $A^4\tilde{V}(\phi)$ in the Einstein frame and that the choice of which frame the potential is defined in arbitrary. A natural class of models that screen using this mechanism then have $n = 4$. Many fundamental theories such as string theory and supergravity have low-energy effective actions that specify the form of these functions in the Jordan frame and so these models are closely connected with fundamental physics.

The Environment-Dependent Dilaton

The starting point for this mechanism [20] is the low-energy effective action for the string dilaton coupled to gravity in the strong coupling limit [84, 87]:

$$S = \int {\rm d}^4x \sqrt{\tilde{g}} \left[\frac{e^{-2\psi(\phi)}}{2l_{\rm s}^2}\tilde{R} + \frac{Z(\phi)}{2l_{\rm s}^2}\nabla_\mu\phi\nabla^\mu\phi - \tilde{V}(\phi) \right] + S_{\rm m}\left[\tilde{g}_{\mu\nu}, g_{\rm i}(\phi); \psi_{\rm i}\right] \tag{2.54}$$

where $\psi(\phi)$ is an unknown function that depends on the details of the string compactification, $l_{\rm s}$ is the string length scale, and, unlike the previous models, the coupling constants $g_{\rm i}$ are dilaton-dependent. Transforming to the Einstein frame by defining

$$A(\phi) = M_{\rm pl} l_{\rm s} e^{\psi(\phi)} \tag{2.55}$$

we have[18]

$$S = \int \mathrm{d}^4x\sqrt{g}\left[\frac{{M_{\rm pl}}^2}{2}R - \frac{1}{2}k^2(\phi)\nabla_\mu\phi\nabla^\mu\phi - A^4(\phi)\tilde{V}(\phi)\right] + S_{\rm m}[A^2(\phi)g_{\mu\nu}, g_{\rm i}(\phi); \psi_{\rm i}] \quad (2.56)$$

where

$$k^2(\phi) = 6\beta^2(\phi) - \frac{A^2(\phi)Z(\phi)}{l_{\rm s}^2}. \quad (2.57)$$

In the strong coupling limit, which corresponds to $\phi \to \infty$ so that $e^{-\phi/M_{\rm pl}} \ll 1$, one can expand the functions appearing in (2.56) as [87]

$$\tilde{V}(\phi) = V_0 e^{-\frac{\phi}{M_{\rm pl}}} + \mathcal{O}\left(e^{-2\frac{\phi}{M_{\rm pl}}}\right) \quad (2.58)$$

$$Z(\phi) = -\frac{l_{\rm s}^2}{\lambda^2} + b_Z e^{-\frac{\phi}{M_{\rm pl}}} + \mathcal{O}\left(e^{-2\frac{\phi}{M_{\rm pl}}}\right) \quad (2.59)$$

$$g_{\rm i}^{-2}(\phi) = \bar{g}^{-2} + b_{\rm i} e^{-\frac{\phi}{M_{\rm pl}}} + \mathcal{O}\left(e^{-2\frac{\phi}{M_{\rm pl}}}\right), \quad (2.60)$$

where the constants λ, b_Z and $b_{\rm i}$ etc. are set by the details of the specific string compactification. We will treat them as free parameters in what follows. One generally expects $b_Z, b_{\rm i} \sim \mathcal{O}(1)$ and $\lambda \sim \mathcal{O}(1)$–$\mathcal{O}(l_{\rm s}^{-1}{M_{\rm pl}}^{-1})$ ($\gg \mathcal{O}(1)$) and so the kinetic factor is

$$k(\phi) \approx \frac{1}{\lambda}\sqrt{1 + 6\beta^2(\phi)}, \quad (2.61)$$

where we have again set $A(\phi) \approx 1$ in accordance with our earlier discussion. The equation of motion for the canonically normalised field $\mathrm{d}\varphi = k(\phi)\mathrm{d}\phi$ is then

$$\Box\varphi = -\frac{1}{M_{\rm pl}k(\phi)}\left[\beta(\phi)\left(4V(\phi) + \rho A'(\phi)\right) - V(\phi)\right] + S_{\rm i}\frac{g_{\rm i}^2(\phi)b_{\rm i}e^{-\frac{\phi}{M_{\rm pl}}}}{2M_{\rm pl}k(\phi)}, \quad (2.62)$$

[18] Note that this requires the inverse transformation to that used to find equation (2.15), which can be found by setting $A \to A^{-1}$ and allowing for the fact that the Planck mass was not included in the Einstein-Hilbert-like term in equation (2.54).

where it is understood that $\phi = \phi(\varphi)$ and

$$S_{\rm i} \equiv \frac{\delta S_{\rm m}}{\delta \ln g_{\rm i}}. \tag{2.63}$$

Typically, $S_{\rm i} \sim \mathcal{O}(\rho)$ and $\exp(-\phi/M_{\rm pl}) \ll 1$ in the strong coupling limit so we can safely ignore the final term in equation (2.62). In this case, we can integrate the equation of motion to find the effective potential for φ:

$$V_{\rm eff}(\varphi) = V_0 A^4(\phi) e^{-\frac{\phi}{M_{\rm pl}}} + \rho(A(\phi) - 1). \tag{2.64}$$

The coupling can then be found using the chain rule and one finds

$$\beta(\varphi) = \frac{\beta(\phi)}{k(\phi)}. \tag{2.65}$$

Minimising the effective potential with respect to ϕ is equivalent to minimising it with respect to φ since $\mathrm{d}\varphi/\mathrm{d}\phi \neq 0$ and so we find

$$\beta(\phi_{\rm min}) = \frac{V(\phi_{\rm min})}{4V(\phi_{\rm min}) + \rho}, \tag{2.66}$$

at the minimum of the effective potential. When $\rho \gg 4V(\phi_{\rm min})$ we have $\beta(\phi_{\rm min}) \approx 0$ and using equation (2.65) we can then see that this mechanism screens via the EDDP since $k(\phi_{\rm min}) \neq 0$. The functional form of $A(\phi)$ is still unknown and there is no natural choice in the strong coupling limit of string theory[19] and so the authors of [20] assume that the function has the requisite minimum for the screening mechanism to be present to expand the coupling function as

$$A(\phi) = 1 + \frac{A_2}{2{M_{\rm pl}}^2}\left(\phi - \phi_{\rm min}\right)^2 + \cdots \tag{2.67}$$

[19] Put another way, the functional form is presently unknown in this limit.

and use laboratory tests to constrain the parameter A_2. We will not examine the dilaton model explicitly in this thesis nor any other theories that screen via the EDDP [20] and so for completeness we will simply state the constraint that they obtain is $A_2 \gg 1$. The reader is referred to [20] for the technical derivation of this constraint[21].

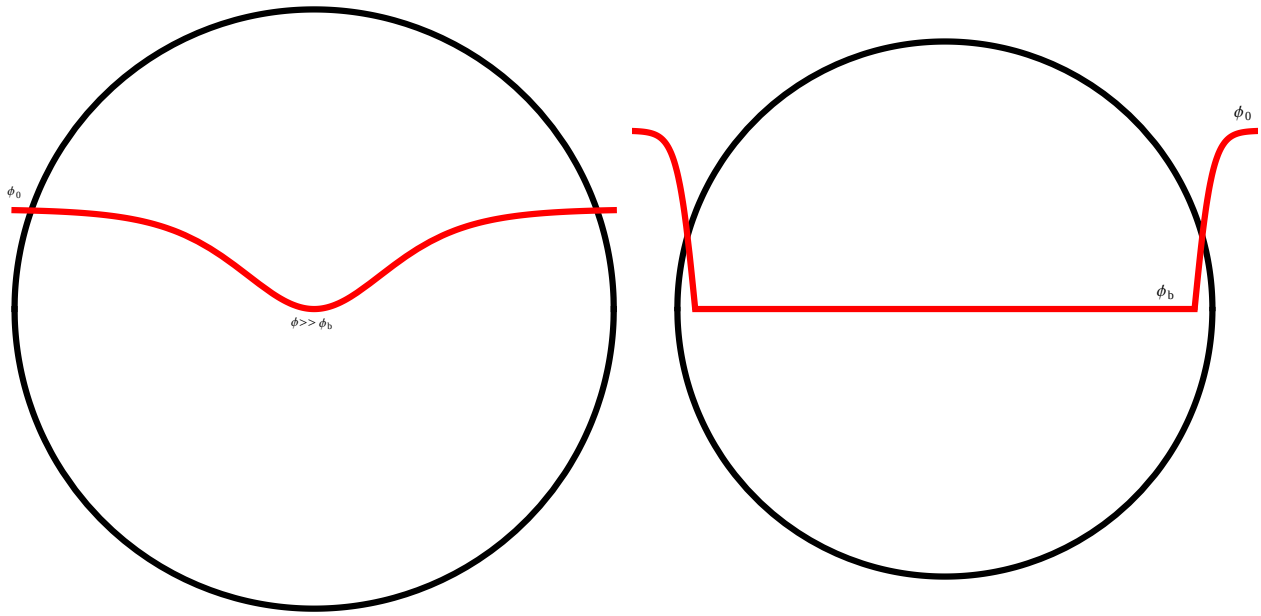
2.2.5 The Screening Mechanism

The previous sections have discussed the three mechanisms by which the fifth-force can be rendered negligible in dense environments but there are still two important questions to address: How is this realised in reality? And exactly which objects are screened? We will answer these questions in this section.

Even if the fifth-force can in theory be screened in dense enthronements, this will only happen if the field can reach the minimum of the effective potential where the screening occurs. Consider then a spherical over-density of radius R with density profile $\rho_{\rm b}(r)$ placed into a much larger (by which we mean its characteristic length scale is $\gg R$) medium with a smaller density $\rho_{\rm c}$. Far away from the object, the field can minimise its effective potential with density $\rho_{\rm c}$ and assumes a field value $\phi_{\rm c}$. The field will want to minimise the effective potential with density $\rho_{\rm b}$ (with corresponding field value $\phi_{\rm b}$) inside the object and so near the object (and inside of course) we expect a field gradient, which according to equation (2.12) implies the presence of a fifth-force. There are then two possible scenarios. Suppose that the object is small enough (to be quantified presently) such that the field is unable to reach this minimum at all. In this case, the field will be a small perturbation about the background value $\phi_{\rm c}$ and will hence mediate a fifth-force that is comparable with the Newtonian force since either $\beta(\phi)$ or $m_{\rm eff}(\phi)$ correspond to those at the minimum in low density environments. In this case, the

[20] They will however be constrained in chapter 4 using a set of model-independent parameters presented in the next section, although we will not translate these constraints into A_2.

[21] Note that their action and expressions for quantities such as $\beta(\phi)$ and $k(\phi)$ differ from ours because they use a dimensionless field variable whereas ours has the canonical mass dimension. Furthermore, their function $k(\phi)$ differs from ours by a factor of 2 because they do not work with a canonically normalised field. We have done this in order to provide a consistent link with the general framework presented in this chapter. There are also several typographical errors in this paper that have been corrected here.



(a) Unscreened (b) Screened

Figure 2.3: The field profile in the screened and unscreened scenarios.

object is *unscreened* and we expect new and novel features compared with those predicted by general relativity. This case is shown in figure 2.3(a). On the other hand, if the object is large enough such that the field can minimise its effective potential at density ϕ_b over most of the radius of the object then the field will only vary very close to the surface of the object and will quickly reach ϕ_c leaving a field gradient in a very thin shell near the surface. In this case, any perturbation in the field will be about ϕ_b and hence corresponds to either a negligible value of $\beta(\phi)$ or a very large effective mass. In this case the object is *screened* and any deviations from general relativity will be unobservable. This is shown in figure 2.3(b).

In general, one expects a situation somewhere between these two extremes so that the field can reach ϕ_b at the centre of the object and remains there until some radius r_s, which we shall refer to as the *screening radius*, at which point it begins to asymptote to ϕ_c. In this case, the region interior to the screening radius is screened and there are no fifth-forces whereas in the region exterior to the screening radius there is a field gradient and this region is unscreened. The screened case then corresponds to $r_s = R$ and the unscreened case to $r_s = 0$; the general

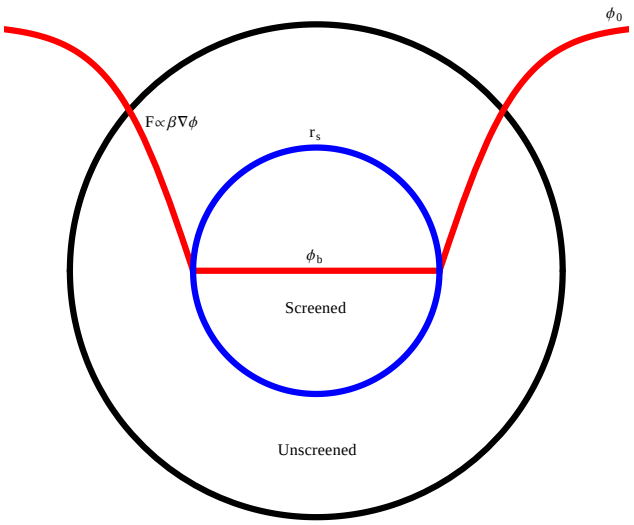


Figure 2.4: The general field profile for a partially unscreened object.

case is an intermediate configuration between the two and we refer to this as the *partially screened* case. This is shown schematically in figure 2.4. We will now derive the field profile for this general case and use it to find the fifth-force.

We begin with the region $r \leq r_s$. In the static, spherically symmetric limit equation (2.23) reduces to

$$\nabla^2\phi = V'(\phi) + \frac{\beta\rho}{M_{\rm pl}}. \tag{2.68}$$

Now suppose that the field minimises its effective potential at $r = 0$ so that $\phi = \phi_b$. This means that the effective potential is minimised and so equation (2.68) becomes

$$\nabla^2\phi \approx 0. \tag{2.69}$$

Since there is no source for this equation, the field will remain at an approximately constant value until this approximation breaks down. This defines the screening radius. In the unscreened region, the field will be a small perturbation $\delta\phi$ about the background value ϕ_c so that $\phi(r) = \phi_c + \delta\phi(r)$. Subtracting the equation of motion (2.68) for the over-dense region

from that for the under-dense one and linearising we have

$$\nabla^2\delta\phi \approx m_{\rm c}^2\delta\phi + \frac{\beta_{\rm c}\delta\rho}{M_{\rm pl}}, \tag{2.70}$$

where $\delta\rho \equiv \rho_{\rm b} - \rho_{\rm c}$, $m_{\rm c}^2 \equiv V_{,\phi\phi}(\phi_c)$ is the mass of the field in the background (the mass of oscillations about the minimum of the effective potential at density $\rho_{\rm c}$) and $\beta_{\rm c} \equiv \beta(\phi_{\rm c})$. Theories that posses screening mechanisms have the property that

$$\frac{{\rm d}\beta}{{\rm d}\phi}\delta\phi \ll \beta(\phi_{\rm c}) \tag{2.71}$$

in the unscreened region and so we have neglected all terms proportional to ${\rm d}\beta/{\rm d}\phi$ in equation (2.70). In all theories of interest, we have $m_{\rm c}R \ll 1$ so that the fifth-force gives rise to novel features on large scales and so we may ignore the first term in equation (2.70), it is negligible compared with the Laplacian. Now we know that $\delta\rho$ is related to the Newtonian potential $\Phi_{\rm N}$ via the Poisson equation (1.8) and so we may substitute this into (2.70) and integrate twice to find the field profile:

$$\delta\phi(r) \approx -\phi_{\rm c} + 2\beta_{\rm c}M_{\rm pl}\left[\Phi_{\rm N}(r) - \Phi_{\rm N}(r_{\rm s}) + r_{\rm s}^2\Phi_{\rm N}'(r_{\rm s})\left(\frac{1}{r} - \frac{1}{r_{\rm s}}\right)\right]H(r - r_{\rm s}), \tag{2.72}$$

where $H(x)$ is the Heaviside step-function. Using the definition of the Newtonian potential ${\rm d}\Phi_{\rm N}/{\rm d}r = GM(r)/r^2$, where $M(r)$ is the mass enclosed within a sphere of radius r (the total mass of the over-density is $M = M(R)$), the fifth-force (2.12) in the unscreened region is given by the derivative of (2.72):

$$\frac{\beta_{\rm c}}{M_{\rm pl}}\frac{{\rm d}\phi}{{\rm d}r} = \alpha_{\rm c}\frac{GM(r)}{r^2}\left[1 - \frac{M(r_{\rm s})}{M(r)}\right], \tag{2.73}$$

where $\alpha_{\rm c} \equiv 2\beta^2(\phi_{\rm c})$. We can see that equation (2.73) reproduces the fully screened and unscreened cases. When $r_{\rm s} = R$ there is no fifth-force and the object is screened whereas when

$r_s = 0$ the object is full unscreened and we have $F_\phi = \alpha_c F_N$, where F_N is the Newtonian force. The parameter α_c therefore determines the strength of the fifth-force.

All that remains is to find the screening radius r_s. Using the fact that $\delta\phi \to 0$ when $r/r_s \to \infty$ as does $\Phi_N(r)$, equation (2.72) gives us an implicit expression for the screening radius:

$$\frac{\phi_c}{2\beta(\phi_c)M_{pl}} \equiv \chi_c = -\Phi_N(r_s) - r_s\Phi_N'(r_s) \geqslant 0. \tag{2.74}$$

It will be useful later to recast this as an integral equation:

$$\chi_c = 4\pi G \int_{r_s}^{R} r\rho_b(r)\,\mathrm{d}r, \tag{2.75}$$

where χ_c is to be viewed as a parameter of the theory to be input by hand and r_s the screening radius to be found using this equation. The parameter χ_c is known as the *self-screening parameter* and is of paramount importance to the screening properties of these theories. Since $\Phi_N < 0$ and $\mathrm{d}\Phi_N/\mathrm{d}r > 0$, there are no solutions when

$$|\Phi_N(R)| = \frac{GM}{R} > \chi_c. \tag{2.76}$$

In this case, the object is fully screened and $r_s = R$. When $\Phi_N < \chi_c$ the object will be at least partially unscreened.

The screening and fifth-force properties in any region are fully specified by α_c and χ_c, however these are environment-dependent and are non-linearly related to the field values in different regions of the universe. The exception to this is unscreened objects, where the field is only a small perturbation around the value in the cosmological background and so these values are roughly constant. Whether or not an object is screened or not depends on its Newtonian potential relative to the cosmological value of χ_c; the same is true of denser objects residing in larger unscreened objects. In each case, the strength of the fifth-force in any unscreened region is proportional to the cosmological value of α_c and so any tests

of these theories using unscreened objects probe the cosmological values of α_c and χ_c. The theory is then parametrised in a model-independent manner by the cosmological values of these parameters, which we denote by α, which measures the strength of the fifth-force in unscreened regions and

$$\chi_0 \equiv \frac{\phi_0}{2M_{\rm pl}\beta(\phi_0)}, \tag{2.77}$$

which determines how small the Newtonian potential must be in order for the object to be unscreened[22]. Note that $f(R)$ theories have $\beta(\phi) = 1/\sqrt{6}$ (see equation (2.36)) and so $\alpha = 1/3$ and there is only one free parameter. When working within an $f(R)$ framework the parameter that is often constrained in the literature is f_{R0}, the present-day value of the first derivative of the function with respect to R. This parameter is equivalent to χ_0 and in this thesis we will only work with this parameter in order to avoid any ambiguity.

This thesis is concerned with both astrophysical probes of modified gravity and the cosmology of supersymmetric chameleon models. α and χ_0 are then perfect parameters to describe both of these scales. In general, cosmological tests probe the cosmological mass and coupling (see [28, 88]), which can be mapped onto χ_0 and α in a straightforward manner. We will see presently that the Milky Way is screened and so laboratory and solar system tests probe the mass as a function of the coupling. These can be mapped onto χ_0 and α in a model-dependent manner but this requires one to know the galactic evolution of χ_c and α_c and how they relate to the cosmological values. This can be done using spherical collapse models [48] although to date no comprehensive analysis has been performed.

This parametrisation may seem esoteric at first, however it is nothing more than the mass and coupling of the field in the cosmological vacuum. $\alpha = 2\beta^2(\phi_0)$ and so α directly measures the coupling $\beta(\phi_0)$ in the cosmological vacuum. Minimising the effective potential, one has

$$\frac{{\rm d}V(\phi)}{{\rm d}\phi} = -\frac{\beta(\phi_0)\rho_0}{M_{\rm pl}}. \tag{2.78}$$

[22] One must note however that this analysis applies to isolated objects only. In the presence of other objects of Newtonian potential $\Phi_{\rm N}^{\rm ext}$ the external potential can be large enough to screen an object that would otherwise be self-unscreened [24].

Setting $\rho_0 \sim H_0^2 {M_{\rm pl}}^2$ and linearising the derivative of the potential about ϕ_0 and using the fact that $\delta\phi \approx -\phi_0$ one finds

$$\chi_0 \approx \left(\frac{H_0}{m_0}\right)^2 \tag{2.79}$$

where $m_0^2 \equiv V''(\phi_0)$ is the free mass of the field in the cosmological vacuum. One can see that χ_0 is a measure of the range of the force mediated on cosmological scales.

2.2.6 Current Constraints

This subsection is somewhat historical in that it refers to the situation before 2012 when the original work presented in this thesis was first reported in [89]. In chapter 4 we will present new and updated constraints. The material is presented in this fashion as a historical background and in order to highlight the relevance of this work to the field.

We now have a method of classifying exactly which objects in the universe are screened and which are not. Any object whose Newtonian potential is less than χ_0 will be screened whereas objects where the converse is true will be at least partially unscreened. We can therefore discern the ranges of χ_0 that can be probed using different astrophysical objects by looking at their Newtonian potentials.

The first task is to ensure that our own solar-system is screened. The Newtonian potential of the Earth is $\Phi_{\rm N}^{\oplus} \sim 10^{-9}$ and so one may think that we need to impose $\chi_0 \lesssim \mathcal{O}(10^{-9})$ in order to satisfy laboratory experiments. In fact, this is too stringent. The Newtonian potential of the Sun is $\Phi_{\rm N}^{\odot} = 2 \times 10^{-6}$ and so one would then need to impose $\chi_0 \lesssim \mathcal{O}(10^{-6})$ in order to satisfy post-Newtonian tests of gravity using light bending around the Sun. This is still too näive a constraint because we have yet to account for the fact that the solar system resides within the Milky Way. If the Milky Way were unscreened there would be discernible effects coming from the motion of stars about the galactic centre and so we must demand that it is screened. Spiral galaxies like the Milky Way have rotational velocities of $\mathcal{O}(100\ \mathrm{kms}^{-1})$ or more and so the virial theorem ($GM/Rc^2 \equiv \Phi_{\rm N} = v^2/c^2$) implies they have Newtonian potentials $\Phi_{\rm N} \gtrsim \mathcal{O}(10^{-6})$. The

Milky Way has $\Phi_N \sim 10^{-6}$ but it is situated in the local group whose Newtonian potential is of order 10^{-4}. There are then two possibilities: we must either impose that the local group screens the Milky Way, in which case we must impose $\chi_0 < 10^{-4}$ or we must demand that the Milky Way is self-screening, in which case we need the stronger constraint $\chi_0 \lesssim 10^{-6}$. Either way, the fact that the Milky Way is screened means that $\chi_c^{\text{Milky Way}} \ll \chi_0$ and so the Sun and Earth are blanket screened and do not impose additional constraints. Whether or not the local group does screen the Milky Way has been debated in the literature. Later on, we will present a new and independent constraint that $\chi_0 < 10^{-6}$ and so we shall adopt this constraint from here on. Note that the symmetron has $\chi_0 = M^2/2{M_{\text{pl}}}^2$ and so compatibility with this constraint demands that $M \leq 10^{-3} M_{\text{pl}}$ as we stated without explanation in section 2.2.3.

At the background level, these models do not alter the expansion history predicted by ΛCDM [58], however they give rise to modifications to the CDM power spectrum and other linear probes on scales inside the horizon. It is difficult to define a Newtonian potential for cosmology because one generally requires a full relativistic treatment. It is tempting to use the metric potential Φ defined in (1.36) in a similar manner to the potential defined in (1.6), however saying that this assumes any value is a gauge-dependent statement and there is no guarantee that one cannot find a gauge where a different metric potential assumes a vastly different value. Inside the horizon, the equations of motion for perturbations are essentially non-relativistic and so should look Newtonian in any gauge. Therefore, we can treat this potential as the equivalent of the Newtonian potential provided that one bears in mind the scales on which such an interpretation is valid. In particular, this will not be a good approximation near the horizon. In this case, the potential on sub-horizon scales is of order 10^{-6} and so we expect novel deviations on linear scales for $\chi_0 \gtrsim 10^{-6}$. Now we have argued above that $\chi_0 \lesssim 10^{-6}$ and so according to equation (2.79) the mass of the field in the cosmological background must satisfy $m_0 \gtrsim 10^3 H_0 \sim 10^{-1} h \text{ Mpc}^{-1}$. Now it is well-known that linear perturbation theory in general relativity is only valid on scales $k < 10^{-1} \text{ Mpc}^{-1}$ and so the constraint coming from the necessity of screening the Milky Way ensures that there are no observable

effects on linear scales. On non-linear scales, one must use N-body simulations to calculate the non-linear cosmological probes such as the halo mass function. A full account of N-body codes and their predictions is beyond the scope of this thesis and so we will simply remark that all cosmological signatures of modified gravity vanish when $\chi_0 \leq 10^{-6}$. One can therefore use non-linear cosmological probes to constrain these theories when $\chi_0 \gtrsim 10^{-6}$. Currently, the strongest constraints come from cluster statistics and impose $\chi_0 < 10^{-4}$ [90]. Recently, a new method using the difference between the hydrostatic and lensing mass of the Coma cluster has been used to impose an independent constraint $\chi_0 \lesssim 6 \times 10^{-5}$.

Given our constraint $\chi_0 \leq 10^{-6}$ one may wonder if there are more under-dense regions with lower Newtonian potentials that can act as new probes of these theories. We have already seen than $GM_\odot/R_\odot = 2 \times 10^{-6}$ but what about other main-sequence stars? There is a well known mass-radius relationship for main-sequence stars

$$\left(\frac{R}{R_\odot}\right) = \left(\frac{M}{M_\odot}\right)^{\nu} \tag{2.80}$$

with $\nu = 0.4$–0.8 depending on the dominant nuclear reaction network in the core. We then have

$$\Phi_{\rm N} = \frac{GM}{R} = \frac{GM_\odot}{R_\odot}\left(\frac{M}{M_\odot}\right)^{(1-\nu)}. \tag{2.81}$$

The lowest mass stars have masses of order $0.1M_\odot$ and have $\nu = 0.4$ corresponding to the PP1 chain giving Newtonian potentials of order 10^{-6} and the highest mass stars have masses around $100M_\odot$ and have $\nu = 0.8$ corresponding to the CNO cycle, which gives Newtonian potentials of order 10^{-5}. Main-sequence stars therefore all have Newtonian potentials $\Phi_{\rm N} \geq 10^{-6}$ and therefore cannot probe $\chi_0 < 10^{-6}$. Post-main-sequence stars such as red giant (RG) and asymptotic giant branch (AGB) stars have masses equal to that of their progenitor main-sequence stars but have radii 10 to 100 times larger and therefore have Newtonian potentials of order 10^{-7} (1–$2M_\odot$) to 10^{-8} (10+ $M_\odot$). We can therefore use post-main-sequence stars to probe the parameter range $10^{-8} \leq \chi_0 \leq 10^{-7}$.

Now we have also argued that spiral galaxies are screened and so we cannot probe this parameter range unless we can find unscreened galaxies in which to observe these stars. Elliptical galaxies have Newtonian potentials similar to spirals but dwarf galaxies have lower rotational velocities of order 50 km s^{-1} and hence have Newtonian potentials $\Phi_N \sim \mathcal{O}(10^{-8})$. Dwarf galaxies are hence perfect laboratories for testing these theories. Dwarf galaxies in clusters will be blanket screened by their neighbours whereas those in cosmic voids will be unscreened. By comparing the properties of these galaxies (or their constituents) in voids and clusters and looking for systematic offsets new constraints can be placed. Tests using dwarf galaxies fall into two classes: first, the fact that the galaxies are unscreened means that the galactic properties such as the rotation curves and morphology are altered relative to the general relativity prediction [91] and second, other objects inside these galaxies such as post-main-sequence stars will also be unscreened and show novel features compared with those situated inside dwarf galaxies in clusters. The first class has been investigated elsewhere [92, 93] and the data is not yet good enough to place new constraints, although this will change with the next generation of galaxy surveys. The second class is the subject of a large proportion of this thesis and will be the focus of chapters 3, 4 and 7.

Below $\chi_0 = 10^{-8}$ dwarf galaxies are screened and so one must look for even more underdense object to test these theories. Unfortunately, there are no such objects; when $\chi_0 < 10^{-8}$ every object in the universe is screened[23]. Whilst these theories can never be completely ruled out because one can always screen everything, when $\chi_0 < 10^{-8}$ the theory is rendered indistinguishable from general relativity on all scales[24] and is hence physically uninteresting. In table 1.2 we summarise the Newtonian potentials of different objects in the universe and their degree of screening.

[23] HI gas in the outer disks of galaxies has $\Phi_N \sim \mathcal{O}(10^{-11})$–$\mathcal{O}(10^{-12})$ [24] however this is blanket screened in all galaxies when $\chi_0 \lesssim 10^{-8}$.

[24] One can construct models with arbitrarily weak matter couplings that cannot be probed astrophysically. In this case, one then has a theory which shows no deviations from general relativity on any scale with the exception that one can look for signatures in the laboratory. These cases are also physically uninteresting since they have no effect on any physical phenomena.

Object	Φ_N	Screening Status
Earth	10^{-9}	Screened by the Milky Way
The Sun	2×10^{-6}	Screened by the Milky Way
Main-sequence stars	10^{-6}–10^{-5}	Screened
Local group	10^{-4}	Screened
Milky Way	$\mathcal{O}(10^{-6})$	Screened
Spiral and elliptical galaxies	10^{-6}–10^{-5}	Screened
Post-main-sequence stars	10^{-7}–10^{-8}	Unscreened in dwarf galaxies in cosmic voids
Dwarf galaxies	$\mathcal{O}(10^{-8})$	Screened in clusters, unscreened in cosmic voids

Table 2.1: The screening status of different collapsed objects in the universe given the constraint $\chi_0 < 10^{-6}$. We do not include linear and non-linear cosmological scales since there is no unequivocal equivalent of the Newtonian potential with which to compare χ_0 (see the discussion above). Post-main-sequence stars located in dwarf galaxies in clusters or in galaxies with any other morphology are blanket screened by their host galaxy.

2.2.7 Identification of Unscreened Galaxies

So far, all of the work we have presented has been theoretical and we have not addressed the question of whether we can determine whether or not an individual galaxy in the real universe is screened. We have already seen that this depends in part on the self-Newtonian potential of the galaxy but this does not account for environmental screening due to nearby galaxies. There has been a great effort to address this problem using N-body simulations and there is indeed a method of determining the screening status of a galaxy. The criterion to determine screening exploits the fact that relativistic particles that move on null geodesics do not distinguish between $g_{\mu\nu}$ and $\tilde{g}_{\mu\nu}$ and therefore do not feel the effects of modified gravity. In particular, photons move on the same trajectories as they would in general relativity and hence the amount of gravitational lensing due to a fixed mass is identical in both theories. This means that if one were to measure an object's mass using lensing measurements — the so-called *lensing mass* — and compare it with the mass inferred from the dynamics of non-relativistic particles about this mass — the so-called *dynamical mass* — the two would only

agree if the object is screened. The necessary quantity for determining whether a dark matter halo of mass M is screened or not is the ratio of the distance to the nearest neighbour whose mass is at least as large as M to the virial radius of the neighbouring halo [94, 95].

Observationally, this is difficult to obtain and so in order to obtain a screening map [96] have used a simpler set of criteria. The first is the condition we described at length above i.e. a galaxy is classified as self-screened if

$$\Phi_{\rm N}^{\rm self} \geq \chi_0, \tag{2.82}$$

where

$$\Phi_{\rm N}^{\rm self} \equiv \frac{GM}{r_{\rm vir}} \tag{2.83}$$

where the virial radius $r_{\rm vir}$ is related to the critical linear density contrast $\delta_{\rm crit} = 3M/4\pi r_{\rm vir}^3$ and the authors take $\rho_{\rm crit} = 200\rho_0$. The masses are measured using either X-ray and lensing observations, or, where no such observations are available, using scaling relations such as the mass-luminosity or mass-velocity dispersion relations. This condition is robust and there is little error in using it. A galaxy is classed as environmentally screened if

$$\Phi_{\rm N}^{\rm env} \geq \chi_0, \tag{2.84}$$

where $\Phi_{\rm N}^{\rm env}$ is defined via

$$\Phi_{\rm N}^{\rm env} = \sum_{\rm d_i < \lambda_C + r_i} \frac{GM_{\rm i}}{d_{\rm i}}. \tag{2.85}$$

Here, $d_{\rm i}$ is the distance to a neighbouring galaxy with mass $M_{\rm i}$ and virial radius $r_{\rm i}$ and $\lambda_{\rm C}$ is the Compton wavelength, which is set by the specific modified gravity model and is a function of χ_0 and α. This condition is an ansatz and as such needs careful consideration. It is motivated by the fact that the range of the fifth-force is $\lambda_{\rm C}$ and hence the galaxy will only feel the fifth-force from neighbouring galaxies within a distance $\lambda_{\rm C}+r_{\rm i}$. The authors of [96] have tested this criterion rigorously against N-body simulations and unknown systematics and the interested

reader is referred there for the technical details (see figure 2 in particular). Here, we will only remark that this criterion is very successful at classifying the screening status of most of the galaxies and any errors are always such that there are more unscreened galaxies than it would predict and so any new constraints found using this map are conservative.

We will use this screening map in chapter 4 in order to place new constraints on chameleon-like theories.

2.2.8 Cosmological Behaviour

The majority of this thesis is devoted to astrophysical tests, however in chapter 7 we will be interested in the cosmology of supersymmetric chameleon models and so here we will briefly present the formalism for describing the cosmological dynamics of these theories. In particular, the non-minimal coupling to matter has the consequence that the equation of state parameter is not the same as we found for simple quintessence models (1.49) and so the main focus will be on deriving this. The cosmological behaviour can vary between models and so here we will state only the model-independent features without a lengthy derivation. We refer the reader to [28] and references therein for further details. We will also derive the cold dark matter power spectrum and so we also present the equations governing the evolution of the CDM linear density contrast in chameleon-like models.

Background Evolution

In order to be compatible with local constraints, the cosmological mass at the time-dependent minimum of the effective potential of the field always satisfies

$$\frac{m_{\rm eff}(\phi)}{H} \gg 1, \tag{2.86}$$

where $H(t)$ is the Hubble parameter at any given time. This means that the time-scale ($m_{\rm eff}^{-1}$) on which the field responds to changes in the position of the minimum is far shorter than the

time-scale on which the minimum moves (H^{-1}) and so given any initial condition, the field tracks the minimum adiabatically throughout all subsequent cosmic evolution[25]. As time progresses, the matter density redshifts as a^{-3} and the position of the minimum (and hence field) moves to increasing field values. Now, the Einstein frame Lagrangian (assuming a conserved matter density) is

$$\frac{\mathscr{L}}{\sqrt{-g}} \supset TA(\phi) \tag{2.87}$$

and so the fermion masses ($T \supset m_{\rm f}^0 \bar{\Psi}\Psi$ where Ψ are Dirac spinors) are $m_{\rm f} = m_{\rm f}^0 A(\phi)$. This means that if the field starts off at some initial value ϕ_i and rolls over some distance in field space $\Delta\phi$ before reaching the minimum then the fermion masses change by an amount

$$\frac{\Delta m_{\rm f}}{m_{\rm f}} \approx \beta \frac{\Delta\phi}{M_{\rm pl}}, \tag{2.88}$$

where we have used the fact that $\beta(\phi)$ does not vary too much in unscreened regions (recall the discussion in section 2.2.5). Now there are stringent constraints on the variation of fermion masses during big bang nucleosynthesis (BBN) stating that they cannot vary by more than 10% or so and so in order to comply with this constraint the field must reach its minimum before the onset of BBN. In practice, this means that there is a small region near the minimum where the field can lie where it will reach the minimum before the onset of BBN. Exactly how this is achieved is irrelevant for this thesis and we will always assume the field has reached its minimum before BBN. The interested reader can find details in [42]; see [57, 97] for a discussion of quantum problems associated with this.

An important question to ask is: can these models account for dark energy? This is tantamount to asking if the equation of state can become -1 at late times. The field is coupled to matter and so finding the equation of state is not as simple as taking T_ϕ^{00}/T_ϕ^{ii} as in the case of quintessence. In order to find a physically meaningful expression for w — i.e. one that has the correct interpretation for an observer whose cosmological measurements are predicated

[25] Another way of stating this is that the time-varying minimum is a global attractor for the dynamics.

on minimally coupled theories — we will write down the Friedmann system and attempt to manipulate it into a form that looks like a quintessence theory. The Friedmann equation is

$$H^2 = \frac{1}{3{M_{\rm pl}}^2}\left[\rho_{\rm m} + \frac{1}{2}\dot{\phi}^2 + V(\phi)\right], \tag{2.89}$$

where we have temporarily reverted to using the non-conserved matter density $\rho_{\rm m}$ in order to account for every factor of ϕ in the problem. The conserved matter energy density satisfies

$$\dot{\rho} + 3H\rho = 0; \quad \rho_{\rm m} \equiv A(\phi)\rho. \tag{2.90}$$

If we try to match this onto a quintessence-like system where the total energy density in the Friedmann equation is $\rho_{\rm T} = \rho + \rho_\phi$ then we can identify

$$\rho_\phi = \frac{1}{2}\dot{\phi}^2 + V(\phi) + \big(A(\phi) - 1\big)\,\rho = \frac{1}{2}\dot{\phi}^2 + V_{\rm eff}(\phi). \tag{2.91}$$

The matter is pressureless and so any pressure in the system is due to the field, in which case we have

$$P_\phi = T_\phi^{|ii|} = \frac{1}{2}\dot{\phi}^2 - V(\phi). \tag{2.92}$$

The equation of state is then

$$w_\phi = \frac{P_\phi}{\rho_\phi} = \frac{\dot{\phi}^2 - 2V(\phi)}{\dot{\phi}^2 + V_{\rm eff}(\phi)}, \tag{2.93}$$

which differs from the quintessence expression by a factor of $V_{\rm eff}(\phi)$. Of course, it is not enough to simply define w_ϕ in this way. One must check that the continuity equation for ρ_ϕ,

$$\frac{{\rm d}\rho_\phi}{{\rm d}t} = -3H\left(1 + w_\phi\right)\rho_\phi, \tag{2.94}$$

and the acceleration equation

$$\frac{\ddot{a}}{a} = -\frac{1}{6{M_{\rm pl}}^2}\left(\rho + (1+3w_\phi)\rho_\phi\right) \tag{2.95}$$

are consistent. It is not difficult to verify that this is indeed the case [98].

Linear Perturbations

The growth of linear perturbations in screened modified gravity has been well studied [28, 42, 43] and the linear density contrast $\delta_{\rm c} = \delta\rho_{\rm c}/\rho_{\rm c}$ in the conformal Newtonian Gauge evolves on sub-horizon scales according to

$$\ddot{\delta}_{\rm c} + 2H\dot{\delta}_{\rm c} - \frac{3}{2}\Omega_{\rm c}(a)H^2\left(1 + \frac{2\beta^2(\varphi)}{1+\frac{m_{\rm eff}^2 a^2}{k^2}}\right)\delta_{\rm c} = 0. \tag{2.96}$$

This is the equivalent of equation (1.41) in general relativity. Comparing with (1.40), the last term in (2.96) can be interpreted as a scale-dependent enhancement of Newton's constant:

$$\frac{G_{\rm eff}(k)}{G} = 1 + \frac{2\beta(\varphi)^2}{1+\frac{a^2 m_{\rm eff}^2}{k^2}}. \tag{2.97}$$

On large scales the screening is effective and $G_{\rm eff} \approx G$ whilst on smaller scales the full enhancement, $G_{\rm eff} = G(1+2\beta(\varphi)^2)$ is felt. One would therefore expect that there is some wave number $\tilde{k}$ below which the modes feel no significant fifth-forces and the general relativity power spectrum is recovered. We will return to this equation in chapter 7.

2.3 The Vainshtein Mechanism

As alluded to in the introduction to this chapter, the Vainshtein mechanism screens in a very different manner to chameleon-like models and here we present a brief discussion of its main features and how it differs from conformal scalar-tensor screening using Galileon models as

an example.

2.3.1 Galileon Theories of Gravity

Unlike conformal scalar-tensor theories. The action for Galileon gravity is defined at the linearised level. A full non-linear completion does exist [69] — either in the form of Horndeski gravity [68] or ghost-free massive gravity [99] — but it will be sufficient to study the linearised theory here. First, discovered as the 0-helicity mode of DGP gravity, the general model is that of a scalar field π whose action is invariant (up to a boundary term) under the Galileon shift symmetry $\partial_\mu\pi \to \partial_\mu\pi + c_\mu$ where c_μ is a constant 4-vector. In particular, this does not forbid a coupling to matter of the form

$$\mathscr{L}/\sqrt{-g} \supset \alpha_{\rm V}\frac{\pi}{M_{\rm pl}}T, \tag{2.98}$$

where $\alpha_{\rm V}$ is a dimensionless coupling constant[26]. These theories then fall into the class of modified gravity models defined by equation (2.9) so the fifth force is then

$$\mathbf{F}_\pi = -\frac{\alpha_{\rm V}}{M_{\rm pl}}\nabla\pi. \tag{2.99}$$

In four dimensions there are five possible terms one can write down that satisfy this symmetry independently[27]. Since we only wish to discuss the main features of the screening mechanism it will suffice to study the *cubic Galileon* only. The linearised action is

$$S = \int \mathrm{d}^4x - \frac{1}{4}h^{\mu\nu}\left(\mathscr{E}h\right)_{\mu\nu} - \frac{1}{2}\partial_\mu\phi\,\partial^\mu\phi - \frac{c_3}{2}\partial_\mu\phi\,\partial^\mu\phi\Box\phi + \alpha_{\rm V}\frac{\phi}{M_{\rm pl}}T, \tag{2.100}$$

where $g_{\mu\nu} = \eta_{\mu\nu} + h_{\mu\nu}$, $\left(\mathscr{E}h\right)_{\mu\nu}$ is the Lichnerowicz operator and all contractions are made with the Minkowski metric. The equation of motion for a static non-relativistic source of density

[26] Note that another coupling to matter of the form $\gamma T^{\mu\nu}\partial_\mu\pi\partial_\nu\pi$ is also allowed. Neglecting it does not alter the main features of the screening mechanism and we will not consider it here.

[27] One is a term linear in π and this is often neglected in the literature.

$\rho(r)$ and mass M is

$$\frac{1}{r^2}\frac{\mathrm{d}}{\mathrm{d}r}\left(r^3\left[\left(\frac{\pi'}{r}\right)+2c_3\left(\frac{\pi'}{r}\right)^2\right]\right)=\alpha_{\mathrm{V}}\frac{\rho}{M_{\mathrm{pl}}}, \tag{2.101}$$

where a prime denotes a radial derivative and we have assumed spherical symmetry. We are interested in the field-profile outside the source and there are two limits to consider. At large enough distances from the source (exactly how large we will quantify presently) the first term dominates and the solution is

$$\frac{\mathrm{d}\pi}{\mathrm{d}r}\approx\alpha_{\mathrm{V}}\frac{M}{4\pi M_{\mathrm{pl}}r^2} \tag{2.102}$$

so that the fifth-force is

$$F_\pi=2\alpha_{\mathrm{V}}F_{\mathrm{N}} \tag{2.103}$$

and so this limit corresponds to an unscreened fifth-force that is a factor of $2\alpha_{\mathrm{V}}$ larger than the Newtonian force. The opposite limit, valid when the second term dominates yields the solution

$$\frac{\mathrm{d}\pi}{\mathrm{d}r}=\left(\frac{\alpha_{\mathrm{V}}}{c_3}\right)^{\frac{1}{2}}\left(\frac{M}{8\pi M_{\mathrm{pl}}}\right)^{\frac{1}{2}}r^{-\frac{1}{2}}. \tag{2.104}$$

In this case the fifth-force is

$$\frac{F_\pi}{F_{\mathrm{N}}}=2\alpha_{\mathrm{V}}^2\left(\frac{r}{r_{\mathrm{V}}}\right)^{\frac{3}{2}}, \tag{2.105}$$

where the *Vainshtein radius* is

$$r_{\mathrm{V}}=\left(\frac{c_3\alpha_{\mathrm{V}}M}{2\pi M_{\mathrm{pl}}}\right)^{\frac{1}{3}}. \tag{2.106}$$

Equating the two terms in equation (2.101), we see that this is precisely the radius dividing the two regimes derived above. One can then see that inside the Vainshtein radius where equation (2.105) is valid, the fifth-force is screened relative to the Newtonian force by a factor of $(r/r_{\mathrm{V}})^{3/2}$. Writing the Vainshtein radius in terms of the Schwarzchild radius $r_{\mathrm{Sch}}\equiv M/4\pi{M_{\mathrm{pl}}}^2$ we have $r_{\mathrm{V}}=(\alpha_{\mathrm{V}}L^2r_{\mathrm{Sch}})^{1/3}$, with $L^2=2M_{\mathrm{pl}}c_3$. The strongest constraints on L^2 currently come

from lunar ranging in the Earth-Moon system[28]. [101] and [102] have used data from [103] to constrain

$$L \gtrsim 150\alpha_V^{-\frac{3}{2}} \text{ Mpc.} \tag{2.107}$$

We are interested in theories where $\alpha_V \sim \mathcal{O}(1)$ and so taking this to be the case, the Vainshtein radius for a solar mass object is[29]

$$r_V^{\odot} \gtrsim \mathcal{O}(10^3) \text{ pc.} \tag{2.108}$$

The radius of the solar system is of order 10^{-4} pc and so the presence of the sun alone is enough to screen any smaller objects within the entire solar system and beyond. Unlike the chameleon models described above, astrophysical objects necessarily have Vainshtein radii that vastly exceed their extent and the orbital radii of their satellites. This makes potential astrophysical tests scarce[30] and it is for this reason that we describe this mechanism as more efficient than chameleon-like screening.

[28] See [100] for a review of lunar ranging.

[29] The reader may be confused that the Vainshtein radius appears to be universal for any object of a given mass. This is because we have ignored the fact that any object has a finite extent and instead integrated equation (2.101) to an arbitrary radius outside the object ignoring the sudden reduction in the density. Accounting for the finite-extent of objects does induce changes in the Galileon field profile [104, 105], however these are small and there is nothing to be gained here by including them.

[30] Although see [24, 106, 107] for a discussion of potential astrophysical effects.

Part I:
Astrophysical Tests of Modified Gravity

Because, sir, upon the strength of the strong nuclear interaction rests the rate at which hydrogen fuses to helium in the core of the Sun. If the interaction strengthens even unnoticeably, the rate of hydrogen fusion in the Sun will increase markedly. The Sun maintains the balance between radiation and gravitation with great delicacy and to upset that balance in favor of radiation, as we are now doing—" "Yes?" "—will cause an enormous explosion. Under our laws of nature, it is impossible for a star as small as the Sun to become a supernova. Under the altered laws, it may not be.

Isaac Asimov, *The Gods Themselves*

My candle burns at both ends;
It will not last the night;
But ah, my foes, and oh, my friends—
It gives a lovely light.

Edna St. Vincent Millay

3

Equilibrium Stellar Structure in Modified Gravity

In the previous chapter we examined the general properties of screened modified gravity and discussed the criteria that determines whether an object is screened or not. Armed with this knowledge, the purpose of the next three chapters is to search for novel astrophysical effects of these theories and to use them to place new constraints as well as discuss future tests using upcoming experiments. In section 2.2.6 we argued that objects with $\Phi_{\rm N} \lesssim \mathcal{O}(10^{-6})$ may be unscreened and suggested main- and post-main-sequence stars as potential candidates. In this chapter we will lay down the theoretical groundwork for calculating how stars behave in modified theories of gravity. Specialising to chameleon-like models, we will then discuss potential observational signatures and present a numerical tool for predicting the structure and evolution of stars for arbitrary values of χ_0 and α that is accurate enough to compare with observational data.

Before proceeding to perform any technical calculations, the new physics arising from stellar structure in modified gravity can be discerned from simple physical considerations. Stars are spheres of gas that reach an equilibrium configuration with a constant radius by

burning nuclear fuel in their cores to create a pressure gradient that combats the inward gravitational force and prevents collapse. Now consider a star in modified gravity compared with an identical star in general relativity[1]. This star feels a stronger gravitational force in its outer layers and hence requires a larger pressure gradient to combat the extra inward force. It hence needs to burn more fuel in its core per unit time in order to provide this gradient. One would therefore expect two new features: first, since a star of fixed mass has a finite supply of fuel this will be depleted faster and the star will have a shorter life-time on any evolutionary phase. Second, the increased burning rate will release more energy per unit time and so we expect that individual stars will be brighter.

First, we will present the equations of motion governing hydrodynamics in modified theories of gravity. This will apply equally to conformal scalar-tensor theories such as chameleon models and those that screen using the Vainshtein mechanism like galileons. The static equations describe the equilibrium structure of stars and perturbations about this configuration describe their oscillations. At the level of the equilibrium structure, theories that screen via the Vainshtein mechanism are too efficient to show novel effects in any environment and so we will subsequently specialise to chameleon-like theories and derive the modified equations of equilibrium stellar structure. At the level of linear perturbations, it is possible that oscillating stars may source scalar radiation in Vainshtein screened theories and so we will return to the general case when discussing the linear perturbations in chapter 5.

Next, we derive the modified gravity analogue of the Lane-Emden stellar structure models presented in chapter 1. In this chapter we will only focus on main-sequence stars since their structure can be solved analytically using Lane-Emden models. We investigate the new properties of these stars in modified gravity, predict the magnitude of the luminosity enhancement and lifetime reduction and discuss possible observational tests of these predictions. We do this by using a simple model of main-sequence stars, the Eddington Standard model, which

[1]We will see later that the notion of identical stars in different theories is somewhat subjective. It depends on which quantities one wishes to keep fixed and in some cases cannot be defined at all. Nonetheless, the analogy presented here is still apt and captures the main idea underpinning stellar structure tests of modified gravity.

is an $n = 3$ Lane-Emden polytrope. Using this, we calculate the luminosity enhancement and lifetime as a function of stellar mass and χ_0 for $f(R)$ gravity ($\alpha = 1/3$, see section 2.2.2). Individual main-sequence stars cannot be resolved outside the Milky Way and we have already argued in section 2.2.6 that only dwarf galaxies in cosmic voids are unscreened. Hence, any test related to these predictions must rely on their contribution to the galactic properties such as the spectra, the luminosity and the colour. In particular, since the constituent stars are brighter we expect that dwarf galaxies in voids will be brighter than those in clusters and therefore looking for systematic offsets between a sample of galaxies in voids and clusters is a potential observational probe of these predictions. This, in theory, should be possible using the screening maps of [96] although to date no such analysis has been performed and so here we present only the theory. We estimate the galactic luminosity enhancement by integrating the stellar luminosity found using the Eddington standard model weighted with the initial mass function (IMF). Both the Eddington standard model and this simple calculation have several drawbacks and are not accurate enough to compare with real data and so a more realistic numerical simulation is needed. In the final part of this chapter we present the details and results of the implementation of the modified gravity equations into the publicly available stellar structure code MESA [108, 109]. This is powerful enough to allow a comparison with data and although this modified gravity version has not yet been used to predict the modified galactic properties[2] it will be used in subsequent chapters to provide models that have been compared with data to place the strongest constraints to date.

3.1 Modified Gravity Hydrodynamics

Hydrodynamics is the study of the motion and thermal properties of bulk fluids described by collective quantities such as the pressure, density, temperature etc. under the motion of external forces. In stellar structure described by general relativity the main contribution to

[2] This is an ambitious project and is currently in progress. Any results are still a long way off.

the dynamics comes from the effect of the inward gravitational force, although other effects such as convection, semi-convection, winds and thermohaline circulation may be important in certain post-main-sequence stars. When one moves to a modified theory of gravity, the nature of the gravitational force is altered leaving all other properties such as nuclear reaction rates, the opacity and convection unaltered[3]. This is the essence of stellar structure tests of modified gravity: Only the gravitational physics is altered, the other sectors are unchanged. Therefore, the only equation to be altered is the fundamental force-law and no others.

We have already seen that chameleon-like theories screen according to the Newtonian potential of the object and we have also argued in section 2.2.6 that since $\chi_0 \lesssim 10^{-6}$ we only expect to see novel effects in objects with Newtonian potentials less than $\mathcal{O}(10^{-6})$. Neutron stars have potentials of order 10^{-1} and are hence screened in these theories (although see [41] for a novel effect where the star may become slightly unscreened over Hubble times). The status of these stars in Vainshtein screened theories is not certain, although given that they screen incredibly efficiently in high densities it is likely that any effects are negligible. Hence, we will deal only with non-relativistic stars where the general relativity corrections are of order $\Phi_N \ll 1$ and will solve the Newtonian force law for the motion of the fluid elements and not the full Tolman-Oppenheimer-Volkov equation.

We will describe bulk quantities such as the pressure and density in the *Eulerian picture*, where these quantities are to be considered as fields which give the value of said quantities at any point in space as a function of time. In contrast, we will describe the position of individual fluid elements (and, when needed, the pressure perturbation) in the *Lagrangian picture*, where the motion of individual fluid elements are followed as a function of time. In this case, the

[3]In fact, these can differ between identical screened and unscreened stars but this is a second order effect. The radial profiles of these quantities depends on the solution of the stellar structure equations which is different between the two stars but the equations governing their physics are identical in both cases. It is also the case that changing the theory of gravity can result in changes due to quantum effects such as a shift in the atomic energy levels. These changes are at most comparable with the changes due to general relativity — which are known to be negligible — and hence do not affect the stellar properties.

Lagrangian position $\mathbf{r}$ of a fluid element satisfies the (non-relativistic) momentum equation:

$$\frac{\partial^2 \mathbf{r}}{\partial t^2} = -\frac{1}{\rho}\nabla P + \mathbf{F}, \tag{3.1}$$

where $P(\mathbf{r})$ is the pressure, $\rho(\mathbf{r})$ is the density and $\mathbf{F}$ is the external force density. In modified gravity, the fluid moves under its own Newtonian gravity and the fifth-force (2.12) due to the scalar field so that

$$\frac{\partial^2 \mathbf{r}}{\partial t^2} = -\frac{1}{\rho}\nabla P - \frac{GM(r)}{r^3}\mathbf{r} - \frac{\beta(\phi)}{M_{\rm pl}}\nabla\phi, \tag{3.2}$$

where $\beta(\phi) = M_{\rm pl}\,\mathrm{d}\ln A/\,\mathrm{d}\phi$ for chameleon-like theories and $\beta(\phi) = \alpha_{\rm V}$ for Vainshtein screened theories. This is the only hydrodynamical equation that is altered relative to general relativity; changing gravity only changes the motion of the fluid elements and does not directly alter other processes such as mass conservation, energy generation and radiative transfer. The quantity $M(r)$ ($r \equiv |\mathbf{r}|$) is the mass enclosed inside a radius r from the centre, and is given via the Poisson equation

$$\nabla^2\Phi_{\rm N} = 4\pi G\rho(r), \tag{3.3}$$

which may be integrated once to give

$$\frac{\mathrm{d}\Phi_{\rm N}}{\mathrm{d}r} = \frac{GM(r)}{r^2}. \tag{3.4}$$

Since mass is a locally-conserved quantity we also have the continuity equation:

$$\frac{\partial\rho}{\partial t} + \boldsymbol{\nabla}\cdot(\rho\mathbf{v}) = 0, \tag{3.5}$$

where $\mathbf{v} \equiv \mathrm{d}\mathbf{r}/\,\mathrm{d}t$ is the velocity of the fluid element. In general, one must also consider the energy generation and radiative transfer equations but these are only important if one wishes to study the effects of perturbations coupled to stellar atmospheres, which is irrelevant in the context of modified gravity. We will include their effects when describing the equilibrium

stellar configuration in order to produce the correct equilibrium stellar properties, however, we will not include them in our perturbation analysis. Since they do not depend on the theory of gravity, they are identical to equations (1.52) and (1.53) at the background level. At the level of perturbations, we will work in the so-called *adiabatic* approximation, where the density and pressure evolve according to

$$\frac{\mathrm{d}P}{\mathrm{d}t} = \frac{\Gamma_1 P}{\rho}\frac{\mathrm{d}\rho}{\mathrm{d}t}. \tag{3.6}$$

The quantity

$$\Gamma_1 \equiv \left(\frac{\mathrm{d}\ln P}{\mathrm{d}\ln \rho}\right)_{\text{adiabatic}} \tag{3.7}$$

is the *first adiabatic index*. It is of paramount importance to the study of stellar pulsation and stability and we will return to discuss it later on in chapter 5.

It is important to note that the first adiabatic index is not simply the equation of state relating $P_0(r)$ to $\rho_0(r)$ and in particular is not equal to the adiabatic index described in equation (1.54) for polytropic gasses, although in very simple cases the two may be equal. It describes the response of the pressure to *adiabatic* compressions whereas the adiabatic index is simply a relation between the density and the pressure and quite often relies on different assumptions. In particular, whilst it is true that simple gasses have equations of state $P \propto \rho^\gamma$ with $\gamma = 4/3$ $(5/3)$ for relativistic (non-relativistic) gasses it is not necessarily the case that $\Gamma_1 = 4/3$ indicates a relativistic system. In fact, it means that the energy from adiabatic compressions are not raising the density like a simple non-relativistic gas. One example of this is the progenitor of a type II supernova where the gas is non-relativistic but Γ_1 drops to $4/3$ because the pressure does not increase upon compression, instead, the rate of photo-disintegration of iron is increased. Another example is the He^+ ionisation region of Cepheid stars where pressure does not change upon a compression but the ionisation fraction is increased.

3.1.1 Equilibrium Structure

The equilibrium stellar configuration is both static and spherically symmetric and can be found by setting time-derivatives to zero and $\mathbf{r} = r$ in the hydrodynamic equations so that this is now the Eulerian radial coordinate. We will denote all equilibrium quantities with a subscript-zero except for $M(r)$, which is defined at the background level only. It is important to note that χ_0 is not a property of the star but is the cosmological value of χ_c found by evaluating (2.74) using the cosmological values of ϕ and β. In what follows, $\phi_0(r)$ is the equilibrium field-profile throughout the star and not the cosmological value. With no time-dependence, (3.5) is trivially satisfied and $\rho(r,t) = \rho(r)$. This simple form of the density profile allows us to find the mass enclosed in any given radius:

$$\frac{\mathrm{d}M(r)}{\mathrm{d}r} = 4\pi r^2 \rho_0(r). \tag{3.8}$$

The momentum equation (3.2) then reduces to the *modified hydrostatic equilibrium equation*

$$\frac{\mathrm{d}P_0(r)}{\mathrm{d}r} = -\frac{GM(r)\rho_0(r)}{r^2} - \frac{\beta(\phi_0)\rho_0(r)}{M_{\rm pl}}\frac{\mathrm{d}\phi_0(r)}{\mathrm{d}r}. \tag{3.9}$$

Physically, this equation describes the pressure profile the star must assume in order for the star to support itself against gravitational collapse. The second term is the fifth-force due to the scalar field; stars in modified gravity need to provide larger pressure gradients in order to combat this extra inward component [27, 89, 110]. These equations are then supplemented by the radiative transfer equation

$$\frac{\mathrm{d}T_0(r)}{\mathrm{d}r} = -\frac{3}{4a}\frac{\kappa(r)}{T_0^3}\frac{\rho_0(r)L_0(r)}{4\pi r^2}, \tag{3.10}$$

which describes how the temperature $T(r)$ varies due to the flux of energy with luminosity $L(r)$ away from regions of energy generation governed by

$$\frac{\mathrm{d}L_0}{\mathrm{d}r} = 4\pi r^2 \rho_0(r)\epsilon(r), \tag{3.11}$$

where $\epsilon(r)$ is the energy generation rate per unit mass. As mentioned above, these are identical to the equations coming from general relativity and are repeated here for completeness.

3.2 Lane-Emden Stars

Lane-Emden stars are perfect tools for studying the effects of modified gravity without the complications of non-gravitational physics. They are spheres of gas that have collapsed under their own gravity to reach a static equilibrium configuration, which is set by the interplay of the pressure and gravitational physics alone. They are not realistic enough to compare with real stellar data but all of the essential new physics is made transparent through their study and this serves as a direction for potential observational probes using more complete numerical models. In this section we will present a general framework for calculating their properties in screened modified gravity.

From here on we will specify to the case of chameleon-like theories and assume the fifth-force profile (2.73). Since we are only concerned with the equilibrium structure in this chapter, we will drop the subscript zeros. We will restore them in chapter 5 where we discuss perturbations about this equilibrium. In this case, the modified hydrostatic equilibrium equation (3.9) becomes

$$\frac{\mathrm{d}P}{\mathrm{d}r} = -\frac{GM(r)\rho(r)}{r^2}\left[1+\alpha\left[1-\frac{M(r_s)}{M(r)}\right]H(r-r_s)\right]. \tag{3.12}$$

Since this is the only equation that is modified we can follow the same derivation in section 1.5.2 to arrive at the equivalent of the Lane-Emden equation. Before doing this however, an examination of equation (3.12) reveals that the equations of stellar structure are no longer

self-similar in modified gravity; there is a second length scale r_s appearing and a second mass scale $M(r_s)$ and so continuing blindly will result in solutions that cannot have every dimensionful quantity scaled out. This means the new solution cannot be directly compared with the general relativity results. If we wish to make a meaningful comparison we must make an approximation that preserves self-similarity and so we will make the approximation that $G \to G(1+\alpha)$ in the region exterior to the screening radius, which is equivalent to ignoring the factor of $M(r_s)/M(r)$ in equation (3.12). This means that in any stellar model we compute over-estimates the effects of modified gravity, however this is not as bad an approximation as it may first seem; the precise stellar structure is not observable and most observable properties are those defined at the surface where this approximation is strongest.

Making this approximation and following the same steps as section 1.5.2 we arrive at the modified Lane-Emden equation:

$$\frac{1}{y^2}\frac{\mathrm{d}}{\mathrm{d}y}\left[y^2\frac{\mathrm{d}\theta}{\mathrm{d}y}\right] = -\begin{cases} (1+\alpha)\theta^n, & y > y_s, \\ \theta^n, & y < y_s, \end{cases} \tag{3.13}$$

where y_s is the Lane-Emden screening radius such that $r_s = r_c y_s$. The boundary conditions are identical to the general relativity case, namely $\theta(0) = 1$ and $\theta'(0) = 0$ where a prime denotes a derivative with respect to the Lane-Emden coordinate y, whose definition (as well as the definition (1.57) of r_c) is (1.56) unchanged in modified gravity. For convenience, we introduce the quantities

$$\omega_R \equiv -y_R^2 \left.\frac{\mathrm{d}\theta}{\mathrm{d}y}\right|_{y=y_R} \quad \text{and} \tag{3.14}$$

$$\omega_s \equiv -y_s^2 \left.\frac{\mathrm{d}\theta}{\mathrm{d}y}\right|_{y=y_s}, \tag{3.15}$$

which are the modified gravity analogues of equation (1.61). We have already seen in subsection (1.5.2) that in general relativity ($\alpha = \chi_0 = 0$, $\omega_R = \omega_s$) there is a unique solution for

any given value of n. We will denote the general relativity values of y_R and ω_R by $\bar{y}_R$ and $\bar{\omega}_R$ respectively. In modified gravity, there is a two-dimensional space of solutions at fixed n given by specific values of χ_0 and α, each with different values of ω_R, ω_s, y_s and y_R. This is a consequence of the fact that, despite our approximation, the modified Lane-Emden equation is still not self-similar. Self-similarity is weakly broken by the screening radius, which still appears as a second length scale in the problem. Despite this, a meaningful comparison with general relativity can still be made provided one is very careful about exactly which quantities are fixed in both cases and is clear about what is actually being compared. We will return to this point when discussing specific solutions. Using these definitions, we can find the mass of the star:

$$M = \int_0^R 4\pi r^2 \rho(r)\,\mathrm{d}r = 4\pi r_c^3 \rho_c \left[\frac{\omega_R + \alpha\omega_s}{1+\alpha}\right], \tag{3.16}$$

where we have used the modified Lane-Emden equation. This differs from the general relativity expression (1.60) in that it does not simply depend on ω_R and the central density. Instead, it depends on the screening radius (and hence χ_0) and α as well. Hence, Lane-Emden models with fixed mass, χ_0 and α correspond to stars with different central densities to those of the same mass in general relativity.

Equation (2.75) gives the screening radius once the density profile and χ_0 is specified. By writing the density in the Lane-Emden variable θ and using the modified Lane-Emden equation (3.13), we can calculate the integral exactly to find an implicit relation for ω_s (and hence the screening radius) in terms of χ_0, M and R:

$$\frac{\chi_0}{GM/R} \equiv X = \left[\frac{y_R\theta(y_s) + \omega_R - \frac{y_R}{y_s}\omega_s}{\omega_R + \alpha\omega_s}\right], \tag{3.17}$$

where we have used equation (3.16) to replace the factors of r_c and ρ_c with M. One can see how it is the ratio of χ_0 to $\Phi_N = GM/R$ that determines the screening radius and not simply the density. As $r_s \to 0$[4], the star becomes increasingly unscreened, $\omega_s \to 0$ and $\theta(y_s) \to 1$.

[4]Strictly speaking, we should impose $r_s/R \to 0$ since r_s is a dimensionful quantity.

This gives the maximum value of X where the star is partially screened. For values greater than this, equation (3.17) has no solutions and the star is always unscreened. From (3.17), we have

$$X_{\rm max} = \frac{y_R + \omega_R}{\omega_R} \tag{3.18}$$

independent of α. Later on, we will specify to the cases $n = 1.5$ and $n = 3$ and so for future reference we note here that $X_{\rm max} \approx 2.346$ for $n = 1.5$ and $X_{\rm max} \approx 4.417$ for $n = 3$.

3.3 Main-Sequence Stars

In this section we will use $n = 3$ polytropes to describe the structure of main-sequence stars in modified gravity. We have already alluded to the fact that the structure itself is not observable. What is observable is the galactic luminosity and, as discussed above, we expect that there will be systematic offset between the luminosity of dwarf galaxies in cosmic voids and those in clusters. The first step towards calculating this is to find the luminosity enhancement of an individual unscreened star compared with its screened counterpart as a function of the stellar mass and χ_0. We will restrict to $f(R)$ theories by setting $\alpha = 1/3$ from here on, however the method can be applied to any other value without the need for any modifications.

3.3.1 Scaling Relations

Before proceeding to solve the stellar structure equations, we can gain a lot of physical intuition into the behaviour of unscreened stars by using simple scaling relations[5]. We have already seen that the stellar structure equations are self-similar in general relativity and that a fully unscreened object can be described by $G \to G(1+\alpha)$ and hence the same is true for any unscreened star. Self-similarity implies that we can replace each quantity e.g. pressure, density, mass etc. by some characteristic quantity multiplying a dimensionless function and use

[5] See [111] for a nice discussion on how scaling relations can be used to provide a similar intuition for how stars behave when other physics is altered.

the equations to derive relationships between these quantities. For example, we can replace the pressure by setting $P = P_c x_P(r)$ where P_c is the central pressure. As an example, making these replacements in the hydrostatic equilibrium equation (1.50) leads to the relation

$$P_c \frac{dx_P}{dx_r} = -\frac{GM^2 x_M x_\rho}{R^4 x_r^2}, \tag{3.19}$$

where we have set $\rho = M/R^3 x_\rho$. Now since all the functions or derivatives of the x_i functions are dimensionless this gives us the scaling relation

$$P_c \propto \frac{M^2}{R^4}. \tag{3.20}$$

Here we ignored the factor of G because it is constant but what happens if we allow it to vary by a constant factor i.e. we change our star from one described by general relativity to an unscreened star in a theory of modified gravity with coupling α? In this case we obtain a new scaling relation

$$P_c \propto \frac{GM^2}{R^4}. \tag{3.21}$$

We know that the equations of stellar structure do not close and so one must specify an equation of state relating the pressure to the density and temperature. Main-sequence stars are predominantly supported by two sources of pressure. Gas pressure is the thermodynamic pressure associated with the motion of the individual atoms, which we take to be well-described by the ideal gas law

$$P_{\rm gas} = \frac{k_B \rho T}{\mu m_H}, \tag{3.22}$$

where m_H is the mass of a hydrogen atom and μ is the mean molecular weight, which represents the average number of particles (nucleons and electrons) per unit hydrogen mass. Gas pressure is the dominant contribution to the pressure in low mass stars. Radiation pressure is the pressure due to the absorption of photons propagating through the gas and is given by

integrating the Planck distribution for radiation in thermal equilibrium:

$$P_{\text{rad}} = \frac{1}{3} a T^4. \tag{3.23}$$

Radiation pressure is the dominant contribution to the pressure in high mass stars. Using these two expressions to find additional scaling relations, one can use these in conjunction with the scaling relations found from the hydrostatic equilibrium and radiative transfer equations to find the mass-luminosity scaling relation

$$L \propto \begin{cases} G^4 M^3 & \text{gas pressure} \\ GM & \text{radiation pressure} \end{cases}. \tag{3.24}$$

We can then find the luminosity enhancement for an unscreened star of fixed mass relative to a screened one:

$$\frac{L_{\text{unscreened}}}{L_{\text{screened}}} = \begin{cases} (1+\alpha_0)^4 & \text{low mass stars} \\ 1+\alpha_0 & \text{high mass stars} \end{cases}. \tag{3.25}$$

One can see that low mass stars receive a large luminosity enhancement when they are unscreened (recall $(1+\alpha) = 4/3$) whereas higher mass stars receive a not so large (but still $\mathcal{O}(1)$) enhancement. Whereas more radiation is being released in high mass stars per unit time, more is being absorbed to provide the pressure and hence cannot escape to the surface and so the stellar luminosity is not as affected. We therefore expect the luminosity enhancement as a function of stellar mass will decrease with increasing mass and, in particular, we expect a sharp turn-off when the radiation pressure comes to dominate. We will see precisely this below.

3.3.2 The Eddington Standard Model

The Eddington standard model is a simple set of assumptions about main-sequence stars that allows us to compute their properties by solving one simple modified Lane-Emden equation rather than an entire system of coupled equations. It makes the simplifying assumptions that the opacity is constant and due mainly to electron scattering $\kappa(T,\rho) \equiv \kappa_{\rm es}$[6] and that the radiation entropy $S_{\rm rad} = 4aT^3/3\rho$ is constant throughout the star. This allows us to simplify the equations considerably since the temperature is now a function of density only, and hence the pressure is barotropic. We assume that the pressure is a combination of the gas and radiation pressure only and so we have

$$P = \frac{1}{3}aT^4 + \frac{k_{\rm B}\rho T}{\mu m_{\rm H}} \tag{3.26}$$

and we introduce the ratio of the gas pressure to the total pressure[7]

$$b \equiv \frac{P_{\rm gas}}{P} \tag{3.27}$$

so that $P_{\rm rad} = (1-b)P$. Equating $bP_{\rm gas}$ with $(1-b)P_{\rm rad}$ we find

$$T^3 = \left(\frac{3k_{\rm B}}{a\mu m_{\rm H}}\right)\frac{1-b}{b}\rho. \tag{3.28}$$

Now in theory b could be a function of the radius, however the Eddington standard models' assumption implies that T^3/ρ is constant and hence so is b. In this case equation (3.26) can be written

$$P = K(b)\rho^{4/3} \tag{3.29}$$

[6]This is a good approximation for most main-sequence stars except the lowest mass stars, which require Kramer's opacity law $\kappa \propto \rho T^{-3.5}$.

[7]This quantity is often denoted by β in the astrophysics literature. Since β has already been used to denote the coupling we shall use b here.

where the constant

$$K(b) = \left[\frac{3}{a}\left(\frac{k_{\rm B}}{\mu m_{\rm H}}\right)^4 \frac{(1-b)}{b^4}\right]^{1/3}. \tag{3.30}$$

We can hence see that the Eddington standard model is a $\gamma = 4/3$ or $n = 3$ polytrope and we can solve for its structure in modified gravity by solving the modified Lane-Emden equation (3.13) to find the structure of the star then using the radiative transfer equation (3.10) to calculate the luminosity.

We begin by calculating the surface luminosity. Differentiating equation (3.23) and substituting the radiative transfer equation (3.10) we have

$$\frac{{\rm d}P_{\rm rad}}{{\rm d}r} = -\frac{\kappa_{\rm es}\rho L}{4\pi r^2}. \tag{3.31}$$

Setting $P_{\rm rad} = (1-b)P$ in the modified hydrostatic equilibrium equation for $r > r_{\rm s}$ and retaining the factor of $M(r_{\rm s})/M(r)$ so that we do not over-estimate the luminosity too much by making the approximation $G \to G(1+\alpha)$ we have

$$\frac{{\rm d}P_{\rm rad}}{{\rm d}r} = -\frac{(1-b)\alpha_{\rm eff} GM\rho}{r^2}; \quad \alpha_{\rm eff} \equiv \alpha\left[1 - \frac{M(r_{\rm s})}{M(r)}\right] \tag{3.32}$$

from which we find the surface luminosity by equating the two expressions at the surface:

$$L = \frac{4\pi(1-b)\alpha_{\rm surf} GM}{\kappa_{\rm es}}; \quad \alpha_{\rm surf} \equiv \alpha_{\rm eff}(R) = \alpha\left[1 - \frac{M(r_{\rm s})}{M}\right]. \tag{3.33}$$

We will see shortly that whereas b is constant throughout a given star, its value depends on χ_0 and α and hence there are two sources of luminosity enhancement in main-sequence stars. First, the factor of $\alpha_{\rm surf}$ gives an enhancement due to the increased rate of nuclear burning. Second, the ratio of gas to radiation pressure changes. Physically, the factor of $1-b$ is present because the luminosity is due only to radiation and not the gas. Next, we must find the constant b, which at this stage is still unknown. This can be found by using the polytropic

relation (3.29) at $r = 0$ in the definition of r_c (1.57) to find

$$r_c^3 = \left(\frac{1}{\pi G}\right)\frac{K(b)^{\frac{3}{2}}}{\rho_c}, \tag{3.34}$$

which can be used in the formula for the mass (3.16) to find

$$4\pi K(b)^{\frac{3}{2}}\left(\frac{1}{\pi G}\right)^{\frac{3}{2}}\left[\frac{\omega_R + \alpha\omega_s}{1+\alpha_0}\right]. \tag{3.35}$$

Now we would like to make contact with the general relativity case in order to compare with modified gravity stars and so we note that this corresponds to the fully screened case so that $r_s = R$. In this case we have $\omega_R = \bar{\omega}_R \approx 2.02$. In the other extreme case where the star is fully unscreened ($r_s = 0$) $\omega_s = 0$ and by rescaling $\xi \to (1+\alpha)^{-1/2}$ to bring the modified Lane-Emden equation into the standard form (1.59) we have $\omega_R \approx 2.02(1+\alpha)^{-1/2}$. It is convenient to define a function α_b that interpolates between these two cases:

$$1 + \alpha_b = \left((1+\alpha)\frac{\bar{\omega}_R}{\omega_R + \alpha_0\omega_s}\right)^{2/3}, \tag{3.36}$$

such that when $r_s = R$, $\omega_R = \omega_s = \bar{\omega}_R$ we have $\alpha_b = 0$ and when $r_s = 0$ the star is fully unscreened and $\alpha_b = \alpha$. We can then invert equation (3.35) using equation (3.30) to find

$$\frac{1-b}{b^4} = (1+\alpha_b)^3\left(\frac{M}{M_{\rm edd}}\right)^2, \tag{3.37}$$

where the Eddington mass is

$$M_{\rm edd} = \frac{4\pi^{1/2}}{G^{3/2}\bar{\omega}_R}\left(\frac{3}{a}\right)^{1/2}\left(\frac{k_B}{\mu m_H}\right)^2, \tag{3.38}$$

which is defined in terms of fundamental constants and the general relativity Lane-Emden solution and is hence independent of α. Numerically, $M_{\rm edd} = 18.3\mu^{-2}M_\odot$. In general relativity, equation (3.37) is known as *Eddington's quartic equation* and here we will refer to it by the

same name.

We now have a system of equations that close. The only technical difficulty is that the screening radius is defined implicitly via equation (3.17), which requires us to know the structure of the star. Now the structure of the star can only be computed once we know the screening radius and so one must use an iterative procedure. This requires the mass-radius relation (2.80) $R \propto M^{0.88}$[8]. Given a star of fixed mass M we can calculate GM/R. We then fix the value of χ_0 and α and assume some test screening radius. This allows us to solve the modified Lane-Emden equation numerically and extract the values of ω_R and ω_s. We then use these in equation (3.17) to calculate X. Next, we iterate through different screening radii until $X = \chi_0/(GM/R)$, in which case we have found the correct screening radius and so the solution of the modified Lane-Emden equation is the correct one. Using ω_R and ω_s, we can calculate α_b and $\alpha_{\rm surf}$ using

$$\frac{\alpha_{\rm surf}}{\alpha} = 1 - \frac{M(r_s)}{M} = \left[\frac{\omega_R - \omega_s}{\omega_R + \alpha}\omega_s\right], \tag{3.39}$$

which can be used in Eddington's quartic equation with the value $\mu = 0.5$, which assumes only fully ionised hydrogen and is appropriate for main-sequence stars, to calculate b. Once we have this, equation we can use equation (3.33) to calculate the luminosity of the star relative to the same star in general relativity

$$\frac{L}{L_{\rm GR}} = \frac{1 - b(\alpha, \chi_0)}{1 - b(\alpha = 0, \chi_0 = 0)}\alpha_{\rm surf}. \tag{3.40}$$

By calculating this for stars of different masses and different χ_0 (recall we are fixing $\alpha = 1/3$) we can numerically fit the enhancement as a function of these two parameters. We have already seen that the star will be fully unscreened when $X = 4.417$ and so it is convenient to

[8]Technically, $n = 3$ polytropes do not have a mass radius relation and the relation we take here assumes an extra component not included in the Eddington standard model, namely nuclear burning. Without the assumption of such a relation it is not possible to compare stars of fixed mass in general relativity and modified gravity or even between stars with two different values of χ_0 and α. The choice of a mass-radius relation is tantamount to deciding to compare the properties of two stars of fixed mass and radius for a given value of χ_0 and α.

use the rescaled quantity $X_3 \equiv \chi_0/(4.417GM/R)$ such that $0 \leqslant X_3 \leqslant 1$. The relation between α_b and α can then be recast as

$$\alpha_b(1+\alpha_b) = \alpha(1+\alpha)f(X_3;\alpha) \tag{3.41}$$

and

$$\frac{\alpha_{\rm surf}}{\alpha} = g(X_3;\alpha), \tag{3.42}$$

where the fitting functions f and g take values between 0 and 1. Numerically, we find

$$\begin{aligned} f(X_3;\alpha=1/3) &= X_3^2(1.94+0.79X_3-2.91X_3^2+1.18X_3^3), \\ g(X_3;\alpha=1/3) &= \sqrt{-\frac{13}{14}+\sqrt{\frac{169}{196}+\frac{20X_3}{7}}}\,. \end{aligned} \tag{3.43}$$

We plot the luminosity enhancement of a star for a given value of χ_0 and $\alpha = 1/3$ in figure 3.1 for $\chi_0 = 1\times10^{-6}$, 5×10^{-6}, 1×10^{-5} and 1×10^{-4}. Several features that we have already discussed are immediately obvious. Firstly, the ratio is always greater than unity; stars are indeed brighter in modified gravity than in general relativity as we argued at the start of this chapter. We also remarked that the Sun has $\Phi_{\rm N} \sim 2\times10^{-6}$ and that according to equation (2.81) lower mass stars have lower Newtonian potentials and so are more unscreened whilst the converse is true for higher mass stars. This is evident in the figure where one can see that the curves with $\chi_0 \sim \mathcal{O}(10^{-6})$ are more unscreened (show higher luminosities) at lower masses. The other two curves with $\chi_0 \geq 10^{-5}$ show a sharp turn-off of the luminosity enhancement at low masses. This is the effect we predicted in section (3.3.1) where we argued that high mass stars are dominated by radiation pressure, which shows a dramatically lower luminosity enhancement. This is the reason for the sharp turn-off: these stars are radiation dominated whereas their general relativity doppelgängers are gas dominated. Increasing χ_0 at fixed α results in stronger pressure gradients, larger temperatures and a higher surface luminosity and so its effects are degenerate with increasing the stellar mass. For this reason, unscreened

stars are more radiation supported than their screened counterparts and the reduction in the luminosity enhancement begins at smaller stellar masses when χ_0 is increased. At low stellar masses, these upper curves flatten out and saturate at a value $(4/3)^4 \approx 3.16$ which is precisely the value we predicted in section (3.3.1) for a fully unscreened, gas pressure-supported star relative to the same star in general relativity. Using the mass-radius relation, the Newtonian potential scales as $\Phi_N \propto M^{0.2}$ and so decreasing the stellar mass also decreases the Newtonian potential making the star more unscreened. When $X > 4.417$, equation (3.17) has no solutions and the star is fully unscreened. Since a fully unscreened star cannot become even more unscreened, lowering the mass (and Newtonian potential) beyond the point where $X = 4.417$ has no further effect and hence the curves flatten off. Finally, we note that when $\chi_0 \sim 10^{-6}$ there is little enhancement in the luminosity. This reflects the fact that these stars all have $\Phi_N \sim \chi_0$ and are heavily screened. Nevertheless, it is important to note that they are not completely screened as the simple aphorism $\Phi_N = \chi_0$ implies screening would suggest. This is because the self-screening condition was derived assuming a fixed density sourcing a field profile whereas this formalism uses an iterative procedure to account for the back reaction of the field on the density. We can see that when a star is treated as a dynamical object that adjusts its equilibrium configuration to match the effects of the fifth-force the object is not as unscreened as one might have näively expected. This means that there are still astrophysical signatures of modified gravity coming from main-sequence stars even at $\chi_0 = 10^{-6}$.

3.3.3 Effects on the Galactic Properties

So far, we have yet to discuss the reduced stellar lifetime we predicted qualitatively at the start of the chapter. Since the stellar lifetime is related to the rate at which fuel is consumed in the core we cannot predict it using the Eddington standard model alone. Indeed, this is an $n = 3$ Lane-Emden star, which is a completely static configuration. In order to include time-dependence, one must use rate equations to calculate the energy generation and use equation (3.11). Since we will present a complete numerical model below that includes both

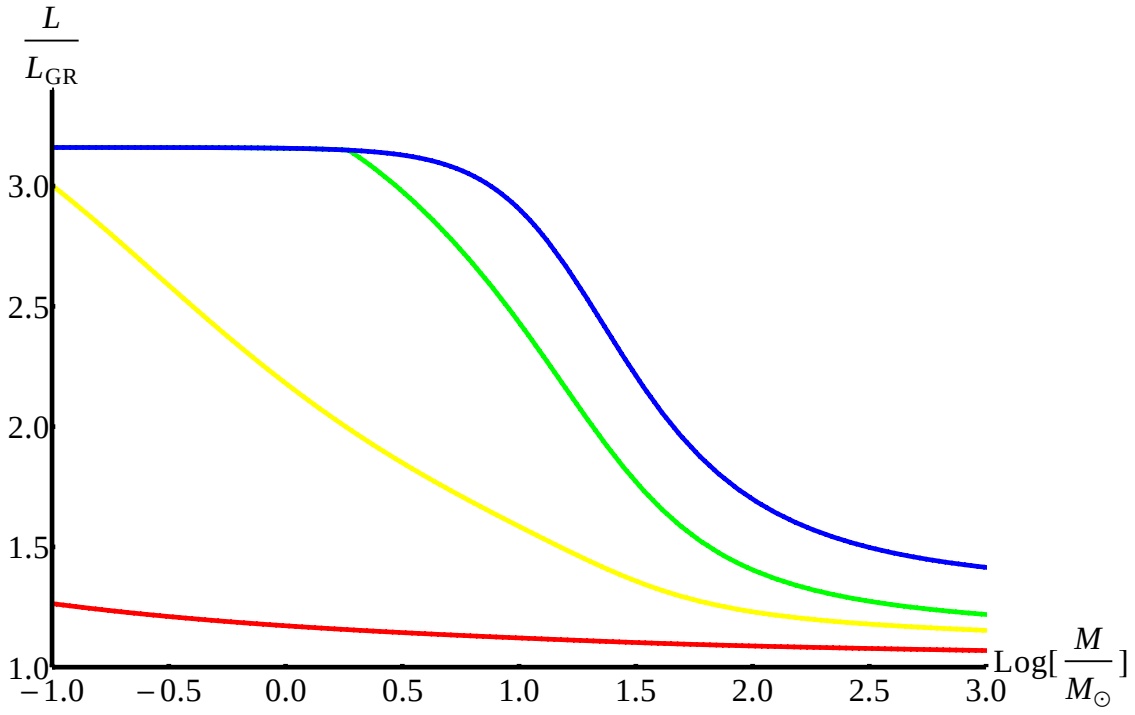


Figure 3.1: The ratio of the stellar luminosity of a partially screened star in $f(R)$ chameleon gravity compared with one that is completely screened as a function of stellar mass M. $L_{\rm std}$ is the luminosity of a completely screened (general relativity) star. From top to bottom: $\chi_0 = (10^{-4}, 10^{-5}, 5\times10^{-6}, 10^{-6})$.

time-dependence and does not use any of the other approximations we have made we will not attempt this here but will instead make a simple estimate. The main-sequence lifetime can be well approximated by

$$\tau_{\rm MS} \approx 10 \left(\frac{M}{M_\odot}\right)\left(\frac{L_\odot}{L}\right) \text{ Gyr} \tag{3.44}$$

and using equation (3.24) we have

$$\frac{L}{L_\odot} = (1+\alpha)^4 \left(\frac{M}{M_\odot}\right)^3 \tag{3.45}$$

for low-mass stars and so we can see that a fully unscreened solar-mass star in $f(R)$ gravity will go off the main-sequence more than three times as quickly than the same star whose structure is governed by general relativity. This has important observational consequences. Unscreened galaxies have hosted more generations of stars than screened galaxies of the same mass and

age and so we expect them to be more metal enriched and appear older.

A quantitative prediction of the properties of unscreened dwarf galaxies is not possible using this simple model since it does not keep track of the chemical evolution of the star. What is possible is a simple estimate of the enhancement of the galactic luminosity at fixed age and mass which we present below in order to demonstrate that this enhancement can be significant and merits further investigation.

The number of stars born with mass M within a galaxy is given by the initial mass function $\Phi(M) = \mathrm{d}N/\mathrm{d}M$, i.e. the number of stars dN within the mass range dM. This relation is empirically found to be roughly universal [9]. For simplicity we use the Salpeter IMF [112], $\Phi(M) \propto M^{-2.35}$ with $0.08M_\odot \leq M \leq 100M_\odot$. We can then estimate the luminosity increase for an unscreened dwarf galaxy by integrating the luminosity using the fitting functions (3.43) over the IMF.

Before doing so however, we must account for the stars that have gone off the main-sequence as the IMF only gives the number of stars born. We do this by making use of equation (3.44). If the age of the galaxy is τ_{age} then we assume that all stars with $\tau_{\text{MS}} > \tau_{\text{age}}$ contribute in their entirety to the luminosity whereas stars whose main-sequence lifetimes are less than the age of the galaxy contribute a fraction $\tau_{\text{MS}}/\tau_{\text{age}}$ of their luminosity. We note that stars that have gone off the main-sequence still have a luminosity enhancement in the red giant phase (and beyond), however we do not account for their contribution here due to the lack of an analytic model. In fact, these stars are brighter by several orders of magnitude than their main-sequence counterparts and so this is a conservative estimate. This effect is accounted for in by including a factor $f_0(M;\tau_{\text{age}})$ where

$$f_0(M;\tau_{\text{age}}) = \begin{cases} 1 & \tau_{\text{MS}} > \tau_{\text{age}} \\ \frac{\tau_{\text{MS}}}{\tau_{\text{age}}} & \tau_{\text{MS}} < \tau_{\text{age}} \end{cases} \tag{3.46}$$

[9] In principle, since the physics of gravitational collapse is expected to be encoded in the IMF, modified gravity may change its functional form. We do not attempt to investigate this here since the IMF is empirical and there is no successful analytic or numerical derivation of this function from known principles. Furthermore, it has been found to be universal in a number of very different environments and so we expect it to be largely robust.

so that the galactic luminosity is

$$L_{\rm gal}(\tau_{\rm age},\chi_0) = \int_{0.08M_\odot}^{100M_\odot} dM f_0(M,\tau_{\rm age}) L(M;\chi_0)\frac{{\rm d}N}{{\rm d}M}. \tag{3.47}$$

We can then immediately see that stars whose main-sequence lifetime are shorter than the age of the galaxy do not contribute to the luminosity enhancement since the factor of $L(M)^{-1}$ in the main-sequence lifetime exactly cancels the factor in the integral. Normalising the integrals so that the total luminous mass of screened and unscreened galaxies are identical (this is required in order to account for the fact that more stars have gone off the main-sequence in the unscreened case), one can perform the integral (3.47) to calculate the ratio of the luminosity enhancement of an unscreened dwarf galaxy compared to a screened one. As an example, in table 3.1 we show this ratio for a dwarf galaxy of mass $M_{\rm gal}$ =$10^{10}M_\odot$ and age $\tau_{\rm age}$ =13 Gyr for χ_0 in the range 10^{-6}–10^{-4} in $f(R)$ gravity. Table 3.1 reveals that the enhancement is

χ_0	Luminosity Enhancement
1x10^{-4}	42%
1x10^{-5}	42%
5x10^{-6}	29%
1x10^{-6}	3%

Table 3.1: The luminosity enhancement in unscreened relative to screened dwarf galaxies as a function of χ_0. All values were computed using the fitting formulae (3.43) and equation (3.46) in (3.47) taking $\alpha = 1/3$.

significant for $\chi_0 \gtrsim 10^{-6}$, which, as argued above, we would expect. The saturation around $\chi_0 \sim 10^{-5}$ is due to the effect of the decreased main-sequence lifetime. If χ_0 is around this value then, as seen in figure 3.1, the low mass stars are all completely unscreened and so increasing its value further cannot make them any more luminous. Hence, the luminosity enhancement saturates around this value. As noted in subsection 2.2.6, red giant stars are still

unscreened if $\chi_0 \lesssim 10^{-6}$ and so even at these low values of χ_0 it is possible that there will be a significant effect, for example, galaxies that have partially unscreened post-main-sequence stars and screened main-sequence stars will produce different spectra from those where all the stars are partially screened. This is beyond the scope of our present model since we cannot calculate the enhancement in post-main-sequence stars analytically.

In practice, one cannot observe two identical galaxies — one screened and the other not — and simply measure the difference in their luminosity. We would, however, expect there to be systematic differences between galaxies located in clusters and those in voids. By looking for these systematic differences it is possible that independent constraints on χ_0 in the range 10^{-4}–10^{-6} (or possibly lower) can be found.

3.4 Numerical Modelling of Stars in Modified Gravity

So far, we have presented a simple model of main-sequence stars in screened modified gravity and have used it to make simple estimates of the luminosity enhancement of both individual stars and dwarf galaxies compared with their general relativity counterparts. Along the way we were very careful to point out any shortcomings or approximations — and indeed there were many — and highlighted the fact that these models are not powerful enough to compare with observational data. For this, a more accurate treatment is required. There are computer programs that include all of the non-gravitational stellar physics neglected in our previous model that are powerful enough to be compared with current data and we have modified the publicly available code MESA [108, 109] to include the effects of modified gravity. Below, we briefly describe the implementation of modified gravity into this code and present some of the resultant predictions. A more detailed account of the implementation is given in appendix C.

MESA [108, 109] is capable of solving the complete system of stellar structure equations coupled to the radiative transfer system, stellar atmosphere models, nuclear burning networks, convective motion and micro-physical processes such as opacity and electron degeneracy. It

also includes effects such as overshooting, mass-loss and rotation in a fully consistent manner. Given some initial mass, it generates a pre-main-sequence stellar model and dynamically evolves it through the main-sequence and subsequent post-main-sequence to its final state, be it a white dwarf, neutron star or core-collapse supernova.

MESA is a one-dimensional code (in that it assumes spherical symmetry) that divides the star into a series of variable-length cells, each with a specific set of quantities such as temperature, density, mass fraction etc. that may correspond to the values at either the cell centre or boundary. Exactly which depends on the quantity in question, however it is always possible to interpolate between the two. We implement the effects of modified gravity by updating these assignments to include a cell-centred value of G, which differs from the Newtonian value in the region exterior to the screening radius. This implementation uses a quasi-static approximation where, given some initial radial profile, the star is evolved to its new equilibrium structure one time-step later. Using this profile, we integrate equation (2.75) to successively deeper cells until it is satisfied. The radius of this cell is then designated the screening radius and we then update the value of G in each cell according to equation (2.73) so that

$$G(r) = G\left[1 + \alpha\left(1 - \frac{M(r_s)}{M(r)}\right)\right] \quad r \geq r_s. \tag{3.48}$$

We then let the model evolve one time-step further to find the modified structure. This approximation is valid provided that the time-step between successive models is smaller than the time-scale on which changes to $G(r)$ are important and MESA provides a facility to ensure this is always the case. Furthermore, [110] have modified MESA for the same purpose of us using a scalar field ansatz and cell interpolation and we have verified that our results are indistinguishable from theirs.

In figure 3.2 we show the Hertsprung-Russell (HR) diagram for stars of one solar mass with initial metallicity $Z = 0.02$ (solar metallicity) evolving from the zero-age main-sequence (ZAMS) to the tip of the red giant branch for $\chi_0 = 5\times10^{-6}, 10^{-6}, 10^{-7}$ and $\chi_0 = 0$ (general rel-

ativity). It is clear from the tracks that stars that are less screened are indeed hotter and more luminous. We can also see that for $\chi_0 = 10^{-7}$ the tracks are identical along the main-sequence but separate in the red-giant phase corresponding to the Newtonian potential dropping due to the increased radius and the star becoming less screened. It appears that the red giant tracks all converge to a similar track. This is due to the fact that the Newtonian potential of these stars is so shallow that they are unscreened to a very high degree, even at $\chi_0 = 10^{-7}$. In fact, if one examines the tracks in detail, small differences can be discerned. One important question to address is: *How do we decide which two points on different tracks correspond to identical stars?* One should be careful which properties to compare if a meaningful comparison is to be made. This is often stars with identical temperatures and luminosities since these are the properties that are observed. In this case, the stars will have different ages, radii and chemical compositions. If instead one wishes to make a more theoretical comparison and ask which points along the tracks correspond to stars at identical evolutionary stages then a useful quantity is the core hydrogen mass fraction[10], whose evolution defines the main-sequence. If one compares two stars with identical core hydrogen mass fractions then the more unscreened star will be younger, brighter and hotter. To show this explicitly, we show the star's age and radius at three points along the star's main-sequence with identical core hydrogen mass fractions. Notice that it is clear that unscreened stars do indeed have shorter lives than their screened counterparts. It also shows that the radii at the same evolutionary stage tend to be smaller as well. Physically, the extra pressure needed to support the star in modified gravity is produced by increased densities and temperatures over the standard case, demanding a more compact star. We have not shown the values for $\chi_0 = 10^{-7}$ since these stars are almost entirely screened on the main-sequence and hence have nearly identical properties to the unmodified stars. Nor have we shown any information about the red giant phase. This is because the red giant phase is far shorter than the main-sequence and so comparing quantities between stars that are screened to different extents is misleading. Despite the assumptions of the simple model

[10]On the main-sequence. Quantities such as the helium mass fraction or core mass are more appropriate for post-main-sequence stars.

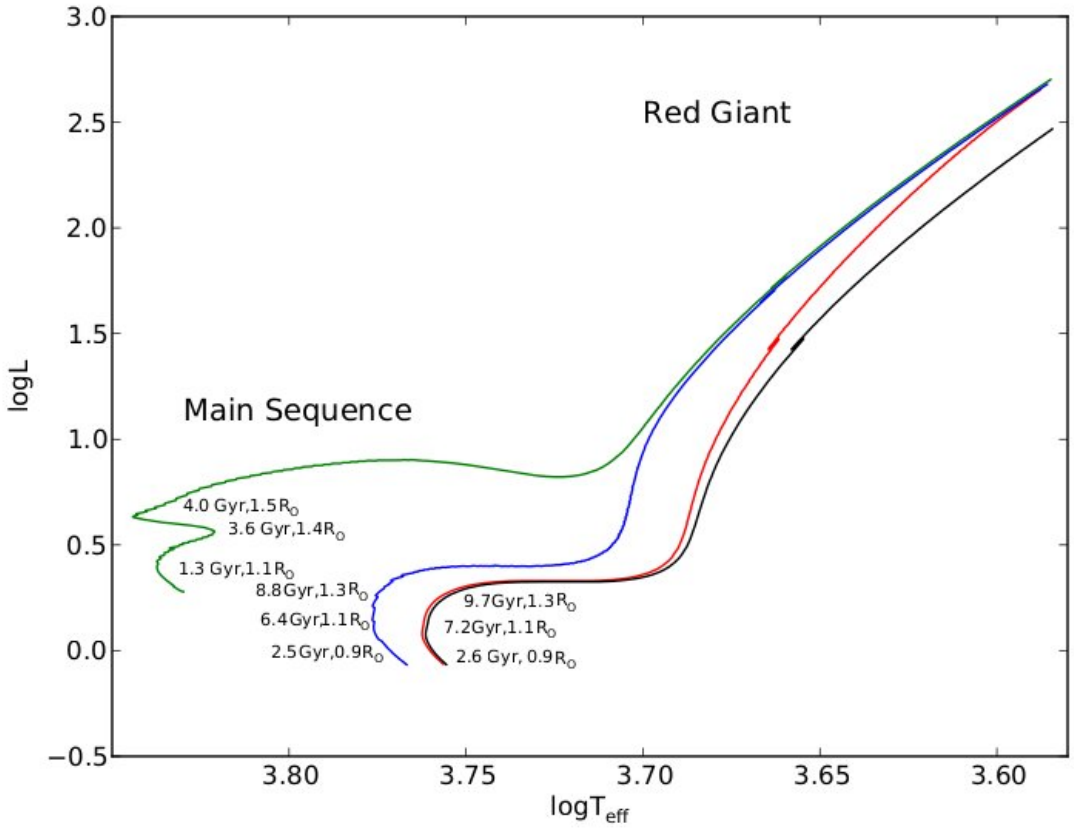


Figure 3.2: The Hertsprung-Russell diagram for stars of one solar mass with initial metallicity $Z = 0.02$. The black line shows the tracks for stars in general relativity while the red, blue and green tracks correspond to stars in modified gravity with $\chi_0 = 10^{-7}, 10^{-6}$ and 5×10^{-6} respectively. The radius and age at the point where the central hydrogen mass fraction has fallen to 0.5, 0.1 and 10^{-5} is shown for each star except the $\chi_0 = 10^{-7}$ case.

above, it is clear that the luminosity increase is still present when more realistic models are used and the missing physics is accounted for. This is a good example of how Lane-Emden models capture all of the new gravitational physics and that there are no major new features present when the non-gravitational physics is re-introduced.

Astrophysics is fun.

Eugene Lim

4

Distance Indicator Constraints on Modified Gravity

In this chapter we will change focus from main-sequence stars to post-main-sequence stars and how they can be used as probes of modified gravity. We will again focus on chameleon-like models and will make use of some of the tools presented in chapter 3.

4.1 Distance Indicators as Probes of Modified Gravity

To date, there are two main methods of probing screened modified gravity using dwarf galaxies. The first looks at their kinematics and morphology and has been presented in [91, 92]; currently these constraints are not competitive with others in the literature. The second uses distance indicators. Suppose one were to set about measuring the distance to a different galaxy from our own. Clearly we cannot measure this directly and so we must infer its value from other measurements. This requires us to use some formula for converting these measurements into the distance but where does this formula come from? There are two possibilities: either it is derived from our current theory or it is calibrated on objects either in our own galaxy or neighbouring ones in the local group. Either way, there is an implicit assumption that the

physics that governs objects in our own and neighbouring galaxies is the same in every other galaxy in the universe. Now chameleon-like theories of gravity do not posses this feature. The Milky Way and local group is screened but dwarf galaxies may not be. In this case, the formula used to infer the distance to these galaxies would not be correct if it depends on the theory of gravity. As an example, lets consider using the luminosity distance as a distance indicator and let us further assume that the galaxy we are interested in is near enough that cosmological effects can be neglected. In this case, one has

$$F = \frac{L}{4\pi d^2}, \tag{4.1}$$

where F is the flux and L is the luminosity of some object in the galaxy. Now the flux is a measured quantity, the number we measure is not sensitive to the theory of gravity but we need some method of inferring the luminosity. One such method is to use some standard candle where we can theoretically predict the value of L and we find that it is universal for all objects of the same type and that we use general relativity to predict its value. Now suppose that the laws governing gravity are different in this other galaxy to our own such that if we use general relativity we over predict the luminosity. The flux is a measured quantity that is insensitive to our theory of gravity and so given any predicted value of the luminosity we must adjust the inferred distance so that equation (4.1) is satisfied. Hence, we over-predict the distance compared with its true value. This means that if we compare the distance inferred using this method to the distance inferred using a different method that is independent of the theory of gravity, the two will only agree if we have used the correct theory of gravity to infer the first distance. Note also that if we had not predicted the luminosity but had instead measured it in nearby galaxies the conclusion would be the same and the two distances will only agree if the same law of gravity holds in the galaxies used to make the calibration.

The simple example above illustrates the premise behind distance indicator tests of modified gravity. We look for distance indicators that are sensitive to the theory of gravity that we

are interested in and make new predictions for the formula used to infer the distance using their properties; we refer to these as *unscreened distance indicators*. We then identify galaxies where we expect this theory of gravity to show strong deviations from general relativity, in this case dwarf galaxies in voids, and look for those with simultaneous distance measurements using *screened distance indicators*, which do not depend on the theory of gravity. Now the data generally gives distances to these galaxies and so what one must do is calculate the difference between distance predicted using the general relativity formula and the new theory. If one then takes the distance coming from the unscreened indicator and compares it with the measurement from the screened one there will be a discrepancy by a known amount if the theory of gravity is not general relativity because the distance calculated using the unscreened indicator has been found using an incorrect formula for that galaxy. The lack of any such deviation — or more realistically the agreement within errors — places new constraints on modified gravity.

This is exactly what we will do in this chapter and we will use three different indicators as probes: water masers, tip of the red giant branch (TRGB) distance indicators and Cepheid variable stars. We will describe each of these briefly below; a full account of these distance indicators may be found in [113].

4.1.1 Cepheid Variable Stars

Cepheid variable stars are stars of 3-10$M_\odot$ that have gone off the main-sequence and evolved onto the red giant phase. During this phase these star's tracks in the HR diagram undergo loops in the temperature direction at approximately constant luminosity. This is shown in figure 4.1 for stars in general relativity; the figure was produced using MESA. Whilst traversing these loops they cross a region in temperature known as the *instability strip*, which is shown in figure 4.1 as two black diagonal lines. Inside the strip, the star is unstable to *Cepheid pulsations* and pulsate with a period of $\mathcal{O}$(days). This gives rise to a variation in the star's luminosity and

there is a known period-luminosity relation calibrated on Cepheid stars in the local group:

$$M_V = a \log \tau + b(B - V) + c, \tag{4.2}$$

where M_V is the V-band magnitude, which is related to the total luminosity, τ is the period of oscillation and $(B - V) \propto \log T_{\rm eff}$, where $T_{\rm eff}$ is the effective temperature. This is the temperature inferred from the peak of the Planck spectrum for the light that reaches us from the photosphere of the star. This is the radius at which the optical depth becomes 2/3 so that the stellar atmosphere is optically transparent and light can escape. a, b and c are constants and $a \approx -3$ [113]. A complete theoretical model of the physics driving period-luminosity relation is still to be found, however equation (4.2) can be understood in a simple manner. Using simple scaling relations (we will show this explicitly in chapter 5) one can show that $\tau \propto (G\rho)^{-1/2}$ and so one can re-write equation (4.2) schematically as

$$\log L \propto \tilde{a} \log R + \tilde{b} \log T_{\rm eff} + \tilde{c}, \tag{4.3}$$

which gives $L \propto R^2 T_{\rm eff}^4$ (R is the stellar radius), which is nothing more than the Steffan-Boltzmann law.

Physically, the oscillations are the result of acoustic waves resonating within the star. Hydrostatic equilibrium is not exact and every star has a set of radial and non-radial eigenfrequencies for the propagation of internal waves. When these waves propagate adiabatically they can neither grow nor decay and are standing waves within the star. When the motion is non-adiabatic, these modes can be excited and the star can pulsate in one or a combination of these modes. The instability strip arises because various mechanisms act to drive these pulsations and the motion within the star is non-adiabatic. In the case of Cepheid stars, the pulsations are driven by the *kappa mechanism*. Stars on the blue loop contain a layer where the temperature is around 4×10^4 K. This corresponds to the ionisation potential of helium and so a small compression of the star will raise the temperature and allow more photons to

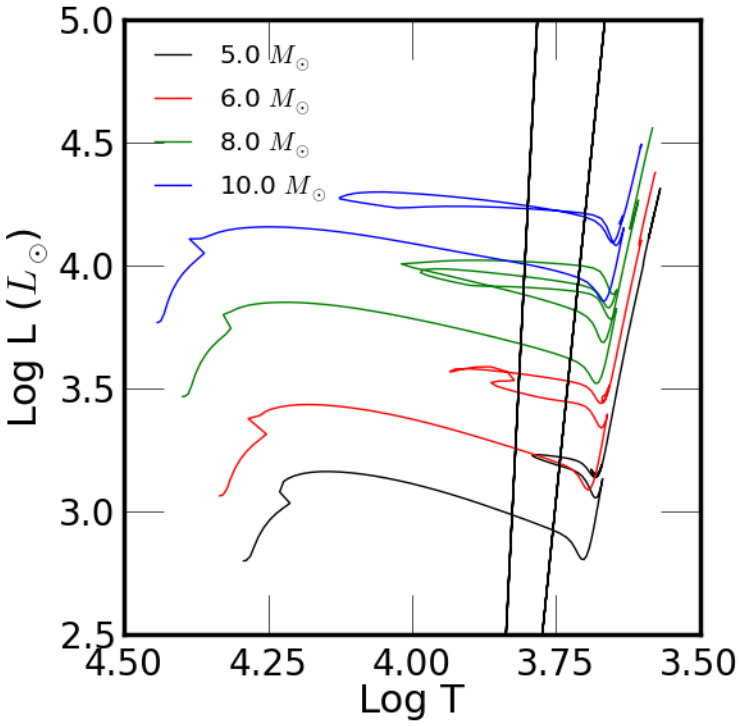


Figure 4.1: The evolution of Cepheid stars in the HR diagram. The instability strip shown in the black lines is taken from [114].

ionise helium in this layer. Usually, an increase in the temperature decreases the opacity (recall Kramer's law give $\kappa \propto T^{-3.5}$) but in this case the opacity increases upon compression. This means that heat is trapped in the layer upon a compression, damming up energy. Since the opacity has increased, more photons are absorbed and the stellar luminosity decreases. Upon an expansion, the converse is true, ionised helium recombines with free electrons releasing photons and the temperature decreases. These extra photons increase the luminosity of the star. This is the driving mechanism behind Cepheid pulsations but we still need to worry about whether the motion is adiabatic or not. If the motion is adiabatic then the photon number is conserved and the luminosity at the base of the ionisation zone must be equal to that at the top and hence the motion is damped. The blue edge of the instability strip corresponds to the motion becoming non-adiabatic inside the ionisation zone. In theory, the pulsations should occur at all temperatures lower than this, however convective effects act to damp the oscillations and the red edge corresponds to temperatures where this damping is non-negligible. In

what follows, we will use the instability strip given by [114]:

$$\log L = 4.2 - 46\left(\log T_{\rm eff} - 3.8\right) \quad \text{blue edge,} \tag{4.4}$$

$$\log L = 4.2 - 23\left(\log T_{\rm eff} - 3.7\right) \quad \text{red edge.} \tag{4.5}$$

We refer to the first time the star crosses the strip whilst moving on a blue loop as the first crossing and ignore the very brief crossing during the transition from the main-sequence to red giant phase. This phase is so short lived that only a handful of observations have been made here.

Cepheid distances have been calibrated using parallaxes for 10 Milky Way Cepheids in the distance range $\approx 0.3 - 0.6$ kpc, with periods ranging from $\approx 3 - 30$ days. The error on the mean distance is $\pm 3\%$ or 0.06 in magnitude. Outside the Local Group, where modified gravity effects may be present, Cepheid distances have been measured to over 50 galaxies. The final uncertainty in the distance modulus, which includes zero point calibration, metallicity, reddening and other effects, is ± 0.09 magnitude or 5% in distance.

4.1.2 Tip of The Red Giant Branch Stars

Stars of 1.5–2 $M_\odot$ do not exhibit blue loops. Instead they continue to ascend the red giant branch with an ever increasing luminosity and a decreasing temperature. After the star leaves the main-sequence its core is composed of neutral hydrogen surrounded by a thin shell where hydrogen burning continues. The temperature in the outer layers is too low to ignite the hydrogen there and so this is inert. This outer layer absorbs high-energy photons from the shell and expands the star to a radius 10–100 times that of its main-sequence progenitor, causing a decrease in the effective temperature. At this point, the entire stellar luminosity is due entirely to the shell. As more and more hydrogen is converted to helium, the core grows more massive and begins to contract, raising the temperature and further increasing the rate of hydrogen burning. Once the temperature in the core reaches $T \sim 10^8$ K helium may be

ignited and will burn to produce carbon and oxygen via the triple alpha process. This moves the star to the horizontal branch — where it has a higher temperature and lower luminosity — over a very small time-scale leaving a visible discontinuity. This is particularly pronounced in the I-band (the flux at 800 nm) and the discontinuity occurs at

$$I = -4.0 \pm 0.1 \tag{4.6}$$

independent of the stellar mass. The relation is robust over a large range of metallicities ($-2.2 < [\mathrm{Fe/H}] < -0.7$ dex) and the small error is due only to a weak dependence. This comes about because the core mass is weakly dependent on the metallicity. This makes the TRGB a standard candle: the luminosity can be inferred directly from the discontinuity since it is related to the I-band magnitude there and hence a distance can be found by measuring the flux and using equation (4.1).

TRGB distances have been measured to approximately 250 galaxies. These are applied to old, metal poor populations which enables distance estimates out to about 20 Mpc, slightly closer than Cepheid distances since TRGB stars are not as bright as Cepheids. However, since single epoch photometry is enough to measure the luminosity at the tip, it is much easier to obtain the data required for a TRGB distance estimate.

4.1.3 Water Masers

H_2O vapour orbiting in Keplarian motion in the accretion disk at a distance of $\mathcal{O}(0.1\ \mathrm{pc})$ from the central black hole of a galaxy has a far smaller number density of molecules than water vapour under terrestrial conditions. This means that the gas cannot achieve thermal equilibrium and hence population inversion can occur. If the galaxy has an active galactic nuclei then X-ray emission or shocks can cause a population inversion between the 6_{56} and 5_{23} rotational levels leading to microwave emission at 22.2 GHz ($\lambda = 1.35$ cm). Given the Keplarian orbits, a measurement of the centripetal acceleration, rotational velocity, angle on

the sky and the angle of inclination of the orbit can be used to obtain a geometric distance estimate. Before proceeding to discuss the more technical aspects of the measurement, we will elucidate the basic idea using a simple example. Figure 4.2 shows a simple illustration of one water maser in circular orbit around the central black hole. Since the orbit is Keplarian we have

$$a = \frac{v^2}{r}, \tag{4.7}$$

where a is the centripetal acceleration and v is the orbital velocity. Geometrically, we have

$$D = \frac{r}{\Delta\theta} \tag{4.8}$$

and so a measurement of v, a and $\Delta\theta$ allows us to infer the geometric distance to the galaxy. In fact, since we observe velocities and accelerations along the line of sight (LOS) we must correct for the inclination of the orbit. If the orbit is inclined at an angle i to the plane perpendicular to the line of sight we have $v_{\text{observed}} = v \sin i$ and $a_{\text{observed}} = a \sin i$, in which case the distance can be found using

$$D = \frac{v^2}{a\Delta\theta} \sin i, \tag{4.9}$$

where v and a are now the measured quantities.

In practice, one requires accretion disks that are edge-on since this allows for a complete measurement of the rotation curve, which, as we will see shortly, is necessary to infer the distance. This means there are relatively few water maser galaxies compared with those containing Cepheid and TRGB stars. In this work, we will only make use of the most studied galaxy, NGC 4258 [116], and so from here on we will concentrate on this galaxy only. The principle is similar for other galaxies and a full account of water masers can be found in [117]. NGC 4258 has a thin, slightly warped accretion disk whose shape has been well-studied (see [118] and references therein). This disk rotates at ≈ 1000 kms^{-1} and contains several masing clouds of water, which are classified into two types. Systemic masers are those on the near-edge of the disk and move with the systemic velocity of the galaxy (≈ 470 kms^{-1}). They drift in position

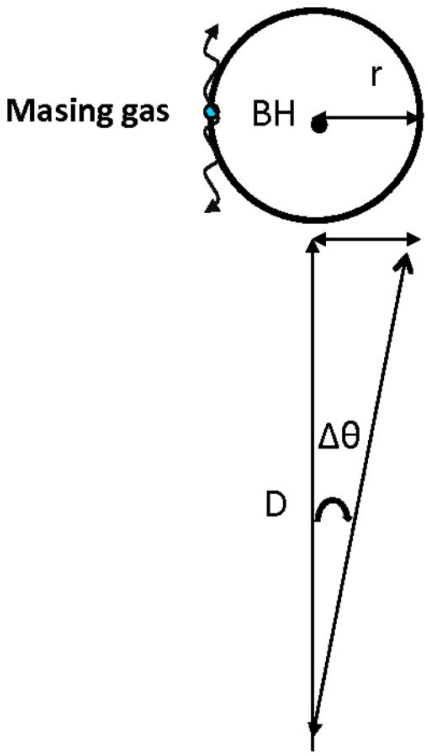


Figure 4.2: Masing gas orbiting the central black hole (labelled BH) at a distance D from an observer. Figure reproduced from [115].

and LOS velocity of 30 μas yr^{-1} and 9 kms^{-1} yr^{-1} respectively with respect to the motion of the disk. High-velocity masers are stationary with respect to the disk and hence show perfect Keplarian rotation curves. This is illustrated in figure 4.3. The rotation curve for the water masers in NGC 4258 is shown in figure (4.4). At small angles on the sky, one is observing the systemic masers, whose velocities are constant. As one moves outward in angle on the sky (impact parameter) the LOS velocity varies linearly since the component of the velocity along the line of sight is $v_{\rm LOS} = v \sin\theta \approx v\theta$. At larger angles on the sky one is observing the high velocity masers, which trace Keplarian orbits. Extrapolating the linear part of the rotation curve until it intersects the Keplarian curves then gives the LOS velocity at the systemic radius and the angle on the sky subtended by the systemic orbit $\Delta\theta$. The LOS velocity is measured using very long baseline interferometry and the acceleration is found using multi-epoch monitoring

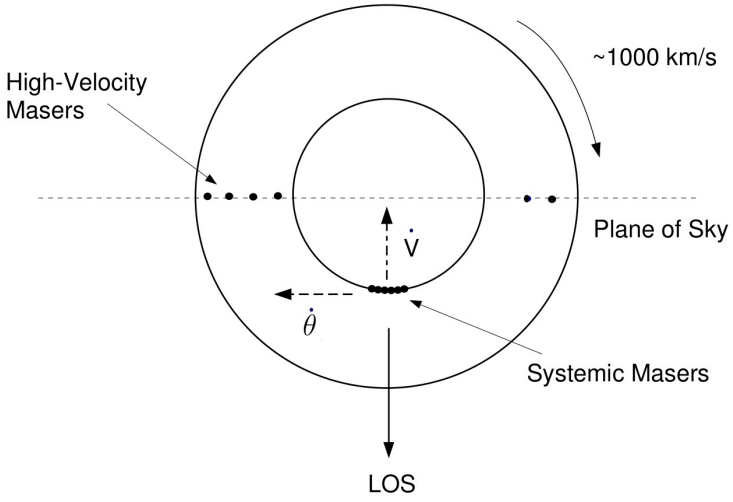


Figure 4.3: An illustration of the accretion disc and water masers in NGC 4258; the black dots show the position of individual masers. This figure has been adapted from [119].

of the maser spectra [1]. Furthermore, since the structure of the accretion disk is well-known, one can find the angle of inclination and make a geometric distance estimate using equation (4.9). Additionally, one can measure $\dot{\theta}$, the drift in position shown in figure 4.3. Since $v \approx D\dot{\theta}$ one can make a second, independent geometric estimate.

4.2 Distance Indicators in Modified Gravity

Water masers are generally found near the central black holes of galaxies and are mostly found in spiral galaxies. We have argued in section 2.2.6 that these are screened given our adopted constraint $\chi_0 < 10^{-6}$. Furthermore, the region around the central black hole in any galaxy has $\Phi_N \sim \mathcal{O}(10^{-5})$ and so water masers are screened distance indicators. Cepheids and TRGB distances are sensitive to modified gravity in different regimes and so below we will derive the effects on the distance estimates for each of these indicators.

[1] This is a complicated exercise in data analysis and fitting and is well beyond the scope of the current section. The interested reader is referred to [115].

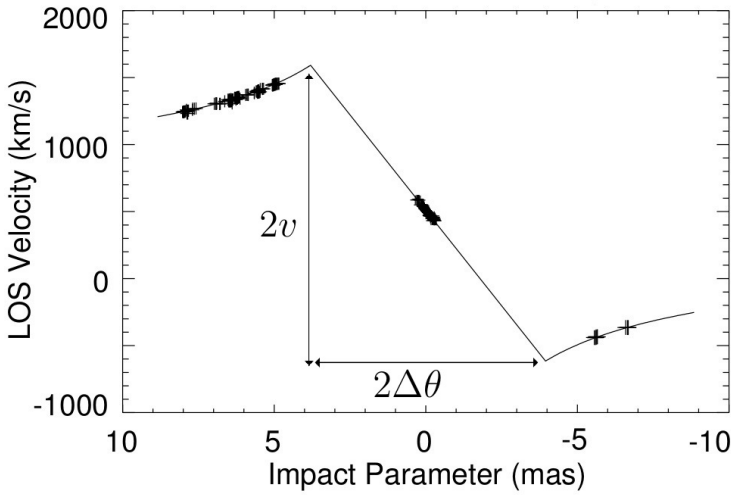


Figure 4.4: The rotation curve for NGC 4258. This figure has been adapted from [116].

4.2.1 Tip of the Red Giant Branch Stars in Modified Gravity

Näively, one would expect these to be screened distance indicators since the location of the tip depends on nuclear and not gravitational physics. In fact, modified gravity does effect the location of the tip if the hydrogen burning shell is unscreened, in particular, the luminosity at the tip is lower the more unscreened the shell. This is because the increased gravity in the shell leads to an enhanced rate of hydrogen burning, which causes the temperature to increase at a faster rate than the equivalent star in general relativity and hence the triple alpha process can begin at a lower effective temperature and surface luminosity. Ultimately, we will determine the magnitude of the difference using MESA, but the physics driving the change can be understood using a simple model.

It is a good approximation to treat the core as a solid isothermal sphere with temperature T_c and mass M_c. The hydrogen burning shell is incredibly thin and can be treated as having constant mass equal to the core value and luminosity L. In this case, the shell pressure and temperature is given by the hydrostatic equilibrium and radiative transfer equations,

$$\frac{\mathrm{d}P}{\mathrm{d}r} = -\frac{GM_c\rho(r)}{r^2}; \quad \frac{\mathrm{d}T^4}{\mathrm{d}r} = \frac{3}{4a}\frac{\kappa(r)\rho(r)L}{4\pi r^2}, \tag{4.10}$$

which can be used to find

$$P \propto \frac{GM_{\rm c}T^4}{L}, \tag{4.11}$$

where the opacity in the hydrogen shell is due mainly to electron scattering and so we have taken it to be constant. The pressure in the shell is due mainly to the gas and so we ignore radiation pressure and take the equation of state to be that of an ideal gas, $P \propto \rho T$. Using this and equation (4.11) in the radiative transfer equation we find

$$T(r) \propto \frac{GM_{\rm c}}{R_{\rm c}}, \tag{4.12}$$

where the integration constant is negligible near the base of the shell. Next, we can estimate the luminosity given an energy generation rate per unit mass $\epsilon \propto \rho(r)T(r)^{\nu}$

$$L = \int 4\pi r^2 \rho(r)\epsilon(r)\,{\rm d}r. \tag{4.13}$$

For temperatures above 10^7 K, which is the case in the shell, hydrogen burning proceeds mainly via the CNO-cycle and so $\nu = 15$. Using the equation of state and the results above in equation (4.13) one finds

$$L \propto \frac{G^{\frac{8}{3}}M_{\rm c}^{7.7}}{R_{\rm c}^6}. \tag{4.14}$$

Now suppose that the core or shell becomes unscreened so that $G(r) \approx G(1+\alpha_{\rm e})$ where

$$\alpha_{\rm e} = \alpha\left[1 - \frac{M(r_{\rm s})}{M(R_{\rm c})}\right] \tag{4.15}$$

is the effective value of α in the shell (see equation (3.48)). The helium flash occurs at a fixed temperature, independent of modified gravity, and so if we set $\xi = M_{\rm c}/R_{\rm c}$ at the point when $T_{\rm c} = 10^8$ K then we have $\xi_{\rm MG}/\xi_{\rm GR} = (1+\alpha_e)^{-1} < 1$. The ratio of the core mass to the core radius at the helium flash in modified gravity is then lower than that in general relativity. In general, this does not tell us anything about the core mass and radius individually,

however, in practice one finds that the core radius is the same in both cases (this is borne out by MESA simulations) and so this is a relation between the core masses at fixed temperature. Substituting equation (4.14) into (4.12) we can find the ratio of the shell luminosity in the unscreened case to the screened case such that the core temperature is identical. One finds

$$\frac{L_{\rm MG}}{L_{\rm GR}} = \frac{1}{(1+\alpha_{\rm e})^5}. \tag{4.16}$$

Since $\alpha_{\rm e} \geq 0$, the shell luminosity when the core is unscreened is lower than its value when the core is screened at fixed temperature. Hence, the peak luminosity, which corresponds to the temperature required for the onset of helium burning, is indeed lower in modified gravity.

Using MESA we find numerically that when $\chi_0 < 10^{-6}$ the shell is screened and the change in the peak luminosity is less than 1%, however when $10^{-6} < \chi_0 < 10^{-5}$ the core becomes increasingly unscreened and the change in the luminosity at the tip falls by 20% to 50% over this range[2]. This is shown in figure 4.5 where we plot the radial profile of $1 + \Delta G/G$ where $\Delta G = G(r) - G$ (see equation (3.48)) as a function of $x \equiv r/R$ for a $1.5M_\odot$ stellar model with $\alpha = 1/3$. It is evident that the hydrogen shell above the core feels the effects of modified gravity when $\chi_0 > 10^{-6}$.

Hence, TRGB distance indicators are screened when $\chi_0 < 10^{-6}$ and unscreened when $\chi_0 > 10^{-6}$. Using equation (4.1), failure to account for the reduced luminosity over-estimates the distance when $\chi_0 > 10^{-6}$.

4.2.2 Cepheid Distances in Modified Gravity

Cepheid distance estimates are found using the period-luminosity relation (4.2) and so in theory, one should derive the new period-luminosity relation in modified gravity. We shall take steps towards this in chapter 5, however, a full theoretical derivation of the relation requires sophisticated non-adiabatic pulsation models and are still not accurate enough to fit

[2]The dramatic change is due to the strong dependence on gravity in equation (4.16).

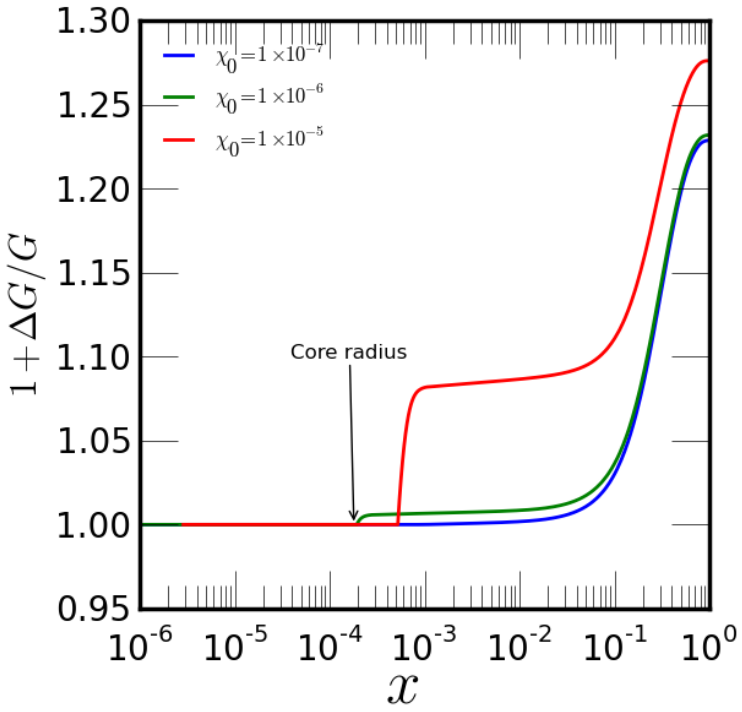


Figure 4.5: The radial profile of $1+\Delta G/G$. We have indicated the core radius for the $\chi_0 = 10^{-5}$ model. Note that since we are using the rescaled radius $x \equiv r/R$ the core radius does not necessarily occur at fixed x for different χ_0. Numerically, we find that the core radius is largely insensitive to the value of χ_0.

the current experimental data correctly and so here we will estimate the error in the distance estimate if the galaxy is unscreened by perturbing the empirically calibrated period-luminosity relation about the general relativity result. In particular, this means that we cannot address the question of whether the location of the instability strip changes by a significant amount in modified gravity, nor can we predict the new amplitude of the period-luminosity relation.

Now the period-luminosity relation is an empirically calibrated formula based on Cepheids in the local group and the Milky Way and so it is a formula derived using objects that behave according to general relativity. What happens if we then try to apply this to a galaxy where gravity is described by a different theory? As a simple example, let us consider changing the value of $G \to G + \Delta G$ for a constant ΔG. In order to use the period-luminosity relation to calculate the distance, one must measure the flux, the period and $B - V$. If one were to use the formula calibrated on systems described by general relativity, one would end up with

an incorrect value of M_V because stars with a fixed period and fixed effective temperature correspond to a different value of M_V if the theory of gravity is changed. If d_0 is the value of the distance that would be inferred had we used the correct formula (i.e. the true distance), using this incorrect formula will result in a different distance $d_{\rm MG}$ being inferred. Cepheid measurements are most robust at the blue edge of the instability strip and so when calculating $d_{\rm MG}$ we will always use MESA models at the first crossing of this edge. In practice, this means that when comparing stars in different theories, we are changing the luminosity of the star at fixed effective temperature. Using the definition of the V-band magnitude

$$M_V = -2.5 \log\left(\frac{L}{d^2}\right) \tag{4.17}$$

we have

$$\frac{\Delta d}{d} = -0.3\frac{\Delta G}{G} - 0.025\frac{\Delta L}{L} \tag{4.18}$$

where we have used $L \propto R^2$ at constant $T_{\rm eff}$ and $\Delta d = d_{\rm MG} - d_0$ with $\Delta d/d \equiv \Delta d/d_0$. Using MESA, we find that $\Delta L/L \ll 1$, in which case the main dependence comes from changing G. We then have

$$\frac{\Delta d}{d} \approx -0.3\frac{\Delta G}{G}; \tag{4.19}$$

if one tries to use the general relativity formula to infer the distance to a galaxy where gravity is stronger one will under-estimate the distance. Physically, the stars in these galaxies pulsate faster than in general relativity at constant temperature but they have an almost identical luminosity. Hence, using the general relativity formula is tantamount to over-estimating the magnitude at a fixed luminosity and hence inferring a smaller distance.

So far, we have assumed that the effective value of G is a constant but we know from equation (3.48) that this is not the case, G increases outward in the region exterior to the screening radius. This means that the magnitude of the deviation should be lower than that predicted using a constant change in G and so it is important to account for this. In chapter 5 we will perturb the equations of modified gravity hydrodynamics to calculate the new period

and so we can find $\Delta d/d$ in terms of $\Delta\tau/\tau$ but here we will do something simpler and use an appropriately averaged value of G so that $\Delta G = \langle G \rangle$. We will see in chapter 5 that this is in fact an under-estimate and so any constraints we obtain are conservative.

In 1950, Epstein [120] used numerical pulsation codes to find the relative importance of different regions of the star for driving pulsations (see figures 1 and 2 in [120]). Using the published values in [120], we have recreated this function $f(r)$ and normalised it such that

$$\int_0^R f(r)\,\mathrm{d}r = 1. \tag{4.20}$$

Figure 4.6 shows this as a function of the dimensionless radial coordinate $x \equiv r/R$. We then

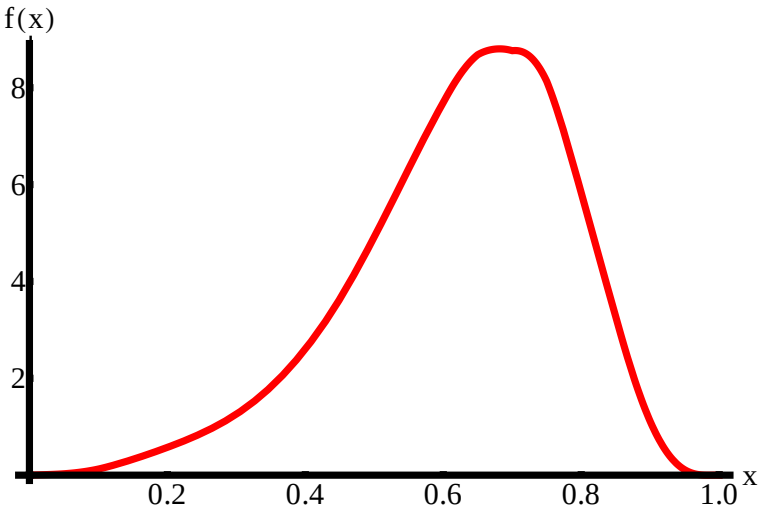


Figure 4.6: The normalised Epstein function $f(x)$ with $x \equiv r/R$. The function was reconstructed by interpolating the data in [120].

define the average value of G via

$$\langle G \rangle = \frac{1}{R}\int_0^R f(r)G(r)\,\mathrm{d}r \tag{4.21}$$

so that

$$\frac{\Delta G}{G} \equiv \frac{\langle G \rangle - G}{G}. \tag{4.22}$$

This procedure accounts for the fact that G is not constant throughout the star but does not

overly penalise the fact that the core is heavily screened because this region does not contribute significantly to the pulsations.

Using MESA, we find that (for $\alpha \sim \mathcal{O}(1)$) $\Delta G/G \sim \mathcal{O}(1)$ when $\chi_0 \gtrsim 10^{-8}$ depending on the stellar mass (higher mass Cepheids are more unscreened) and so we can use these stars to probe this parameter range. This is shown in figure 4.7, where we plot the radial profile of $1+\Delta G/G$ (again $\Delta G = G(r) - G$) for a $6M_\odot$ stellar model at the first crossing of the blue edge of the instability strip for $\alpha = 1/3$ and different values of χ_0. The gravitational enhancement drops rapidly when $\chi_0 < 4\times 10^{-7}$, however larger Cepheids ($M \sim 10M_\odot$) show enhancements when $\chi_0 \gtrsim 10^{-8}$.

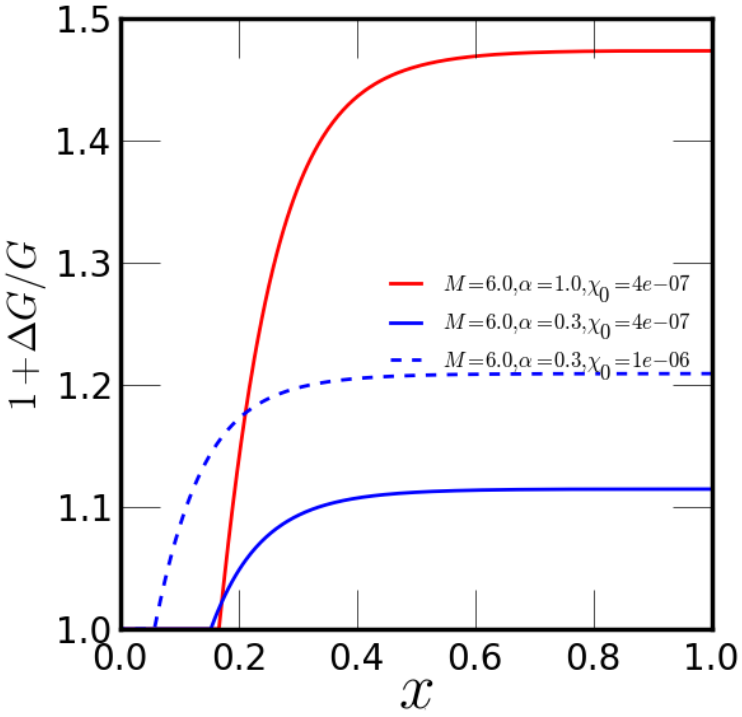


Figure 4.7: The radial profile of $1+\Delta G/G$ as a function of $x \equiv r/R$ for a $6M_\odot$ star at the blue edge of the instability strip. Different values of χ_0 are indicated and $\alpha = 1/3$ in each case.

4.3 Distance Indicator Constraints on Modified Gravity

We have argued above that water masers are screened distance indicators, TRGB stars are screened when $\chi_0 \lesssim 10^{-6}$ and Cepheid stars are screened when $\chi_0 \lesssim 10^{-8}$. This means that any deviation between water maser and TRGB distances can probe the range $\chi_0 > 10^{-6}$ and any deviation between TRGB and Cepheid stars can probe the range $10^{-8} < \chi_0 < 10^{-6}$. In theory, comparing water maser distances with Cepheid distances could also probe smaller values of χ_0. In practice there are no water maser distances to dwarf galaxies so this comparison is not currently possible. We will perform both of these tests below and will derive new constraints in each case.

4.3.1 Comparison of Water Maser and TRGB distances

Using MESA, we have evolved $1.5M_\odot$ stellar models to the onset of the helium flash for a variety of different values of χ_0 and α and compared the luminosity at the tip with that of the corresponding general relativity model. Using this, we can calculate $\Delta d/d = d_{\rm MG} - d_0$ using equation (4.1). In this case, $d_{\rm MG} = d_{\rm TRGB}$ is the incorrect distance found by assuming the general relativity luminosity at the tip and $d_0 = d_{\rm maser}$ is the correct, geometric distance found using water maser measurements. As an example of the size of the discrepancy, we tabulate the change in the luminosity at the tip and the value of $\Delta d/d$ for various different values of χ_0 and $\alpha = 1/3$ (corresponding to $f(R)$ models) in table 4.3.1. We have also varied α as well but these values are not given for brevity.

As discussed in section 4.1.3, there is only one galaxy for which we have simultaneous distance estimates from water masers and other methods: the spiral galaxy NGC 4258. The two distance estimates using the positional drift and the Keplarian motion methods agree within errors (see [116, 121]) and a comparison with the TRGB and Cepheid distance estimates

α	χ_0	$\log L/L_\odot$	$\Delta d/d$
0	0	3.34	0
1/3	1×10^{-6}	3.32	0.02
1/3	2×10^{-6}	3.30	0.04
1/3	4×10^{-6}	3.25	0.12
1/3	8×10^{-6}	<3	>0.20

Table 4.1: Change in the inferred distance using the TRGB indicator for $f(R)$ chameleon models for a $1.5M_\odot$ stellar model.

(taken from [113]) is shown below:

$$\text{NGC4258 Maser} : d = 7.2 \pm 0.2 \text{ Mpc} \tag{4.23}$$

$$\text{NGC4258 Maser} : d = 7.1 \pm 0.2 \text{ Mpc} \tag{4.24}$$

$$\text{NGC4258 Cepheid} : d = 7.18 \pm 0.07(\text{statistical}) \text{ Mpc} \tag{4.25}$$

$$\text{NGC4258 TRGB} : d = 7.18 \pm 0.13 \pm 0.40 \text{ Mpc.} \tag{4.26}$$

The distances agree within estimated errors that are at the few percent level for the maser distances and (allowing for systematics, which are not included in the Cepheid measurement) at the 5-10% level for Cepheid and TRGB distances. The agreement of TRGB and water maser distances probes $\chi_0 > 10^{-6}$. The precise range probed depends on the value of α and the stellar mass. For $\alpha = 1/3$ the range probed is $\chi_0 > 4\times10^{-6}$ and a typical star of mass $1.5M_\odot$, the TRGB luminosity is smaller by over 20%, corresponding to an inferred distance that is larger by over 10%. Thus, given the measurements above, $f(R)$ models with this parameter range are excluded. Shortly after this new constraint was presented in [89], [122] reported a new maser distance to NGC 4258 using the Keplarian method accounting for the warping of the accretion disk, elliptical orbits of the masers and orbital precession. This yielded an updated distance 7.60 ± 0.17 (random) ±0.15 (systematic) Mpc. Although not as good, this still agrees with the TRGB and Cepheid distances within errors and the conclusions are unchanged.

The agreement of the Cepheid distance with the water maser distances would probe $\chi_0 < 10^{-6}$ if the galaxy were not a spiral and the Cepheid was not screened. The megamaser cosmology project [123] will provide new maser galaxies and estimate their distance. Since the goal of this survey is to determine H_0 the morphology of the galaxies surveyed is not relevant and it is unclear whether this data will be suitable for testing modified gravity or indeed if masers can be found in galaxies with shallower Newtonian potentials.

Since TRGB distances vary from the general relativity value by larger amounts with increasing χ_0 the agreement of the maser and TRGB distances rules out the entire range $\chi_0 \gtrsim 10^{-6}$ for $\alpha \geq \mathcal{O}(1)$. Previously, this constraint had been assumed by demanding that the Sun or the Milky Way is unscreened but no comparison of data with theoretical models was ever attempted and these objects could have been blanket screened by the local group if $\chi_0 < 10^{-4}$. This is a new and independent constraint that resolved the debate as to how the Milky Way is screened: it is self-screening.

4.3.2 Comparison of Cepheid and TRGB distances

We now turn our attention to the parameter range $\chi_0 < 10^{-6}$, which can be probed by comparing TRGB distances, which are screened in this range, with Cepheid distances, which are not. We require simultaneous Cepheid and TRGB distances to the same galaxy, which we classify as screened or unscreened (this is a function of χ_0) using the screening map of [96] discussed in section 2.2.7. The TRGB and Cepheid data used here is taken from the literature; a full discussion of the various telescopes and experimental methods is given in [89] and references therein. In appendix B we list the various galaxies used in the comparison, their TRGB and Cepheid distance measurements as well as their literary references. In order to calculate theoretical predictions of $\Delta d/d$ for various χ_0 and α we evolve $6M_\odot$ stellar models of initial metallicity $Z = 0.004$ using MESA to the first crossing of the blue edge of the instability strip and apply the procedure detailed in section 4.2.2. As an example, we show both $\Delta G/G$ and $\Delta d/d$ for a selection of models used in the analysis in table 4.3.2. In this case

$\Delta d = d_{\rm Cepheid} - d_{\rm TRGB}$, $d_{\rm MG} = d_{\rm Cepheid}$ and $d_0 = d_{\rm TRGB}$.

α_0	χ_0	$\Delta G/G$	$\Delta d/d$
1/3	4×10^{-7}	0.11	-0.03
1/3	1×10^{-6}	0.21	-0.06
1/2	4×10^{-7}	0.17	-0.05
1/2	1×10^{-6}	0.34	-0.09
1	2×10^{-7}	0.21	-0.06
1	4×10^{-7}	0.45	-0.12

Table 4.2: Change in inferred distance due to the change in the Cepheid periods for different modified gravity parameters. In each case the quantities were computed using $6M_\odot$ stellar models with initial metallicity $Z = 0.004$.

As mentioned in the introduction to this chapter, the analysis of this data was performed by the other authors of [89] and so here we will only briefly describe the method, the interested reader is referred to [89] for the full details. We began with a sample of 27 galaxies with both TRGB and Cepheid distances taken from the literature. In general, we only use galaxies with several Cepheid distances, which are combined to give a lower error on the measurement. After removing one galaxy with only two confirmed Cepheids and one with a TRGB distance greater than 10 Mpc we are left with 25 galaxies. We perform a likelihood analysis on the data to estimate the best fit value of $\Delta d/d$. The best values and 1-σ errors are given in table (4.3) along with the reduced χ^2 and the number of galaxies. We included empirically estimated systematic errors in the estimate of the distance to each galaxy from multiple measurements, as well as in the average deviation $\Delta d/d$ for each sub-sample of galaxies. For the latter, we made the ansatz that each galaxy has an additional unknown systematic error that can be added in quadrature to the reported error. By further assuming that the systematic error was the same for each galaxy, we could estimate $\sigma_{\rm sys}$ iteratively such that the reduced χ^2 was unity. We found that the systematic error thus estimated is sub-dominant for the majority of galaxies. Figure 4.8 shows the observed period-luminosity relation for both the screened and

Table 4.3: Best fit values for $\Delta d/d$ and uncertainty σ in the fractional difference between Cepheid and TRGB distances for the screened and unscreened sub-samples. Our estimated σ includes systematic errors. The number of galaxies N in each sub-sample is given as is the reduced χ^2.

Sample	N	$\Delta d/d$	σ	Reduced χ^2
Unscreened	13	0.003	0.017	1.0
Screened	12	−0.005	0.022	1.3

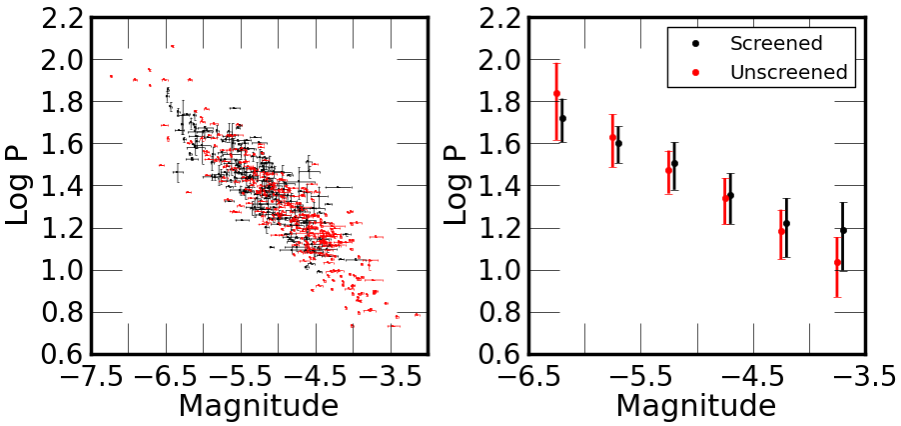


Figure 4.8: The period-luminosity relation for the galaxies in our sample; the black and red points denote screened and unscreened galaxies respectively. *Left panel*: we show all the Cepheids observed along with the reported error bars. *Right panel*: the mean period and dispersion within bins in absolute magnitude of size 0.5.

unscreened galaxies in our sample. There are no major differences evident and any disparity must be searched for using statistical methods.

Figure 4.9 shows the Cepheid distance compared with the TRGB distance for both sub-samples; both are clearly consistent and again one must use statistical methods to quantify any small discrepancies. As an example, the two green lines show the predictions for chameleon theories with coupling strength $\alpha = 1/3$ and $\alpha = 1$ and values of χ_0 as indicated in the caption. These two models are ruled out at over 95% confidence.

We have checked several sources of systematic errors in our analysis including metallicity corrections to the period-luminosity relation, different screening criteria for classifying galaxies into specific sub-samples, including only the best distance measurements to a specific

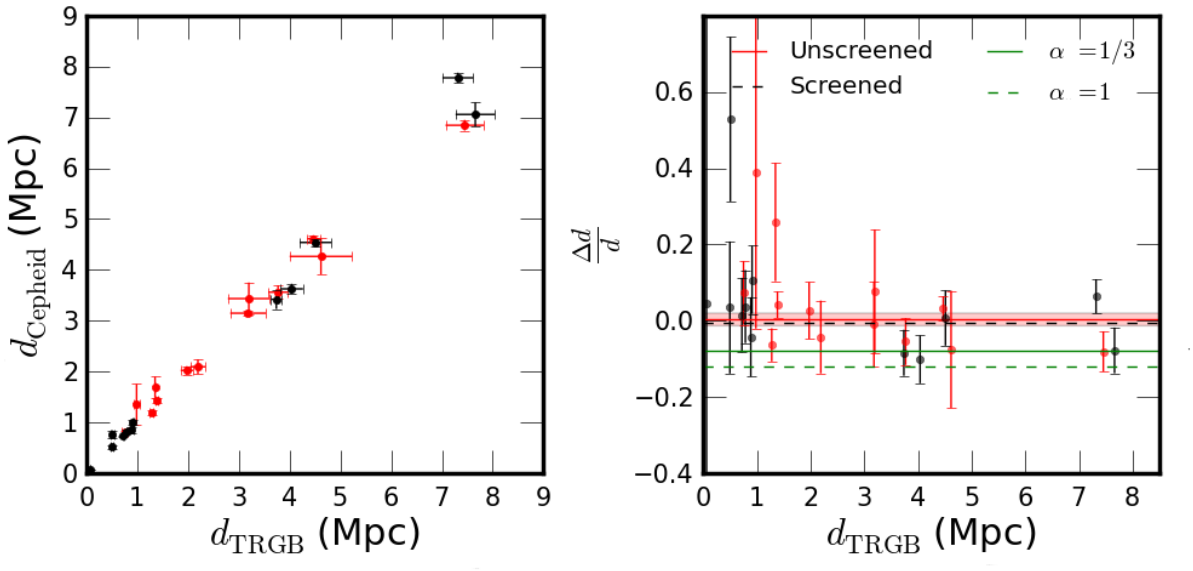


Figure 4.9: *Left panel:* A comparison of distances measured using the Cepheid period-luminosity relation and TRGB luminosities. The black and red points show galaxies from the screened and unscreened sub-samples respectively. *Right panel:* $\Delta d/d$, the fractional difference between Cepheid and TRGB distances, as a function of TRGB distance. The shaded region in the right panel shows the 68% confidence region around our best fit to the unscreened sample (red line). The best fit to the screened sample is shown by the dashed black line. Both sub-samples are consistent with the general relativity expectation of zero deviation. The dotted and dashed green lines show two possible predictions of chameleon theories with $\alpha = 1$, $\chi_0 = 4 \times 10^{-7}$ and $\alpha = 1/3$, $\chi_0 = 1 \times 10^{-6}$, which corresponds to $f(R)$ gravity.

galaxy and including galaxies we previously rejected (technical details can be found in [89]). In all cases, the best-fit line for $\Delta d/d$ moves in the opposite direction to that predicted by modified gravity i.e. more positive values and so we conclude that our analysis is robust to these sources of systematics.

Constraints

Whereas the modified stellar structure can be calculated in a model-independent way using χ_0 and α, the screening of dark matter haloes is model-dependent and this needs to be accounted for when constructing the screening map. So far, the map has been calibrated using chameleon N-body codes [96] and so this is where the most robust constraints can be found. In figure 4.10 we plot the regions in the χ_0–α plane that are excluded with 68% (light region)

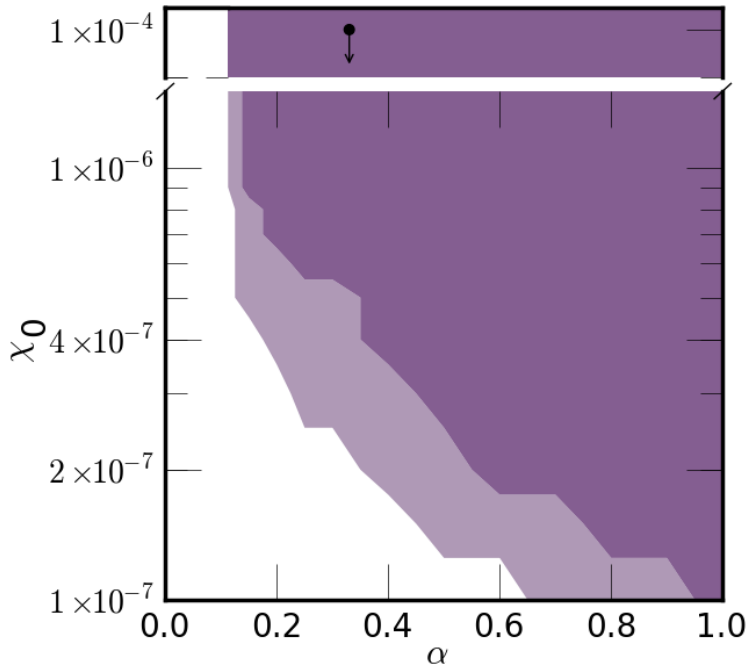


Figure 4.10: The excluded region in the χ_0–α plane for chameleon models. The boundaries of the shaded regions show the upper limits at 68% and 95% confidence level. The black arrow shows the previous constraint, $\chi_0 \leq 10^{-4}$, coming from cosmological and cluster constraints, which was obtained for $f(R)$ theories with $\alpha = 1/3$.

and 95% (dark region) confidence for chameleon models. The jaggedness of the contours is due to the small sample size; decreasing χ_0 will cause galaxies to move from the unscreened to screened sub-sample and so the quality of the data can change rapidly with a small change in χ_0. Also plotted is the previous constraint coming from cosmological probes [124, 125] $\chi_0 \lesssim 10^{-4}$. These new constraints are three orders of magnitude stronger than those coming from cosmological probes. After these results were published, [126] published an independent constraint coming from the equivalence of the hydrostatic and lensing mass of the Coma cluster. They find $\chi_0 < 6 \times 10^{-5}$ for $f(R)$ theories; our results are stronger than theirs by two orders of magnitude.

Two theories of particular interest are $f(R)$ theories with $\alpha = 1/3$ and $\mathcal{O}(1)$ chameleons.

Our analysis reveals the new upper limit on χ_0 (at the 95% confidence level) for these theories:

$$\alpha = 1/3: \quad \chi_0 \leq 4 \times 10^{-7} \tag{4.27}$$

$$\alpha = 1: \quad \chi_0 \leq 1 \times 10^{-7}. \tag{4.28}$$

These limits correspond to a cosmological Compton wavelength of the field of order 1 Mpc. As discussed in section (2.2.7), the Compton wavelength is important for determining whether or not a galaxy is screened. Symmetron models with $\alpha = 2$ have similar Compton wavelengths to these models and so one can place the constraint

$$\chi_0 \leq 3 \times 10^{-7} \tag{4.29}$$

for this model, however other models require a re-calibration of the screening map. We have not attempted this here, nor have we attempted to place a constraint on theories which screen using the EDDP effect. In principle, a new screening map calibrated on symmetron and dilaton N-body simulations (which have been performed [51]) could be used in conjunction with the same data to place new constraints although no attempt has been made to date.

4.4 Summary of Main Results

Simultaneous measurements of the distance to unscreened dwarf galaxies will not agree if one of the methods used to infer the distance is sensitive to the theory of gravity. In this chapter, we have used three distance indicators to place new constraints on chameleon and chameleon-like theories of gravity. Water masers are insensitive to the theory of gravity considered here. TRGB distances are screened when $\chi_0 \gtrsim 10^{-6}$ and unscreened otherwise, making them versatile tools for probing these theories. Cepheid variable stars are unscreened when $\chi_0 \gtrsim 10^{-8}$ and hence have the potential to probe the entire parameter range of interest. The only obstacle to this is a lack of unscreened galaxies for $\chi_0 \lesssim 10^{-7}$. Future surveys will improve the number of

Cepheid measurements to distant galaxies and we will discuss these in chapter 8.

Only the galaxy NGC 4258 has simultaneous maser, TRGB and Cepheid measurements. It is a spiral galaxy and the agreement of these measurements places the new independent constraint $\chi_0 < 10^{-6}$. By comparing simultaneous measurements of Cepheid and TRGB distances to a sample of screened and unscreened galaxies we have been able to probe into the previously unexplored range $\chi_0 < 10^{-6}$. Our analysis is data limited due to the small sample size but nonetheless we have been able to place new constraints summarised in figure 4.10. In particular, we can exclude $\chi_0 > 4 \times 10^{-7}$ for $f(R)$ ($\alpha = 1/3$) theories of gravity. These constraints are currently the strongest in the literature.

In order to obtain these results, we had to use an approximation to find the change in the pulsation period of Cepheid stars. In particular, we were unable to predict the new pulsation period as a function of χ_0 and α due to an incomplete theoretical framework and instead had to perturb the relation found using general relativity. In the next chapter, we will construct such a framework and use it to assess the validity of this approximation and the robustness of our results. Ultimately, we will find that the constraints presented here are conservative and, it is possible to improve them using the same data and statistical analysis.

Self-education is, I firmly believe, the only kind of education there is.

Isaac Asimov

5

Stellar Oscillations in Modified Gravity

In the previous chapter we obtained new constraints on chameleon-like theories of modified gravity by comparing Cepheid and TRGB distance indicators to unscreened dwarf galaxies. In theory, it is possible to improve these constraints using the same or upcoming data, however there were three main uncertainties which prevented this: systematic errors in the data, approximations used to determine whether a galaxy is screened or not and an incomplete theoretical model of Cepheid pulsations. Recall that we did not calculate the new period-luminosity relation but instead perturbed the general relativity calibrated formula. Furthermore, we did not account for the radial profile of G completely and used an averaging procedure. The systematics were investigated and we found that the constraints are largely robust to their effects. A better understanding of which galaxies are screened requires better data with lensing masses and dynamical masses [47] and further N-body simulations and it is not currently possible to address this issue.

In this chapter, we will address the final issue and take the first steps towards a model of Cepheid pulsations in modified gravity. As discussed in the previous chapter, this has applications beyond the current methods of placing constraints. A full theoretical model would allow a prediction of both the amplitude and slope of the period-luminosity relation as well as the lo-

cation of the blue edge of the instability strip[1]. All of these are potential new and independent probes of modified gravity. So far, we have been treating the stars at the level of perturbations (Cepheid pulsations are oscillations about the equilibrium profile) but we have not addressed the issue of perturbations of the scalar field. At the background level, we assumed the field was static, however, since we have a time-varying density profile we expect time-dependent perturbations in the scalar field. This corresponds to scalar radiation, which can back-react and modify the oscillation period.

To address these issues, in this chapter we will perturb the equations of modified gravity hydrodynamics coupled to the scalar field equation of motion to first-order and derive a system of equations governing the evolution of radial perturbations. The system is a coupled Sturm-Liouville eigenvalue problem whose eigenfrequencies give the period of oscillation. We will specialise to radial perturbations since we are interested in stars in other galaxies for which non-radial modes are unobservable. This allows for a calculation of the new oscillation period in modified gravity that does not rely on perturbing the general relativity result. Furthermore, using equilibrium profiles from MESA we can fully account for the radial dependence of G. Since the equations of modified gravity hydrodynamics apply equally to all theories of modified gravity that can be written in the form (2.9), the resulting equations are valid equally for chameleon-like theories and Vainshtein-screened theories provided one perturbs the relevant equation of motion for the scalar. There are three new effects in modified gravity:

1. When the star is unscreened, the period of oscillation can be reduced by an $\mathcal{O}(1)$ amount and is larger than one would find by simply changing the value of G. For Cepheid stars in chameleon-like theories we find that the change in the period can result in differences from the general relativity inferred distance measurement of up to three times what we found in the previous chapter by perturbing the general relativity formula.

2. When the star is unscreened, the star is more stable to perturbations. There is a well-

[1] In theory, including convection could predict the location of the red edge as well, however there are already theoretical uncertainties in this in general relativity.

known result in stellar astrophysics that when the first adiabatic index falls below 4/3 the squared-frequency of the fundamental mode is negative and so the mode is unstable. We will show that in modified gravity the first adiabatic index can fall below 4/3 without any instability. In modified gravity, there is no universal bound on the critical index for the appearance of the instability; its precise value depends on the structure and composition of the star as well as how unscreened it is.

3. The perturbations of the star can source scalar radiation and vice versa.

The first two effects require the star to be unscreened whilst the third does not. Vainshtein-screened theories are too efficient to leave any star unscreened and so it is only the third effect that may be used to probe this theory. Here, we will only investigate the first two effects with the aim of improving the Cepheid constraints of the previous chapters and so once the general result has been presented we will specialise to chameleon-like theories. In fact, scalar radiation in chameleon theories has been previously studied. [127] approximated pulsating stars as solid spheres whose radius and density are oscillating and calculated the resultant scalar radiation using linear perturbations of the scalar equation of motion. This reduced the problem to a forced harmonic oscillator being driven at the frequency of the oscillation of the star. [128] modelled the system as a thin-shell solution that adjusts itself adiabatically to match the changing radius of the star. In both cases, they concluded that scalar-radiation is negligible. These approaches both ignored the fact that the star is not an isolated system unaffected by modified gravity. Its internal structure is coupled to the scalar field profile and hence the correct method of calculating the scalar radiation and the oscillation period is to couple perturbations in the stellar structure equations to the scalar field perturbations. The formalism presented here will capture this fully and it is for this reason that we obtain an eigenvalue problem and not a forced oscillator. That being said, the two approaches above are enough to estimate the amount of scalar radiation to the correct order of magnitude and so we will decouple the equations by ignoring scalar perturbations. Scalar radiation is not necessarily negligible in other theories of modified gravity and so the formalism presented here may be

useful in the future to provide a consistent framework for calculating new constraints on other theories — galileons being one example — using scalar radiation.

When deriving the equations governing the stellar oscillations we will make an adiabatic approximation for simplicity and to discern the new physics. This means that the formalism is not powerful enough to predict the amplitude of the period-luminosity relation, its slope or the location of the blue edge of the instability strip. Non-adiabatic extensions are required for this. Since the non-adiabatic driving processes in Cepheids do not depend on gravitational physics, the adiabatic result can be extended in the same manner as the equivalent equation in general relativity without introducing new features. All of the new physics driving the change in the period-luminosity relation and the location of the instability strip is included in the modified equilibrium structure of the star and the perturbation analysis presented below.

The extension to non-adiabatic systems has yet to be investigated. Non-adiabatic processes tend to drive Cepheids in the fundamental mode of oscillation and so the periods calculated using the adiabatic equations do not differ significantly from those that would result had we solved the full non-adiabatic system.

We will solve the new equation governing radial oscillations of the star numerically using both Lane-Emden and MESA models to calculate $\Delta\tau/\tau$ (which is found from the eigenfrequency of the Sturm-Liouville problem) and investigate the modified stellar stability properties. The former has implications for the tests presented in the previous chapter and upcoming experimental tests of modified gravity and we discuss these in light of these new predictions. The latter may lead to interesting observational consequences such as an enhanced type II supernova rate in unscreened dwarf galaxies or the presence of super-massive blue stars. It is currently unclear whether these effects can be used as the basis for any new observational tests but a further investigation is certainly merited.

5.1 Modified Gravity Hydrodynamics: Linear Perturbation Theory

The dynamics of stellar oscillations are governed by the hydrodynamics of small perturbations about the equilibrium configuration and so we shall linearise the equations (3.2), (3.3), (3.5) about some assumed background profile $\{P_0(r), \rho_0(r), \Phi_{\mathrm{N},0}(r), \Gamma_{1,0}(r), \phi_0(r)\}$ ignoring second-order terms in the perturbations.

The fundamental object of interest is the linearised perturbation to the Lagrangian position of each fluid element $\boldsymbol{\delta}\mathbf{r}(\mathbf{r})$, which describes the oscillation of the fluid from equilibrium at each radius. The equations of modified gravity hydrodynamics presented in section 3.1 are completely general and describe the full three-dimensional hydrodynamic problem. Continuing with the full three dimensional framework would result in a complete treatment of both radial and non-radial modes of oscillation. The aim of this section is to provide a consistent framework with which to predict the oscillation properties of partially unscreened stars residing in unscreened dwarf galaxies. The extra-galactic nature of these stars ensures that only their fundamental radial mode (and possibly the first-overtone) are observable and so non-radial modes are independent for observational tests of modified gravity. We therefore specify to the case of radial oscillations so that $\boldsymbol{\delta}\mathbf{r}(r)$ is a purely radial vector. A more convenient quantity to work with is the relative displacement, given by

$$\zeta(r) \equiv \frac{\delta r(r)}{r}, \tag{5.1}$$

and the aim of the present section is to derive its equation of motion.

We shall work with Eulerian perturbations of the background profile, which we will distin-

guish from Lagrangian perturbations by the use of a tilde so that

$$P(r,t) = P_0(r) + \tilde{P}(r,t) \tag{5.2}$$

$$\rho(r,t) = \rho_0(r) + \tilde{\rho}(r,t) \tag{5.3}$$

$$\Phi_{\rm N}(r) = \Phi_{\rm N,0}(r) + \tilde{\Phi}_{\rm N}(r,t) \tag{5.4}$$

$$\phi(r,t) = \phi_0(r) + \tilde{\phi}(r,t). \tag{5.5}$$

As remarked above, the Lagrangian perturbations may provide more physical insight on occasion and the two are related, for example, via

$$\delta P(r,t) = P(\mathbf{r} + \boldsymbol{\delta}\mathbf{r}, t) - P_0(r) \tag{5.6}$$

$$= \tilde{P}(r,t) + \delta r \frac{\mathrm{d}P_0(r)}{\mathrm{d}r}. \tag{5.7}$$

It will be useful later to have the Lagrangian pressure perturbation in terms of our system-variables. This is given by

$$\frac{\delta P}{P_0} = \Gamma_{1,0}\frac{\delta\rho}{\rho_0} = -\Gamma_{1,0}\left(3\zeta + r\frac{\mathrm{d}\zeta}{\mathrm{d}r}\right), \tag{5.8}$$

which only holds in the adiabatic approximation.

We begin by perturbing equation (3.5) to obtain the Eularian density perturbation

$$\tilde{\rho} = -\frac{1}{r^2}\frac{\partial}{\partial r}(r^3\rho_0\zeta). \tag{5.9}$$

This may be used in the perturbed form of (3.2) to find[2]

$$\rho_0 r\frac{\partial^2\zeta}{\partial t^2} = -\frac{\mathrm{d}\tilde{P}}{\mathrm{d}r} - \rho_0\frac{\mathrm{d}\tilde{\Phi}_{\rm N}}{\mathrm{d}r} + \frac{\beta_0}{M_{\rm pl}r^2}\frac{\partial}{\partial r}(r^3\rho_0\zeta)\frac{\mathrm{d}\phi_0}{\mathrm{d}r} - \frac{\beta_0\rho_0}{M_{\rm pl}}\frac{\mathrm{d}\tilde{\phi}}{\mathrm{d}r}. \tag{5.10}$$

[2]We have neglected terms proportional to $\mathrm{d}\beta(\phi)/\mathrm{d}\phi$ in accordance with the discussion in section 2.2.5. Chameleon-like theories have $\delta\phi\,\mathrm{d}\beta/\mathrm{d}\phi \ll 1$ in the unscreened region and theories that utilise the Vainshtein mechanism have $\mathrm{d}\beta/\mathrm{d}\phi = 0$.

The perturbed Poisson equation is

$$\nabla^2\tilde{\Phi}_{\rm N} = 4\pi G\tilde{\rho}, \tag{5.11}$$

which can be integrated once using (5.9) yielding

$$\frac{{\rm d}\tilde{\Phi}_{\rm N}}{{\rm d}r} = -4\pi G r\rho_0\zeta. \tag{5.12}$$

Now

$$\frac{{\rm d}P}{{\rm d}t} = \frac{\partial P}{\partial t} + \mathbf{v}\cdot\nabla P = \frac{\partial\tilde{P}}{\partial t} + r\frac{\partial\zeta}{\partial t}\frac{\partial P_0}{\partial r} \tag{5.13}$$

and using (3.6) this is

$$\tilde{P} + r\zeta\frac{\partial P_0}{\partial r} = \frac{\Gamma_{1,0}P_0}{\rho_0}\left(\tilde{\rho} + r\zeta\frac{\partial\rho_0}{\partial r}\right). \tag{5.14}$$

We wish to eliminate $\tilde{P}$ and $\tilde{\rho}$ and so we substitute (5.9) into (5.14) to give

$$\begin{aligned}\tilde{P} &= -\frac{\Gamma_{1,0}P_0}{\rho_0}\left(\frac{1}{r^2}\frac{\partial}{\partial r}(r^3\rho_0\zeta) - r\zeta\frac{{\rm d}P_0}{{\rm d}r} + \frac{\rho_0}{\Gamma_{1,0}P_0}\frac{{\rm d}P_0}{{\rm d}r}r\zeta\right)\\ &= -\Gamma_{1,0}P_0 r\left(\frac{\partial\zeta}{\partial r} + \frac{3}{r}\zeta + \frac{1}{\Gamma_{1,0}P_0}\frac{{\rm d}P_0}{{\rm d}r}\zeta\right).\end{aligned} \tag{5.15}$$

We then have

$$\begin{aligned}\frac{\partial\tilde{P}}{{\rm d}r} &= -\frac{\partial}{\partial r}(\Gamma_{1,0}rP_0\frac{\partial\zeta}{\partial r})\\ &\quad -\frac{\partial}{\partial r}(3\Gamma_{1,0}P_0\zeta) - \frac{\partial}{\partial r}(r\frac{{\rm d}P_0}{{\rm d}r}\zeta).\end{aligned} \tag{5.16}$$

This may then be used with (5.11) and (5.10) to find:

$$r^4\rho_0\frac{\partial^2\zeta}{\partial t^2} = \frac{\partial}{\partial r}\left(r^4\Gamma_{1,0}P_0\frac{\partial\zeta}{\partial r}\right) + r^3\frac{\partial}{\partial r}\left[\left(3\Gamma_{1,0}-4\right)P_0\right]\zeta - \frac{r^3\beta_0\rho_0}{M_{\rm pl}}\frac{\partial\tilde{\phi}}{\partial r} - \frac{\beta_0\rho_0}{M_{\rm pl}}r^4\frac{{\rm d}^2\phi_0}{{\rm d}r^2}\zeta - 2\frac{r^3\beta_0\rho_0}{M_{\rm pl}}\frac{{\rm d}\phi_0}{{\rm d}r}\zeta. \tag{5.17}$$

This is the equation of motion governing the evolution of ζ. In general relativity, $\partial\tilde{\phi}/\partial r = 0$ and we obtain a single equation. In modified gravity, however, we need a separate equation for $\tilde{\phi}$. This is where we will specify to the case of chameleon-like theories and perturb the equation of motion (2.16)[3]:

$$-\frac{\partial^2\tilde{\phi}}{\partial t^2} + \nabla^2\tilde{\phi} = m_0^2\tilde{\phi} - 3\frac{\beta}{M_{\rm pl}}\rho_0\zeta - \frac{\beta}{M_{\rm pl}}r\frac{\partial}{\partial r}(\rho_0\zeta), \tag{5.18}$$

where $m_0^2 \equiv V_{\phi\phi}(\phi_0)$ is the mass of the unperturbed field at zero density and equation (5.9) has been used. We are interested in stationary-wave solutions and so we expand

$$\zeta(r,t) = \xi(r)e^{i\omega t} \tag{5.19}$$

$$\tilde{\phi}(r,t) = \varphi(r)e^{i\omega t} \tag{5.20}$$

to yield two coupled equations

$$(\nabla^2+\omega^2)\varphi = m_0^2\varphi - 3\frac{\beta}{M_{\rm pl}}\rho_0\xi - \frac{\beta}{M_{\rm pl}}r\frac{\partial}{\partial r}(\rho_0\xi), \tag{5.21}$$

$$\frac{\rm d}{{\rm d}r}\left(r^4\Gamma_{1,0}P_0\frac{{\rm d}\xi}{{\rm d}r}\right) + r^3\frac{\rm d}{{\rm d}r}\left[\left(3\Gamma_{1,0}-4\right)P_0\right]\xi - \frac{r^4\beta_0\rho_0}{M_{\rm pl}}\frac{{\rm d}^2\phi_0}{{\rm d}r^2}\xi - 2\frac{r^3\beta_0\rho_0}{M_{\rm pl}}\frac{{\rm d}\phi_0}{{\rm d}r}\xi + r^4\rho_0\omega^2\xi = \frac{r^3\beta_0\rho_0}{M_{\rm pl}}\frac{{\rm d}\varphi}{{\rm d}r}. \tag{5.22}$$

Equations (5.21) and (5.22) constitute the main result of this section. One could combine them into a single equation, however, it is more instructive to treat the system as two coupled

[3]Equation (5.17) is equally valid for any scalar-tensor theory of modified gravity where ${\rm d}\beta(\phi)/{\rm d}\phi$ can be neglected provided that one perturbs the equation of motion for the scalar field coming from that theory.

equations. In general relativity, we have $\varphi = \beta_0 = \mathrm{d}\phi_0/\mathrm{d}r = 0$ and (5.22) reduces to

$$\frac{\mathrm{d}}{\mathrm{d}r}\left(r^4\Gamma_{1,0}P_0\frac{\mathrm{d}\xi}{\mathrm{d}r}\right) + r^3\frac{\mathrm{d}}{\mathrm{d}r}\left[\left(3\Gamma_{1,0}-4\right)P_0\right]\xi + r^4\rho_0\omega^2\xi = 0,$$

which describes linear, adiabatic, radial waves moving in the stellar interior. It is known at the *linear adiabatic wave equation* (LAWE) and its eigenfrequencies ω^2 give the frequency of stellar oscillations about equilibrium. We will hence refer to (5.22) as the *modified linear adiabatic wave equation* (MLAWE). It's properties will be the subject of the next section. Note that the effects of modified gravity alter the oscillation properties of the star via the MLAWE in two different ways. Firstly, the MLAWE contains extra terms not present in the general relativity problem. These represent the effects of perturbing the modified gravity hydrodynamics. In particular, the new term proportional to $\mathrm{d}\phi_0/\mathrm{d}r \sim G(r)$ encodes the effects of the radial-dependence of Newton's constant not present in general relativity. The term proportional to $\mathrm{d}\phi_0/\mathrm{d}r \sim \mathrm{d}G(r)/\mathrm{d}r$ encodes the effects of the rate of change of this constant. Steeper gradients make it more difficult for acoustic waves to propagate and this will have important consequences for the stability of unscreened stars. Secondly, the equilibrium profiles represented by P_0 etc. are computed using the modified equations of stellar structure. We will discern how each of these contributes to the change in the oscillation period below.

Using the profile (2.73), we have

$$\frac{\beta_0}{M_{\mathrm{pl}}}\left[2\frac{\mathrm{d}\phi_0}{\mathrm{d}r} + r\frac{\mathrm{d}^2\phi_0}{\mathrm{d}r^2}\right] = 4\pi\alpha G r\rho_0(r) \quad r > r_{\mathrm{s}}, \tag{5.23}$$

which we shall use in all analytic and numerical computations from here on.

5.2 Properties of the Modified Linear Adiabatic Wave Equation

The MLAWE describes the behaviour of stellar oscillations in modified gravity. There are two major differences with respect to the general relativity equation. Firstly, there are two additional terms in the homogeneous part, proportional to the first and second derivatives of the background field. When $r < r_s$ these are negligible and the homogeneous part behaves as it would in general relativity, however, these are comparable to the other terms when $r > r_s$ and encode the effect of modified gravity on wave propagation in the region exterior to the screening radius. Physically, the term proportional to $\mathrm{d}\phi_0/\mathrm{d}r$ acts as a varying enhancement of Newton's constant $G(r)$ given by equation (2.73) and the term proportional to $\mathrm{d}^2\phi_0/\mathrm{d}r^2$ can schematically be viewed as $\mathrm{d}G(r)/\mathrm{d}r$ and so it encodes the effect of a radially varying Newtonian force in the outer regions.

The second effect is a driving term proportional to $\beta_0\,\mathrm{d}\varphi/\mathrm{d}r$. This is clearly the effect of the fifth-force due to perturbations in the field. This was modelled by [127] as an inhomogeneous forcing term at a single frequency. Here it appears as coupling between the field and stellar perturbations: the stellar perturbations source the scalar field perturbations and vice versa. Physically, $\tilde{\phi}(r,t)$ corresponds to scalar radiation (or rather the flux $T_{\phi\,0i}$ at infinity). As mentioned in the introduction to this chapter, there is evidence from previous studies [127, 128] that this is negligible in chameleon-like systems and so from here on we will neglect the dynamics of the field perturbations and treat only the homogeneous part of the MLAWE (5.22).

5.2.1 Boundary Conditions

The MLAWE requires two boundary conditions in order to fully specify the solution given a specific value of ω[4]. Firstly, our system is spherically symmetric and so we must impose $\delta r = 0$ at $r = 0$. The MLAWE then requires

$$\left.\frac{\mathrm{d}\xi}{\mathrm{d}r}\right|_{r=0} = 0. \tag{5.24}$$

The surface boundary condition depends on the stellar atmosphere model (see [129] for a discussion) but the lowest modes, where the period of oscillation is longer than the inertial response time of the atmosphere can be described by solutions with vanishing surface pressure so that $\delta P(R) = 0$. This gives the surface condition [129]

$$\left.\frac{\delta P}{P_0}\right|_{r=0} = \left(\frac{\omega^2 R^3}{GM} + 4\right)\zeta(R), \tag{5.25}$$

where the Lagrangian pressure perturbation is given by (5.8). Note that the additional terms in the MLAWE vanish at the stellar centre and radius if we take $\rho_0(R) = 0$ so that these conditions are identical to those required by general relativity.

5.2.2 Sturm-Liouville Nature of the Equation

The MLAWE can be written in Sturm-Liouville form

$$\hat{\mathscr{L}}\xi + w(r)\omega^2\xi, = 0 \tag{5.26}$$

where the weight function $w(r) = r^4\rho_0(r)$ and the operator can be written

$$\hat{\mathscr{L}}^{\mathrm{GR}} = \frac{\mathrm{d}}{\mathrm{d}r}\left(r^4\Gamma_{1,0}P_0\frac{\mathrm{d}}{\mathrm{d}r}\right) + r^3\frac{\mathrm{d}}{\mathrm{d}r}\left[\left(3\Gamma_{1,0} - 4\right)P_0\right], \tag{5.27}$$

$$\hat{\mathscr{L}}^{\mathrm{MG}} = \hat{\mathscr{L}}^{\mathrm{GR}} - \frac{\beta\rho_0}{M_{\mathrm{pl}}}r\frac{\mathrm{d}^2\phi_0}{\mathrm{d}r^2} - 2\frac{\beta\rho_0}{M_{\mathrm{pl}}}\frac{\mathrm{d}\phi_0}{\mathrm{d}r}. \tag{5.28}$$

[4]Of course, we also need to derive the value of ω^2 from the solution of the equation. This can be done by looking for values such that the solutions satisfy both boundary conditions and is discussed in section 5.2.2.

The problem of finding the pulsation frequencies is then one of finding the eigenvalues of these equations that correspond to eigenfunctions satisfying the boundary conditions (5.24) and (5.25). In practice, it is not possible to solve these equations analytically for physically realistic stars and numerical methods must be used. We will do just this in section 5.4. Despite the need for numerics, a lot of the new modified gravity features can be discerned and elucidated using well-known Sturm-Liouville techniques and so we shall investigate these first.

5.2.3 Scaling Behaviour of the Eigenfrequencies

Using the dimensionless quantities:

$$\bar{P}_0(r) \equiv \frac{R^4}{GM^2} P_0(r), \tag{5.29}$$

$$\bar{\rho}_0(r) \equiv \frac{R^3}{M} \rho_0(r) \quad \text{and} \tag{5.30}$$

$$x \equiv \frac{r}{R}, \tag{5.31}$$

the MLAWE (5.22) can be cast into dimensionless form:

$$\frac{\mathrm{d}}{\mathrm{d}x}\left(x^4 \Gamma_{1,0} \bar{P}_0 \frac{\mathrm{d}\xi}{\mathrm{d}x}\right) \tag{5.32}$$

$$+ x^3 \frac{\mathrm{d}}{\mathrm{d}x}\left[\left(3\Gamma_{1,0} - 4\right)\bar{P}_0\right]\xi + x^4 \bar{\rho}_0 \left[\Omega^2 - 4\pi\alpha\bar{\rho}_0\right] = 0, \tag{5.33}$$

where

$$\Omega^2 \equiv \frac{\omega^2 R^3}{GM} \tag{5.34}$$

is the dimensionless eigenfrequency and the term proportional to α is only present when $r > r_s$. In general relativity, $\alpha = 0$ and one can solve this given some equilibrium stellar model to find Ω^2. Since this must be a dimensionless number one has $\omega^2 \propto GM/R^3$. In modified gravity, there are two independent effects that act to change this value at fixed mass: the change due to the different equilibrium structure and the change due to the additional term

in the MLAWE. At the level of the background, we expect that stars of fixed mass have smaller radii and larger values of $\langle G \rangle$ (where by $\langle\rangle$ we mean some appropriate average over the entire star) so that the frequencies are higher in modified gravity. At the level of perturbations, one can replace Ω^2 in the general relativity equation by the effective frequency $\Omega^2 - 4\pi\alpha\langle\bar{\rho}_0\rangle$ so that $\Omega^2_{\rm MG} \approx \Omega^2_{\rm GR} + 4\pi\alpha\langle\bar{\rho}_0\rangle$ and we therefore expect the modified gravity eigenfrequency to be larger still.

One can gain some insight by considering scaling relations in a similar manner to the methods of section 3.3.1 when the star is fully unscreened so that $G \to G(1+\alpha)$. Let us assume a polytropic equation of state of the form

$$P = K\rho^\gamma, \tag{5.35}$$

where K is a constant and γ differs from $\Gamma_{1,0}$ since the system need not be adiabatic. In this case, equations (3.8) and (3.9) give

$$\rho_{\rm c} \propto \frac{M}{R^3} \tag{5.36}$$

$$\rho_{\rm c}^{\gamma-1} \propto \frac{GM^2}{R}, \tag{5.37}$$

which can be combined to find the scaling of the radius for a fully-unscreened star in modified gravity:

$$\frac{R_{\rm MG}}{R_{\rm GR}} = (1+\alpha)^{-\frac{1}{3\gamma-4}} \tag{5.38}$$

at fixed mass. Ignoring the modified gravity perturbations, one would then expect

$$\frac{\omega^2_{\rm MG}}{\omega^2_{\rm GR}} = (1+\alpha)^{\frac{3\gamma-1}{3\gamma-4}}. \tag{5.39}$$

We shall confirm this limit numerically for some simple models later in section 5.4.1. In the

fully unscreened limit, we would then expect the eigenfrequencies to scale approximately like

$$\frac{\omega^2_{\rm MG}}{\omega^2_{\rm GR}} \sim (1+\alpha)^{\frac{3\gamma-1}{3\gamma-4}} \left(1 + \frac{4\pi\alpha}{\Omega^2_{\rm GR}}\langle\bar{\rho}_0\rangle\right) \tag{5.40}$$

so that they are always larger than the general relativity prediction (assuming $\gamma > 4/3$), at least when $\omega^2_{\rm GR} > 0$.

5.3 Stellar Stability

Given the Sturm-Liouville nature of the problem, we can find an upper bound on the fundamental frequency ω_0 using the variational principle. Given an arbitrary trial function $\Psi(r)$, one can construct the functional

$$F[\omega] \equiv -\frac{\int_0^R \mathrm{d}r\, \Psi^*(r)\hat{\mathscr{L}}\Psi(r)}{\int_0^R \mathrm{d}r\, \Psi^*(r)\Psi(r)\rho_0 r^4}, \tag{5.41}$$

which has the property that $\omega_0^2 \leq F[\omega]$. Ignoring modified gravity for now and taking the simplest case where χ is constant, the fundamental eigenfrequencies of the LAWE (5.23) satisfy

$$\omega_0^2 \leq \frac{\int_0^R \mathrm{d}r\, 3r^2(3\Gamma_{1,0}-4)P_0}{\int_0^R \mathrm{d}r\, \rho_0 r^4}, \tag{5.42}$$

where we have used $\hat{\mathscr{L}} = \hat{\mathscr{L}}^{\rm GR}$ defined in (5.27). When the right hand side is negative we have $\omega_0^2 < 0$ and the eigenfunctions have growing modes. This is the well-known result in stellar astrophysics that stars where the first adiabatic index falls below 4/3 are unstable to linear perturbations and cannot exist[5].

[5]Corrections from general relativity increase this critical value to $4/3 + \mathcal{O}(1)GM/R$ [130], where the $\mathcal{O}(1)$ factor depends on the specific composition of the star. We are interested in the properties of main-sequence stars with $GM/R \sim 10^{-6}$ and Cepheid stars with $GM/R \sim 10^{-7} - 10^{-8}$ and so this correction is always negligible compared with the effects of modified gravity, which are of the same order as the non-relativistic contribution when the star is unscreened.

In modified gravity, we have $\hat{\mathscr{L}} = \hat{\mathscr{L}}^{\rm MG}$ and so using equation (5.28) we have

$$\omega_0^2 \leq \frac{\int_0^R \mathrm{d}r\, 3r^2 \left[(3\Gamma_{1,0}-4)P_0\right] + \int_{r_s}^R \frac{\beta\rho_0}{M_{\rm pl}} \left(r^4 \frac{\mathrm{d}^2\phi_0}{\mathrm{d}r^2} + 2r^3 \frac{\mathrm{d}\phi_0}{\mathrm{d}r}\right)}{\int_0^R \mathrm{d}r\, \rho_0 r^4} \tag{5.43}$$

and so this stability condition is altered in stars which are at least partially unscreened. This is not surprising given the form of equation (5.22). The term proportional to the derivative of $[(3\Gamma_{1,0}-4)P_0]$ behaves like a position-dependent mass for ξ, which is negative when $\Gamma_{1,0} < 4/3$ so that one would expect growing modes. The additional terms in (5.43) are due to the two new terms in (5.22), which are of precisely the same varying mass form with the opposite sign. A negative mass, which would signify an instability, coming from the general relativity term can then be compensated by the new terms in modified gravity, restoring stability[6].

Physically, the first adiabatic index is a measure of how the pressure responds to a compression of the star. Given a compression from one radius R_1 to a smaller radius R_2, a larger adiabatic index will result in more outward pressure. If this increase in pressure is faster than the increase in the gravitational force, the star can resist the compression and is hence stable. Below the critical value of $4/3$, the converse is true and the star is unstable. We have already seen above that the new terms contributing to the stability correspond to a varying value of G and its derivative in the outer layers. Since modified gravity enhances the gravity, one may näively expect that its effect is to destabilise stars, however, we will argue below that this is not the case. The MLAWE describes acoustic waves propagating in the star. If the force of gravity and its gradient is larger in the outer layers then it is more difficult for these waves to propagate and hence modes which would usually have been unstable are stabilised.

Once again, we must disentangle the effects of the modified equilibrium structure and the

[6]The reader may wonder why the star is more stable in modified gravity when the stability criterion in general relativity does not change if one changes the value of G. When the star is unscreened we have $G \to G(1+\alpha)$ and so one may expect any modified gravity effects to vanish in this limit. In general relativity, there is an exact cancellation coming from the perturbations to the momentum equation (3.1) and the Newtonian potential. In modified gravity, the additional gravitational force is not derived from the Newtonian potential but from the field profile and so any cancellation must come from the perturbation to the field equation. A priori, there is no reason why the field perturbations should cancel this new contribution and, indeed, we see here that they do not.

perturbations on the critical value of $\Gamma_{1,0}$. Consider first the modified equilibrium structure only. In this case, the stability condition is given by the general relativity expression, equation (5.42), however the pressure and density profiles will be different. Clearly, the critical value for the instability is still 4/3 since this is the only value which makes the integral vanish but this does not necessarily mean the stability is altered away from this value. Scaling the pressure and density using the dimensionless quantities defined in (5.29), (5.30) and (5.31), we have

$$\omega_0^2 \leq (3\Gamma_{1,0} - 4)\frac{GM}{R^3} f(\chi_0, \alpha), \tag{5.44}$$

where f is a dimensionless function which depends on the composition of the star[7]. In modified gravity, the radius of the star will be smaller than its general relativity counterpart and the effective value of G is larger. Hence, when $\Gamma_{1,0} > 4/3$ the maximum possible frequency is greater than in general relativity whereas when $\Gamma_{1,0} < 4/3$ the maximum frequency is more negative. If a star is unstable in general relativity then modified gravity enhances the instability, moving the frequency further away from zero. This can also be seen from the scaling relation (5.39). If $\omega^2_{\rm GR} < 0$ then $\omega^2_{\rm MG}$ is even more negative. At the background level, the effects of modified gravity are to destabilise stars that are already unstable, without altering the stability condition.

Let us now turn our attention to the effects of perturbations. Using equation (5.23), we have

$$\omega_0^2 \leq \frac{\int_0^R \mathrm{d}r\, 3r^2 \left[(3\Gamma_{1,0} - 4)P_0\right] + \int_{r_s}^R 4\pi\alpha G r^4 \rho_0^2}{\int_0^R \mathrm{d}r\, \rho_0 r^4}. \tag{5.45}$$

The additional term is clearly positive and so one may lower the value of $\Gamma_{1,0}$ below 4/3 and still find positive eigenfrequencies, confirming our earlier intuition that the effect of modified gravity is to stabilise stars compared with general relativity. We will denote the critical index by $\Gamma^{\rm crit}_{1,0}$. When $\Gamma_{1,0} < \Gamma^{\rm crit}_{1,0}$ the star is unstable to linear perturbations. Unlike general relativity, there is no universal critical index in modified gravity. The precise value depends on χ_0 and α

[7]The reader should note that this is a varying function of χ_0 and α and so is not universal.

and is composition-dependent. We will investigate the stability of some simple semi-analytic models in section 5.4.1 but before doing so, one can gain some insight into the full effects of modified gravity on the stability by using the same scaling relations as section 5.2.3. In particular, we can set the numerator in (5.45) to zero to find the modified critical index:

$$\Gamma_{1,0}^{\text{critical}} = \frac{4}{3} - g(\chi_0, \alpha)\alpha, \tag{5.46}$$

where

$$g(\chi_0, \alpha) = \frac{4\pi G}{3} \frac{\int_{r_s}^{R} r^4 \rho_0^2(r)}{\int_0^R r^2 P_0(r)} \tag{5.47}$$

is a dimensionless function that encodes the effects of the structure of the star. In $f(R)$ theories, $\alpha = 1/3$ [82] and so we expect the critical value of $\Gamma_{1,0}$ to change by $\mathcal{O}(10^{-1})$ assuming that $g \sim \mathcal{O}(1)$. We will verify numerically that this is indeed the case for a simple model in section 5.4.1.

5.4 Numerical Results

We now proceed to solve the MLAWE for various different stars. We will do this for two different stellar models: Lane-Emden and MESA models. The first models are simple compared with the second but they have the advantage that the non-gravitational physics (e.g. nuclear burning) is absent, which will allow us to gain a lot of physical intuition about the new modified gravity features. They are simple semi-analytic models and this allows us to first investigate the MLAWE using a controlled system with known scaling properties and limits without the complications arising from processes such as radiative transfer. This also allows us to test that the code is working correctly since we can compare our results with both the general relativity case, which has been calculated previously, and the fully unscreened case, which can be predicted analytically given the general relativity one. Their perturbations can also be described using an arbitrary value of $\Gamma_{1,0}$, independent of their composition and so we will use them to

study the modifications to stellar stability. These models are not realistic enough to compare with observational data and the power of MESA lies in that it can produce realistic models of stars such as main-sequence and Cepheid stars, which will allow us to predict the effects of modified gravity on realistic stars in unscreened galaxies. In the previous chapter, we used MESA predictions to obtain the strongest constraints on chameleon-like models to date. Combining these models with the modified gravity oscillation theory has the potential to provide even tighter constraints.

Details of the numerical procedure used to solve the MLAWE are given in appendix C. The shooting method has been used to solve the MLAWE in all instances.

5.4.1 Perturbations of Lane-Emden Models

In this section we numerically solve the MLAWE for stars whose equilibrium configurations are given by the Lane-Emden models described in section 3.2.

Oscillation Periods of Lane-Emden Models

We solve the MLAWE by first tabulating solutions of the modified Lane-Emden equation and using these to numerically solve the MLAWE. The dimensionless eigenvalues (see section C.2.2 in appendix C for a derivation and discussion of this expression)

$$\tilde{\omega}^2 \equiv \frac{(n+1)\omega^2}{4\pi G\rho_c} \tag{5.48}$$

for Lane-Emden models in general relativity were numerically calculated in 1966 by [131] and so as a code comparison, we have compared our fundamental frequencies and first overtones with theirs for different values of n and $\Gamma_{1,0}$. Their values are given to five decimal places and in each case our results agreed with theirs to this accuracy.

Self-similarity is not completely preserved in modified gravity Lane-Emden models. This means that given values of χ_0 and α we are not free to choose the mass and radius of the

modified gravity star to be identical to those of the general relativity star because the ratio GM/R is constrained via equation (3.17). Therefore, given a star in general relativity of mass M and radius R, one must decide upon the correct comparison in modified gravity. In what follows, we will fix the mass and composition (this implies that K is fixed) of the star and allow the radius to vary so that the stars we compare are stars of the same mass whose radii (and pressure and density profiles) have adjusted to provide an equilibrium configuration given a specific value of χ_0 (and hence r_s)[8]. In particular, this means that it is not possible (or rather not meaningful) to compare stars of fixed GM/R since these stars have different masses and radii to their general relativity ($\alpha = 0$) counterparts. This means that the stars we compare have fixed masses but different Newtonian potentials[9]. In order to fix the mass, one must fix the central density and so in modified gravity we have $\rho_c = \rho_c(\chi_0, \alpha)$, highlighting the consequences of breaking self-similarity. For concreteness, we will work with $n = 1.5$. This is a good approximation to stellar regions which are fully convective (see [63], sections 7 and 13 for more details) and hence have physical applications to red giant and Cepheid stars[10]. In terms of an equation of state of the form (5.35), this model corresponds to $\gamma = 5/3$. In what follows, we will assume that γ is identical to the first adiabatic index and set $\Gamma_{1,0} = 5/3$, however, we will relax this assumption when considering stellar stability and allow for more general models.

Using equation (3.16), we have

$$\rho_c = \left(\frac{M}{4\pi}\right)^2 \left[\frac{8\pi G}{2K}\right]^3 \left(\frac{1+\alpha}{\omega_R + \alpha\omega_s}\right)^2, \tag{5.49}$$

[8]This is not possible in the case $n = 3$ since there is no mass-radius relation. The absence of such a relation has the result that the constant K must vary as a function of stellar mass, χ_0 and α. Indeed, this is what we found in chapter 3 where we studied the Eddington standard model. For this reason, there is no meaningful way to compare perturbations of stars in modified gravity since one is comparing stars with different equations of state. For this reason, we will not consider perturbations of these models.

[9]This is another illustration of how including the effects of the fifth-force on the structure of an object can violate the condition that $\Phi_N \sim \chi_0$ implies screening. The field-profile is only set once one knows the structure of the object and, as we have seen here, even when observable properties (such as the mass) are fixed the Newtonian potential may vary if the star is unscreened and a näive estimate using the general relativity value may not give the correct screening radius.

[10]The $n = 1.5$ polytrope model is a far better approximation to red giant stars than Cepheids.

which may be used to find the modified Mass-Radius-χ_0 relation (as opposed to the Mass-Radius relation found in general relativity).

$$R = \frac{1}{(4\pi)^{\frac{3}{2}}}\left(\frac{5K}{2G}\right)\left(\frac{\omega_R + \alpha\omega_s}{1+\alpha}\right)^{\frac{1}{3}}. \tag{5.50}$$

In the cases of red giant stars and low-mass Cepheids, we have $GM/R \sim 10^{-7}$ and so we can pick $M = M_{\rm GR}$ and $R = R_{\rm GR}$ in the general relativity case ($\alpha = 0$) such that $GM_{\rm GR}/R_{\rm GR} = 10^{-7}$ and

$$\frac{GM}{R} = 10^{-7}\left(\frac{M_{\rm GR}}{M}\right)\left(\frac{R}{R_{\rm GR}}\right) \tag{5.51}$$

and equation (3.17) is (fixing $M = M_{\rm GR}$ and recalling that $\bar{y}_R$ is the value of y_R found using general relativity)

$$\frac{\chi_0}{10^{-7}} = \frac{\bar{y}_R}{y_R}\left[\frac{y_R\theta(y_s) + \omega_R - \frac{y_R}{y_s}\omega_s}{\left(\bar{\omega}_R(1+\alpha)\right)^{\frac{1}{3}}\left(\omega_R + \alpha\omega_s\right)^{\frac{2}{3}}}\right]. \tag{5.52}$$

The procedure is then as follows: Given specific values of χ_0 and α, we use a trial value of y_s to solve the Modified-Lane Emden equation until equation (5.52) is satisfied. We then use the Lane-Emden solution in the MLAWE to numerically calculate the value of $\tilde{\omega}^2$ given a value of $\Gamma_{1,0}$. Using equation (5.49), we can find the ratio of the period in modified gravity to that predicted by general relativity:

$$\frac{\tau_{\rm MG}}{\tau_{\rm GR}} = \sqrt{\frac{\tilde{\omega}^2_{\rm GR}}{\tilde{\omega}^2_{\rm MG}}}\,\frac{\omega_R + \alpha\omega_s}{\bar{\omega}_R(1+\alpha)}. \tag{5.53}$$

We can then calculate this ratio for any value of χ_0 and α.

Before presenting the numerical results, it is worth noting that the fully-unscreened behaviour of the star, at least in the case where only the effects of the modified equilibrium structure are considered, can be calculated in terms of the general relativity properties of the star. In the fully-unscreened case, one has $\omega_s = y_s = 0$. One can then set $y \to (1+\alpha)^{-\frac{1}{2}}y$ to bring equation (3.13) into the same form as in general relativity. This then gives $y_R^{\rm unscreened} = (1+\alpha)^{-\frac{1}{2}}\bar{y}$ and $\omega_R{}^{\rm unscreened} = (1+\alpha)^{-\frac{1}{2}}\bar{\omega}_R$. For $n = 1.5$, one has $\bar{y}_R \approx 3.654$

and $\bar{\omega}_R \approx 2.72$. One then has, by rescaling the MLAWE (see appendix C for the equation in these coordinates), $\tilde{\omega}^2_{\text{unscreened}}/\tilde{\omega}^2_{\text{GR}} = (1+\alpha)$ and so, using (5.49), $\omega^2_{\text{unscreened}}/\omega^2_{\text{GR}} = (1+\alpha)^4$, which exactly matches our prediction in (5.39) for $\gamma = 5/3$. From equation (5.53), we have $\tau^{\text{unscreened}}_{\text{MG}}/\tau_{\text{GR}} = (1+\alpha)^{-2} = 0.5625$ for $\alpha = 1/3$. These unscreened results can be used to check that the numerical results are behaving as expected[11].

We would like to investigate the effect of the different modifications coming from the altered equilibrium structure and the modified perturbation equation separately. They appear at the same order in the MLAWE and so we expect them to contribute equally and it is important to disentangle their effects, especially since we have already argued in section 5.3 that they may contribute differently to the stellar stability and that the equilibrium structure acts to make negative general relativity frequencies more negative. Lane-Emden models are perfectly suited for this study since we do not have to worry about altered evolution histories and so we will consider two cases:

- Case 1: We solve the LAWE (5.23) using modified Lane-Emden profiles. This case only includes the modified equilibrium structure.

- Case 2: We solve the full MLAWE using the modified background structure. This is the physically realistic case.

The case where we ignore the modified equilibrium structure and solve the MLAWE is highly unphysical. There is no screening radius and so we are introducing the perturbations about an arbitrary radius. Furthermore, the size of the effect depends on whether we take the radius of the star as corresponding to the general relativity solution (in which case we are ignoring the effects on the period coming from the change in the central density (5.49)) or the equivalent modified gravity solution (in which case our profiles do not satisfy the boundary conditions and we are including some of the modified equilibrium properties in our analysis). For these

[11] One should note that whereas (5.53) is an exact analytic expression it is not possible to evaluate its numerical value analytically. One must still solve the modified Lane-Emden equation and the MLAWE for quantities such as ω_R and $\tilde{\omega}^2_{\text{GR}}$.

reasons, we do not investigate this scenario. In each case, we assume the profile (2.73). Since we have solved the modified Lane-Emden equation with constant α in the region $r > r_s$ (this is required for a physically meaningful comparison with general relativity) this profile is not technically correct since it does not satisfy the stellar structure equations. In fact, it is an under-estimate [12]. In each case we will fix $\alpha = 1/3$, corresponding to $f(R)$ gravity and vary χ_0.

In figure 5.1 we plot the ratio of the modified gravity period to the general relativity one as a function of $\log \chi_0$ for case 1. In chapter 4, the approximation

$$\frac{\tau_{\rm MG}}{\tau_{\rm GR}} = \sqrt{\frac{G}{\langle G \rangle}}, \tag{5.54}$$

where $\langle G \rangle$ is the average value of the effective Newtonian constant using the Epstein weighting function was used in order to obtain new constraints on the model parameters. This was found by perturbing the general relativity prediction that $\tau \propto G^{-1/2}$ at fixed radius and describing the effects of the radial variation of G using $\langle G \rangle$. This approximation is based on the change in the equilibrium structure only and so it is important to test not only how it compares with the predictions from the full numerical prediction at the background level but also how well it can be used to approximate the frequency once modified gravity perturbations are taken into account. Hence, we also plot the prediction coming from this approximation. In each case we have calculated $\langle G \rangle$ using the modified Lane-Emden solution at given χ_0. One should emphasise that in chapter 4 we used this approximation for MESA models whereas this comparison is purely for the hypothetical case of Lane-Emden models. We will investigate how well this holds for MESA models in section 5.4.2. The figure reveals that the approximation (5.54) is an over-estimate for very screened stars whereas it is a large under-estimate for stars that are significantly unscreened. The Epstein function favours the regions of Cepheid stars

[12] Compared to the result that would be obtained if we had used a fully-unscreened profile. The equilibrium structure is still a small over-estimate of the effects of modified gravity. For our purposes, this is not an issue since we seek only to investigate the new effects of modified gravity oscillations and do not compare any of these results with real stars. When we analyse MESA predictions we will use a fully consistent approach.

that are most important for pulsations. This tends to be the outer layers and so it is no surprise that it over-estimates the effects in the screened case: it places a large emphasis on the small region where the gravity is enhanced even though this region has little to no effect on the structure of the star. The approximation (5.54) assumes that the stellar radius is fixed but in Lane-Emden models this is clearly a decreasing function of χ_0 and α according to (5.50). According to (5.34), the period scales as $R^{\frac{3}{2}}$, which explains why the approximation is an underestimate when the star is very unscreened and the change in the radius is significant. This is also the reason for the slow divergence of the two curves: since we are solving the LAWE, the deviation of the two curves is driven entirely by the change in the stellar radius, which is not significant when the star is very screened. As soon as the effects of the fifth-force are significant the curves begin to diverge. We can also see that the ratio asymptotes to the value predicted in (5.53) when the star is fully-unscreened confirming that the numerics are behaving as expected.

In figure 5.2 we plot the ratio of the modified gravity period to the general relativity one for case 2. We can see that the approximation (5.54) fails very rapidly and that the change in the period is significant and can be as large as 50% for significantly unscreened stars. Unlike the previous case, we can see that the red and blue curves diverge very rapidly, even when the star is very screened. This is because the blue curve is based entirely on the LAWE and does not capture the additional $\mathcal{O}(1)$ effects included in the MLAWE. When the star is very screened any deviations from general relativity are small so the curves agree well but as soon as the star becomes even slightly unscreened and the additional terms in the MLAWE are very important, hence the rapid divergence.

We plot the two cases together in figure 5.3. One can see that the effect of the new terms coming from the modified structure of hydrodynamics has a significant effect on the period and that if one were to consider only the equilibrium structure, the change in the period would be a large under-estimate. That being said, the change in the period from the general relativity value is $\mathcal{O}(1)$ as soon as one calculates using the modified equilibrium structure and the effect

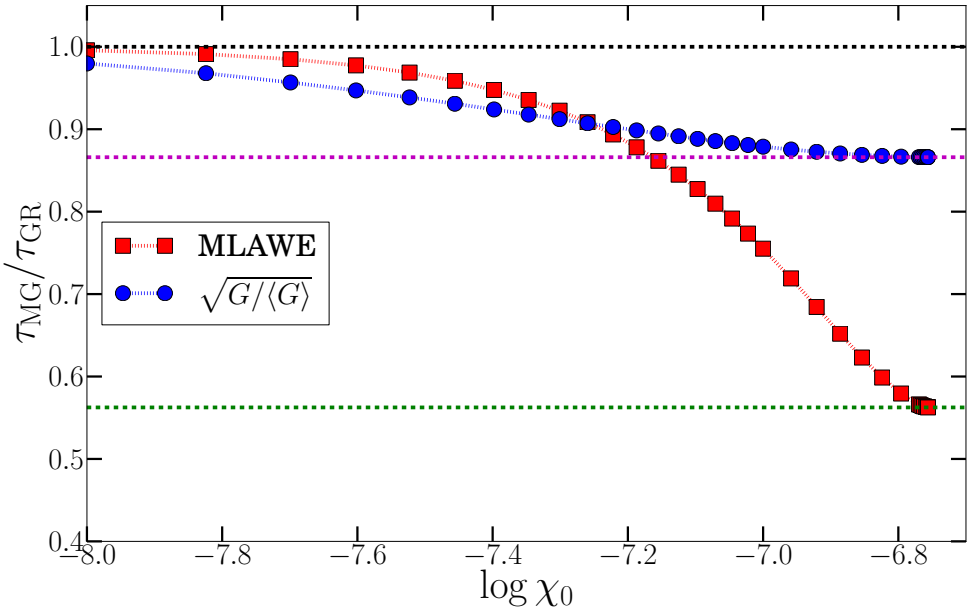


Figure 5.1: The fractional change in the stellar pulsation period as a function of $\log_{10}\chi_0$ when only the change to the equilibrium structure is considered (case 1). The red squares correspond to eigenfrequencies of the LAWE whereas the blue circles show the approximation (5.54). The green dashed line shows the ratio for a fully unscreened star and the black dashed line shows a ratio of 1, corresponding to a general relativity star. The magenta line shows the fully-unscreened value of $\sqrt{\frac{G}{\langle G\rangle}} = (1+\alpha)^{-\frac{1}{2}}$.

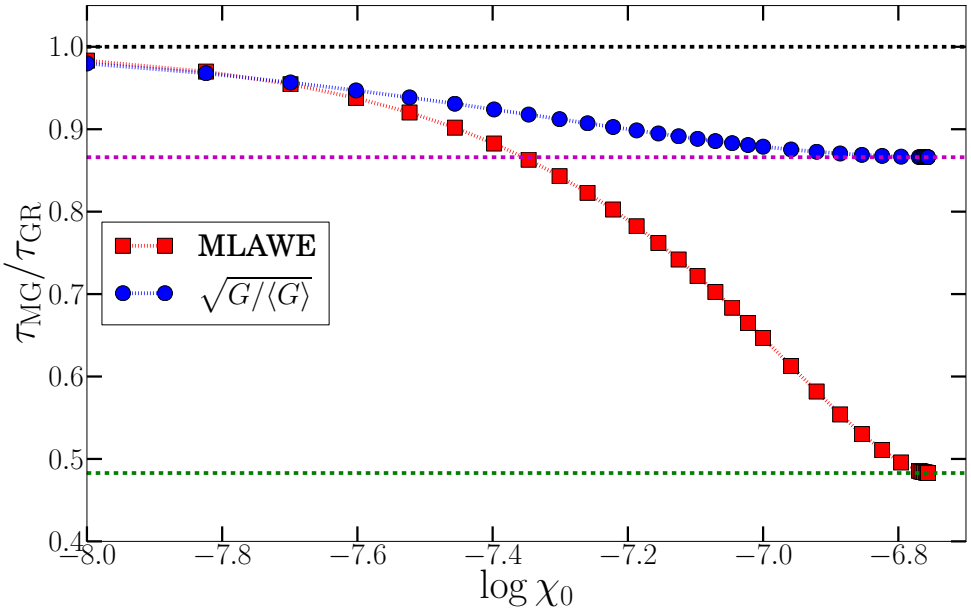


Figure 5.2: The fractional change in the stellar pulsation period as a function of $\log_{10}\chi_0$ when both the effects of the modified equilibrium structure and modified perturbation equation are considered (case 2). The red squares correspond to eigenfrequencies of the MLAWE whereas the blue circles show the approximation (5.54). The green dashed line shows the ratio for a fully unscreened star and the black dashed line shows a ratio of 1, corresponding to a general relativity star. The magenta line shows the fully-unscreened value of $\sqrt{\frac{G}{\langle G\rangle}} = (1+\alpha)^{-\frac{1}{2}}$.

of the perturbation is to increase this by an amount not as large as this initial change. These results seem to suggest that convective stars such as Cepheids and red giants may show very large changes in the oscillation periods due to their modified background structure and that the approximation will tend to under-estimate this change. Furthermore, the effects of the hydrodynamic perturbations will make these changes more drastic but not as large as those coming from the modified background. In fact, we will see below that this is not the case for Cepheid models. We will see that the approximation holds very well when only the background structure is considered but when the perturbations are included the resulting change in the period can be three times as large as that due to the modified equilibrium structure alone. One assumption we have made here is that K is constant. This is tantamount to having a uniform composition throughout the entire star. This is a good approximation for red giant stars, which are fairly homogeneous, but Cepheids have shells of varying composition and several ionised layers and so this is not an accurate approximation. In particular, we will see below that the radius of Cepheid stars does not change significantly in modified gravity, contrary to what this model would predict and this is why we find the approximation holds well when the modified gravity perturbations are ignored, despite this model's predictions.

Stability of Lane-Emden Models

Before moving on to look at realistic models from MESA, we will first use Lane-Emden models to investigate the modification to the stellar stability criterion. In section 5.3 we derived the new properties relating to stellar stability in modified gravity and argued that there are two new features: first, that when there are unstable modes present in general relativity such that $\omega_0^2 < 0$, then, when only the change equilibrium structure is taken into account, the instability is worse i.e. ω_0^2 is more negative; second, that the new term appearing in the MLAWE makes stars more stable, the critical value of $\Gamma_{1,0}$ required for $\omega_0^2 < 0$ is less than the general relativity value of $4/3$ and the correction is of order $g(\chi_0, \alpha)\alpha$ given in (5.46). $g(\chi_0, \alpha)$ encodes the competing effects of the new term in the MLAWE and the modified structure and composition

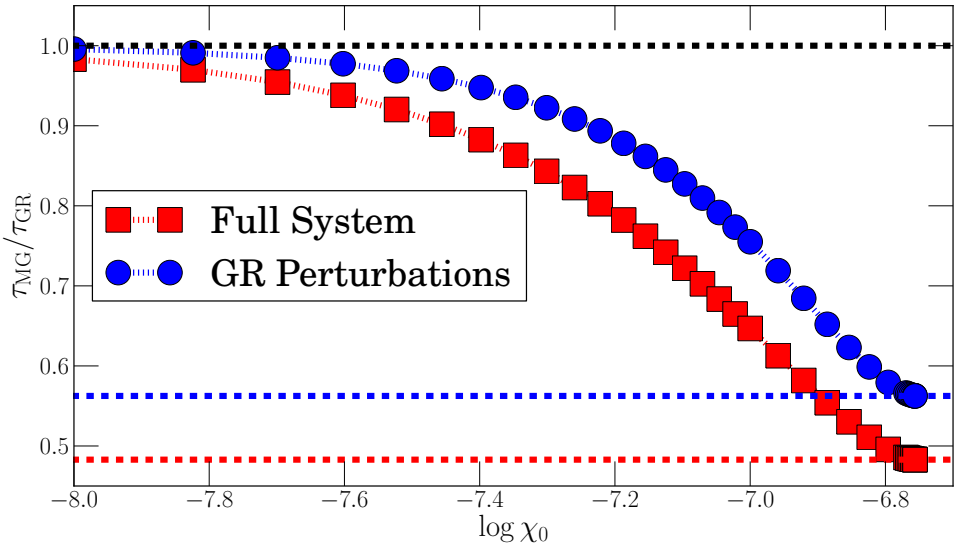


Figure 5.3: The fractional change in the stellar pulsation period as a function of $\log_{10}\chi_0$ for case 1 (blue circles) and case 2 (red squares). The black dashed line shows the general relativity ratio of 1 and the red and blue lines show the fully-unscreened ratio for the full simulation and the one including only the modified equilibrium structure respectively.

coming from the new equilibrium structure. Here, we will verify these predictions numerically.

In order to investigate the first, we have solved for the modified eigenfrequencies of the same $n = 1.5$ modified Lane-Emden model investigated in the previous section using the LAWE for various values of $\Gamma_{1,0} < 4/3$. This corresponds to a star whose adiabatic perturbations are governed by a different index to that appearing in the equation of state that fixes the equilibrium structure. In each case, the modified eigenfrequencies are indeed more negative the more unscreened the stars are and, as an example, we plot the ratio $\omega^2_{\rm MG}/\omega^2_{GR}$ in the case $\Gamma_{1,0} = 37/30 \approx 1.23333$, which is close to being stable. In this case one has $\omega^2_{\rm GR} = -0.314$ and so the larger this ratio, the more negative the modified gravity value. This is plotted in figure 5.4 and it is evident that the instability is indeed worse in stars which are more unscreened. We have checked that this is the case for other values of $\Gamma_{1,0} < 4/3$.

Next, we turn our attention to the modification of the critical value of $\Gamma_{1,0}$. In order to investigate this, we again use the $n = 1.5$ model above and vary $\Gamma_{1,0}$ as a function of χ_0. We scan through different values of $\Gamma_{1,0}$ at fixed χ_0 in order to find the value where $\omega^2 \approx 0$ (to

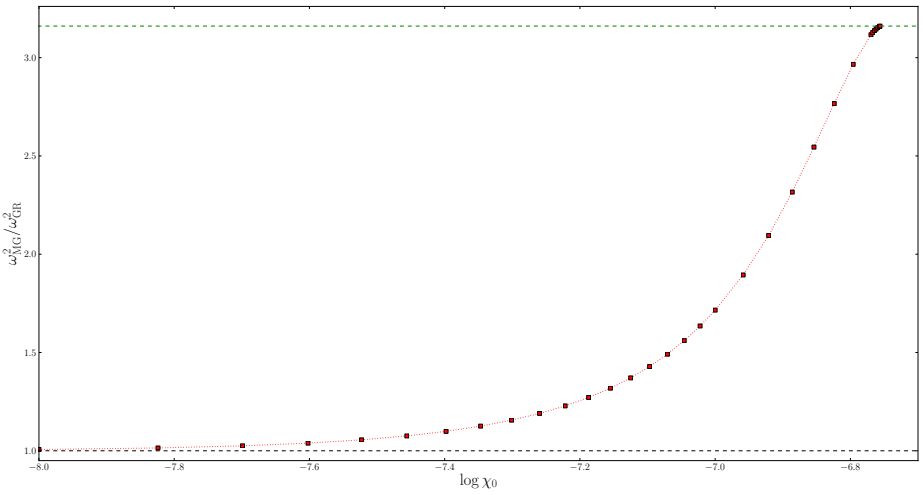


Figure 5.4: The ratio of the modified gravity to general relativity eigenfrequencies as a function of $\log_{10}\chi_0$ when $\Gamma_{1,0} \approx 1.2333$. The black dotted line shows the general relativity ratio of 1 and the green dotted line shows the ratio for a fully unscreened star.

8 decimal places), which is the new critical value in modified gravity. We solve for the zero-eigenfrequencies in two cases: the case where we ignore the modified equilibrium structure[13] and include only the modified gravity perturbations and the full MLAWE. The values of the critical value of $\Gamma_{1,0}$ vs $\log\chi_0$ are plotted in figure 5.5.

It is evident from the figure that the critical value is indeed lower than 4/3 showing that these models are indeed more stable in modified gravity. One can also see that the red curve lies above the blue one so that the effect of the modified equilibrium structure is to stabilise the star compared with how stable it would have been had only the modified perturbation structure been present. This can be seen from equation (5.47), where the effects of the modified equilibrium structure appear in the denominator of $g(\chi_0, \alpha)$. When the star is more unscreened the integrated pressure is larger, which increases the denominator and therefore reduces the size of the correction to the general relativity value. The critical value when the modified background structure is ignored decreases monotonically, however, the full MLAWE

[13]We have already argued in the previous subsection that this case is highly unphysical and ambiguous. This is true if we wish to discern how the modified gravity perturbations affect the numerical value of the oscillation periods but here we seek only to qualitatively investigate how the modified equilibrium structure influences the critical index. Hence, for this purpose it is a reasonable case to investigate.

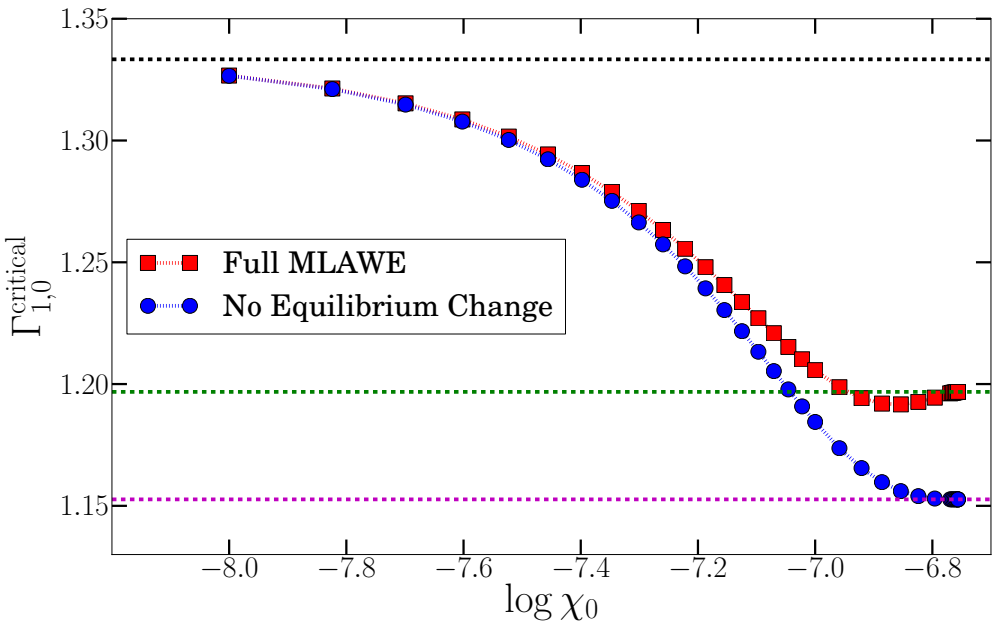


Figure 5.5: The critical value of $\Gamma_{1,0}$ as a function of $\log_{10} \chi_0$. The blue circles show the critical values when the modifications to the equilibrium structure are ignored and the red squares show the critical values when the full MLAWE is solved. The black dashed line shows the general relativity value of 4/3 and the magenta line shows the fully unscreened value when we ignore the modified equilibrium structure. The green line shows the fully unscreened value found by solving the full MLAWE.

predicts an increase in stars that are significantly unscreened, showing that the effects of this altered equilibrium structure become more important when the star is more unscreened. Finally, we note that the change in the critical index is indeed of order 10^{-1}, which we predicted using analytic arguments in section 5.3.

5.4.2 Perturbations of MESA Models

Having studied some simple stellar models and gained some intuition about the MLAWE, we now turn our attention to realistic stellar models from MESA. We will limit the discussion to Cepheid stars, firstly because we have already studied them in detail in chapter 4 and secondly because they are the only stars whose oscillations can be observed in distant galaxies[14].

Perturbations of Cepheid Models

Equation (4.19) was derived by assuming that the effect of modified gravity is to rescale Newton's constant by a constant factor. We would now like to account for the fact that this is not the case and that the effective value of G is radially varying and so it is no longer appropriate to work with ΔG since this requires some sort of averaging. Instead we will leave the perturbed period-luminosity relation in terms of $\Delta\tau/\tau$ so that one has

$$\frac{\Delta d}{d} \approx -0.6\frac{\Delta\tau}{\tau}. \tag{5.55}$$

Note that we still need to perturb the empirically calibrated period-luminosity relation since this formalism is not powerful enough to predict it. We are now in a position to calculate $\Delta\tau/\tau$ for the same models we used in table 4.3.2 and check how well the approximation we used in the previous chapter holds. We first calculate the modified periods by ignoring the effects of the modified gravity perturbations. This is equivalent to solving the general relativity problem with the modified gravity equilibrium structure and hence corresponds to finding the same

[14]Some other pulsating objects such as RR Lyrae stars can be resolved in the local group but this is necessarily screened and so these objects cannot be used to probe modified gravity.

period that we attempted to find in the previous chapter using the averaging procedure, this time including the full radial dependence of the effective value of G. Recall that in the previous chapter we assumed that the formula for the period in modified gravity is identical to that in general relativity by replacing G by an appropriate average. Implicit in this is the assumption that the dynamics of the pulsations are governed by the same underlying equations. We have already seen that this is not the case and hence our procedure was oblivious to the extra terms in the MLAWE. Next, we solve the full MLAWE and calculate the new oscillation periods, which allows us to discern how well the approximation of perturbing the general relativity formula works. The models with $\alpha = 1/3$, $\chi_0 = 10^{-6}$, $\alpha = 1/2$, $\chi_0 = 10^{-6}$ and $\alpha = 1$, $\chi_0 = 4 \times 10^{-7}$ all execute one loop that does not cross the instability strip and cross only on the second loop. This is because these stars are so unscreened that their tracks in the HR diagram are significantly different from the general relativity tracks[15]. There is hence no model to compare to the general relativity first-crossing and so we do not analyse these models[16]. Comparing table 4.3.2 with figure (4.10), we see that the remaining models correspond to those with the lowest values of χ_0 at fixed α that were ruled out by the analysis in the previous chapter and hence represent the tightest constraints placed using the previous approximation.

In table 5.1 we show $\Delta\tau/\tau$ calculated for each model using the approximation, the case where modified gravity perturbations are neglected and the full MLAWE. In table 5.2 we show

α	χ_0	$\Delta\tau/\tau$ (approximation)	$\Delta\tau/\tau$ (no perturbations)	$\Delta\tau/\tau$ (full MLAWE)
1/3	4×10^{-7}	0.086	0.092	0.266
1/2	4×10^{-7}	0.054	0.064	0.207
1	2×10^{-7}	0.102	0.122	0.314

Table 5.1: The change in the period of Cepheid pulsations due to modified gravity effects.

[15]Recall that we are using the observed instability strip to define the first crossing, which inherently assumes general relativity since it is found empirically using Cepheid stars in our own galaxy and the local group. Its location may change once one solves the full non-adiabatic problem. As discussed above, this is beyond the scope of this thesis.

[16]This is not to say that the approximation used in the previous chapter is not applicable, rather that numerically calculating the period will give spurious results due to the lack of a suitable general relativity model to compute the unmodified period.

α	χ_0	$\Delta d/d$ (approximation)	$\Delta d/d$ (no perturbations)	$\Delta d/d$ (full MLAWE)
1/3	4×10^{-7}	-0.03	-0.04	-0.12
1/2	4×10^{-7}	-0.05	-0.06	-0.16
1	2×10^{-7}	-0.06	-0.07	-0.19

Table 5.2: The change in the inferred Cepheid distance due to modified gravity. In each case $\Delta d/d$ was found using the perturbed period-luminosity relation 5.55.

how these changes propagate to $\Delta d/d$, which is the astrophysical quantity used to place constraints. MESA gives the change in the radius between modified gravity and general relativity as $\Delta R/R \sim \mathcal{O}(10^{-2})$ and so most of the change in the period is due to the enhanced gravity and not the size of the star. This is very different from the $n = 1.5$ Lane-Emden model in section 5.4.1, which predicts a large reduction in the radius when the star is unscreened. One can see that when we neglect the modified gravity perturbations the approximation we used in the previous chapter is very close to the true value, indicating that the Epstein function is very successful at describing which regions of the star determine the period of oscillation. This agreement is hardly surprising. The radius is almost constant between the two theories and the approximation was found by perturbing the LAWE prediction $\tau \propto G^{-\frac{1}{2}}$ at fixed radius. When the modified gravity perturbations are included, we see that this approximation breaks down and the relative difference in the period is $\mathcal{O}(10^{-1})$, which is approximately a day. We can see that $\Delta d/d$ can be up to three times as large as we predicted in the previous chapter using the approximation. We therefore conclude that the constraints we placed there (and that were reported in [89]) are conservative, and it is possible that they could be improved using the same data and analysis. With this in mind, we estimate the values of χ_0 and α that can be probed using the full MLAWE rather than the approximation used in chapter 4. We accomplish this by taking the same initial stellar conditions and running a series of new simulations using MESA for successively decreasing values of χ_0 at fixed α. Using the same procedure as chapter 4 to identify the Cepheid models at the blue edge, we calculate $\Delta d/d$ using the MLAWE until it is equal to the value predicted by the approximation i.e. the value that gave the tightest

α	χ_0
1/3	9×10^{-8}
1/2	7×10^{-8}
1	3×10^{-8}

Table 5.3: The lower bounds on χ_0 and α that could potentially be placed if one were to use the same procedure and data-sets as [89] using the full MLAWE instead of the approximation.

constraint before experimental errors prevented any further analysis. In table 5.3 we show the values of χ_0 and α such that the MLAWE gives the same result as the approximation.

These then represent an estimate of the range of parameters that one could hope to constrain using the same data and the MLAWE. Of course, this is just a simple estimate and a more rigorous method would be to repeat the data analysis. Nevertheless, this simple estimate serves to show that we expect the new constraints to be significantly stronger. In particular, the MLAWE predictions suggest that the constraints could be pushed into the $\mathcal{O}(10^{-8})$ regime[17].

5.5 Summary of Main Results

In this chapter we have perturbed the equations of modified gravity hydrodynamics to first-order and have found the new equations governing the oscillations of stars about their equilibrium configurations. We have specialised to radial modes since only these are observable in distant galaxies where chameleon-like theories can be tested. The MLAWE (5.22) was the resultant equation and the rest of the chapter was dedicated to its study. We have identified two new effects: firstly, the new oscillation periods of stars in these theories are always smaller than the general relativity prediction and can be up to three times smaller than one would predict if one only accounted for the modified equilibrium structure. Secondly, stars are more stable in chameleon-like theories, by which we mean that the critical first adiabatic in-

[17] One must also worry about the fact that at lower values of χ_0, galaxies will move from the unscreened to the screened sub-sample, reducing the quality of the statistics. We do not attempt to estimate the effect this will have on the lowest values of χ_0 that could potentially be constrained but we note that it will raise them above the values predicted in table 5.3.

dex for the onset of unstable radial modes is lower than the value of 4/3 predicted by general relativity. The nev value is not universal but is instead model- and composition-dependent.

Using a pulsation calculator that calculates the new eigenfrequencies by solving the MLAWE, we investigated these effects quantitatively using Lane-Emden models. These are useful to discern the new physics but are not realistic enough to compare with observational data and so we then used the calculator to find the new frequencies of MESA models. In the previous chapter, we used these MESA models to place the strongest constraints on the model parameters χ_0 and α to date using an approximation based on the LAWE. By using the same models and solving the MLAWE exactly we have found that this approximation is very conservative and that the true modified periods can be up to three times shorter than it predicts. This means that it is possible to improve the constraints shown in figure 4.10 using the same data and statistical techniques. In order to estimate the amount by which the constraints can be improved we chose three fiducial models and fixed α whilst lowering the value of χ_0 until the MLAWE prediction for $\Delta d/d$ matches the value that gave the strongest constraint in the previous chapter. This is an optimistic estimate since lowering χ_0 reduces the number of galaxies in the unscreened sample and therefore increases the statistical error. The results are shown in table 5.3, which shows that it may be possible to probe into the regime $\chi_0 \sim \mathcal{O}(10^{-8})$ provided there are a sufficient number of galaxies in the unscreened sample at these low values.

Part II:
Supersymmetric Models of Modified Gravity

There should be a science of discontent. People need hard times to develop psychic muscles.

Frank Herbert, *Dune*

You can prove anything you want by coldly logical reason — if you pick the proper postulates.

Isaac Asimov, *Reason*

6

Supersymmetric Models of Modified Gravity

In this chapter, we will change directions completely and focus on more theoretical aspects of chameleon-like models. In particular, we are interested in studying supersymmetric models. There are many reasons why one might wish to look for supersymmetric completions of these theories. One might be interested in unifying these models with particle physics within a more fundamental framework. Many beyond the standard model theories such as string theory are supersymmetric and so any supersymmetric model is a step towards this goal. Another reason is the powerful non-renormalisation theorems that supersymmetric theories enjoy. Recently, the quantum stability of these models has come into question. Symmetron models do not have a shift symmetry yet we have fine-tuned the mass to allow for screening in our own galaxy and novel features on cosmological scales. Without some symmetry protecting this value, we expect scalar loops in the matter sector to raise it considerably and so inherent in this tuning is the assumption that such a symmetry exists at some level. Chameleon models screen by increasing the mass by several orders of magnitude in dense environments. Now the Coleman-Weinberg one-loop quantum correction to the scalar potential is

$$\Delta V_{1-\text{loop}} = -\frac{1}{64\pi^2} m_\phi^4 \ln\left(\frac{m_\phi^2}{\mu^2}\right), \tag{6.1}$$

where μ is the renormalisation group scale. Clearly the more efficient the mechanism is the more we expect that quantum corrections are important and may act to negate the mechanism completely. This has been studied by [56] who have found there are large regions of parameter space where chameleon models are dominated by quantum corrections. Furthermore, [57,97] have studied the quantum effects during the radiation era and have again found that quantum corrections can act to destroy the classical dynamics. One may hope to circumvent all of these problems by including some sort of symmetry that either removes or greatly reduces the quantum corrections. This would then imply that the field is a Goldstone boson with a technically natural small mass, however this is incompatible with the screening mechanisms. Chameleon models require a very large mass in order to screen and hence this symmetry would be completely broken, thus making its introduction obsolete. Symmetron models have the field screen by moving over large regions in field space to zero and so even if the symmetry is present at one field value, it will be broken as soon as the field moves and quantum corrections will reappear. This is not the case if the symmetry imposed is supersymmetry. Supersymmetric theories have a Goldstone fermion instead and the field can therefore have a large mass whilst still enjoying small quantum corrections.

This has motivated several previous attempts at finding supersymmetric completions of chameleon-like models. The first was that of Brax & Martin [132–134] who constructed a general framework within $\mathcal{N} = 1$ supergravity where supersymmetry breaking in a hidden sector can generate non-supersymmetric corrections to the scalar potential for an arbitrary number of dark sector fields and induce a coupling between these fields to the minimum supersymmetric standard model (MSSM). This is precisely what we need for chameleon-like models; the corrections to the scalar potential may allow us to find run-away models, which is difficult in supergravity due to the power-law nature of the Kähler potential and the superpotential. Furthermore, the coupling to matter provides the scalar-tensor structure and an extra density-dependent term in the effective potential. Unfortunately, the final result was a no-go theorem precluding the existence of viable chameleon models [134]. When supersymmetry is

broken in the hidden sector it is generally at a scale M_s and particle physics typically requires this to be around 1–10^3TeV. The corrections to the scalar potential are then of $\mathcal{O}({M_{pl}}^2 M_s^2)$, leading to an effective potential for the chameleon of order

$$V_{eff}(\phi) \sim {M_{pl}}^2 M_s^2 f(\phi) + \rho(A(\phi) - 1) + \cdots, \tag{6.2}$$

where f is some $\mathcal{O}(1)$ dimensionless function. In this case the density-dependent part of the effective potential is negligible on all scales of interest for modified gravity and the mechanism cannot operate.

Another attempt has been made by [78] who have used a type IIB string theory approach where the low-energy effective action is no-scale[1] $\mathcal{N} = 1$ supergravity with corrections coming from the KKLT mechanism [135] to provide a run-away chameleon potential. In this case the volume modulus for the six-dimensional internal manifold plays the role of the chameleon in the four-dimensional theory. The coupling to matter is provided by the warp factor on the six-dimensional internal manifold and arises from the ansatz that once the compactification has been performed, the four-dimensional matter fields couple to the 10-dimensional Jordan frame metric. This is motivated by the fact that the 10-dimensional matter fields are coupled to the 10-dimensional Jordan frame metric, although a direct demonstration that this remains the case has yet to be seen. The combination of the compactification to $\mathcal{N} = 1$ with a no-scale Kähler potential, corrections from the KKLT mechanism and gaugino condensation leads to an effective potential of the form

$$V_{eff}(\phi) = V(\phi) + \rho e^{\beta \frac{\phi}{M_{pl}}} \tag{6.3}$$

where β is a constant and $V(\phi)$ is found using the supergravity formula for the scalar potential (1.72) and adding the KKLT correction. The exact form is not relevant here and the reader is referred to [78] for the technical details. This model can indeed produce a chameleon theory with constant β but only if one changes the sign of one of the constants in the gaugino

[1] The original model had $n = 3$, however this is ruled out in this set-up by accelerator searches for extra dimensions and so an updated model uses $n = 2$ [79].

condensation superpotential. Typically, $W \sim \exp(ia\sigma)$ where σ is the volume modulus and $a > 0$. This does not give rise to a run-away potential and so one is forced to take $a < 0$, which is not realised within the standard KKLT set-up, however the authors argue that situations where this is the case are possible. When the standard case of $a > 0$ is assumed the chameleon mechanism operates in reverse and the evolution of the universe acts to decompactify the extra dimensions [136]. This model has subsequently been generalised to racetrack like models [137], however this does not improve the situation.

In this chapter we will take a more bottom-up approach. Chameleon-like theories are low-energy IR modifications of gravity and so a bottom-up approach will capture all of the new supersymmetric features without the technical complications of more fundamental theories. Of course, one would ultimately like to realise these models in more fundamental theories and using results from a bottom-up approach such as this will allow us to determine which models are viable once they are supersymmetrised and therefore exactly where to concentrate the search efforts in more fundamental theories. In particular, we will see that under the most general assumptions (only global supersymmetry and corrections coming from supergravity) only $n = 3$ no-scale Kähler potentials can give rise to models that show any deviation from general relativity in the laboratory and astrophysical objects. This then gives us a clear indication of the types of models we should examine in supergravity and string theory.

Since supergravity is broken at higher energy scales than those where the screening mechanism operates we will concentrate on global supersymmetry coupled to gravity. This avoids the problem of large breaking scales appearing in the effective potential since supersymmetry is not broken in a hidden sector at very high scales[2]. Instead, we will see that supersymmetry is broken at finite density where the density-dependence in the effective potential moves the field away from the zero-density minimum, which preserves supersymmetry. In this case the scale of supersymmetry breaking is set by the ambient density and not by particle physics. This is an interesting new feature that allows one to decouple the supersymmetry breaking scales in

[2]Or rather, it is but we assume that the hidden sector fields do not couple to the sector containing the modified gravity field and so there are no corrections and the Lagrangian retains global supersymmetry.

the dark and observable sector, which may have important consequences for supersymmetric cosmology. We will only consider a theory where the field is coupled to dark matter fermions and not the observable sector. This will allow us to discern all of the new supersymmetric features without dealing with the technical complications of the entire MSSM. A generalisation of this model that includes couplings to the standard model is straight forward, although we will not examine it here.

6.1 The Framework

We will take a bottom-up approach and attempt to find the most general $\mathcal{N} = 1$ globally supersymmetric model that gives rise to an effective potential of the form (2.51). The gravitational scalar is taken to be the lowest component of a chiral superfield $\Phi = \phi + \ldots$. This is coupled to two other fields $\Phi_\pm = \phi_\pm + \sqrt{2}\theta\psi_\pm + \ldots$, whose fermions act as dark matter. The Kähler potential is

$$K(\Phi, \Phi^\dagger, \Phi_\pm, \Phi_\pm^\dagger) = \Phi_+\Phi_+^\dagger + \Phi_-\Phi_-^\dagger + \hat{K}(\Phi, \Phi^\dagger), \tag{6.4}$$

where $\hat{K}(\Phi, \Phi^\dagger)$ is left arbitrary for now. Its specific form must be chosen carefully to obtain an effective potential that realises one of the screening mechanisms described in chapter 2. When $\hat{K}(\Phi\Phi^\dagger) \neq \Phi^\dagger\Phi$ the field is not canonically normalised, indeed

$$\mathscr{L}_{\text{kin}} \supset K_{\Phi\Phi^\dagger}\nabla_\mu\Phi\nabla^\mu\Phi^\dagger \tag{6.5}$$

so that the mass of the field is

$$m_\Phi^2 = \frac{1}{K_{\Phi\Phi^\dagger}}\frac{\partial^2 V(\Phi)}{\partial\Phi\partial\Phi^\dagger}. \tag{6.6}$$

The superpotential is

$$W(\Phi, \Phi_\pm) = \hat{W}(\Phi) + mA(\Phi)\Phi_+\Phi_-, \tag{6.7}$$

where $A(\Phi)$ is an arbitrary holomorphic function of the gravitational chiral scalar only. Ultimately, it will play the role of the coupling function and so one must choose its functional form depending on which screening mechanism one wishes to realise. Again, we leave $\hat{W}$ unspecified; a specific choice of its form leads to different models. With this arrangement, $\langle\phi_+\rangle = \langle\phi_-\rangle = 0$ and so the potential is

$$V(\Phi) = V_{\rm F}(\Phi) = \hat{K}^{\Phi\Phi^\dagger}\left|\frac{\mathrm{d}\hat{W}}{\mathrm{d}\Phi}\right|^2 \tag{6.8}$$

There is a Φ-dependent contribution to the dark matter fermion mass

$$\mathscr{L}_{\rm f} = \frac{\partial^2 W}{\partial\Phi_+\partial\Phi_-}\psi_+\psi_- = mA(\Phi)\psi_+\psi_-. \tag{6.9}$$

When these fermions condense to finite density such that $\langle\psi_+\psi_-\rangle = \rho_{\rm c}/m$ this term provides an additional contribution to the potential resulting in an effective potential

$$V_{\rm eff}(\Phi) = V_{\rm F}(\Phi) + \rho_{\rm c}(A(\Phi) - 1), \tag{6.10}$$

where $\rho_{\rm c}$ is the conserved matter density. In practice, it will be necessary to decompose ϕ as $\phi = |\phi|e^{i\theta}$ and stabilise the angular field at the minimum, however several general results can be derived before specialising to specific models and so we shall continue to work with Φ for the time being. When this decomposition is used we shall set $\phi \equiv |\phi|$ and use φ to denote the field found by bringing the kinetic term for ϕ into canonical form.

6.2 Supersymmetric Features

In this section we will discuss some of the new model-independent features that accompany the embedding of these theories into a supersymmetric framework.

6.2.1 Environment-Dependent Supersymmetry Breaking

Minimising (6.10) with respect to Φ, one has

$$\left(\frac{K_{\Phi\Phi^\dagger\Phi^\dagger}}{K^2_{\Phi\Phi^\dagger}} - \frac{1}{K_{\Phi\Phi^\dagger}}\frac{\mathrm{d}^2\hat{W}}{\mathrm{d}\Phi^2}\right)\frac{\mathrm{d}\hat{W}}{\mathrm{d}\Phi} = \rho_\mathrm{c}\frac{\mathrm{d}A(\Phi)}{\mathrm{d}\Phi}. \tag{6.11}$$

The vacuum expectation value (VEV) of the dark matter scalars is $\langle\phi_\pm\rangle = 0$ and so $F_\Phi = -\mathrm{d}W/\mathrm{d}\Phi = -\mathrm{d}\hat{W}/\mathrm{d}\Phi$. Any coupling to dark matter necessarily breaks supersymmetry at finite density. This is one of the new features of supersymmetric screened modified gravity; by secluding the dark sector from the observable one (up to supergravity breaking effects described below) the scale of supersymmetry breaking is not set by particle physics effects but rather by the ambient density and so our model is not plagued with issues such as the cosmological constant being associated with TeV scale breaking effects or detailed fine-tunings. That being said, this is far from a solution to the cosmological constant problem since we do not attempt to explain why the vacuum energy in the observable sector associated with QCD and electroweak symmetry breaking does not contribute to the cosmological dynamics. We also offer no explanation for the cancelling of the cosmological constant in the hidden sector which is of order $M_\mathrm{pl}{}^2m_{3/2}^2$.

6.2.2 Absence of Observational Signatures

When working in the low-energy framework of global supersymmetry it is important to ensure that any corrections coming from supergravity breaking in the hidden sector are negligible. We will see presently that once these corrections are accounted for the vast majority of supersymmetric screened theories of modified gravity necessarily have $\chi_0 \ll 10^{-8}$ and hence there are no unscreened objects in the universe. Whereas this does not rule these theories out, it renders them observationally indistinguishable from general relativity[3].

[3]Technically, this is not quite correct, we will see in chapter 7 that there is a small region in parameter space where there are still potential deviation in the cold dark matter power spectrum on linear scales where the non-linear screening mechanism does not operate and χ_0 is not an indicator of how much modified gravity effects are

Supergravity Corrections

The most important supergravity correction for these models are those coming from $|D_\Phi W|^2$ of the form

$$\Delta V_{\cancel{\text{SUGRA}}} = \frac{K^{\Phi\Phi^\dagger}|K_\Phi|^2|W|^2}{{M_{\rm pl}}^4} e^{\frac{K}{{M_{\rm pl}}^2}} = m_{3/2}^2 K^{\Phi\Phi^\dagger}|K_\Phi|^2. \tag{6.12}$$

This correction must be negligible compared to $V_{\rm F}$ and $\rho_c A(\Phi)$ if they alone are to be responsible for the screening mechanism [4]. This correction introduces an important new feature into these models: the mass of the field is always at least as large as the gravitino mass. To see this, one can take derivatives of (6.12) and focus on certain terms only to find

$$\frac{\partial^2 V(\Phi)}{\partial\Phi\partial\Phi^\dagger} \supset m_{3/2}^2 K_{\Phi\Phi^\dagger}. \tag{6.13}$$

Recalling that the field may not be canonically normalised and applying (6.6) one finds there is a contribution to the field's mass of exactly $m_{3/2}$. This can be anywhere from 1 eV as predicted by gauge mediated supersymmetry breaking scenarios to $\mathcal{O}$(TeV) corresponding to gravity mediated breaking [138]. Consequently, the Compton wavelength of the field is $\lambda_{\rm C} \sim m_{3/2}^{-1}$ and so the range of the fifth-force in such models is always less than 10^{-6} m depending on the gravitino mass. It should be noted that this result is completely independent of the form of the matter coupling or the potential, it is not even sensitive to their origins or whether the field is coupled to dark matter or the standard model. When one has scalars coupled to matter and the theory has an underlying $\mathcal{N} = 1$ supergravity at some high energy scale then the range of the fifth-force will always be less than $m_{3/2}^{-1}$. In supergravity breaking scenarios with a large gravitino mass this precludes the need for screening mechanisms altogether.

Another immediate consequence of this is that canonical symmetrons [19] cannot be accommodated within a supersymmetric framework. The supersymmetric symmetron is found by imposing a $\mathbb{Z}_2$ symmetry upon the effective potential. This is achieved by including only

suppressed.

[4] If this is not the case then one is really working within the framework of supergravity and can therefore not realise any screening mechanisms due to the no-go result of [134].

odd powers of Φ in $\hat{W}(\Phi)$ and only even powers in the coupling $A(\Phi)$. The Kähler potential is $\hat{K}(\Phi\Phi^\dagger) = \Phi^\dagger\Phi$ so that the fields are canonically normalised and, at lowest relevant order, the superpotential is

$$W(\Phi) = M^2\Phi + \frac{1}{3}g\Phi^3 + m\left(1 - h\frac{\Phi^2}{2m\Lambda_3} + f\frac{\Phi^4}{4m\Lambda_3^3}\right)\Phi_+\Phi_-, \tag{6.14}$$

where the explicit introduction of the $-$ sign in the coupling will become clear momentarily. The F-term potential is then

$$V_{\rm F}(\phi,\theta) = M^4 + g^2\phi^4 + 2gM^2\phi^2\cos(2\theta), \tag{6.15}$$

which is minimised when $\cos(2\theta) = -1$ so that the model is a symmetron:

$$\begin{aligned} V(\phi) &= M^4 - 2gM^2\phi^2 + g^2\phi^4 = (g\phi^2 - M^2)^2, \\ A(\phi) &= 1 + h\frac{\phi^2}{2m\Lambda_3} + f\frac{\phi^4}{4m\Lambda_3^3}. \end{aligned} \tag{6.16}$$

Note that this has a supersymmetric minimum ($V = 0$) at $\phi_0 = M/\sqrt{g}$; at finite density the field moves to smaller value thereby breaking this supersymmetry. Now the symmetron mechanism requires that the bare mass be negative, however there is a contribution from supergravity corrections of $\mathcal{O}(m_{3/2}^2)$ and so either we must demand that there is a fine-tuned cancellation or we must take $M > m_{3/2}$ (recall that the canonical symmetron model requires $M \leq 10^{-29}eV$ whereas $m_{3/2} \geq 1$ eV). If this is not the case the symmetron mechanism is lost. Suppose then that $M > m_{3/2}$. We have

$$\beta(\phi) = M_{\rm pl}\frac{{\rm d}\ln A(\phi)}{{\rm d}\phi} \sim \frac{M_{\rm pl}\phi_0}{m\Lambda_3} \tag{6.17}$$

in the cosmological background when the $\mathbb{Z}_2$ symmetry is broken. So if the force is to be of comparable strength to gravity in free space we need $MM_{\rm pl} \sim m\Lambda_3$. Now the symmetry is

broken (or restored) at a density

$$\rho_\star \sim M^2 m \Lambda_3 \sim M^3 M_{\rm pl} > m_{3/2}^3 M_{\rm pl} > 10^{27}\ {\rm eV}^4 = 10^{39}\rho_0, \tag{6.18}$$

where we have taken the best case scenario of an eV mass gravitino. This means that in the late-time universe only objects whose densities exceed 10^{27} eV^4 can restore the $\mathbb{Z}_2$ symmetry locally and screen the fifth-force. This immediately precludes screening in all dark matter haloes (whose density is typically $10^6\rho_0$) and Earth based laboratories (with density $10^{29}\rho_0$). This problem is not ameliorated if we instead allow the force in free space to be stronger than gravity since this increases the lower bound on $\rho_\star$. Either the symmetron mechanism does not exist or $\mathcal{O}(1)$ fifth-forces are present in our solar system. One should note that this does not rule out the symmetron as a viable model of modified gravity but it is the case that if the universe is supersymmetric (including an underlying supergravity) then the symmetron mechanism cannot be realised.

One may then also wonder whether the same is true of generalised symmetrons? In this case, a correction to the mass of $\mathcal{O}(m_{3/2})$ does not affect the choices for the parameters in the theory since a mass term is not present in the effective potential before supergravity corrections are included (see equation (2.49)), however, it does add a term proportional to $m_{3/2}^2\phi^2$ to the effective potential and hence changes the transition from second to first order. In this case, the mechanism is lost and $\beta(\phi)$ does not approach zero smoothly in increasingly dense environments. Therefore, it is not possible to realise generalised symmetrons within a supersymmetric framework either.

No-Scale-Type Models

Given that the mere presence of an underlying supergravity imposes such stringent restrictions on the mass of the field one might naturally wonder how general these restrictions really are and whether they can be circumvented. There are indeed a class of models where the

supergravity correction, i.e. the mass (6.13) is not present. Clearly if $K^{\Phi\Phi^\dagger}|K_\Phi|^2$ is constant then (6.13) is spurious since the second derivative of the corrections are zero and there are no corrections to the field's mass. These are the no-scale type models, a particularly common example of which is the logarithmic Kähler potential that arises in type IIB superstring theory $K = -n{M_{\rm pl}}^2 \ln[(\Phi+\Phi^\dagger)/M_{\rm pl}]$ ($n = 1$ for the dilaton and $n = 3$ for T-moduli, which corresponds to the pure no-scale case where $V_{\rm F}(\phi) = 0$ at the minimum). In more complicated scenarios one typically has many chiral scalars which parametrise a no-scale type manifold given by $K^{\Phi_i\Phi_j^\dagger}K_{\Phi_i}K_{\Phi_j^\dagger} = c$ with $c = 3$ in the pure no-scale case.

These models evade the corrections so one may wonder if they are re-introduced by loop corrections. The one-loop effective potential is

$$\Delta V_{1-\rm loop} = -\frac{1}{64\pi^2}\mathrm{STr}\left[M^4 \ln\frac{M^2}{\mu^2}\right], \tag{6.19}$$

where M is the mass matrix and μ is the renormalisation group scale. At tree level we have, for the scalar, $M^2 \sim |\hat{W}_{\Phi\Phi}|^2$ and so if $\hat{W} \sim \mathcal{O}(\mathscr{M}^3)$ we expect $\mathscr{M} \ll M_{\rm pl}$ since $\hat{W}$ is associated with low-energy behaviour well below the supergravity breaking scale. In this case, the quantum corrections are set entirely by the tree-level parameters[5], which a priori are independent of the gravitino mass.

The equation (6.19) encompasses only supersymmetric corrections and so we must also account for the soft masses induced by hidden sector supersymmetry breaking. These have been studied extensively by [139–141] (and references therein) who find that whenever the manifold is not pure no-scale i.e. $K^{\Phi_i\Phi_j^\dagger}K_{\Phi_i}K_{\Phi_j^\dagger} \neq 3$ the soft masses are always of order $m_{3/2}$ and so one can conclude that these models do not evade the supergravity breaking constraints. Furthermore, in the pure no-scale case the same analyses have shown that only no-scale models

[5]Note that since the theory is supersymmetric we do not expect corrections to the scalar mass coming from fermion loops that would usually be present in non-supersymmetric theories and be of a similar order to the largest fermion mass. We have already seen above that the underlying supersymmetry is broken at finite density and that the scale of breaking is set by the local density and hence we expect corrections to be present at this scale, which we will see in the next chapter is generally a lot lower than any standard model (and hence also supersymmetric partner) fermion masses.

where the isometry group of the scalar manifold is

$$\mathscr{M} = \frac{\mathrm{SU}(1,n)}{\mathrm{U}(1)\times\mathrm{SU}(n-1)}, \tag{6.20}$$

do not acquire soft masses. Any no-scale model whose isometry group differs from this must necessarily include gravitino-mass scalars in its low-energy effective theory.

One should note however that it is very difficult to find screening mechanisms with this class of Kähler potentials. For example, in the simplest case where $K = -3{M_{\rm pl}}^2 \ln(T+T^\dagger)/M_{\rm pl}$, the canonically normalised field is $\Phi = \exp(\sqrt{2/3}\,\phi/M_{\rm pl})$. Now any term in the superpotential is of the form $W(\Phi) \propto \Phi^n$ and so at best one has an exponentially decreasing scalar potential and an exponentially increasing coupling function. It is very difficult to obtain a thin shell solution for an Earth-like density profile in such a model [20]. One must then rely on non-perturbative effects to generate a viable potential and no satisfactory mechanism has been found to date.

We can then discern the conditions under which globally supersymmetric theories are not bound by constraints from supergravity breaking; they must be no-scale models with the isometry group (6.20). At the level of string theory, models such as these receive corrections to their Kähler potentials in string perturbation theory, which are then used in the tree-level supergravity formula to find the scalar potential. Hence, only string theory models which preserve this no-scale property to all orders in perturbation theory and under non-perturbative corrections can evade the supergravity corrections. At the level of field theory, any no-scale model with this isometry group will always lead to a low-energy model which is not bound by these constraints.

Efficient Screening

When the models do not evade the supergravity corrections the presence of a contribution of order $m_{3/2}$ to the field's mass is enough to ensure that the screening in these models is so

efficient that no object in the universe is unscreened. This can be deduced as follows. Working with the canonically normalised field φ and assuming that θ is stabilised at its minimum, the new effective potential is[6]

$$V_{\rm eff}(\varphi) = V_{\rm F}(\varphi) + \rho(A(\phi) - 1) + \frac{1}{2}m_{3/2}^2\varphi^2. \tag{6.21}$$

At the minimum, we have

$$-\frac{\beta(\varphi_0)\rho_0}{M_{\rm pl}\varphi_0} = m_{3/2}^2 + \frac{1}{\varphi_0}\frac{{\rm d}V_{\rm F}(\varphi)}{{\rm d}\varphi} \tag{6.22}$$

where we have used the fact that $A(\varphi_0) \approx 1$. If this equation has no solutions then there is no minimum and the theory is not one of screened modified gravity. We are interested in situations where this is not the case and so we will assume that a minimum exists. Now the left hand side of this equation — barring any fine-tuned cancellation — must be as large as $m_{3/2}^2$, in which case

$$\frac{\varphi_0}{\beta_\varphi(\varphi_0)} \leq \frac{\rho_0}{m_{3/2}^2 M_{\rm pl}}. \tag{6.23}$$

The quantity on the left hand side of the inequality is precisely χ_0 (see equation (2.77)). Taking equation (6.23) and inserting it into (2.77) we have

$$\chi_0 \leq \left(\frac{H_0}{m_{3/2}}\right)^2, \tag{6.24}$$

where $\rho_0 \sim 3\Omega_{\rm c}^0 H_0^2 {M_{\rm pl}}^2$. In the best case scenario we have $m_{3/2} \sim \mathcal{O}({\rm eV})$ and so we have $\chi_0 \leq 10^{-66}$. In section 2.2.6 we showed that most unscreened objects in the universe are dwarf galaxies with $\Phi_{\rm N} \sim 10^{-8}$ and so this condition ensures that no object in the universe is unscreened; hence, there are no observational signatures of fifth-forces in any astrophysical object. Since $\chi_{\rm MW} \ll \chi_0$ ($\chi_{\rm MW}$ is the value of χ_c in the Milky Way), the mass of the field in the Milky Way is $m_{\rm MW} \gg m_0 \gg 10^{33}H_0$ (see the discussion in section 2.2.5) whereby $\gg$ we

[6]Note that we are using ρ and not $\rho_{\rm c}$ since this argument holds even when the field is coupled to baryons

mean several orders of magnitude. The Compton wavelength corresponding to a mass this large is well below the length scales that can be probed using current laboratory probes of fifth-forces [76]. Therefore, this bound also precludes any possibility of a laboratory detection and will continue to do so for the foreseeable future.

This behaviour can alternatively be seen by considering the derivation of the field profile presented in section 2.2.5 in the unscreened region of a spherical over-density. Consider a spherical object of constant dark matter density ρ_b embedded in a much larger medium of density ρ_c so that

$$\rho(r) = \begin{cases} \rho_b, & r < R \\ \rho_c, & r > R \end{cases} . \tag{6.25}$$

When the object is static, equation (2.23) becomes $\nabla^2\varphi = V_{\rm eff}(\varphi)_{,\varphi}$ and when the object is unscreened the field only differs from the exterior value by a small perturbation $\delta\varphi$ and we can expand this to first order to find

$$\nabla^2\delta\varphi \approx m_c^2\delta\varphi + \frac{\beta_\varphi(\varphi_0)\delta\rho}{M_{\rm pl}}, \tag{6.26}$$

where $\delta\rho = \rho_b - \rho_c$ and m_c^2 is the mass of the field in the outer medium. The next step was to use the fact that models with screening mechanisms have the property that the Compton wavelength of the field $\lambda_{\rm C}m_c^{-1}$ is much greater than the size of the object and so we neglected the mass term for the perturbation. In these models however, we have $m_c \geq m_{3/2} \geq 1$ eV$\sim 10^{28}$Mpc^{-1} and therefore the Compton wavelength is incredibly small compared with typical galactic, stellar and planetary scales. Therefore, the unscreened solution does not exist in any object in the universe.

If there is such a thing as reincarnation, knowing my luck I'll come back as me.

John Sullivan, *Rodney Trotter in: Only Fools and Horses*

7

Phenomenology of Supersymmetric Chameleons

In the previous chapter we presented a general framework for embedding screened modified gravity into global supersymmetry and proved several model-independent results. We showed that supersymmetric symmetrons do not exist and that supersymmetric chameleons (and theories that screen via the environment-dependent Damour-Polyakov effect) have $\chi_0 < 10^{-66}$. This implies that there are no unscreened objects in the universe and hence astrophysical or laboratory tests of modified gravity cannot probe these models. No-scale models are an exception, however we showed that the simplest models do not screen and, to date, more complicated models have not been found. Whereas χ_0 sets the screening properties of collapsed objects, there are two regimes where it is not enough to specify whether modified gravity effects are present: the cosmological background and linear scales in cosmological perturbation theory. In this chapter, we will construct a class of supersymmetric chameleon models using the framework of the previous chapter and use them as prototypes to investigate both of these regimes.

On cosmological scales, the homogeneous time-evolution of the scalar field is a source

of pressure and density in the Friedmann equation in the Einstein frame, which may lead to different cosmological dynamics from ΛCDM[1]. The first part of this chapter examines the background cosmology of the supersymmetric chameleon model we will construct using the tools presented in section 2.2.8. We will find that the dynamics are indistinguishable from ΛCDM and so we require a cosmological constant to act as dark energy[2]. This presents a new problem not present in more phenomenological chameleon models. Supersymmetry is broken if the vacuum energy density is positive and so we cannot include a cosmological constant at the level of the action, one must be induced via the dynamics. One could appeal to supergravity breaking, which contributes an amount of order $M_{\rm pl}{}^2 m_{3/2}^2$ to the vacuum energy density. This is the same order as the supergravity breaking scale and is far too large compared with the measured value and so this contribution needs to be fine-tuned away in most supersymmetric models and chameleons are no exception. Instead, we will present a new and novel mechanism where a cosmological constant in the form of a Fayet-Illiopoulos term appears at late times due to the coupling of the chameleon to two charged scalars. The scalar potential for these scalars is $\mathbb{Z}_2$ symmetric with a mass term that depends on the chameleon VEV. At early times, the symmetry is broken and the charged scalars have non-zero VEVs but as time progresses, the chameleon evolves towards larger field values and the coefficient of the mass term becomes increasing larger, eventually becoming positive and restoring the symmetry. At this time, the scalar's VEV moves towards zero, leaving only an FI term in the potential which acts as a cosmological constant. FI terms have no natural value within global supersymmetry and run logarithmically at most with the energy scale [142] and so tuning this term to match the current observed energy density is technically natural and an appealing model, which merits further study in terms of the cosmological constant problem[3]. We will investigate the range of

[1] [58] have proved a general no-go result stating that chameleon-like models are indistinguishable from ΛCDM. One of their key assumptions is that the coupling to matter $\beta(\phi) \sim \mathcal{O}(1)$. Supersymmetric models do not satisfy this property and since $\beta \gg \mathcal{O}(1)$ and so this theorem does not apply to these models.

[2] Technically, any other dynamical degrees of freedom whose phenomenology can reproduce the current data could be included in the model, however this is more complicated and we will consider dark energy to be a cosmological constant for simplicity.

[3] Of course, this is far from a solution to the cosmological constant problem. We are fine-tuning all the contributions to the vacuum energy density coming from supergravity breaking in the hidden sector and any symmetry

parameters that allow this cosmological constant to be generated before last scattering so that its effects are imprinted on the CMB and will use this to rule out certain regions in the model parameter space.

We next turn our attention to linear perturbations of CDM. The screening mechanism is inherently non-linear, and so we do not expect to see any deviation in the CDM power spectrum on scales greater than $0.1h$ Mpc^{-1}[4], however, on scales less than this the mechanism cannot operate and χ_0 is a meaningless parameter for describing the extent of the modifications of gravity. We therefore expect that deviations from general relativity may be present. In order to investigate this, we solve the modified equations governing CDM perturbations and calculate the modified CDM power spectrum. This indeed shows an enhancement on large scales due to the enhanced gravitational force arising from the unscreened fifth-force. This enhancement can be made arbitrarily large or small by tuning the model parameters due to the lack of other constraints. We rule out some parameter ranges by demanding that these deviations are not larger than the error of 10% reported by the WiggleZ survey [143] and indicate the regions in parameter space that could potentially be probed using Euclid.

7.1 Supersymmetric Chameleon Models

So far, we have not presented any specific chameleon models. In this section we will use the framework of section (6.1) to construct one possible class. In theory, it is possible to construct other classes of models although to date none have been studied. We will argue at the end of this chapter than the phenomenology of these models will not differ too drastically from the ones we will construct here and are no more appealing.

The Kähler potential for Φ is non-canonical — this is a requirement for it to give rise to a

breaking in the matter sector including the electroweak and QCD phase transitions to zero. Furthermore, we have no natural mechanism that sets the magnitude of the FI term and appeal to supergravity (or possibly more fundamental physics) to provide this mechanism

[4]We assume that the scale on which perturbations become non-linear is approximately the same as the non-linear scale in general relativity. This is motivated by the efficient screening theorem of the previous chapter.

run-away potential — whilst the dark matter fields are canonically normalised:

$$K(\Phi,\Phi^\dagger)=\frac{\Lambda_1^2}{2}\left(\frac{\Phi^\dagger\Phi}{\Lambda_1^2}\right)^\gamma+\Phi_+^\dagger\Phi_++\Phi_-^\dagger\Phi_-, \tag{7.1}$$

where γ is an arbitrary integer exponent whose value determines how steep the run-away potential is. The self-interacting part of the superpotential is

$$\hat{W}=\frac{\gamma}{\sqrt{2}\alpha}\left(\frac{\Phi^\alpha}{\Lambda_0^{\alpha-3}}\right)+\frac{1}{\sqrt{2}}\left(\frac{\Phi^\gamma}{\Lambda_2^{\gamma-3}}\right), \tag{7.2}$$

where $\Phi=\phi+\sqrt{2}\theta\psi+\ldots$ contains a scalar ϕ whose modulus ultimately plays the role of the superchameleon and $\Phi_\pm=\phi_\pm+\sqrt{2}\theta\psi_\pm+\ldots$ are chiral superfields containing dark matter fermions $\psi_\pm$. Splitting the superchameleon field as $\phi(x)=|\phi|e^{i\theta}$ and identifying $\phi\equiv|\phi|$ from here on, one can minimise the angular field (this is done explicitly in appendix E where a coupling to two U(1) charged scalars, which we will introduce later, is also examined) and define the new quantities

$$\Lambda^4\equiv\left(\frac{\Lambda_1}{\Lambda_2}\right)^{2\gamma-2}{\Lambda_2}^4,\quad M^{n+4}=\left(\frac{\Lambda_1}{\Lambda_0}\right)^{2\gamma-2}{\Lambda_0}^{n+4},\quad \phi_{\min}=\left(\frac{M}{\Lambda}\right)^{\frac{4}{n}}M,\quad n=2(\alpha-\gamma) \tag{7.3}$$

to find the F-term potential

$$V_{\rm F}(\phi)=K^{\Phi\Phi^\dagger}\left|\frac{\mathrm{d}W}{\mathrm{d}\Phi}\right|^2=\left(\Lambda^2-\frac{M^{2+\frac{n}{2}}}{\phi^{\frac{n}{2}}}\right)^2=\Lambda^4\left[1-\left(\frac{\phi_{\min}}{\phi}\right)^{\frac{n}{2}}\right]^2. \tag{7.4}$$

The parameters Λ_i appearing in the Kähler potential and superpotential are scales associated with non-renormalisable operators and one would expect them to be large, however, we can see that the scales governing the low-energy dynamics are M and Λ. We will explore their values in detail when discussing the parameter space in section 7.2.2. In practice, it is easier to work with other low-energy parameters, which will be introduced later, and their relation to these parameters is given in appendix F. The index n should be even and one would expect

γ and α to be small (but not 1) given their origin as indices in the superpotential and so we will often consider the case $n = 2$ when the need to elucidate specific calculations arises.

When $\phi \ll \phi_{\rm min}$ equation (7.4) reduces to the Ratra-Peebles potential

$$V_{\rm F}(\phi) \approx \Lambda^4 \left(\frac{\phi_{\rm min}}{\phi}\right)^n, \tag{7.5}$$

which has been well studied in the context of dark energy [144] (although one should be aware that we have not yet canonically normalised our field). At larger field values the potential has a minimum at $\phi = \phi_{\rm min}$ where $V(\phi_{\rm min}) = 0$ and $\mathrm{d}W/\mathrm{d}\Phi = 0$. Supersymmetry is therefore broken whenever $\phi \neq \phi_{\rm min}$.

The coupling function is found by considering the part of the superpotential containing the interactions of Φ and $\Phi_\pm$

$$W_{\rm int} = m\left[1 + \frac{g}{m}\frac{\Phi^\delta}{\Lambda_3^{\delta-1}}\right]\Phi_+\Phi_-, \tag{7.6}$$

which gives a superchameleon-dependent mass to the dark matter fermions

$$\mathscr{L} \supset \frac{\partial^2 W}{\partial\Phi_+\partial\Phi_-}\psi_+\psi_-. \tag{7.7}$$

When the dark matter condenses to a finite density $\rho_{\rm c} = m\langle\psi_+\psi_-\rangle$ this term provides a density-dependent contribution to the scalar potential resulting in the scalar-tensor effective potential $V_{\rm eff} = V + \rho_{\rm c}(A-1)$. With the above choice of superpotential, the coupling function is

$$A(\phi) = 1 + \frac{g}{m{\Lambda_3}^{\delta-1}}\phi^\delta = 1 + \left(\frac{\phi}{\mu}\right)^\delta; \quad \mu^\delta \equiv \frac{m\Lambda_3^{\delta-1}}{g}. \tag{7.8}$$

The scale Λ_3 is not present when $\delta = 1$, which may make fine-tuning of the dark matter mass necessary. For this reason, we will always consider $\delta \geq 2$. As it stands, the field ϕ is not canonically normalised since the kinetic term in the Lagrangian reads

$$\mathscr{L}_{\rm kin} = -K_{\phi\phi^\dagger}\partial_\mu\phi\partial_\mu\phi^\dagger = -\frac{1}{2}\gamma^2\left(\frac{|\phi|}{\Lambda_1}\right)^{2\gamma-2}\partial_\mu\phi\partial_\mu\phi^\dagger. \tag{7.9}$$

The normalised field is

$$\varphi = \Lambda_1 \left(\frac{\phi}{\Lambda_1} \right)^{\gamma} \tag{7.10}$$

so that the coupling function (7.8) becomes

$$A(\varphi) = 1 + x \left(\frac{\varphi}{\varphi_{\min}} \right)^{\frac{\delta}{\gamma}}; \quad x \equiv \frac{g \phi_{\min}^{\delta}}{m \Lambda_3{}^{\delta-1}} \tag{7.11}$$

and the effective potential is

$$V_{\text{eff}}(\varphi) = \Lambda^4 \left[1 - \left(\frac{\varphi_{\min}}{\varphi} \right)^{\frac{n}{2\gamma}} \right]^2 + x \rho_{\text{c}} \left(\frac{\varphi}{\varphi_{\min}} \right)^{\frac{\delta}{\gamma}}, \tag{7.12}$$

which is shown in figure 7.1. We may then find the coupling $\beta(\varphi)$:

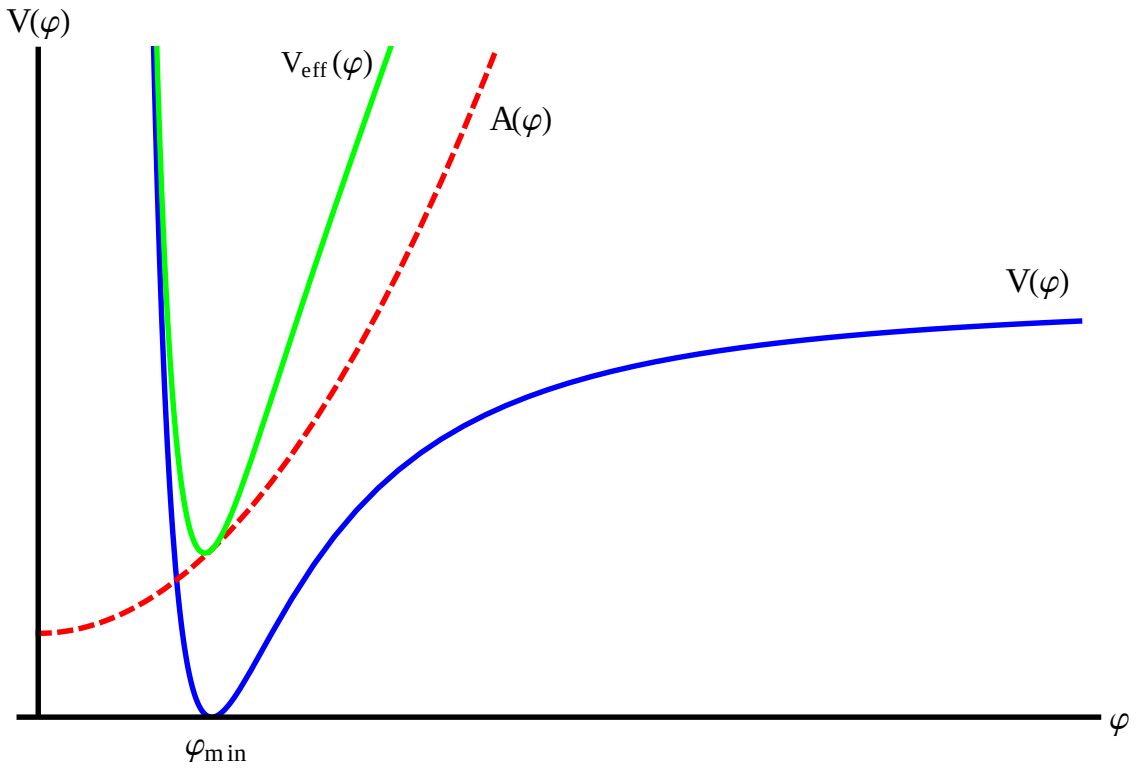


Figure 7.1: The effective potential.

$$\beta(\varphi) = \frac{x\delta M_{\rm pl}}{\gamma\varphi_{\rm min}}\left[1+\left(\frac{\varphi}{\varphi_{\rm min}}\right)^{\frac{\delta}{\gamma}}\right]^{-1}\left(\frac{\varphi}{\varphi_{\rm min}}\right)^{\frac{\delta}{\gamma}-1}. \tag{7.13}$$

Equation (7.12) is the effective low-energy potential for a scalar-tensor theory described in section 2.2 with the scalar coupled to dark matter via the coupling function $A(\varphi)$. Minimising the effective potential we have[5]

$$\left(\frac{\varphi_{\rm min}}{\varphi}\right)^{\frac{n+\delta}{\gamma}} - \left(\frac{\varphi_{\rm min}}{\varphi}\right)^{\frac{n+2\delta}{2\gamma}} = \frac{\rho_{\rm c}}{\rho_\infty}, \tag{7.14}$$

where

$$\rho_\infty \equiv \frac{n\Lambda^4}{\delta x} \equiv \rho_{\rm c}^0(1+z_\infty)^3 = 3\Omega_{\rm c}^0 {M_{\rm pl}}^2 H_0^2(1+z_\infty)^3, \tag{7.15}$$

which defines the quantity z_∞. This is an important model parameter; we will see later that it is the redshift at which the field settles into its supersymmetric minimum. It turns out that this redshift controls the large scale behaviour of the modified linear CDM power spectrum, whose features change very rapidly for modes which enter the horizon after this redshift.

At zero density the field sits at the supersymmetric minimum $\varphi = \varphi_{\rm min}$ where its mass is

$$m_\infty^2 \equiv \frac{n\delta x\rho_\infty}{2\gamma^2\varphi_{\rm min}^2} = \frac{3n\delta x}{2\gamma^2}\Omega_{\rm c}^0(1+z_\infty)^3\left(\frac{M_{\rm pl}}{\varphi_{\rm min}}\right)^2 H_0^2. \tag{7.16}$$

When $\rho_{\rm c} \gtrsim \rho_\infty$ the field minimum is moved to smaller values by the matter coupling term and supersymmetry is broken. Supersymmetry is therefore broken locally in our model depending on the ambient density and ρ_∞. The scale of this breaking is set by the cold dark matter density and the model parameters, however this is generally far lower than the TeV scale associated with particle physics in the observable sector. This is one advantage of decoupling the dark and observable sectors, the dark sector does not suffer from an unnatural hierarchy of scales set by the decoupling of standard model particles. Away from the supersymmetric minimum,

[5]The careful reader may notice that taking the limit $\delta = 1$ gives a different equation from that found in [145], which contains a typographical error.

the field's mass is

$$m_\varphi^2 = m_\infty^2 \left[\frac{2(n+\gamma)}{n} \left(\frac{\varphi_{\rm min}}{\varphi} \right)^{\frac{n}{\gamma}+2} - \frac{n+2\gamma}{n} \left(\frac{\varphi_{\rm min}}{\varphi} \right)^{\frac{n}{2\gamma}+2} + \frac{2(\delta-\gamma)}{n} \frac{\rho_{\rm c}}{\rho_\infty} \left(\frac{\varphi_{\rm min}}{\varphi} \right)^{2-\frac{\delta}{\gamma}} \right]. \tag{7.17}$$

Clearly $m_{\rm eff}(\varphi) > m_\infty$ when $\varphi < \varphi_{\rm min}$ and so these models are indeed chameleons with a mass at the minimum of the effective potential which depends on the matter density.

7.1.1 Supergravity Corrections and Screening

We saw in section 6.2.2 that supergravity corrections place extremely stringent constraints on combinations of the model parameters and ensure that the screening is too efficient to allow laboratory or astrophysical tests. Here we will briefly elucidate how this works in practice by calculating the corrections to this specific class of models.

The correction to the potential coming from supergravity breaking is

$$\Delta V_{\not{\rm SG}} = \frac{m_{3/2}^2 \left| K_\Phi \right|^2}{K_{\Phi\Phi^\dagger}} \sim \frac{m_{3/2}^2 \phi^{2\gamma}}{\Lambda_1^{2\gamma-2}}, \tag{7.18}$$

which competes with the density-dependent term in the effective potential (7.12) to set the position of the minimum. Since we focus on the branch of the potential where $\phi \leq \phi_{\rm min}$, this term can always be neglected provided that it is far less than the density-dependent term when ϕ has converged to its supersymmetric minimum. This requires that the supergravity corrections are negligible at densities around ρ_∞ so that

$$\left(\frac{\varphi_{\rm min}}{M_{\rm pl}} \right)^2 \ll \frac{x\rho_\infty}{{M_{\rm pl}}^2 m_{3/2}^2}. \tag{7.19}$$

The denominator is proportional to the supergravity contribution to the vacuum energy, which is typically very large and is usually fine-tuned away whereas the numerator is proportional to the vacuum energy when the supersymmetric minimum is reached (see below), which we

expect to be well below this. This condition tells us that the supersymmetric minimum must be well below the Planck scale and is simply the statement that the matter coupling and fifth-force is a low-energy, IR phenomena. It will be useful to express this condition in the alternative form

$$\left(\frac{\varphi_{\min}}{M_{\rm pl}}\right)^2 \ll 3x\Omega_{\rm c}^0(1+z_\infty)^3\left(\frac{H_0}{m_{3/2}}\right)^2, \tag{7.20}$$

from which it is immediately evident that $\varphi_{\min} \ll M_{\rm pl}$ even when the gravitino mass is as low as the gauge mediated supersymmetry breaking value of 1 eV. Using (7.15) equation (7.19) can be recast as a condition on the normalised field's mass at the supersymmetric minimum

$$m_\infty^2 \gg \frac{3n\delta}{2\gamma^2}m_{3/2}^2. \tag{7.21}$$

The field's mass is at least as large as the gravitino mass. The condition (7.19) also has implications for the coupling $\beta(\varphi)$. Using it in conjunction with equation (7.13), the coupling when the field reaches the supersymmetric minimum (we will see in the next section that this happens at late times) satisfies

$$\beta(\varphi_{\min}) \gg \frac{x^{\frac{1}{2}}\delta}{\sqrt{3\Omega_{\rm c}^0}\gamma}\left(\frac{m_{3/2}}{H_0}\right) \gg 10^{33}x^{\frac{1}{2}} \tag{7.22}$$

and so we see that $\beta(\varphi) \gg \mathcal{O}(1)$ unlike more conventional chameleon models that assume order-one couplings.

7.2 Cosmology

In this section we will examine the cosmology of these models with the aim of accounting for dark energy. As alluded to in the introduction to this chapter, we will ultimately find that a cosmological constant is required in order to match both the present day equation of state w and the energy density in dark energy.

7.2.1 Background Cosmology

Solving (7.14) for the minimum in the limit of both large and small dark matter density we have

$$\frac{\varphi}{\varphi_{\rm min}} \approx \begin{cases} \left(\frac{\rho_\infty}{\rho_{\rm c}}\right)^{\frac{\gamma}{n+\delta}}, & \rho_{\rm c} \gg \rho_\infty \\ 1, & \rho_{\rm c} \ll \rho_\infty \end{cases}. \tag{7.23}$$

We can now find the contribution to the vacuum energy density

$$V_{\rm eff}(\varphi) \approx \begin{cases} \frac{x(\delta+n)}{n}\rho_{\rm c}\left(\frac{\rho_\infty}{\rho_{\rm c}}\right)^{\frac{\delta}{n+\delta}}, & \rho_{\rm c} \gg \rho_\infty \\ x\rho_{\rm c}, & \rho_{\rm c} \ll \rho_\infty \end{cases} \tag{7.24}$$

and the mass of the field using (7.17)

$$\left(\frac{m_\varphi}{m_\infty}\right)^2 \approx \begin{cases} \frac{2(\delta+n)}{n}\left(\frac{\rho_{\rm c}}{\rho_\infty}\right)^{\frac{n+2\gamma}{n+\delta}}, & \rho_{\rm c} \gg \rho_\infty \\ 1, & \rho_{\rm c} \ll \rho_\infty \end{cases}. \tag{7.25}$$

Finally, one can find the equation of state for the field w_φ using equation (2.93). so that

$$w_\varphi = \begin{cases} -\frac{\delta}{n+\delta}, & \rho_{\rm c} \gg \rho_\infty \\ 0, & \rho_{\rm c} \ll \rho_\infty \end{cases}. \tag{7.26}$$

In order to match this with current observations we would like $w_\varphi \approx -1$, which can be achieved by taking the limits $\rho_{\rm c} \gg \rho_\infty$, $\delta \gg n$ and imposing the condition

$$x\delta(1+z_\infty)^3 \approx 3n\Omega_{\rm c}^0. \tag{7.27}$$

This corresponds to the case where $z_\infty < 0$ and the supersymmetric minimum has not been reached by the current epoch. Both n and δ appear as indices (or a combination of indices) in the superpotential and so we would expect them to be of similar order; taking $\delta \gg n$ is

then tantamount to neglecting many lower order operators in the superpotential, making the model appear somewhat contrived. When these conditions are not met — we will see shortly that this scenario gives rise to unacceptably large deviations in the CDM power spectrum — a cosmological constant is required in order to account for the present-day dark energy observations. Unlike most models however, it is not so simple to add a cosmological constant by hand within a supersymmetric framework. Global supersymmetry is broken if $\langle V \rangle \neq 0$ and so the addition of a cosmological constant to the system is non-trivial. One method is to appeal to supergravity breaking, which adds a cosmological constant of the order ${M_{\rm pl}}^2 m_{3/2}^2 \gg \rho_0$ and so one must somehow fine-tune to great extent in order to arrive at the small value observed today. Here, we will take a different approach. If we assume that the cosmological constant problem in the matter and observable sectors is solved then we can dynamically generate a cosmological constant at late times in the form of a Fayet-Illiopoulos term provided that there exists a coupling between the chameleon and two U(1) charged scalars. Unfortunately, this does not remove the need for some degree of fine-tuning, since the value of the Fayet-Illiopoulos constant must be set by hand in this framework, however, this method has the advantage that this constant receives no quantum corrections from decoupling particles and so if one can find a more UV complete theory where its value is set in terms of other constants then this value would be preserved at low energy scales. The study of globally supersymmetric chameleons is aimed as a first step towards realising them within a more UV complete theory and a lot of insight can be gained by studying this mechanism.

7.2.2 A Late-time Cosmological Constant

An effective cosmological constant can be implemented by introducing two new scalars[6] $\Pi_\pm = \pi_\pm + \ldots$ with charges $\pm q$ under a local U(1) gauge symmetry. These have the canonical Kähler

[6] One new scalar is not sufficient since there is no U(1)-invariant superpotential that can be written down for a single charged scalar and so it is not possible to couple the gravitational scalar to the charged sector.

potential

$$K = \Pi_+^\dagger e^{2qX}\Pi_+ + \Pi_-^\dagger e^{-2qX}\Pi_-, \tag{7.28}$$

where X is the U(1) vector multiplet containing the gauge field and couple to the superchameleon via the superpotential

$$W_\pi = g'\Phi\Pi_+\Pi_-. \tag{7.29}$$

This construction gives rise to a new structure for the F-term potential as well as a D-term potential for the fields $\pi_\pm$:

$$V_{\rm D} = \frac{1}{2}\left(q\pi_+^2 - q\pi_-^2 - \xi^2\right)^2, \tag{7.30}$$

where we have included a Fayet-Illiopoulos term $2\xi^2$ which will later play the role of the cosmological constant. The new scalar potential is far more complicated with the addition of these new fields but when $\langle\pi_-\rangle = 0$ it reduces to the original effective potential for the superchameleon (7.12) and an effective potential for π_+:

$$V(\pi_+) = \frac{1}{2}\left(q\pi_+^2 - \xi^2\right)^2 + g'^2\phi^2\pi_+^2; \quad \langle\pi_-\rangle = 0, \tag{7.31}$$

where in this expression we have set $\pi_+ = |\pi_+|$ and will continue to do so from here on. In appendix E we minimise the entire global F- and D-term potentials with respect to the angular fields coming from $\pi_\pm$ and show that $\langle\pi_-\rangle = 0$ is indeed a stable minimum of the system.

The mass of the charged scalar π_+ is $m_{\pi_+}^2 = g'^2\phi^2 - q^2\xi^2$. At early times the superchameleon is small ($\ll \phi_{\rm min}$) and this mass is negative and the $U(1)$ symmetry is therefore broken ($\langle\pi_+\rangle \neq 0$). However, as the cosmological field evolves towards its minimum this mass slowly increases until it reaches zero, restoring the symmetry so that $\langle\pi_+\rangle = 0$. We would therefore expect $\pi_+ = 0$ in the late-time universe leaving us with the FI term, which plays the

role of a cosmological constant. Indeed, minimising (7.31) with respect to π_+ one finds

$$q^2\pi_+^2 = \begin{cases} 0 & \phi \geq \Delta \\ q\xi^2 - g'^2\phi^2 & \phi < \Delta \end{cases}, \tag{7.32}$$

where

$$\Delta \equiv \sqrt{\frac{q}{g'^2}}\,\xi \tag{7.33}$$

and $\phi = \Delta$ is equivalent to the statement $m_{\pi_+} = 0$. When $\langle \pi_+ \rangle = 0$ equation (7.31) reduces to $V(\pi_+) = \xi^2/2$ and so we shall set $\xi \sim 10^{-3}$ eV in order to match the present-day energy density in dark energy. There is no natural choice for this parameter within our globally supersymmetric framework and so this value is completely arbitrary. Once set, this value is largely robust to quantum corrections; when supersymmetry is unbroken they do not run and when this is not the case they run logarithmically at most [142]. Therefore, if one could find a natural mechanism by which a small FI term is present in a more UV complete theory, for example a suitable combination of two or more large mass scales, then its value at lower energy scales will remain at the same magnitude[7]; the same is not true of scalar VEVs, which receive large corrections from heavy particle loops.

7.2.3 The Model Parameter Space

Given the above mechanism, it is prudent to examine the model parameter space to determine the viable regions where a cosmological constant can appear. Firstly, when $\langle \pi_+ \rangle \neq 0$ (i.e. at early times) there are corrections to the superchameleon potential which can act to alter its cosmological dynamics. Secondly, we must ensure that the cosmological constant has the correct properties to reproduce current observations. We require the symmetry to be restored

[7] Here we are assuming that the cosmological constant problem in the hidden and observable sectors is resolved.

at field values lower than the supersymmetric minimum, which requires

$$\phi_{\min} > \Delta \quad \text{or equivalently} \quad \left(\frac{M}{\Lambda}\right)^{\frac{4}{n}} > \left(\frac{q}{2g'^2}\right)^{\frac{1}{2}} \frac{\xi}{M}. \tag{7.34}$$

Furthermore, if our model is to produce the correct imprint on the CMB then the cosmological constant must be generated before last scattering. We shall do this by imposing that the cosmological density ρ_Δ (given in (F.4)) at which the U(1) symmetry is restored is greater than 1 eV^4.

Corrections to the Scalar Potential

At late times (defined by the time at which $\phi = \Delta$) we have a FI cosmological constant, but at earlier times the non-zero VEV of π_+ induces corrections to the effective potential for ϕ[8]:

$$V_{\text{corr}} = \frac{g'^2\xi^2}{q}\phi^2 - \frac{g'^4}{2q^2}\phi^4. \tag{7.35}$$

These corrections compete with the density-dependent term coming from the dark matter coupling and therefore act to negate the chameleon mechanism. When they are important, they lead to a new, density-independent minimum. Since the magnitude of the density-dependent term decreases as the dark matter redshifts away it is possible to have a scenario where the field gets stuck at the new minimum and the cosmological constant is never generated.

There are several possible scenarios involving these corrections, which either allow or preclude the generation of a cosmological constant depending on the model parameters. If the corrections are negligible compared to the density-dependent term throughout the entire time that $\phi < \Delta$ then they are never important to the model dynamics and vanish once $\phi > \Delta$. If, on the other hand, the corrections are important before they vanish then their dynamics must

[8]At first glance, one may be concerned that the correction proportional to $-\phi^4$ results in a potential that is unbounded from below, but this form of the potential is deceptive. If one were to consider allowing the field to run away down this potential then at some point we would be in a situation where $\phi > \Delta$ and these corrections are no longer present; what looks like an unbounded potential is in fact a hill in the global potential.

be included. However, if ϕ can still pass Δ then a cosmological constant can still be generated since the corrections vanish after Δ is passed. If the only important correction is the quadratic one then a minimum always develops and therefore the cosmological constant will only be generated if the field value at this minimum is larger than Δ. If either the quartic correction or both corrections simultaneously are important then the potential may or may not develop a minimum. If no minimum develops then the field will eventually pass Δ since the potential takes on a (locally) run-away form. If a minimum does develop then we again require the field value at this minimum be larger than Δ in order to generate a viable cosmology. The exact details of how one can determine which scenario is applicable to a certain choice of parameters and whether or not the dynamics are affected to the extent that the model is not viable are given in full detail in appendix F. Below, we shall only present the resulting parameter space once every possible scenario is taken into account.

Low-Energy Parameters

In order to classify the parameter space into viable regions we will need to derive certain conditions on combinations of the model parameters and so it is important to know which parameters are fixed in terms of certain combinations of the others. It will be sufficient to examine the position of the minima and the values of ϕ relative to Δ and at no point will we need to use the dynamics of φ. For this reason, we will work exclusively with the field ϕ and not its canonically normalised counterpart since this avoids unnecessary powers of γ. We have already seen in section 7.1 that three of the underlying parameters Λ_i $(i = 0, 1, 2)$ combine to form two derived parameters M and Λ. What are observable (or rather, what governs the low-energy dynamics) however are the low-energy parameters $n, \delta, \gamma, x, \mu, z_\infty, g'$, which are either combinations of M and Λ or indices that appear in the low-energy effective potentials (7.8) and (7.31); μ is a combination of the underlying parameter Λ_3 and the dark matter mass

m. It will prove useful to introduce the parameter

$$\mathscr{G} \equiv g'/\sqrt{q}. \tag{7.36}$$

A static analysis therefore probes the six dimensional parameter space $n, \delta, x, \mu, z_\infty, \mathscr{G}$ and leaves γ unspecified.

In what follows, we will be interested in regions of parameter space where the background cosmology is viable and the parameters themselves assume *sensible* values. In order to decide exactly what is meant by "sensible" it is instructive to pause and think about their physical significance. n and δ are indices (or are combinations of indices) that appear in a superpotential and so these should naturally have values close to 1 as argued in section 7.2.1. $g' = \sqrt{q}\mathscr{G}$ is a U(1) coupling constant that appears in the coupling of the charged fields to ϕ and so we would expect values of $\mathcal{O}(10^{-2} - 10^{-3})$ so that the theory is not strongly coupled. Values much smaller than this would be tantamount to fine-tuning. Similarly, x parametrises the ratio of the vacuum energy density to the matter density when the field has converged to its supersymmetric minimum. The energy density in the field today is (see equation (7.24)) $V_{\rm eff}(\phi_{\rm min}) = x\rho_{\rm c}$, which must be less than ξ^4 so that the dominant contribution to dark energy comes from the cosmological constant and so we require $x \lesssim \mathcal{O}(1)$. Naïvely, one might argue that x should be small since it also parametrises the coupling to matter (see equations (7.11) and (7.13)) and so directly controls the enhanced gravitational force. We have already seen that supergravity corrections ensure that all astrophysical fifth-force effects are screened and so this argument does not apply.

Finally, we are left $\mu = m^{\frac{1}{\delta}}\Lambda_3^{\frac{\delta-1}{\delta}}$. When $\delta = 1$ this is simply the dark matter mass and thus varying μ is tantamount to fine-tuning the dark matter mass to produce an acceptable cosmology. When $\delta \neq 1$ however we are free to fix the dark matter mass and what we are really varying is Λ_3. In this sense we are not fine-tuning when we vary μ but are in fact scanning the space of viable cosmologies as a function of Λ_3. For this reason, we shall always

fix $\delta \neq 1$. Now the dark matter mass can be any where from $\mathcal{O}$(eV) to $\mathcal{O}$(TeV) depending on the model and Λ_3 appears as a mass scale in the underlying supersymmetric theory and so we would naturally expect it to be large (at least compared to the scales involved in the low-energy dynamics). Hence, in what follows we will treat anywhere in the region $\mathcal{O}(\text{eV}) \lesssim \mu \lesssim \mathcal{O}(M_{\text{pl}})$ as sensible.

7.2.4 Constraints on the Parameter Space

Given the above considerations and the procedure for dealing with corrections to the effective potential in appendix F we are now in a position to explore the parameter space at the background level.

We have performed a thorough investigation into the exact effects of varying each of the six parameters on the cosmology and can find a large region where the parameters are indeed sensible and the background cosmology is viable. It is difficult to gain any insight from the equations since they are all heavily interdependent in a complicated fashion and a large number of plots can be misleading since they can change very abruptly when a single parameter is varied by a small amount. For these reasons, here we shall simply describe the qualitative effects of varying some of the more constrained and less interesting parameters and present only a few two-dimensional cross-sections once these have been fixed at sensible values. We will also indicate the regions where the linear CDM power spectrum deviates from the general relativity prediction by up to 10% and can therefore be probed with upcoming experiments such as Euclid [9] whilst the other regions will show a negligible deviation. This region is found using the power spectrum derived in section 7.3 and parameters that give deviations already ruled out by WiggleZ [143] are not shown in the plots.

Let us begin with the indices. n[9] and δ have very similar effects: if their value is increased whilst fixing the other five parameters then the region of parameter space where the corrections can be neglected will increase. Being indices, these should not stray too far from $\mathcal{O}(1)$

[9]Note that $n = 2(\gamma - \alpha)$ and n can only assume even values.

and so their effects are far less pronounced than the other parameters, some of which can vary over many orders of magnitude. Hence, from here on we will fix $n = \delta = 2$. In figure 7.2 we plot the z_∞–log(x) plane with $\mu = 10^3$ TeV and $\mathcal{G} = 10^{-2}$ corresponding to what we have argued above are sensible values. For the sake of brevity we will set $z_\infty = 5$ from here on. This choice is completely arbitrary and different choices may give rise to very different cross-sections of parameter space, however, the region where the corrections are negligible is both ubiquitous and generically large when $z_\infty \gtrsim 0$ and so it is not necessary to scan this parameter in great detail in order to narrow down a viable region.

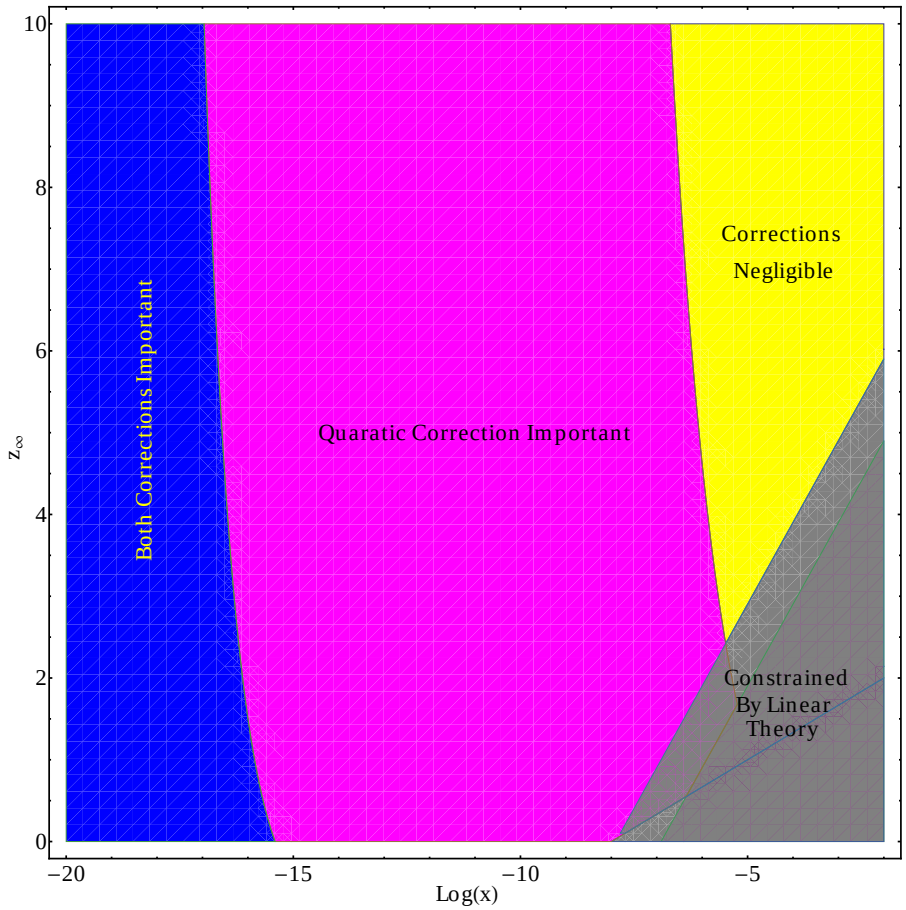


Figure 7.2: The various regions in the z_∞–log(x) plane with $n = \delta = 2$, $\mu = 10^3$ TeV and $\mathcal{G} = 10^{-2}$. The yellow region shows the parameter range where the corrections are negligible. The magenta region shows the ranges where the quadratic correction is important, the dark blue region where both corrections are important. The grey region corresponds to parameters where the model deviates from ΛCDM at the level of linear perturbations.

Next, we plot the log(μ)–log(x) plane with $n = \delta = 2$ and $\mathscr{G} = 10^{-2}$ in figure 7.3 to investigate the effects of varying μ on the viable region. It is evident from the figure that large ($\gtrsim \mathcal{O}$(TeV)) values of μ are required for there to be a large region with negligible corrections; in fact, if one steadily increases μ one finds that this region grows, replacing the regions where the corrections are important. This behaviour can be traced back to equations (F.4) and (F.7) in appendix F where it is shown that $M^{4+n} \propto \mu^n$ and therefore the density at which the corrections disappear increases slightly faster with μ than the densities at which the corrections become important. Finally, now that we have some idea of the viable values of z_∞ and μ we plot the log($\mathscr{G}$)-log(x) plane with $n = \delta = 2$ and $\mu = 10^3$ TeV in figure 7.4 in order to investigate the values of $\mathscr{G}$ where the corrections are negligible. One can see that when $\mathscr{G} \gtrsim \mathcal{O}(1)$ the corrections are generally negligible, which is a result of (F.4) in appendix F, which show that the density at which the corrections disappear generally grows faster with $\mathscr{G}$ than the density at which they become important. The density at which the corrections are important both include an explicit factor of x^{-1} which is absent from the density at which the corrections disappear (there are other factors of x coming from the scale M though these vary with a far smaller power). This is the reason that the region where the corrections are negligible is larger when x is closer to 1. The plot clearly shows that there is a large region around $\mathscr{G} \approx 10^{-2}$, which we have argued above is a sensible range where there is no excessive fine-tuning or strong U(1) coupling. With the parameters we have chosen this only exists when $x \gtrsim 10^{-10}$, however this does not really constrain x. If one were to increase either n, δ, z_∞ or μ this region would extend further in the direction of decreasing x. Thus, we have found that when the model parameters assume sensible values there is a large region of parameter space where the corrections to the effective potential are negligible before they vanish and an FI cosmological constant appears at late times. When the FI cosmological constant is generated, the background cosmology is indistinguishable from ΛCDM and so one must look at the growth of structure on linear scales in order to probe this theory. This will be examined in detail in the next section.

7.3 Linear Perturbations

In this section we calculate the modified linear CDM power spectrum predicted by these models. This allows us to rule out parameters that give deviations in tension with current experiments such as WiggleZ [143] and identify those regions that could be probed by upcoming experiments such as Euclid [9].

The equation governing the evolution of CDM perturbations in the conformal Newtonian gauge was given in equation (2.96). Given (7.21), we have $am_{3/2} \gg 2.5 \times 10^{28} a$ Mpc^{-1} and so on the scales of interest we are always in the limit $k \ll m_\varphi a$. In this limit we can linearise (2.96) to find

$$\ddot{\delta}_c + 2H\dot{\delta}_c - \frac{3}{2}\Omega_c(a)H^2\left(1 + 2k^2\frac{\beta^2(\varphi)}{m_{\rm eff}^2 a^2}\right)\delta_c \approx 0. \tag{7.37}$$

Equation (7.37) will be our starting point in what follows; it has solutions that can be written in terms of *modified Bessel functions*. A short introduction to these functions, including how equations of the form (7.37) can be transformed into the modified Bessel equation is provided in appendix D. The quantity δ_c is gauge-dependent and so is not a physical observable. Previous works have put constraints on their models by looking for the parameters where the final term in (7.37) is small and the general relativity result is recovered. "Small", is a gauge-dependent statement and it is the linear power spectrum that is the physical observable so here we shall study its deviations from the ΛCDM predictions as a potential observable probe of supersymmetric chameleons.

In the radiation era, we have

$$\ddot{\delta}_c + 2H\dot{\delta}_c - \frac{3}{2}H^2\left(\frac{G_{\rm eff}(k)}{G}\right)\frac{\bar{\rho}_c}{\bar{\rho}_c + \bar{\rho}_r}\delta_c = 0, \tag{7.38}$$

where $G_{\rm eff}(k)$ is defined in (2.97) and $\bar{\rho}_c/(\bar{\rho}_c + \bar{\rho}_r) \approx (1+z_{\rm eq})/(1+z)$. In general relativity, $G_{\rm eff} = G$ and this final term is negligible compared with the time derivatives of δ_c, which scale as $H^2\delta_c$, and can be neglected to give a logarithmic growth of the density contrast, $\delta_c \propto \ln(t)$.

With the inclusion of modified gravity, one has

$$\frac{G_{\rm eff}-G}{G}\left(\frac{1+z_{\rm eq}}{1+z}\right)\approx\mathcal{O}(1)\,x\left(\frac{k}{10^{-5}\ {\rm Mpc}^{-1}}\right)^2\frac{1}{(1+z)^{\frac{2n+5\delta}{n+\delta}}}, \tag{7.39}$$

where $H_0^2\sim 10^{-5}h^2\ {\rm Mpc}^{-1}$. Now modes deep inside the horizon can have arbitrarily large values of k, however, we know that, in general relativity at least, modes with $k>0.1h\ {\rm Mpc}^{-1}$ will be non-linear today even if they were not in the past so that we do not need to keep track of their evolution. In modified gravity, we expect this number to be smaller, however here we will use the general relativity value in order to be conservative. In this case, the largest mode which is linear today satisfies $k/10^{-5}h\ {\rm Mpc}^{-1}\sim 10^4$. Now $z\gg z_{\rm eq}\sim 10^3$ and the minimum possible value of $(2n+5\delta)/(n+\delta)$ is 2 so that the maximum deviation from general relativity satisfies

$$\left.\frac{G_{\rm eff}-G}{G}\left(\frac{1+z_{\rm eq}}{1+z}\right)\right|_{\rm max}\ll 10^2 x. \tag{7.40}$$

Unless x assumes unrealistically large values $x\sim\mathcal{O}(1)$, which we shall see below gives large deviations from the CDM power spectrum today in tension with current observations, the final term in (7.38) is negligible and the modes evolve in an identical manner to general relativity.

We can use the standard general relativity result and for simplicity we will not use the full logarithmic form but will treat the modes as constant inside the radiation era[10]. Outside the horizon, both during the matter and radiation eras, we have $G_{\rm eff}\approx G$ since the modifications of general relativity are suppressed and so the perturbations do not evolve. We hence treat the modes as constant until the time of horizon re-entry. Finally, we shall treat the change from radiation to matter domination as a sharp transition. Whilst not strictly necessary, this allows us to compute the power spectrum analytically and there are no subtleties associated with modified gravity in treating the full transition period. We make this approximation in the interest of discerning the new features introduced by supersymmetric chameleons as simply

[10]This approximation may be relaxed with little effort and indeed should be if one wishes to compare with observational data. Given that we shall not do so here there is little to be gained by including the logarithmic term.

as possible.

On the scalar field side, we assume that the field settles into its supersymmetric minimum instantaneously at $\rho_c = \rho_\infty$, thereby ignoring the short-lived transition period when equation (7.14) has no analytic solution and any oscillations around the minimum. This was studied in a specific case in [42], where it was found that the sharp settling is a very good approximation and so we do not expect the short-lived transition period to impact upon the power spectrum. Our power spectrum therefore exhibits unphysical sharp discontinuities at the scales which enter the horizon at matter-radiation equality and (as we shall see momentarily) at z_∞, which would be found to be smooth curves had we solved the full equations numerically. We will primarily be concerned with the power spectrum on large scales, since this is where it is least constrained and so these unphysical features will play no part in our conclusions.

In what follows we shall consider two distinct cases. In the previous subsection we found that we can account for dark energy without a cosmological constant by imposing $z_\infty < 0$, $\rho_c \gg \rho_\infty$ and $\delta \gg n$ and so we shall first investigate this case. We will find that this gives unacceptably large deviations from the general relativity prediction and so we then proceed to investigate the general case $z_\infty \gtrsim 0$. The field is assumed to reach its supersymmetric minimum sometime around the current epoch i.e. $z_\infty \lesssim 10$ although our treatment will be valid for $z_\infty \leq z_{\rm eq}$.

In the following we focus on the power spectrum in the matter era. After the end of the matter era around a redshift $z \sim 1$, the growth of structure is slowed down by the presence of dark energy. Hence deviations of the power spectrum from ΛCDM are maximally dependent on the features of modified gravity when calculated at the end of the matter era. Here we shall only make sure that the deviations from general relativity are no larger than around 10% to comply with recent observations [143]. Upcoming large scale surveys like Euclid will measure the linear CDM power spectrum to the percent level [9] and so have the power to place further constraints on superchameleon models. The results of these calculations have been used in figures 7.2–7.4 in section 7.2.4 to indicate where exactly in the parameter space

these deviations occur.

7.3.1 $z_\infty < 0$

This is the case where the field is displaced from the supersymmetric minimum at all times prior to the present epoch and will settle into it at some point in the future. We have seen in section 7.2.1 that when $\delta \gg n$ and $x\delta(1+z_\infty)^3 \approx 3n\Omega_c^0$ we can have $w_\varphi \approx -1$ and $V_{\rm eff} \sim {M_{\rm pl}}^2 H_0^2$, consistent with the current dark energy observations. Since this case is of particular interest to us we will enforce these conditions below and refer to them as the *dark energy conditions*. Assuming a matter dominated era we can use equations (7.13) and (7.17) in (7.37) to find

$$t^2\ddot{\delta}_c + \frac{4}{3}t\dot{\delta}_c - \left[\frac{2}{3}\Omega_c^0 + 9x(1+z_\infty)^3(kt_0)^2\left(\frac{t}{t_0}\right)^{\frac{8}{3}}\right]\delta_c. \tag{7.41}$$

Following appendix D, the growing mode solution is

$$\delta_c(t) = C_{\rm MG}(k)t^{-\frac{1}{6}}I_\nu\left[\sigma k t_0\left(\frac{t}{t_0}\right)^{\frac{4}{3}}\right], \tag{7.42}$$

where

$$\nu^2 = \frac{1}{8}\left(\frac{1}{8}+3\Omega_c\right) \quad \text{and} \quad \sigma^2 \equiv \frac{81x(1+z_\infty)^3}{16} \approx \frac{243}{16}\frac{n\Omega_c^0}{\delta}, \tag{7.43}$$

where the last equality for σ holds when we impose the dark energy conditions conditions. This should be compared with the general relativity prediction

$$\delta_c(t) = C_{\rm GR}(K)t^n; \quad \text{where} \quad n = -\frac{1}{6}+\frac{1}{2}\sqrt{\frac{1}{9}+\frac{8}{3}\Omega_c^0}, \tag{7.44}$$

where $\Omega_c^0 \sim 1$ at the end of the matter era. For small x, we have $I_\nu(x) \sim x^\nu\left[1+\mathcal{O}(x^2)\right]$ to leading order (see appendix D) and noting that $8\nu = 6n+1$ we can see that these expressions agree for small k as indeed they should since $G_{\rm eff} \approx G$ in this limit.

Given the solution (7.42) we are now in a position to calculate the power spectrum. We start by noting that the time at which a given mode crosses the horizon ($k = 2\pi aH$) is

$$t_{\rm H} = t_0 \left(\frac{4\pi}{3t_0 k}\right)^3 \tag{7.45}$$

and assume that the modes are constant during the radiation era and outside the horizon in the matter era as discussed above. In this case, the contrast during the radiation era (and outside the horizon in the matter era) is given by the primordial fluctuations from inflation, $\delta_{\rm c}^{\rm I}$. Modes that enter the horizon during the matter era, that is modes with $k < k_{\rm eq} = 0.01h$ Mpc^{-1}, will begin evolving according to (7.42) and so we have the boundary condition $\delta_{\rm c}(t_{\rm H}) = C_{\rm MG}(k) t_{\rm H}^{-1/6} I_\nu[\sigma k t_0 (t_{\rm H}/t_0)^{4/3}]$, which allows us to find $C_{\rm MG}(k)$ and hence the power spectrum

$$P(k) = \langle \left|\delta_{\rm c}(t_0)\right|^2 \rangle = \langle \left|\delta_{\rm c}^{\rm I}\right|^2 \rangle \begin{cases} \left(\frac{t_{\rm H}}{t_0}\right)^{\frac{1}{3}} \frac{I_\nu^2(\sigma k t_0)}{I_\nu^2\left[\sigma k t_0 \left(\frac{t_{\rm H}}{t_0}\right)^{\frac{4}{3}}\right]} & k < k_{\rm eq} \\ \left(\frac{t_{\rm eq}}{t_0}\right)^{\frac{1}{3}} \frac{I_\nu^2(\sigma k t_0)}{I_\nu^2\left[\sigma k t_0 \left(\frac{t_{\rm eq}}{t_0}\right)^{\frac{4}{3}}\right]} & k > k_{\rm eq} \end{cases} . \tag{7.46}$$

Modified Bessel functions diverge from their leading order general relativity behaviour very rapidly and so if the modified power spectrum is not to deviate from the general relativity prediction too greatly the arguments of both functions in (7.46) must be small enough such that the leading order behaviour is a good approximation, at least over the entire range of k where linear theory is valid. Since $t_0 > t_{\rm H}$ this is equivalent to demanding $\sigma k t_0 \ll 1$. When this is satisfied the power spectrum will show no deviations from general relativity and when this begins to break down we expect to see small deviations. One can verify using equation (D.5) in appendix D that the leading order dependence is k^4, the same as predicted by general relativity. Alternatively, according to (2.97) we should recover the general relativity prediction whenever $k \ll m_{\rm eff}/\beta(\varphi)$. Using equations (7.13) and (7.17) one finds an equivalent condition up to an order unity coefficient.

One can then define scale $\tilde{k}$ below which no gravitational enhancement is felt:

$$\tilde{k}^2 \simeq \frac{H_0^2}{x(1+z_\infty)^3} = \frac{\delta H_0^2}{3n\Omega_c^0}, \tag{7.47}$$

where the last equality holds when we impose the dark energy conditions. Since $k \sim H_0$ corresponds to modes which enter the horizon today we expect deviations from general relativity on smaller scales. Unless $\delta \gg 10^6 n$, the linear CDM power spectrum differs from the general relativity one by several orders of magnitude. Since δ appears as an index in the superpotential such a large value seems highly unnatural. With this in mind, we will abandon this limit and proceed to study the general case where we allow n and δ to vary independently and φ to converge to its supersymmetric minimum at some point in the recent past.

7.3.2 $z_\infty > 0$

This is the case where the field has settled into its supersymmetric minimum sometime in the past. We start by noting that when $z_\infty > 0$ the final term in (7.37) will exhibit a different time dependence after the field has converged to its supersymmetric minimum, so we must keep track of modes that enter the horizon before and after this and match the time evolution appropriately. We therefore begin by solving (7.37) for the case where $z < z_\infty$ so that $\varphi \approx \varphi_{\min}$ and $m_\varphi \approx m_\infty$. Assuming a matter dominated epoch and defining $k_\infty = 2\pi a(t_\infty)H(t_\infty)$ to be the mode which enters the horizon when $z = z_\infty$ ($t_\infty = t_0(1+z_\infty)^{-3/2}$) we have

$$t^2\ddot{\delta}_c + \frac{4}{3}t\dot{\delta}_c - \left[\frac{2}{3}\Omega_c^0 + \frac{9x\delta}{n(1+z_\infty)^3}(kt_0)^2\left(\frac{t_0}{t}\right)^{\frac{4}{3}}\right]\delta_c \quad k < k_\infty. \tag{7.48}$$

Following appendix D we can again write down the solution in terms of modified Bessel functions. Since the final term decreases with increasing t the growing mode is the modified Bessel

function of the second kind:

$$\delta_{\rm c}(t) = C_{\rm MG}^{k<k_\infty}(k) t^{-\frac{1}{6}} K_\omega \left[\zeta k t_0 \left(\frac{t_0}{t} \right)^{\frac{2}{3}} \right], \tag{7.49}$$

where

$$\zeta^2 \equiv \frac{27 x \delta}{2n(1+z_\infty)^3}; \quad \text{and} \quad \omega^2 = \frac{9}{4}\left(\frac{1}{36} + \frac{2}{3}\Omega_{\rm c}^0\right). \tag{7.50}$$

Next, we must find the solution when $k > k_\infty$. In this case we have (using equations (7.13), (7.23) and (7.25))

$$t^2 \ddot{\delta}_{\rm c} + \frac{4}{3} t \dot{\delta}_{\rm c} - \left[\frac{2}{3}\Omega_{\rm c}^0 + 9 \frac{x\delta}{n+\delta} (1+z_\infty)^{\frac{3\delta}{n+\delta}} k^2 t_0^2 \left(\frac{t}{t_0} \right)^{\frac{8\delta+2n}{3(\delta+n)}} \right] \delta_{\rm c}, \tag{7.51}$$

the solution of which is

$$\delta_{\rm c}(t) = C_{\rm MG}^{k>k_\infty}(k) I_\nu \left[\sigma k t_0 \left(\frac{t}{t_0} \right)^r \right]; \quad \nu^2 = \left(\frac{\delta+n}{4\delta+n} \right)^2 \left[\frac{1}{4} + 6\Omega_{\rm c}^0 \right], \tag{7.52}$$

with

$$\sigma^2 \equiv \frac{81 x \delta (\delta+n)(1+z_\infty)^{\frac{3\delta}{\delta+n}}}{(4\delta+n)^2} \quad \text{and} \quad r = \frac{4\delta+n}{3(\delta+n)}. \tag{7.53}$$

We can use this to calculate the power spectrum in the general case. Modes that enter the horizon during the radiation dominated era (i.e. $k > k_{\rm eq}$) are constant until matter radiation equality when they start growing according to equation (7.52). In this case we have $C_{\rm MG}^{k>k_\infty}(k > k_{\rm eq}) I_\nu[\sigma(t_{\rm eq}/t_k)^r] = \delta_{\rm c}(t_{\rm eq})$. On the other hand, modes which enter during matter domination are subject to the condition $C_{\rm MG}^{k>k_\infty}(k < k_{\rm eq}) I_\nu \left[\sigma(t_{\rm H}/t_k)^r\right] = \delta_{\rm c}(t_{\rm H})$. Thus, modes that enter the horizon before z_∞ evolve according to

$$\delta_{\rm c}(t) = \delta_{\rm c}^{\rm I} \begin{cases} \left(\frac{t_{\rm eq}}{t}\right)^{\frac{1}{6}} \frac{I_\nu\left[\sigma k t_0 \left(\frac{t}{t_0}\right)^r\right]}{I_\nu\left[\sigma k t_0 \left(\frac{t_{\rm eq}}{t_0}\right)^r\right]} & k > k_{\rm eq} \\ \left(\frac{t_{\rm H}}{t}\right)^{\frac{1}{6}} \frac{I_\nu\left[\sigma k t \left(\frac{t}{t_0}\right)^r\right]}{I_\nu\left[\sigma k t_0 \left(\frac{t_{\rm H}}{t_0}\right)^r\right]} & k < k_{\rm eq} \end{cases}. \tag{7.54}$$

Near z_∞, modes inside the horizon (whether they entered during the radiation or matter era) thus evolve according to the general form $\delta_c(t) = D(k)t^{-1/6}I_\nu[\sigma k t_0(t/t_0)^r]$ where the form of $D(k)$ varies depending on when the mode entered the horizon as detailed in (7.54). When $z = z_\infty$ the field converges to its supersymmetric minimum and the evolution now proceeds according to equation (7.49) and we must again match the two solutions at $z = z_\infty$ so that $\delta_c(t_\infty) = D(k)t_\infty^{-1/6}I_\nu[\sigma k t_0(t_\infty/t_0)^r]$. Modes that enter the horizon later than this simply evolve according to (7.49), matching at the time when they enter the horizon, in which case we have $\delta_c(t_H) = C_{MG}^{k<k_\infty}(k)t_H^{-1/6}K_\omega[\zeta k t_0(t_0/t_H)^{2/3}]$. Thus, the power spectrum taking on different functional forms in three different regimes (this is to be contrasted with the two predicted in general relativity):

$$P(k) = \left\langle \left|\delta_c^I\right|^2 \right\rangle \begin{cases} \left(\frac{t_{eq}}{t_0}\right)^{\frac{1}{3}} \frac{I_\nu^2\left[\sigma k t_0\left(\frac{t_\infty}{t_0}\right)^r\right]}{I_\nu^2\left[\sigma k t_0\left(\frac{t_{eq}}{t_0}\right)^r\right]} \frac{K_\omega^2\left[\zeta k t_0\right]}{K_\omega^2\left[\zeta k t_0(1+z_\infty)\right]} & k > k_{eq} > k_\infty \\ \left(\frac{t_H}{t_0}\right)^{\frac{1}{3}} \frac{I_\nu^2\left[\sigma k t_0\left(\frac{t_\infty}{t_0}\right)^r\right]}{I_\nu^2\left[\sigma k t_0\left(\frac{t_H}{t_0}\right)^r\right]} \frac{K_\omega^2\left[\zeta k t_0\right]}{K_\omega^2\left[\zeta k t_0(1+z_\infty)\right]} & k_\infty < k < k_{eq} \\ \left(\frac{t_H}{t_0}\right)^{\frac{1}{3}} \frac{K_\omega^2\left[\zeta k t_0\right]}{K_\omega^2\left[\zeta k t_0\left(\frac{t_0}{t_H}\right)^{\frac{2}{3}}\right]} & k < k_\infty \end{cases} . \tag{7.55}$$

We are now in a position to explore the deviations from the general relativity prediction, but we must first check that general relativity is indeed recovered on large scales. We know from our analysis in the previous subsection that this requires taking the argument of all modified Bessel functions of the first kind to be small, however the second kind functions require more thought. As detailed in appendix D, these grow with decreasing argument and diverge as it approaches zero and so one may be concerned that taking the argument to be small is not the correct limit. In fact, $K_\omega[y] \sim y^{-\omega} + \mathcal{O}(y^{2-\omega})$ (see appendix D) and so in this limit one may neglect the higher order terms. One can indeed check by expanding the functions according to (D.5) that this leading order behaviour coincides with the general relativity prediction.

We can then go beyond leading order to find the predicted deviations from ΛCDM. Mod-

ified Bessel functions deviate from their leading order terms very rapidly and so one is interested in the case where the deviations are given by the next-to-leading order expansion. In this regime, the power spectrum (7.55) can be expanded (using the power series given in appendix D) and deviates from the ΛCDM case by $\Delta P(k)$, which is scale-dependent:

$$\frac{\Delta P(k)}{P_{\Lambda\mathrm{CDM}}(k)} = \begin{cases} \frac{2}{\nu+1}\left(\frac{\sigma k t_0}{2}\right)^{2r}\left(\frac{t_\infty}{t_0}\right)^{2r}\left[1-\left(\frac{t_{eq}}{t_\infty}\right)^{2r}\right] + 2F(\omega)\left(\frac{\zeta k t_0}{2}\right)^2\left[(1+z_\infty)^2-1\right] & k > k_{\mathrm{eq}} > k_\infty \\ \frac{2}{\nu+1}\left(\frac{\sigma k t_0}{2}\right)^{2r}\left(\frac{t_\infty}{t_0}\right)^{2r}\left[1-\left(\frac{t_{\mathrm{H}}}{t_\infty}\right)^{2r}\right] + 2F(\omega)\left(\frac{\zeta k t_0}{2}\right)^2\left[(1+z_\infty)^2-1\right] & k_\infty < k < k_{\mathrm{eq}} \\ 2F(\omega)\left(\frac{\zeta k t_0}{2}\right)^2\left[\left(\frac{t_0}{t_{\mathrm{H}}}\right)^{4/3}-1\right] & k < k_\infty \end{cases} . \tag{7.56}$$

The factor $F(\omega)$ is given by

$$F(\omega) = \begin{cases} \frac{1}{\omega-1} & \omega > 1 \\ \frac{\pi\omega}{\Gamma^2(1+\omega)\sin(\pi\omega)} & \omega < 1 \end{cases} . \tag{7.57}$$

The case $\omega = 1$ corresponds to $\Omega_c^0 = 0.625$, which is not physically relevant and so is not considered here. This factor arises as a result of different terms in the expansion of $K_\omega[y]$ becoming sub-leading when ω assumes different values. The technical details are given in appendix D.

The deviation monotonically increases with k in the linear regime. On large scales entering the horizon after t_∞, the growth of the deviation $\Delta P/P_{\Lambda\mathrm{CDM}}$ is in k^6 whereas for smaller scales entering the horizon before t_∞, the discrepancy grows as k^2. Of course, this result is only valid in the linear regime of perturbation theory. On smaller scales, typically $k \gtrsim 0.1\mathrm{hMpc}^{-1}$, non-linear effects become important and the screening mechanism is active. We therefore expect that the deviations from ΛCDM will be rapidly suppressed. As a result, we expect the full power spectrum to show large deviations from ΛCDM in the linear regime and only mild deviations in the non-linear one. A complete analysis of this phenomenon requires N-body simulations which are well beyond the scope of this work.

The CDM power spectrum predicted by the superchameleon is very different from other

chameleons that have been previously studied. Indeed, in the vast majority of models linear scales are slightly outside the Compton wavelength of the scalar field whose range is around 1 Mpc (see the discussion in chapter 2). Deviations from ΛCDM are small until the quasi-linear regime for scales around 1 Mpc where the effects of the scalar peaks before being damped in the non-linear regime by the screening mechanism. Here, scales are always outside the Compton wavelength of the scalar field and the deviation from ΛCDM is due to the large coupling $\beta(\varphi)$ to matter. This can be strong enough to lead to k-dependent effects in the linear regime before being heavily Yukawa suppressed in the non-linear one. Hence we have found that superchameleons leave a drastically different signature on large scale structure formation than the majority of previously studied, non-supersymmetric models.

7.4 Other Models

Before concluding this chapter, we pause to discuss how generic the phenomenology of the specific model studied here really is. This model is by no means the most general or even the simplest. Indeed, the index γ appears in the Kähler potential and the superpotential but this was not necessary and we could have used two distinct indices. From this point of view, our model here is a special point in the parameter space of all indices. The phenomenology of these models does not differ drastically from the model presented here. The scalar potential (7.4) is locally run-away when $\phi \lesssim \phi_{\rm min}$ and tends to a constant when $\phi \gg \phi_{\rm min}$. Generalising these models does not affect the small-ϕ behaviour of the potential but changes the behaviour when $\phi \gg \phi_{\rm min}$. Depending which index is larger the potential either decays to zero tends to ∞ as $\phi \to \infty$. The large-field behaviour is irrelevant since the field never passes $\phi_{\rm min}$. It is hardly surprising then that these models do not alleviate the need for a cosmological constant.

One may also wonder why two terms in the superpotential are necessary? Indeed, if one is ignored then we obtain an F-term potential of the form $V_{\rm F} \sim \tilde{M}^{4+p}/\phi^p$ provided the index appearing in the Kähler potential higher than the one appearing in the superpotential.

In this case the potential is more similar to the well-studied potentials found in many non-supersymmetric models. One also finds that a cosmological constant is required in these models but the absence of any supersymmetric minimum ensures that supersymmetry is broken at all densities and so these are somewhat less appealing than the more complicated models investigated here given our original motivations for studying supersymmetric completions.

We can therefore conclude that the qualitative features found in this chapter are ubiquitous in many classes on supersymmetric models that are not of the no-scale type.

7.5 Summary of Main Results

In this chapter and the previous one we have presented a bottom-up approach for constructing globally supersymmetric theories that include chameleon-like screening. In the previous chapter, we presented the general framework and discussed the new supersymmetric features that arise. In particular, we showed that when one accounts for supergravity corrections, any supersymmetric model (with the exception of $n = 3$ no-scale models) necessarily has $\chi_0 \ll 10^{-8}$ and so every object in the universe is self-screened, thereby precluding the possibility of probing these theories using laboratory or astrophysical methods[11]. Furthermore, we showed that the symmetron mechanism cannot operate at all in supersymmetric theories that include an underlying supergravity.

In this chapter we used the general framework to construct a class of supersymmetric chameleon models and examined their cosmology. We found that they cannot account for the cosmic acceleration and, rather than appeal to an external cosmological constant or supergravity breaking corrections, we introduced a novel mechanism where the coupling of the superchameleon to two U(1) charged chiral scalars induces the appearance of a cosmological constant at late times in the form of an FI term. This mechanism requires one to set all other

[11] Binary pulsar tests evade this theorem since the observational signatures of modified gravity result from time-dependent effects not included in the χ_0–α parametrisation [41].

contributions to the cosmological constant to zero[12] and so is not a solution to the cosmological constant problem. However, we have argued that the value of the FI term is more robust to quantum corrections than scalar VEVs (it runs logarithmically at most) and so a small value, which must be set by hand in our framework, is largely robust to the effects of particle loops in the matter sector. The no-go theorem of the previous chapter does not apply on linear scales and so next we derived and solved the equations governing CDM perturbations and calculated the modified form of the power spectrum. We identified regions of parameter space that are excluded by current measurements and other regions that can be probed using upcoming experiments. Finally, we explored the full parameter space and identified regions where the FI cosmological constant can be generated dynamically without interfering with the chameleon mechanism and the theory is not yet ruled out by current observations of linear cosmological probes. Such regions are ubiquitous and so there is no need to fine-tune the model parameters. We identified a small region that can be probed by future surveys but there are large viable regions that will remain unexplored, at least for the foreseeable future.

[12] I.e. assume the old cosmological constant problem in all other sectors is solved.

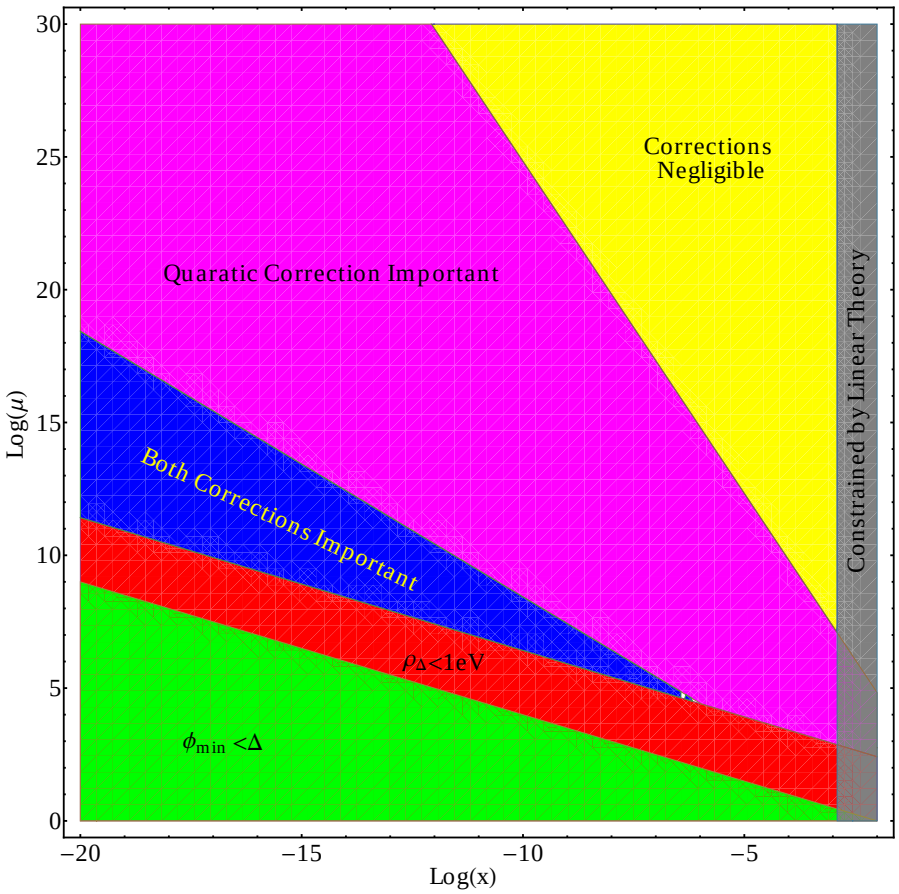


Figure 7.3: The various regions in the $\log(\mu)$–$\log(x)$ plane with $n = \delta = 2$, $z_\infty = 5$ and $\mathcal{G} = 10^{-2}$. The yellow region shows the parameter range where the corrections are negligible. The magenta region shows the ranges where the quadratic correction is important and the dark blue region where both corrections are important. The red region corresponds to models where a cosmological constant is generated after last scattering and are therefore excluded and the green region corresponds to models where $\phi_{\rm min} < \Delta$ and a cosmological constant is only generated at some time in the future. The grey region corresponds to parameters where the model deviates from ΛCDM at the level of linear perturbations.

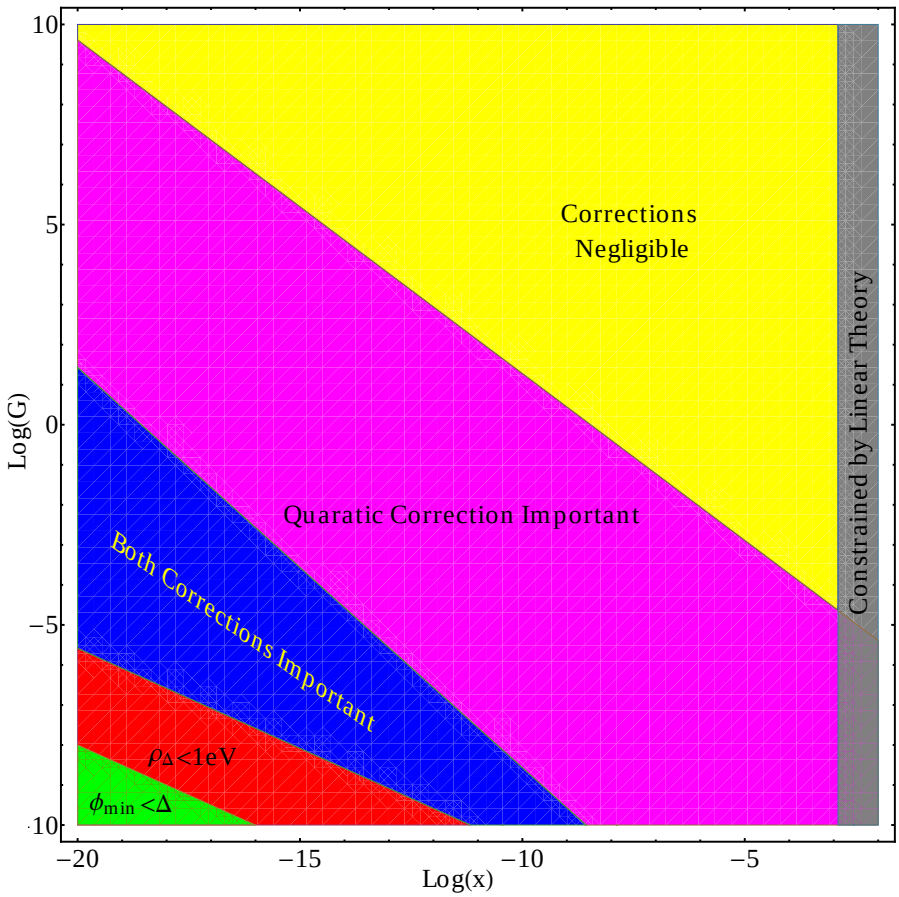


Figure 7.4: The various regions in the $\log(\mathcal{G})$-$\log(x)$ plane with $n = \delta = 2$, $z_\infty = 5$ TeV and $\mu = 10^3$ TeV. The yellow region shows the parameter range where the corrections are negligible. The magenta region shows the ranges where the quadratic correction is important and the dark blue region where both corrections are important. The red region corresponds to models where a cosmological constant is generated after last scattering and are therefore excluded and the green region corresponds to models where $\phi_{\rm min} < \Delta$ and a cosmological constant is only generated at some time in the future. The grey region corresponds to parameters where the model deviates from ΛCDM at the level of linear perturbations.

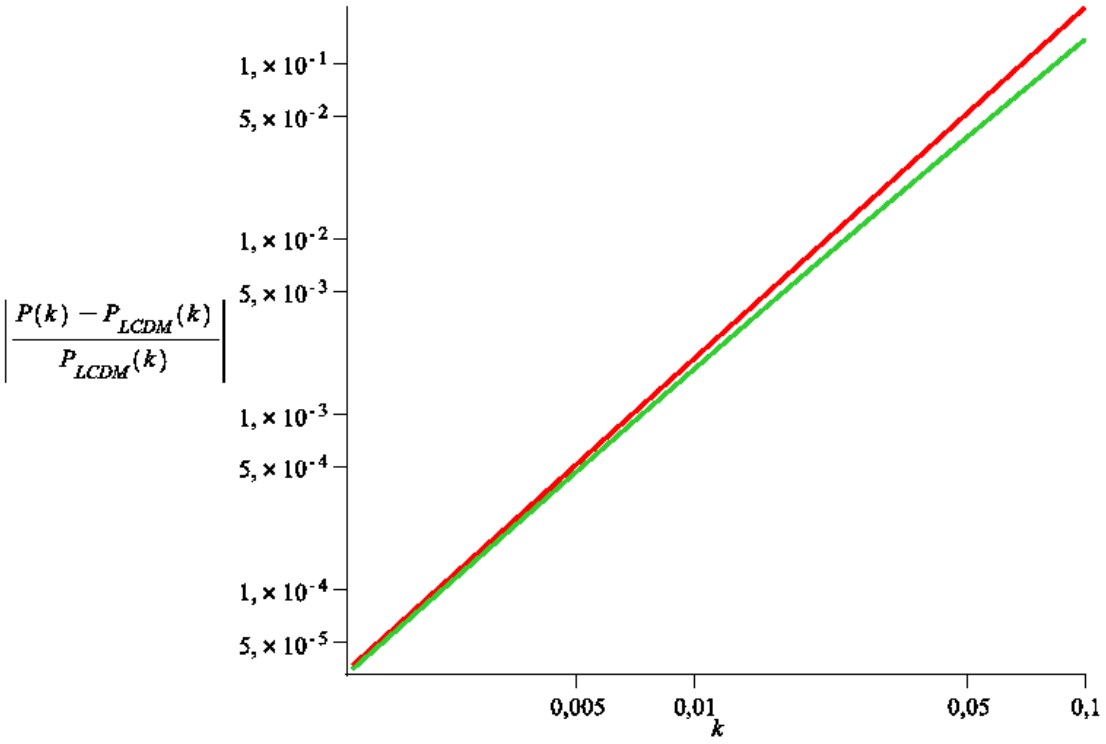


Figure 7.5: The deviation from the ΛCDM power spectrum when a cosmological constant is present, with $\delta = n = 2$, $x = 5 \times 10^{-7}$ and $z_\infty = 5$. In red we show the exact power spectrum deviation. The linearised deviation found using equation (7.56) is shown in green. Smaller values of x result in smaller deviations.

A lot of the cosmologists and astrophysicists clearly had been reading science fiction.

Frederik Pohl

8

Discussion and Conclusions

This thesis has been concerned with several different aspects of modified theories of gravity that include screening mechanisms. Our primary focus has been on those theories that can be embedded into the conformal scalar-tensor class — including the chameleon and symmetron models as well as those that screen using the environment-dependent Damour-Polyakov effect — but many of the results presented apply equally to theories that screen using the Vainshtein mechanism. Below we will summarise some outstanding problems this thesis has attempted to address and review the progress that has been made. We finish by discussing the prospects for using the work presented here in light of future experimental surveys.

8.1 Problems Addressed in this Thesis

Modified theories of gravity have attracted a renewed interest ever since the acceleration of the universe was first discovered in 1998. Many theories that can account for the cosmic acceleration fail to satisfy the solar system tests of gravity and this has prompted an effort towards finding theories that include screening mechanisms. These allow for interesting effects on intergalactic and cosmological scales but are indistinguishable from general relativity in our own galaxy. Although they cannot account for the cosmic acceleration, conformal

scalar-tensor theories can show interesting effects on intergalactic scales and may have important consequences for outstanding problems in structure formation. One popular method of probing modified theories of gravity is to look at cosmological probes such as the luminosity distance-redshift relation or baryon acoustic oscillations but any effects here are not smoking-gun signals because they are degenerate with other theories of modified gravity and dark energy. Another testing ground is the laboratory. This has provided some constraints but these tests suffer from the drawback that they are testing in the heavily screened regime and so one is looking for small deviations from the Newtonian force law.

In this thesis we have identified a new regime for testing modified theories of gravity. Astrophysical tests probe scales between the Milky Way and the Hubble flow. These scales are mildly non-linear and so some degree of screening is present. This allows for smoking-gun tests since the environment-dependence of this theory predicts that the magnitude of any deviation from general relativity varies depending on where in the universe one looks. Since the screening is not totally efficient, the theory predicts novel features in the structure and dynamics of certain stars and galaxies whose magnitude are order-unity compared with the general relativity predictions. This means that the theories make quantitative predictions of large new signals in the experimental data. The drawback is that some of these effects can be degenerate with other, non-gravitational, astrophysical phenomena and it is important to understand the systematic uncertainties in any astrophysical data-set. Furthermore, unlike laboratory and cosmological probes, there are currently no dedicated surveys searching for signals of modified gravity on astrophysical scales. This is not as large an issue as one may initially think. Since the signals are large, one only needs a small sample size (of order 100 galaxies or so) in order to place quantitative constraints and so many of the proposed tests can piggyback on existing astrophysical surveys with no need for any specific targeting strategy[1].

The theories this thesis is concerned with screen according to the Newtonian potential; objects with lower Newtonian potentials are more unscreened provided that they are not

[1]We have seen that dwarf galaxies are particularly useful testing grounds for modified gravity and so this statement assumes that the survey does not target galaxies with any specific morphologies.

screened by any larger neighbours. The current constraints[2] rule out theories which self-screen in Newtonian potentials $\Phi_N \geq 10^{-6}$ and so one must look for objects with lower Newtonian potentials if one wishes to place stronger constraints. In practice, this means one is interested in post-main-sequence stars and dwarf galaxies situated in cosmological voids. This thesis has used both of these objects to place new constraints on the model parameters.

Recently, several investigations into the quantum stability of these models has provided mounting evidence that they suffer from quantum instabilities. One may hope to alleviate this problem by imposing some sort of symmetry on the theory so that it is technically natural. Supersymmetry is a natural choice for this since it enjoys powerful non-renormalisation theorems and it does not predict Goldstone bosons. This allows the field to vary over many orders of magnitude in field space whilst retaining the benefits of the underlying symmetry. It is also a natural framework for making contact with more fundamental theories such as string theory. The second part of this thesis has investigated possible supersymmetric completions of conformal-scalar tensor theories and investigated the new features and the cosmological dynamics.

8.2 Summary of Original Results

8.2.1 Astrophysical Tests of Conformal Scalar-Tensor Theories

In chapter 2 we presented a model-independent framework for dealing with conformal-scalar tensor theories with screening mechanisms and introduced two parameters that fully specify the theory[3]. These are χ_0, whose value determines how efficient and object is at screening itself, and α, which sets the strength of the fifth-force relative to the Newtonian one in unscreened regions. Prior to the work presented in this thesis, α was constrained by laboratory

[2] Current meaning prior to the original work presented in this thesis.

[3] In fact, we specified these parameters as values of the fundamental functions $V(\phi)$ and $A(\phi)$ evaluated at the present time. One can reconstruct their entire cosmic history from these two numbers alone for any individual theory using tomography [28, 88]. If one wishes to look at these functions inside screened objects such as the Milky Way then these functions must be specified on a model-by-model basis.

experiments on a model-by-model basis and $\mathcal{O}(1)$ values were not ruled out for a large class of models. Cluster counting surveys placed the constraint $\chi_0 < 10^{-4}$ and it was often assumed that $\chi_0 \lesssim \mathcal{O}(10^{-6})$ so that the Milky Way is self-screening. This latter assumption had been heavily debated in the field since the Milky Way could instead be screened by the local group and no formal analysis had been performed.

In chapter 3 we derived the equations of modified gravity hydrodynamics and used them to find the equations governing stellar structure in theories of modified gravity. We then presented a general framework for solving these equations using the Lane-Emden approximation. Lane-Emden models are particularly useful for studying the effects of modified gravity since they decouple the gravitational physics from other physics such as nuclear burning and radiative transfer. We argued that an unscreened star is brighter, hotter and more ephemeral than its screened counterpart. In order to verify this, we used the Eddington standard model in conjunction with the modified Lane-Emden equation to find the altered structure of main-sequence stars. Whereas these are screened given current constraints, their study is still useful since they are far simpler object than post-main-sequence stars and the effects of modified gravity are unambiguous[4]. The criterion that $\chi_0 < \Phi_N$ implies screening was derived by assuming that the object in question is a static source in the field equations. In fact, stars are dynamical objects whose equilibrium configuration is set by their interaction with gravity. Our model included this back-reaction and we subsequently found that main-sequence stars are slightly more unscreened than one may initially believe. Our semi-analytic treatment confirmed that low-mass, gas pressure-supported main-sequence stars are far brighter than their screened equivalents. High-mass, radiation supported stars also show an enhancement but this is somewhat reduced since the extra radiation is absorbed to provide the extra pressure needed to combat the inward gravitational force. We also found that unscreened stars in $f(R)$ gravity have a main-sequence lifetime that can be up to three times shorter than that of a screened star.

[4]In addition to this, the parameter range where main-sequence stars are unscreened had not yet been ruled out at the time this work was initiated.

Our simple prescription applied strictly to main-sequence stars and neglected many important effects such as convection and nuclear burning. It is also completely static and so it is somewhat ambiguous as to which point in a star's life these models correspond. If one wishes to compare with observational data and investigate the structure of post-main-sequence stars a full numerical treatment is needed. To this end, we presented a modified version of the publicly available code MESA that can predict the structure and evolution of stars of any initial mass and metallicity including all the absent effects in the simple Lane-Emden model. This means that its predictions can be compared with experimental data and it is a powerful and versatile tool for making quantitative predictions of the new effects of modified gravity.

Since the degree of screening varies between different galaxies, the laws of gravitational physics are different in screened and unscreened galaxies. This means that any theoretical or empirical[5] formulae used to infer the distance to an unscreened galaxy will give an incorrect measurement if they are sensitive to the laws of gravity. Hence, screened and unscreened distance estimates will agree if the galaxy is screened but will disagree if not. In chapter 4 we exploited this feature to place new constraints on the model-independent parameters. Cepheid variable stars are unscreened distance indicators, tip of the red giant branch stars are unscreened when $\chi_0 > 10^{-6}$ and screened otherwise. Water masers provided a geometric distance estimate and so are screened.

Using MESA models, we predicted the change in the inferred distance using screened and unscreened indicators for both TRGB and Cepheid measurements. By comparing waster maser and TRGB distances to the spiral galaxy NGC 4258 we were able to place a new and independent constraint $\chi_0 < 10^{-6}$, resolving the debate in the literature. We then compared Cepheid and TRGB distances to sub-samples of screened and unscreened galaxies taken from the screening map of [96] to place new constraints in the χ_0–α place for chameleon models. We ruled out self-screening parameters $\chi_0 > 4 \times 10^{-7}$ for $f(R)$ theories and $\chi_0 > 3 \times 10^{-7}$ for symmetron models. These constraints are currently the strongest in the literature and

[5] Calibrated on Milky Way or local group objects.

are three orders of magnitude tighter than the previous bounds from cluster statistics. These bounds imply that the only unscreened objects in the universe are dwarf galaxies and heavy post-main-sequence stars with $M \gtrsim 8M_{\odot}$.

Chapter 4 used several assumptions about the period-luminosity relation for Cepheid stars in modified gravity. In particular, the new relation was found using the general relativity formula, which only accounts of the modified equilibrium structure and ignores the effects of modified gravity on the perturbations about this configuration. In order to investigate these assumptions, in chapter 5 we perturbed the equations of modified gravity hydrodynamics to first-order and found the new equation governing radial, adiabatic oscillations, the modified linear adiabatic wave equation. Using the Sturm-Liouville nature of this equation we were able to predict two new effects. First, an unscreened star is more stable to linear perturbations than an equivalent screened star and second, the oscillation period of an unscreened star is far shorter than previously predicted using the assumptions above. We investigated the first effect using Lane-Emden models and found that the change in the critical value of the first adiabatic index for the onset of the instability is of order $10^{-1}\alpha$. We then investigated the second effect using both Lane-Emden models of convective stars and MESA models of Cepheid stars at the blue edge of the instability strip. We found that the period is indeed shorter than one would predict by simply perturbing the general relativity relation. Using this in the period-luminosity relation, we investigated how the predictions found in chapter 4 were altered by this new effect. When one neglects the effect of modified gravity perturbations but retains the altered equilibrium structure we found that the approximations hold very well. When the perturbations are included we found that the difference in the inferred distance to an unscreened galaxy between screened and unscreened indicators can be up to three times as large. Hence, the constraints we found in chapter 4 are conservative and it is possible to improve them using the same data-sets. We estimated that one could probe into the region $\chi_0 \sim \mathcal{O}(10^{-8})$ but the exact value depends on how many unscreened galaxies are left at these small values and this is beyond the scope of this work.

Many of the general results derived here apply equally to Vainshtein screened theories, however in practice the new effects are not present since these theories are far more efficient at screening an object and the Vainshtein radius is often far larger than the object's radius.

8.2.2 Supersymmetric Completions of Conformal-Scalar Tensor Theories

In chapter 6 we presented a general framework for embedding conformal scalar-tensor theories into global supersymmetry. This bottom-up approach is useful because chameleon-like models are infra-red modifications of general relativity and one can examine their basic properties using global supersymmetry without the technical complications of supergravity. For simplicity, we only coupled the gravitational scalar to two dark matter fermions but the extension to the standard model is straightforward. Furthermore, many of the new results including environment-dependent supersymmetry breaking and efficient screening are independent of the form of the matter coupling.

Using this framework, we were able to show that supersymmetry is always broken at non-zero dark matter densities and showed how the scale of the breaking is set by the ambient density and the model parameters. Including supergravity corrections, we were able to prove a general no-go theorem showing that the mass of the scalar in any supersymmetric theory of modified gravity is at least as large as the gravitino mass and hence mediates a force whose range is less than 10^{-6} m. Using this, we were able to show that $\chi_0 \ll 10^{-66}$ and hence astrophysical and laboratory experiments cannot be used to probe these theories. The exception to the theorem is pure no-scale models where the gravitino mass is undetermined at tree-level. We argued that these models do not generically include screening mechanisms but this is far from a proof and it remains to be seen if the mechanisms can be realised using more complicated models. We also showed that supersymmetric symmetrons cannot exist once supergravity corrections are accounted for unless the model parameters are heavily fine-tuned.

On cosmological scales, χ_0 is not enough to determine whether deviations from general relativity are present. At the level of the background cosmology, χ_0 has no influence on the

homogeneous dynamics of the scalar and on linear scales the screening mechanism cannot operate efficiently and the large coupling to matter allows for deviations in the cold dark matter power spectrum. This is in contrast to non-supersymmetric models with $\mathcal{O}(1)$ couplings that are constrained to affect non-linear scales only. On non-linear scales the screening mechanism can operate and any deviations form general relativity are highly suppressed.

In order to investigate this regime, we presented a class of supersymmetric chameleon models and studied their cosmological dynamics. We found that the field could not account for dark energy without giving deviations in the CDM power spectrum that are in tension with current experiments and so a cosmological constant is needed. This presented a new problem in that supersymmetry is broken if the vacuum energy is positive and it is not possible to include a cosmological constant at the level of the action. We presented a novel mechanism where the coupling of the field to two charged scalars can drive their VEV's to zero at late times leaving a cosmological constant in the form of a Fayet-Illiopoulos term. This is more robust to quantum corrections that scalar VEVs since it is not overly sensitive to loop corrections and runs logarithmically at most. This is by no means a solution to the cosmological constant problem since it does not explain why the contribution to the cosmological constant coming from quantum effects in the other sectors are absent. We investigated the model parameter space where this mechanism is viable and found that regions where this is the case are ubiquitous.

Finally, we calculated the CDM power spectrum in closed form and found that it deviates from the general relativity prediction on intermediate scales by an amount dependent on the model parameters. We were able to exclude parameters that are in tension with current measurements and indicated the region that can be probed using upcoming surveys.

8.3 Outlook

These are exciting times for modified gravity. The past decade has been theoretically dominated with many new theories being investigated and a plethora of observational tests pro-

posed. The next decade and beyond will see a shift in focus towards more data-oriented aspects. Upcoming data releases such as SDSS IV MaNGA will provide spectral measurements of nearly 10000 galaxies. DES saw first light in September 2012 and scientific measurements have begun to be made as of September 2013. This will provide data pertaining to weak lensing, galaxy cluster counts, supernovae distance measurements and baryon acoustic oscillations, all of which can be used as cosmological probes of dark energy and modified gravity. The megamaser cosmology project is under way and has already detected water masers in 62 galaxies. The aim of this project is to determine the Hubble constant geometrically with a precision of 3% in order to constrain the properties of dark energy. Spitzer [146] provides infra-red data pertaining to stars and galaxies and will significantly improve the uncertainties in the slope of the period-luminosity relation for Cepheid variable stars in the infra-red.

Looking to the future, missions such as LSST and WFIRST will provide spectroscopic data for a large number of galaxies and Euclid will provide complementary probes using phenomena such as weak lensing. GAIA [147] will provide spectroscopic measurements of about one billion stars in the Milky Way and the local group.

The prospects are also good for testing gravity in the strong field regime. Future gravitational wave interferometers such as Advanced-LIGO and eLISA will provide data relating to black hole mergers and in-spirals and very recently [148] a millisecond pulsar has been observed in stellar triple system. This offers new possibilities to for testing gravity using the energy radiated into gravitational waves.

What does this mean for the results presented in this thesis and future astrophysical tests of modified gravity? We have already alluded to the fact that these tests can piggyback on other missions and many of the surveys described above could potentially improve the current constraints.

In chapters 6 and 7 we investigated supersymmetric models of screened modified gravity and we argued that Euclid could constrain these by measuring the cold dark matter power spectrum to a precision greater than 10%.

In chapter 3 we argued that the combined effects of the increased luminosity and reduced lifetime of stars should alter the colour, spectra and luminosity of dwarf galaxies in voids relative to those in clusters and that looking for systematic offsets could constitute a new observational test. Our simple estimate is by no means accurate enough to compare with observational data but the tools to make a more quantitative prediction are available. Using MESA to generate mock stellar populations it is possible to create theoretical isochrones that can be used in conjunction with existing galaxy synthesiser codes to make predictions that are accurate enough to compare with data. This is a complicated task because the galactic properties are the result of cumulative effects that begin far in the past when the galaxy was more screened. In practice, this requires one to account for the time-evolution of the self-screening parameter inside haloes using non-linear spherical collapse models but this is possible [48]. Progress towards this goal has been made but any quantitative results are still a long way off.

In chapter 4 we presented new constraints on chameleon-like models using Cepheid variable stars in unscreened galaxies. In chapter 5 we argued that these constraints could be greatly improved using the same data-analysis. We were careful to remark that the small sample of unscreened galaxies is responsible for the jaggedness of the contours and that testing values of $\chi_0 \lesssim \mathcal{O}(10^{-8})$ is very data-limited due to the small number of unscreened galaxies. Surveys such as LSST will provide spectroscopic data for variable stars in a variety of different environments and help to combat this issue. Furthermore, reducing the uncertainty of the slope in the period-luminosity relation using Spitzer data has the potential to improve the systematics. Furthermore, there are other tests that have been alluded to that are not yet possible. Updating the MLAWE to include non-adiabatic processes will allow for a prediction of the slope of the period-luminosity relation as well as the location of the blue edge of the instability strip. Data from the surveys mentioned above could then be compared with these predictions therefore providing further tests.

Recently, a Cepheid variable star in an eclipsing binary system has been discovered for the

first time [149, 150]. This has allowed an accurate measurement of the Cepheid's mass using both the orbital properties and the period-luminosity-mass relation and the two agree at the 1% level. This provides a unique testing ground for modified theories of gravity. The agreement of the mass measurements can probe chameleon models once the MLAWE is updated to include non-adiabatic driving processes since the orbit is screened but the pulsation is not. For Vainshtein screened theories, this test can be reversed since the star is screened but its finite extent may lead to deviations in the mass inferred from its orbit [104].

RR Lyrae variable stars are another class of pulsating object. They have smaller masses and temperatures than Cepheids and pulsate due to the same mechanism. Currently, they are not as powerful as distance indicators. This will change with data coming from GAIA, which will provide new measurements allowing them to become competitive with Cepheid distances. GAIA will not probe stars outside the local group and so it is unlikely that these will be useful for testing chameleon-like models. We argued in chapter 5 that Vainshtein screened theories may give rise to scalar radiation from pulsating stars and this may be detectable by looking for beating effects in the period-luminosity relation or decays in its amplitude. Since this effect is insensitive to the degree of screening it is possible that Cepheid and RR Lyrae stars in the local group could provide a possible testing ground.

Another distance indicator that has yet to be exploited is the planetary nebula luminosity function (PNLF). Planetary nebulae are the remnants of asymptotic giant branch (AGB) stars that blow off their convective envelopes leaving a hot, dense core that emits ionising radiation. This radiation causes transitions in [OIII] atoms, which is detectable as emission lines at approximately 507 nm. The luminosity function for these lines has a universal turn-off and the PNLF is hence a distance indicator [151]. Since the core of AGB stars is screened but the envelope is not, it is possible that the extra centripetal force felt by the envelope could move it away from the core so that the PLNF is greatly diminished. The PLNF may therefore be an unscreened distance indicator and could be used to place new constraints. This effect certainly merits further investigation.

Chameleon-like models are already heavily constrained by much of the work presented in this thesis and it is only a matter of time before the theory is rendered astrophysically uninteresting but what about Vainshtein screened theories? These are far less constrained due to the lack of astrophysical effects. We have already alluded to some potential tests above but are there other possible signatures? [106] have argued that the central black holes in under-dense galaxies should be offset from the galactic centre by an amount of order 0.1 kpc, which presents several possible avenues for testing these theories. The black hole has a sphere of influence on the surrounding stellar matter and will drag a disk of stars away from the galactic centre. One may expect an offset between the optical and dark matter centroids in under-dense galaxies. This is a smoking-gun signal since the direction of the offset should be correlated with the direction of motion of the galaxy. Work on these tests is already under way and optical, near-infra-red and X-ray data from many of the surveys above could be used to place new constraints.

In conclusion, in this thesis we have presented a thorough theoretical, numerical and observational investigation into the properties of various astrophysical objects when the theory of gravity includes chameleon-like screening. We have already placed the most stringent constraints to date but there is more work to be done and many potential new features to be exploited. The next decade will see numerous astrophysical surveys, all of which could constrain the theory of gravity with unprecedented precision. The future is bright, and if gravity really is described by these theories, it may be brighter than we expect!

Mit der Dummheit kämpfen Götter selbst vergebens.

Against stupidity the gods themselves contend in vain.

Friedrich Schiller, *The Maid of Orleans*

Bibliography

[1] A. Einstein, *The Foundation of the General Theory of Relativity*, *Annalen Phys.* **49** (1916) 769–822, [doi:10.1002/andp.200590044].

[2] C. Will, *The confrontation between general relativity and experiment*, *Pramana* **63** (2004) 731–740, [doi:10.1007/BF02705195].

[3] **Supernova Search Team** Collaboration, A. G. Riess *et al.*, *Observational evidence from supernovae for an accelerating universe and a cosmological constant*, *Astron.J.* **116** (1998) 1009–1038, [arXiv:astro-ph/9805201], [doi:10.1086/300499].

[4] **Supernova Cosmology Project** Collaboration, S. Perlmutter *et al.*, *Measurements of Omega and Lambda from 42 high redshift supernovae*, *Astrophys.J.* **517** (1999) 565–586, [arXiv:astro-ph/9812133], [doi:10.1086/307221].

[5] E. J. Copeland, M. Sami, and S. Tsujikawa, *Dynamics of dark energy*, *Int.J.Mod.Phys.* **D15** (2006) 1753–1936, [arXiv:hep-th/0603057], [doi:10.1142/S021827180600942X].

[6] T. Clifton, P. G. Ferreira, A. Padilla, and C. Skordis, *Modified Gravity and Cosmology*, *Phys.Rept.* **513** (2012) 1–189, [arXiv:1106.2476], [doi:10.1016/j.physrep.2012.01.001].

[7] **Planck Collaboration** Collaboration, P. Ade *et al.*, *Planck 2013 results. I. Overview of products and scientific results*, arXiv:1303.5062, doi:10.1051/0004-6361/201321529.

[8] R. Bean and M. Tangmatitham, *Current constraints on the cosmic growth history*, *Phys.Rev.* **D81** (2010) 083534, [arXiv:1002.4197], [doi:10.1103/PhysRevD.81.083534].

[9] **Euclid Theory Working Group** Collaboration, L. Amendola *et al.*, *Cosmology and fundamental physics with the Euclid satellite*, *Living Rev.Rel.* **16** (2013) 6, [arXiv:1206.1225].

[10] **LSST Collaboration** Collaboration, Z. Ivezic, J. Tyson, R. Allsman, J. Andrew, and R. Angel, *LSST: from Science Drivers to Reference Design and Anticipated Data Products*, arXiv:0805.2366.

[11] A. Albrecht, G. Bernstein, R. Cahn, W. L. Freedman, J. Hewitt, *et al.*, *Report of the Dark Energy Task Force*, arXiv:astro-ph/0609591.

[12] D. Spergel, N. Gehrels, J. Breckinridge, M. Donahue, A. Dressler, *et al.*, *Wide-Field InfraRed Survey Telescope-Astrophysics Focused Telescope Assets WFIRST-AFTA Final Report*, arXiv:1305.5422.

[13] **LIGO Scientific Collaboration** Collaboration, B. Abbott *et al.*, *LIGO: The Laser interferometer gravitational-wave observatory*, *Rept.Prog.Phys.* **72** (2009) 076901, [arXiv:0711.3041], [doi:10.1088/0034-4885/72/7/076901].

[14] P. Amaro-Seoane, S. Aoudia, S. Babak, P. Binetruy, E. Berti, *et al.*, *eLISA/NGO: Astrophysics and cosmology in the gravitational-wave millihertz regime*, *GW Notes* **6** (2013) 4–110, [arXiv:1201.3621].

[15] S. Weinberg, *Photons and gravitons in perturbation theory: Derivation of Maxwell's and Einstein's equations*, *Phys.Rev.* **138** (1965) B988–B1002, [doi:10.1103/PhysRev.138.B988].

[16] T. Damour and G. Esposito-Farese, *Nonperturbative strong field effects in tensor - scalar theories of gravitation*, *Phys.Rev.Lett.* **70** (1993) 2220–2223, [doi:10.1103/PhysRevLett.70.2220].

[17] J. Khoury and A. Weltman, *Chameleon fields: Awaiting surprises for tests of gravity in space*, *Phys.Rev.Lett.* **93** (2004) 171104, [arXiv:astro-ph/0309300], [doi:10.1103/PhysRevLett.93.171104].

[18] J. Khoury and A. Weltman, *Chameleon cosmology*, *Phys.Rev.* **D69** (2004) 044026, [arXiv:astro-ph/0309411], [doi:10.1103/PhysRevD.69.044026].

[19] K. Hinterbichler and J. Khoury, *Symmetron Fields: Screening Long-Range Forces Through Local Symmetry Restoration*, *Phys.Rev.Lett.* **104** (2010) 231301, [arXiv:1001.4525], [doi:10.1103/PhysRevLett.104.231301].

[20] P. Brax, C. van de Bruck, A.-C. Davis, and D. Shaw, *The Dilaton and Modified Gravity*, *Phys.Rev.* **D82** (2010) 063519, [arXiv:1005.3735], [doi:10.1103/PhysRevD.82.063519].

[21] A. Vainshtein, *To the problem of nonvanishing gravitation mass*, *Phys.Lett.* **B39** (1972) 393–394, [doi:10.1016/0370-2693(72)90147-5].

[22] J. Sakstein, *Disformal Theories of Gravity: From the Solar System to Cosmology*, *JCAP* **1412** (2014), no. 12 012, [arXiv:1409.1734], [doi:10.1088/1475-7516/2014/12/012].

[23] J. Sakstein, *Towards Viable Cosmological Models of Disformal Theories of Gravity*, *Phys.Rev.* **D91** (2015), no. 2 024036, [arXiv:1409.7296], [doi:10.1103/PhysRevD.91.024036].

[24] L. Hui, A. Nicolis, and C. Stubbs, *Equivalence Principle Implications of Modified Gravity Models*, *Phys.Rev.* **D80** (2009) 104002, [arXiv:0905.2966], [doi:10.1103/PhysRevD.80.104002].

[25] B. Jain and J. Khoury, *Cosmological Tests of Gravity*, *Annals Phys.* **325** (2010) 1479–1516, [arXiv:1004.3294], [doi:10.1016/j.aop.2010.04.002].

[26] J. Khoury, *Theories of Dark Energy with Screening Mechanisms*, arXiv:1011.5909.

[27] A.-C. Davis, E. A. Lim, J. Sakstein, and D. Shaw, *Modified Gravity Makes Galaxies Brighter*, *Phys.Rev.* **D85** (2012) 123006, [arXiv:1102.5278], [doi:10.1103/PhysRevD.85.123006].

[28] P. Brax, A.-C. Davis, B. Li, and H. A. Winther, *A Unified Description of Screened Modified Gravity*, *Phys.Rev.* **D86** (2012) 044015, [arXiv:1203.4812], [doi:10.1103/PhysRevD.86.044015].

[29] J. Sakstein, *Stellar Oscillations in Modified Gravity*, *Phys.Rev.* **D88** (2013) 124013, [arXiv:1309.0495], [doi:10.1103/PhysRevD.88.124013].

[30] J. Sakstein, B. Jain, and V. Vikram, *Testing Gravity Theories Using Stars*, arXiv:1409.3708, doi:10.1142/S0218271814420024.

[31] D. F. Mota and D. J. Shaw, *Strongly coupled chameleon fields: New horizons in scalar field theory*, *Phys.Rev.Lett.* **97** (2006) 151102, [arXiv:hep-ph/0606204], [doi:10.1103/PhysRevLett.97.151102].

[32] D. F. Mota and D. J. Shaw, *Evading Equivalence Principle Violations, Cosmological and other Experimental Constraints in Scalar Field Theories with a Strong Coupling to Matter*, *Phys.Rev.* **D75** (2007) 063501, [arXiv:hep-ph/0608078], [doi:10.1103/PhysRevD.75.063501].

[33] P. Brax, C. van de Bruck, A.-C. Davis, D. F. Mota, and D. J. Shaw, *Testing Chameleon Theories with Light Propagating through a Magnetic Field*, *Phys.Rev.* **D76** (2007) 085010, [arXiv:0707.2801], [doi:10.1103/PhysRevD.76.085010].

[34] H. Gies, D. F. Mota, and D. J. Shaw, *Hidden in the Light: Magnetically Induced Afterglow from Trapped Chameleon Fields*, *Phys.Rev.* **D77** (2008) 025016, [arXiv:0710.1556], [doi:10.1103/PhysRevD.77.025016].

[35] P. Brax, C. van de Bruck, A.-C. Davis, D. F. Mota, and D. J. Shaw, *Detecting chameleons through Casimir force measurements*, *Phys.Rev.* **D76** (2007) 124034, [arXiv:0709.2075], [doi:10.1103/PhysRevD.76.124034].

[36] P. Brax, C. van de Bruck, A.-C. Davis, and D. Shaw, *Laboratory Tests of Chameleon Models*, arXiv:0911.1086.

[37] P. Brax, C. van de Bruck, A. Davis, D. Shaw, and D. Iannuzzi, *Tuning the Mass of Chameleon Fields in Casimir Force Experiments*, *Phys.Rev.Lett.* **104** (2010) 241101, [arXiv:1003.1605], [doi:10.1103/PhysRevLett.104.241101].

[38] P. Brax and C. Burrage, *Atomic Precision Tests and Light Scalar Couplings*, *Phys.Rev.* **D83** (2011) 035020, [arXiv:1010.5108], [doi:10.1103/PhysRevD.83.035020].

[39] P. Brax, A. Lindner, and K. Zioutas, *Detection prospects for solar and terrestrial chameleons*, *Phys.Rev.* **D85** (2012) 043014, [arXiv:1110.2583], [doi:10.1103/PhysRevD.85.043014].

[40] A. Upadhye, *Particles and forces from chameleon dark energy*, arXiv:1211.7066.

[41] P. Brax, A.-C. Davis, and J. Sakstein, *Pulsar Constraints on Screened Modified Gravity*, arXiv:1301.5587.

[42] P. Brax, C. van de Bruck, A.-C. Davis, J. Khoury, and A. Weltman, *Detecting dark energy in orbit - The Cosmological chameleon*, *Phys.Rev.* **D70** (2004) 123518, [arXiv:astro-ph/0408415], [doi:10.1103/PhysRevD.70.123518].

[43] P. Brax, C. van de Bruck, A.-C. Davis, and A. M. Green, *Small scale structure formation in chameleon cosmology*, *Phys.Lett.* **B633** (2006) 441–446, [arXiv:astro-ph/0509878], [doi:10.1016/j.physletb.2005.12.055].

[44] W. Hu and I. Sawicki, *Models of f(R) Cosmic Acceleration that Evade Solar-System Tests*, *Phys.Rev.* **D76** (2007) 064004, [arXiv:0705.1158], [doi:10.1103/PhysRevD.76.064004].

[45] A.-C. Davis, C. A. Schelpe, and D. J. Shaw, *The Effect of a Chameleon Scalar Field on the Cosmic Microwave Background*, *Phys.Rev.* **D80** (2009) 064016, [arXiv:0907.2672], [doi:10.1103/PhysRevD.80.064016].

[46] K. Hinterbichler, J. Khoury, A. Levy, and A. Matas, *Symmetron Cosmology*, *Phys.Rev.* **D84** (2011) 103521, [arXiv:1107.2112], [doi:10.1103/PhysRevD.84.103521].

[47] B. Li, G.-B. Zhao, and K. Koyama, *Halos and Voids in f(R) Gravity*, *Mon.Not.Roy.Astron.Soc.* **421** (2012) 3481, [arXiv:1111.2602], [doi:10.1111/j.1365-2966.2012.20573.x].

[48] B. Li and G. Efstathiou, *An Extended Excursion Set Approach to Structure Formation in Chameleon Models*, *Mon.Not.Roy.Astron.Soc.* **421** (2012) 1431, [arXiv:1110.6440], [doi:10.1111/j.1365-2966.2011.20404.x].

[49] P. Brax and P. Valageas, *Structure Formation in Modified Gravity Scenarios*, *Phys.Rev.* **D86** (2012) 063512, [arXiv:1205.6583], [doi:10.1103/PhysRevD.86.063512].

[50] B. Li, W. A. Hellwing, K. Koyama, G.-B. Zhao, E. Jennings, *et al.*, *The nonlinear matter and velocity power spectra in f(R) gravity*, *Mon.Not.Roy.Astron.Soc.* **428** (2013) 743–755, [arXiv:1206.4317], [doi:10.1093/mnras/sts072].

[51] P. Brax, A.-C. Davis, B. Li, H. A. Winther, and G.-B. Zhao, *Systematic Simulations of Modified Gravity: Symmetron and Dilaton Models*, *JCAP* **1210** (2012) 002, [arXiv:1206.3568], [doi:10.1088/1475-7516/2012/10/002].

[52] C. Llinares and D. F. Mota, *Shape of Clusters of Galaxies as a Probe of Screening Mechanisms in Modified Gravity*, *Phys.Rev.Lett.* **110** (2013), no. 15 151104, [arXiv:1205.5775], [doi:10.1103/PhysRevLett.110.151104].

[53] E. Jennings, C. M. Baugh, B. Li, G.-B. Zhao, and K. Koyama, *Redshift space distortions in f(R) gravity*, *Mon.Not.Roy.Astron.Soc.* **425** (2012) 2128–2143, [arXiv:1205.2698], [doi:10.1111/j.1365-2966.2012.21567.x].

[54] J. Lee, G.-B. Zhao, B. Li, and K. Koyama, *Modified Gravity Spins Up Galactic Halos*, *Astrophys.J.* **763** (2013) 28, [arXiv:1204.6608], [doi:10.1088/0004-637X/763/1/28].

[55] P. Brax, A.-C. Davis, B. Li, H. A. Winther, and G.-B. Zhao, *Systematic simulations of modified gravity: chameleon models*, *JCAP* **1304** (2013) 029, [arXiv:1303.0007], [doi:10.1088/1475-7516/2013/04/029].

[56] A. Upadhye, W. Hu, and J. Khoury, *Quantum Stability of Chameleon Field Theories*, *Phys.Rev.Lett.* **109** (2012) 041301, [arXiv:1204.3906], [doi:10.1103/PhysRevLett.109.041301].

[57] A. L. Erickcek, N. Barnaby, C. Burrage, and Z. Huang, *Chameleons in the Early Universe: Kicks, Rebounds, and Particle Production*, *Phys.Rev.* **D89** (2014) 084074, [arXiv:1310.5149].

[58] J. Wang, L. Hui, and J. Khoury, *No-Go Theorems for Generalized Chameleon Field Theories*, *Phys.Rev.Lett.* **109** (2012) 241301, [arXiv:1208.4612], [doi:10.1103/PhysRevLett.109.241301].

[59] P. Brax and A.-C. Davis, *Modified Gravity and the CMB*, *Phys.Rev.* **D85** (2012) 023513, [arXiv:1109.5862], [doi:10.1103/PhysRevD.85.023513].

[60] **Planck Collaboration** Collaboration, P. Ade *et al.*, *Planck 2013 results. XVI. Cosmological parameters*, arXiv:1303.5076.

[61] B. D. Sherwin, J. Dunkley, S. Das, J. W. Appel, J. R. Bond, *et al.*, *Evidence for dark energy from the cosmic microwave background alone using the Atacama Cosmology Telescope lensing measurements*, *Phys.Rev.Lett.* **107** (2011) 021302, [arXiv:1105.0419], [doi:10.1103/PhysRevLett.107.021302].

[62] D. Prialnik, *An Introduction to the Theory of Stellar Structure and Evolution*. Cambridge University Press, 2000.

[63] R. Kippenhahn and A. Weigert, *Stellar structure and evolution*. Astronomy and astrophysics library. Springer, 1990.

[64] F. Quevedo, S. Krippendorf, and O. Schlotterer, *Cambridge Lectures on Supersymmetry and Extra Dimensions*, arXiv:1011.1491.

[65] J. Wess and J. Bagger, *Supersymmetry and Supergravity*. Princeton series in physics. Princeton University Press, 1992.

[66] T. Jacobson and D. Mattingly, *Gravity with a dynamical preferred frame*, *Phys.Rev.* **D64** (2001) 024028, [arXiv:gr-qc/0007031], [doi:10.1103/PhysRevD.64.024028].

[67] P. Horava, *Quantum Gravity at a Lifshitz Point*, *Phys.Rev.* **D79** (2009) 084008, [arXiv:0901.3775], [doi:10.1103/PhysRevD.79.084008].

[68] G. W. Horndeski, *Second-order scalar-tensor field equations in a four-dimensional space*, *Int.J.Theor.Phys.* **10** (1974) 363–384, [doi:10.1007/BF01807638].

[69] C. Deffayet, G. Esposito-Farese, and A. Vikman, *Covariant Galileon*, *Phys.Rev.* **D79** (2009) 084003, [arXiv:0901.1314], [doi:10.1103/PhysRevD.79.084003].

[70] M. Fierz and W. Pauli, *On relativistic wave equations for particles of arbitrary spin in an electromagnetic field*, *Proc.Roy.Soc.Lond.* **A173** (1939) 211–232, [doi:10.1098/rspa.1939.0140].

[71] D. Boulware and S. Deser, *Can gravitation have a finite range?*, *Phys.Rev.* **D6** (1972) 3368–3382, [doi:10.1103/PhysRevD.6.3368].

[72] C. de Rham, G. Gabadadze, and A. J. Tolley, *Resummation of Massive Gravity*, *Phys.Rev.Lett.* **106** (2011) 231101, [arXiv:1011.1232], [doi:10.1103/PhysRevLett.106.231101].

[73] K. Hinterbichler, *Theoretical Aspects of Massive Gravity*, *Rev.Mod.Phys.* **84** (2012) 671–710, [arXiv:1105.3735], [doi:10.1103/RevModPhys.84.671].

[74] R. Woodard, *Nonlocal Models of Cosmic Acceleration*, *Found.Phys.* **44** (2014) 213–233, [arXiv:1401.0254], [doi:10.1007/s10701-014-9780-6].

[75] T. Clemson and K. Koyama, *The Distinguishability of Interacting Dark Energy from Modified Gravity*, *JCAP* **1301** (2013) 010, [arXiv:1209.2618], [doi:10.1088/1475-7516/2013/01/010].

[76] D. Kapner, T. Cook, E. Adelberger, J. Gundlach, B. R. Heckel, *et al.*, *Tests of the gravitational inverse-square law below the dark-energy length scale*, *Phys.Rev.Lett.* **98** (2007) 021101, [arXiv:hep-ph/0611184], [doi:10.1103/PhysRevLett.98.021101].

[77] P. Brax, C. van de Bruck, D. F. Mota, N. J. Nunes, and H. A. Winther, *Chameleons with Field Dependent Couplings*, *Phys.Rev.* **D82** (2010) 083503, [arXiv:1006.2796], [doi:10.1103/PhysRevD.82.083503].

[78] K. Hinterbichler, J. Khoury, and H. Nastase, *Towards a UV Completion for Chameleon Scalar Theories*, *JHEP* **1103** (2011) 061, [arXiv:1012.4462], [doi:10.1007/JHEP06(2011)072, 10.1007/JHEP03(2011)061].

[79] K. Hinterbichler, J. Khoury, H. Nastase, and R. Rosenfeld, *Chameleonic inflation*, *JHEP* **1308** (2013) 053, [arXiv:1301.6756], [doi:10.1007/JHEP08(2013)053].

[80] P. Brax, A.-C. Davis, and J. Sakstein, *SUPER-Screening*, *Phys.Lett.B* **719** (2013) 210–217, [arXiv:1212.4392], [doi:10.1016/j.physletb.2013.01.044].

[81] P. Brax, A.-C. Davis, and J. Sakstein, *Dynamics of Supersymmetric Chameleons*, *JCAP* **1310** (2013) 007, [arXiv:1302.3080], [doi:10.1088/1475-7516/2013/10/007].

[82] P. Brax, C. van de Bruck, A.-C. Davis, and D. J. Shaw, *f(R) Gravity and Chameleon Theories*, *Phys.Rev.* **D78** (2008) 104021, [arXiv:0806.3415], [doi:10.1103/PhysRevD.78.104021].

[83] A.-C. Davis, B. Li, D. F. Mota, and H. A. Winther, *Structure Formation in the Symmetron Model*, *Astrophys.J.* **748** (2012) 61, [arXiv:1108.3081], [doi:10.1088/0004-637X/748/1/61].

[84] T. Damour and A. M. Polyakov, *The String dilaton and a least coupling principle*, *Nucl.Phys.* **B423** (1994) 532–558, [arXiv:hep-th/9401069], [doi:10.1016/0550-3213(94)90143-0].

[85] T. S. Koivisto, D. F. Mota, and M. Zumalacarregui, *Screening Modifications of Gravity through Disformally Coupled Fields*, *Phys.Rev.Lett.* **109** (2012) 241102, [arXiv:1205.3167], [doi:10.1103/PhysRevLett.109.241102].

[86] M. Zumalacarregui, T. S. Koivisto, and D. F. Mota, *DBI Galileons in the Einstein Frame: Local Gravity and Cosmology*, *Phys.Rev.* **D87** (2013) 083010, [arXiv:1210.8016], [doi:10.1103/PhysRevD.87.083010].

[87] M. Gasperini, F. Piazza, and G. Veneziano, *Quintessence as a runaway dilaton*, *Phys.Rev.* **D65** (2002) 023508, [arXiv:gr-qc/0108016], [doi:10.1103/PhysRevD.65.023508].

[88] P. Brax, A.-C. Davis, and B. Li, *Modified Gravity Tomography*, *Phys.Lett.* **B715** (2012) 38–43, [arXiv:1111.6613], [doi:10.1016/j.physletb.2012.08.002].

[89] B. Jain, V. Vikram, and J. Sakstein, *Astrophysical Tests of Modified Gravity: Constraints from Distance Indicators in the Nearby Universe*, *Astrophys.J.* **779** (2013) 39, [arXiv:1204.6044], [doi:10.1088/0004-637X/779/1/39].

[90] F. Schmidt, M. V. Lima, H. Oyaizu, and W. Hu, *Non-linear Evolution of f(R) Cosmologies III: Halo Statistics*, *Phys.Rev.* **D79** (2009) 083518, [arXiv:0812.0545], [doi:10.1103/PhysRevD.79.083518].

[91] B. Jain and J. VanderPlas, *Tests of Modified Gravity with Dwarf Galaxies*, *JCAP* **1110** (2011) 032, [arXiv:1106.0065], [doi:10.1088/1475-7516/2011/10/032].

[92] V. Vikram, A. CabrÃľ, B. Jain, and J. VanderPlas, *Astrophysical Tests of Modified Gravity: the Morphology and Kinematics of Dwarf Galaxies*, *JCAP* **1308** (2013) 020, [arXiv:1303.0295], [doi:10.1088/1475-7516/2013/08/020].

[93] V. Vikram, J. Sakstein, C. Davis, and A. Neil, *Astrophysical Tests of Modified Gravity: Stellar and Gaseous Rotation Curves in Dwarf Galaxies*, arXiv:1407.6044.

[94] M. R. Haas, J. Schaye, and A. Jeeson-Daniel, *Disentangling galaxy environment and host halo mass*, *Mon.Not.Roy.Astron.Soc.* **419** (2012) 2133, [arXiv:1103.0547], [doi:10.1111/j.1365-2966.2011.19863.x].

[95] G.-B. Zhao, B. Li, and K. Koyama, *Testing General Relativity using the Environmental Dependence of Dark Matter Halos*, *Phys.Rev.Lett.* **107** (2011) 071303, [arXiv:1105.0922], [doi:10.1103/PhysRevLett.107.071303].

[96] A. Cabre, V. Vikram, G.-B. Zhao, B. Jain, and K. Koyama, *Astrophysical Tests of Modified Gravity: A Screening Map of the Nearby Universe*, *JCAP* **1207** (2012) 034, [arXiv:1204.6046], [doi:10.1088/1475-7516/2012/07/034].

[97] A. L. Erickcek, N. Barnaby, C. Burrage, and Z. Huang, *Catastrophic Consequences of Kicking the Chameleon*, *Phys. Rev. Lett.* **110:171101** (2013) [arXiv:1304.0009].

[98] P. Brax and A.-C. Davis, *Supersymmetron*, *Phys.Lett.* **B707** (2012) 1–7, [arXiv:1109.0468], [doi:10.1016/j.physletb.2011.11.060].

[99] E. Babichev, C. Deffayet, and R. Ziour, *The Vainshtein mechanism in the Decoupling Limit of massive gravity*, *JHEP* **0905** (2009) 098, [arXiv:0901.0393], [doi:10.1088/1126-6708/2009/05/098].

[100] K. Nordtvedt, *Lunar laser ranging: A Comprehensive probe of postNewtonian gravity*, arXiv:gr-qc/0301024.

[101] G. Dvali, S. Hofmann, and J. Khoury, *Degravitation of the cosmological constant and graviton width*, *Phys.Rev.* **D76** (2007) 084006, [arXiv:hep-th/0703027], [doi:10.1103/PhysRevD.76.084006].

[102] N. Afshordi, G. Geshnizjani, and J. Khoury, *Do observations offer evidence for cosmological-scale extra dimensions?*, *JCAP* **0908** (2009) 030, [arXiv:0812.2244], [doi:10.1088/1475-7516/2009/08/030].

[103] J. Murphy, T.W., E. Adelberger, J. Battat, C. Hoyle, N. Johnson, *et al.*, *APOLLO: millimeter lunar laser ranging*, *Class.Quant.Grav.* **29** (2012) 184005, [doi:10.1088/0264-9381/29/18/184005].

[104] T. Hiramatsu, W. Hu, K. Koyama, and F. Schmidt, *Equivalence Principle Violation in Vainshtein Screened Two-Body Systems*, *Phys.Rev.* **D87** (2013), no. 6 063525, [arXiv:1209.3364], [doi:10.1103/PhysRevD.87.063525].

[105] M. Andrews, Y.-Z. Chu, and M. Trodden, *Galileon forces in the Solar System*, *Phys.Rev.* **D88** (2013) 084028, [arXiv:1305.2194], [doi:10.1103/PhysRevD.88.084028].

[106] L. Hui and A. Nicolis, *Proposal for an Observational Test of the Vainshtein Mechanism*, *Phys.Rev.Lett.* **109** (2012) 051304, [arXiv:1201.1508], [doi:10.1103/PhysRevLett.109.051304].

[107] L. Hui and A. Nicolis, *No-Hair Theorem for the Galileon*, *Phys.Rev.Lett.* **110** (2013), no. 24 241104, [arXiv:1202.1296], [doi:10.1103/PhysRevLett.110.241104].

[108] B. Paxton, L. Bildsten, A. Dotter, F. Herwig, P. Lesaffre, *et al.*, *Modules for Experiments in Stellar Astrophysics (MESA)*, *Astrophys.J.Suppl.* **192** (2011) 3, [arXiv:1009.1622], [doi:10.1088/0067-0049/192/1/3].

[109] B. Paxton, M. Cantiello, P. Arras, L. Bildsten, E. F. Brown, *et al.*, *Modules for Experiments in Stellar Astrophysics (MESA): Planets, Oscillations, Rotation, and Massive Stars*, *Astrophys.J.Suppl.* **208** (2013) 4, [arXiv:1301.0319], [doi:10.1088/0067-0049/208/1/4].

[110] P. Chang and L. Hui, *Stellar Structure and Tests of Modified Gravity*, *Astrophys.J.* **732** (2011) 25, [arXiv:1011.4107], [doi:10.1088/0004-637X/732/1/25].

[111] F. C. Adams, *Stars In Other Universes: Stellar structure with different fundamental constants*, *JCAP* **0808** (2008) 010, [arXiv:0807.3697], [doi:10.1088/1475-7516/2008/08/010].

[112] E. E. Salpeter, *The Luminosity function and stellar evolution*, *Astrophys.J.* **121** (1955) 161–167, [doi:10.1086/145971].

[113] W. L. Freedman and B. F. Madore, *The Hubble Constant*, *Ann.Rev.Astron.Astrophys.* **48** (2010) 673–710, [arXiv:1004.1856], [doi:10.1146/annurev-astro-082708-101829].

[114] Y. Alibert, I. Baraffe, P. Hauschildt, and F. Allard, *Period - luminosity - color - radius relationships of cepheids as a function of metallicity: evolutionary effects*, *Astron.Astrophys.* **344** (1999) 551–572, [arXiv:astro-ph/9901294].

[115] C.-Y. Kuo, *The megamaser cosmology project : geometric distances to megamaser galaxies and accurate masses of supermassive black holes at their centers*. PhD thesis, University of Virginia, 2011.

[116] J. Herrnstein, J. Moran, L. Greenhill, P. Diamond, M. Inoue, *et al.*, *A Geometric distance to the galaxy NGC 4258 from orbital motions in a nuclear gas disk*, *Nature* **400** (1999) 539–541, [doi:10.1038/22972].

[117] K. Lo, *Mega-masers and galaxies*, *Annual Review of Astronomy and Astrophysics* **43** (2005), no. 1 625–676, [http://www.annualreviews.org/doi/pdf/10.1146/annurev.astro.41.011802.094927], [doi:10.1146/annurev.astro.41.011802.094927].

[118] J. Moran, L. Humphreys, L. Greenhill, M. Reid, and A. Argon, *The structure of the accretion disk in NGC 4258 derived from observations of its water vapor masers*, *IAU Symp.* (2007) [arXiv:0707.1032].

[119] J. Herrnstein, *Cosmology with high-redshift water masers*, arXiv:astro-ph/9803039.

[120] I. Epstein, *Pulsation Properties of Giant-Star Models.*, *Astrophys. J.* **112** (July, 1950) 6, [doi:10.1086/145316].

[121] E. Humphreys, M. Reid, L. Greenhill, J. Moran, and A. Argon, *Toward a New Distance to the Active Galaxy NGC 4258: II. Centripetal Accelerations and Investigation of Spiral Structure*, *Astrophys.J.* **672** (2008) 800–816, [arXiv:0709.0925], [doi:10.1086/523637].

[122] E. Humphreys, M. J. Reid, J. M. Moran, L. J. Greenhill, and A. L. Argon, *Toward a New Geometric Distance to the Active Galaxy NGC 4258. III. Final Results and the Hubble Constant*, *Astrophys.J.* **775** (2013) 13, [arXiv:1307.6031], [doi:10.1088/0004-637X/775/1/13].

[123] C. Henkel, J. Braatz, M. Reid, J. Condon, K. Lo, *et al.*, *Cosmology and the Hubble Constant: On the Megamaser Cosmology Project (MCP)*, arXiv:1205.0823.

[124] L. Lombriser, A. Slosar, U. Seljak, and W. Hu, *Constraints on f(R) gravity from probing the large-scale structure*, *Phys.Rev.* **D85** (2012) 124038, [arXiv:1003.3009], [doi:10.1103/PhysRevD.85.124038].

[125] F. Schmidt, *Dynamical Masses in Modified Gravity*, *Phys.Rev.* **D81** (2010) 103002, [arXiv:1003.0409], [doi:10.1103/PhysRevD.81.103002].

[126] A. Terukina, L. Lombriser, K. Yamamoto, D. Bacon, K. Koyama, *et al.*, *Testing chameleon gravity with the Coma cluster*, *JCAP* **1404** (2014) 013, [arXiv:1312.5083], [doi:10.1088/1475-7516/2014/04/013].

[127] A. Silvestri, *Scalar radiation from Chameleon-shielded regions*, *Phys.Rev.Lett.* **106** (2011) 251101, [arXiv:1103.4013], [doi:10.1103/PhysRevLett.106.251101].

[128] A. Upadhye and J. H. Steffen, *Monopole radiation in modified gravity*, arXiv:1306.6113.

[129] J. Cox, *The Theory of Stellar Pulsation*. Princeton series in astrophysics. Princeton Univversity Press, 1980.

[130] S. Chandrasekhar, *Dynamical Instability of Gaseous Masses Approaching the Schwarzschild Limit in General Relativity*, *Phys.Rev.Lett.* **12** (1964) 114–116, [doi:10.1103/PhysRevLett.12.114].

[131] M. Hurley, P. H. Roberts, and K. Wright, *The Oscillations of Gas Spheres*, *Astrophys. J.* **143** (1966) 535.

[132] P. Brax and J. Martin, *The SUGRA Quintessence Model Coupled to the MSSM*, *JCAP* **0611** (2006) 008, [arXiv:astro-ph/0606306], [doi:10.1088/1475-7516/2006/11/008].

[133] P. Brax and J. Martin, *Dark Energy and the MSSM*, *Phys.Rev.* **D75** (2007) 083507, [arXiv:hep-th/0605228], [doi:10.1103/PhysRevD.75.083507].

[134] P. Brax and J. Martin, *Moduli Fields as Quintessence and the Chameleon*, *Phys.Lett.* **B647** (2007) 320–329, [arXiv:hep-th/0612208], [doi:10.1016/j.physletb.2007.02.019].

[135] S. Kachru, R. Kallosh, A. D. Linde, and S. P. Trivedi, *De Sitter vacua in string theory*, *Phys.Rev.* **D68** (2003) 046005, [arXiv:hep-th/0301240], [doi:10.1103/PhysRevD.68.046005].

[136] J. P. Conlon and F. G. Pedro, *Moduli-Induced Vacuum Destabilisation*, *JHEP* **1105** (2011) 079, [arXiv:1010.2665], [doi:10.1007/JHEP05(2011)079].

[137] H. Nastase and A. Weltman, *Chameleons on the Racetrack*, *JHEP* **1308** (2013) 059, [arXiv:1301.7120], [doi:10.1007/JHEP08(2013)059].

[138] H. P. Nilles, *Supersymmetry, Supergravity and Particle Physics*, *Phys.Rept.* **110** (1984) 1–162, [doi:10.1016/0370-1573(84)90008-5].

[139] A. Brignole, L. E. Ibanez, and C. Munoz, *Towards a theory of soft terms for the supersymmetric Standard Model*, *Nucl.Phys.* **B422** (1994) 125–171, [arXiv:hep-ph/9308271], [doi:10.1016/0550-3213(94)00068-9].

[140] A. Brignole, L. E. Ibanez, and C. Munoz, *Soft supersymmetry breaking terms from supergravity and superstring models*, arXiv:hep-ph/9707209.

[141] D. Farquet and C. A. Scrucca, *Scalar geometry and masses in Calabi-Yau string models*, *JHEP* **1209** (2012) 025, [arXiv:1205.5728], [doi:10.1007/JHEP09(2012)025].

[142] I. Jack and D. Jones, *Renormalization of the Fayet-Iliopoulos D term*, *Phys.Lett.* **B473** (2000) 102–108, [arXiv:hep-ph/9911491], [doi:10.1016/S0370-2693(99)01484-7].

[143] **WiggleZ Collaboration** Collaboration, C. Contreras *et al.*, *The WiggleZ Dark Energy Survey: measuring the cosmic growth rate with the two-point galaxy correlation function*, arXiv:1302.5178, doi:10.1093/mnras/sts608.

[144] B. Ratra and P. J. E. Peebles, *Cosmological consequences of a rolling homogeneous scalar field*, *Phys. Rev. D* **37** (Jun, 1988) 3406–3427, [doi:10.1103/PhysRevD.37.3406].

[145] P. Brax, A.-C. Davis, and H. A. Winther, *Cosmological supersymmetric model of dark energy*, *Phys.Rev.* **D85** (2012) 083512, [arXiv:1112.3676], [doi:10.1103/PhysRevD.85.083512].

[146] M. Werner, T. L. Roellig, F. Low, G. Rieke, M. Rieke, *et al.*, *The Spitzer Space Telescope mission*, *Astrophys.J.Suppl.* **154** (2004) 1–9, [arXiv:astro-ph/0406223], [doi:10.1086/422992].

[147] F. ThÃľvenin, *Measuring stars with gaia*, *EAS Publications Series* **null** (1, 2013) 85–88, [doi:10.1051/eas/1363010].

[148] S. Ransom, I. Stairs, A. Archibald, J. Hessels, D. Kaplan, *et al.*, *A millisecond pulsar in a stellar triple system*, arXiv:1401.0535, doi:10.1038/nature12917.

[149] G. Pietrzyński, I. B. Thompson, W. Gieren, D. Graczyk, G. Bono, A. Udalski, I. Soszyński, D. Minniti, and B. Pilecki, *The dynamical mass of a classical Cepheid variable star in an eclipsing binary system*, *nature* **468** (Nov., 2010) 542–544, [doi:10.1038/nature09598].

[150] M. Marconi, R. Molinaro, G. Bono, G. Pietrzynski, W. Gieren, *et al.*, *The Eclipsing Binary Cepheid OGLE-LMC-CEP-0227 in the Large Magellanic Cloud: pulsation modelling of light and radial velocity curves*, *Astrophys.J.* **768** (2013) L6, [arXiv:1304.0860], [doi:10.1088/2041-8205/768/1/L6].

[151] R. Ciardullo, *The Planetary Nebula Luminosity Function at the Dawn of Gaia*, *Astrophys.Space Sci.* **341** (2012) 151–161, [arXiv:1203.5551], [doi:10.1007/s10509-012-1061-2].

[152] R. Wald, *General Relativity*. Physics, astrophysics. University of Chicago Press, 1984.

[153] G. Pietrzynski, W. Gieren, P. Fouque, and F. Pont, *The araucaria project. discovery of cepheid variables in ngc 300 from a wide-field imaging survey*, arXiv:astro-ph/0202494.

[154] A. Saha, F. Thim, G. Tammann, B. Reindl, and A. Sandage, *Cepheid distances to sne ia host galaxies based on a revised photometric zero-point of the hst-wfpc2 and new p-l relations and metallicity corrections*, *Astrophys.J.Suppl.* **165** (2006) 108–137, [arXiv:astro-ph/0602572], [doi:10.1086/503800].

[155] N. A. Silbermann, P. Harding, B. F. Madore, R. C. Kennicutt, Jr., A. Saha, P. B. Stetson, W. L. Freedman, J. R. Mould, J. A. Graham, R. J. Hill, A. Turner, F. Bresolin, L. Ferrarese, H. Ford, J. G. Hoessel, M. Han, J. Huchra, S. M. G. Hughes, G. D. Illingworth, R. Phelps, and S. Sakai, *The Hubble Space Telescope Key Project on the Extragalactic Distance Scale. VI. The Cepheids in NGC 925*, *Astrophys. J.* **470** (Oct., 1996) 1, [doi:10.1086/177845].

[156] L. Ferrarese, F. Bresolin, J. Kennicutt, Robert C., A. Saha, P. B. Stetson, *et al.*, *The HST Key Project on the extragalactic distance scale. 12. The Discovery of Cepheids and a new distance to NGC 2541*, *Astrophys.J.* (1998) [arXiv:astro-ph/9805365].

[157] S. Sakai, L. Ferrarese, R. C. Kennicutt, J. A. Graham, N. Silbermann, *et al.*, *The Hubble Space Telescope Extragalactic Distance Scale Key Project. 23. The Discovery of Cepheids in NGC 3319*, *Astrophys.J.* (1999) [arXiv:astro-ph/9906487].

[158] C. F. Prosser, J. Kennicutt, Robert C., F. Bresolin, A. Saha, S. Sakai, *et al.*, *The hst key project on the extragalactic distance scale. xxii. the discovery of cepheids in ngc 1326-a*, arXiv:astro-ph/9906486.

[159] R. L. Phelps, S. Sakai, W. L. Freedman, B. F. Madore, A. Saha, P. B. Stetson, R. C. Kennicutt, J. R. Mould, L. Ferrarese, H. C. Ford, B. K. Gibson, J. A. Graham, M. Han, J. G. Hoessel, J. P. Huchra, S. M. Hughes, G. D. Illingworth, and N. A. Silbermann, *The Hubble Space Telescope Extragalactic Distance Scale Key Project. IX. The Discovery of Cepheids in NGC 2090*, *Astrophys. J.* **500** (June, 1998) 763, [doi:10.1086/305766].

[160] W. L. Freedman, S. M. Hughes, B. F. Madore, J. R. Mould, M. G. Lee, P. Stetson, R. C. Kennicutt, A. Turner, L. Ferrarese, H. Ford, J. A. Graham, R. Hill, J. G. Hoessel, J. Huchra, and G. D. Illingworth, *The Hubble Space Telescope Extragalactic Distance Scale Key Project. 1: The discovery of Cepheids and a new distance to M81*, *Astrophys. J.* **427** (June, 1994) 628–655, [doi:10.1086/174172].

[161] D. D. Kelson, G. D. Illingworth, A. Saha, J. A. Graham, P. B. Stetson, W. L. Freedman, R. C. Kennicutt, J. R. Mould, L. Ferrarese, J. P. Huchra, B. F. Madore, C. F. Prosser, F. Bresolin, H. C. Ford, B. K. Gibson, J. G. Hoessel, S. M. G. Hughes, L. M. Macri, S. Sakai, and N. A. Silbermann, *The Hubble Space Telescope Key Project on the Extragalactic Distance Scale. XIX. The Discovery of Cepheids in and a New Distance to NGC 3198*, *Astrophys. J.* **514** (Apr., 1999) 614–636, [doi:10.1086/306989].

[162] J. A. Graham, R. L. Phelps, W. L. Freedman, A. Saha, L. Ferrarese, P. B. Stetson, B. F. Madore, N. A. Silbermann, S. Sakai, R. C. Kennicutt, P. Harding, F. Bresolin, A. Turner, J. R. Mould, D. M. Rawson, H. C. Ford, J. G. Hoessel, M. Han, J. P. Huchra, L. M. Macri, S. M. Hughes, G. D. Illingworth, and D. D. Kelson, *The Hubble Space Telescope Extragalactic Distance Scale Key Project. VII. The Discovery of Cepheids in the Leo I Group Galaxy NGC 3351*, *Asteophys. J.* **477** (Mar., 1997) 535, [doi:10.1086/303740].

[163] D. M. Rawson, L. M. Macri, J. R. Mould, J. P. Huchra, W. L. Freedman, *et al.*, *The Extragalactic Distance Scale Key Project. 8. The Discovery of Cepheids and a new distance to NGC 3621 using the Hubble Space Telescope*, *Astrophys.J.* (1997) [arXiv:astro-ph/9705259].

[164] A. Turner, L. Ferrarese, A. Saha, F. Bresolin, R. C. Kennicutt, Jr., P. B. Stetson, J. R. Mould, W. L. Freedman, B. K. Gibson, J. A. Graham, H. Ford, M. Han, P. Harding, J. G. Hoessel, J. P. Huchra, S. M. G. Hughes, G. D. Illingworth, D. D. Kelson, L. Macri, B. F. Madore, R. Phelps, D. Rawson, S. Sakai, and N. A. Silbermann, *The Hubble Space*

Telescope Key Project on the Extragalactic Distance Scale. XI. The Cepheids in NGC 4414, *Astrophys. J.* **505** (Sept., 1998) 207–229, [doi:10.1086/306150].

[165] L. M. Macri, J. Huchra, P. Stetson, N. Silbermann, W. Freedman, *et al.*, *The Extragalactic Distance Scale Key Project. 18. The Discovery of Cepheids and a new distance to NGC 4535 using the Hubble Space Telescope*, arXiv:astro-ph/9901332.

[166] J. A. Graham, L. Ferrarese, W. L. Freedman, R. C. Kennicutt, Jr., J. R. Mould, A. Saha, P. B. Stetson, B. F. Madore, F. Bresolin, H. C. Ford, B. K. Gibson, M. Han, J. G. Hoessel, J. Huchra, S. M. Hughes, G. D. Illingworth, D. D. Kelson, L. Macri, R. Phelps, S. Sakai, N. A. Silbermann, and A. Turner, *The Hubble Space Telescope Key Project on the Extragalactic Distance Scale. XX. The Discovery of Cepheids in the Virgo Cluster Galaxy NGC 4548*, *Astrophys. J.* **516** (May, 1999) 626–646, [doi:10.1086/307151].

[167] B. K. Gibson, S. M. Hughes, P. B. Stetson, W. L. Freedman, J. Kennicutt, Robert C., *et al.*, *The HST Key Project on the extragalactic distance scale. 17. The Cepheid distance to NGC 4725*, *Astrophys.J.* (1998) [arXiv:astro-ph/9810003].

[168] D. D. Kelson, G. D. Illingworth, W. F. Freedman, J. A. Graham, R. Hill, B. F. Madore, A. Saha, P. B. Stetson, R. C. Kennicutt, Jr., J. R. Mould, S. M. Hughes, L. Ferrarese, R. Phelps, A. Turner, K. H. Cook, H. Ford, J. G. Hoessel, and J. Huchra, *The Extragalactic Distance Scale Key Project. III. The Discovery of Cepheids and a New Distance to M101 Using the Hubble Space Telescope*, *Astrophys. J.* **463** (May, 1996) 26, [doi:10.1086/177221].

[169] S. M. G. Hughes, M. Han, J. Hoessel, W. L. Freedman, R. C. Kennicutt, Jr., J. R. Mould, A. Saha, P. B. Stetson, B. F. Madore, N. A. Silbermann, P. Harding, L. Ferrarese, H. Ford, B. K. Gibson, J. A. Graham, R. Hill, J. Huchra, G. D. Illingworth, R. Phelps, and S. Sakai, *The Hubble Space Telescope Extragalactic Distance Scale Key Project. X. The*

Cepheid Distance to NGC 7331, *Astrophys. J.* **501** (July, 1998) 32, [doi:10.1086/305808].

[170] D. Sugimoto, K. Nomoto, and Y. Eriguchi, *Stable Numerical Method in Computation of Stellar Evolution*, *Progress of Theoretical Physics Supplement* **70** (1981) 115–131, [doi:10.1143/PTPS.70.115].

A

Weyl Rescalings of the Metric

In this appendix we will study the transformation properties of several important geometric tensors that are used to derive the results presented in chapter 2. We will then go on to show how the conservation law for the Einstein frame energy-momentum tensor can be obtained from the Jordan frame equation. Here we will present only those properties necessary to derive the results of chapter 2. A more general account can be found in [152], appendix D[1].

A.1 Transformation of the Ricci Scalar

We are interested in the transformation of various curvature tensors constructed using the Jordan frame metric $\tilde{g}_{\mu\nu}$ in order to find the equivalent tensors constructed using the Einstein frame metric $g_{\mu\nu}$. The two metric are related via

$$\tilde{g}_{\mu\nu} = A^2(\phi) g_{\mu\nu}. \tag{A.1}$$

We are interested in quantities such as the Riemann tensor and the Ricci tensor and scalar, which are constructed using the metric and the Christoffel symbols and so we must first find

[1] Note that the method used in our derivation will differ from theirs but identical results are obtained.

how these are related. Defining

$$\mathcal{K}^{\alpha}_{\mu\nu} = \tilde{\Gamma}^{\alpha}_{\mu\nu} - \Gamma^{\alpha}_{\mu\nu}, \tag{A.2}$$

which, by direct computation using equation (A.1) is

$$\mathcal{K}^{\alpha}_{\mu\nu} = 2\delta^{\alpha}_{(\mu}\nabla_{\nu)}\ln A - g_{\mu\nu}\nabla^{\alpha}\ln A. \tag{A.3}$$

Next, using the definition of the Riemann tensor,

$$2\tilde{\nabla}_{[\mu}\tilde{\nabla}_{\nu]}v^{\alpha} = \tilde{R}^{\alpha}_{\beta\mu\nu}v^{\beta} \tag{A.4}$$

we have

$$\tilde{R}^{\alpha}_{\beta\mu\nu} = R^{\alpha}_{\beta\mu\nu} + 2\nabla_{[\mu}\mathcal{K}^{\alpha}_{\nu]\beta} + 2\mathcal{K}^{\alpha}_{\gamma[\mu}\mathcal{K}^{\gamma}_{\nu]\beta}. \tag{A.5}$$

Contracting the α and μ index[2] and inserting equation (A.3) we can calculate the Ricci tensor:

$$\tilde{R}_{\mu\nu} = R_{\mu\nu} - 4\nabla_{\mu}\nabla_{\nu}\ln A - g_{\mu\nu}\Box\ln A + 2\nabla_{\mu}\ln A\nabla_{\nu}\ln A - 4g_{\mu\nu}\nabla_{\rho}\ln A\nabla^{\rho}\ln A. \tag{A.6}$$

Contracting with $\tilde{g}^{\mu\nu} = A^{-2}(\phi)g^{\mu\nu}$ we obtain the Ricci scalar:

$$\tilde{R} = \frac{1}{A^2}\left[R - 6\Box\ln A - 6\nabla_{\mu}\ln A\nabla^{\mu}\ln A\right]. \tag{A.7}$$

This is precisely the transformation we need to find the Einstein frame expression for a theory whose action is defined in the Jordan frame. Indeed, this is how we obtained equation (2.7) from equation (2.1). In section 2.2 we defined our model in the Einstein frame and so the inverse transformation is needed to calculate the Jordan frame expression in equation (2.15). Clearly this can be achieved using equation (A.7) and treating the tilded Ricci scalar as the Einstein frame quantity. In this case we have $g_{\mu\nu} = A^{-2}\tilde{g}_{\mu\nu}$ and so if we set $A \to A^{-1}$ in equation

[2]Note that it does not matter which metric we use for this contraction since we are contracting with a δ-symbol.

(A.7) and swap the tilded and untilded Ricci scalars we can find the equivalent expression for the Einstein frame Ricci scalar. Note that the term proportional to $\Box \ln A$ is a total derivative and so does not contribute to the equations of motion. For this reason, we have ignored this term when transforming between different frames in chapter 2.

A.2 The Energy-Momentum Tensor

Finally, we want to derive equation (2.11), which gives the conservation law for the energy-momentum tensor in the Einstein frame. Now particles move on geodesics of the Jordan frame metric and so it is this frame where the energy momentum is covariantly conserved:

$$\tilde{\nabla}_\mu \tilde{T}^{\mu\nu} = 0. \tag{A.8}$$

In terms of the Einstein frame energy-momentum tensor, we have

$$\tilde{T}^{\mu\nu} = \frac{2}{\sqrt{-\tilde{g}}}\frac{\delta S_{\rm m}}{\delta \tilde{g}_{\mu\nu}} = \frac{2}{A^4\sqrt{-g}}\frac{\delta S_{\rm m}}{\delta g_{\alpha\beta}}\frac{\delta g_{\alpha\beta}}{\delta \tilde{g}_{\alpha\beta}} = A^{-6}T^{\mu\nu} \tag{A.9}$$

and so the problem is then to calculate the transformation law from the Jordan frame relation $\tilde{\nabla}_\mu(A^{-6}T^{\mu\nu}) = 0$. Using equation (A.2) we have

$$\tilde{\nabla}_\mu\left(A^{-6}T^{\mu\nu}\right) = \nabla_\mu\left(A^{-6}T^{\mu\nu}\right) + A^{-6}\left(\mathscr{K}^{\mu}_{\mu\rho} + \mathscr{K}^{\nu}_{mu\rho}\right)T^{\rho\mu}. \tag{A.10}$$

Replacing the factors of $\mathscr{K}$ using equation (A.3) we then have

$$\nabla_\mu T^{\mu\nu} = \frac{A'(\phi)}{A(\phi)}T\nabla^\nu\phi, \tag{A.11}$$

which can be used with the definition of $\beta(\phi)$ (equation (2.18)) to recover equation (2.11).

B

Cepheid and TRGB Data

In this appendix we present a list of the galaxies that were used in the distance indicator comparison performed in chapter 4 along with their journal references. In table B.1 we list the galaxies used in the period-luminosity relation and in table B.2 we list the TRGB and Cepheid distances for each galaxy used to obtain the constraints in figure 4.10.

Table B.1: The galaxies used in the period-luminosity relation and their references. The second column labelled *N* gives the number of Cepheids observed in each galaxy. Names that end with * are galaxies with unacceptably large dispersion in period-luminosity relation.

Name	*N*	Reference
NGC300	117	[153]
NGC5253	5	[154]
IC4182	13	[154]
NGC925	79	[155]
NGC2541	28	[156]
NGC3319	28	[157]
NGC1326A	17	[158]
NGC 2090	34	[159]
NGC 3031	25	[160]
NGC 3198	52	[161]
NGC 3351*	49	[162]
NGC 3621*	69	[163]
NGC 4321*	52	[156]
NGC 4414*	9	[164]
NGC 4535	50	[165]
NGC 4548*	24	[166]
NGC 4725	20	[167]
NGC 5457	29	[168]
NGC 7331	13	[169]

Table B.2: Cepheid and TRGB based distances to the galaxies used in the comparison. The final column gives the screening for $\phi = 4 \times 10^{-7}$ as follows: 0: Unscreened, 1: environmentally screened, 2: self-screened.

Name	Cepheid distance (Mpc)	TRGB distance (Mpc)	Screening
DDO 069	0.71 ± 0.01	0.78 ± 0.03	0
NGC 3109	1.15 ± 0.03	1.27 ± 0.02	0
DDO 216	1.27 ± 0.27	0.97 ± 0.03	0
Sextans A	1.31 ± 0.03	1.38 ± 0.03	0
Sextans B	1.49 ± 0.11	1.34 ± 0.02	0
GR8	1.80 ± 0.06	2.19 ± 0.15	0
NGC 0300	2.03 ± 0.05	1.95 ± 0.06	0
NGC 2403	3.20 ± 0.15	3.18 ± 0.35	0
NGC 2366	3.28 ± 0.30	3.19 ± 0.41	0
NGC 5253	3.43 ± 0.08	3.77 ± 0.19	0
NGC 4395	4.45 ± 0.37	4.61 ± 0.62	0
IC 4182	4.68 ± 0.04	4.47 ± 0.12	0
NGC 3621	7.17 ± 0.06	7.45 ± 0.38	0
SMC	0.06 ± 0.00	0.06 ± 0.00	1
NGC 6822	0.51 ± 0.03	0.48 ± 0.01	1
IC 1613	0.69 ± 0.01	0.72 ± 0.01	1
IC 0010	0.72 ± 0.05	0.50 ± 0.04	1
M33	0.90 ± 0.02	0.88 ± 0.02	1
WLM	0.95 ± 0.05	0.91 ± 0.02	1
M31	0.86 ± 0.02	0.78 ± 0.02	2
NGC 5128	3.44 ± 0.19	3.73 ± 0.24	2
M81	3.84 ± 0.06	4.04 ± 0.22	2
M83	5.01 ± 0.23	4.51 ± 0.31	2
M101	7.13 ± 0.14	7.66 ± 0.39	2
M106	8.41 ± 0.07	7.31 ± 0.30	2

C

Numerical Methods

In this appendix we describe the various numerical methods used throughout this thesis. We first present a brief introduction to the architecture of MESA and explain how the effects of modified gravity are implemented numerically. Next, we describe the numerical methods used to obtain the solutions of the MLAWE presented in chapter 5.

C.1 MESA

In this section we introduce the basic numerical features of MESA. A complete description is well beyond the scope of this appendix and the reader is referred to [108] for the full details; in this appendix we will only present the features used to obtain the results presented in this thesis. In particular, we have not made use of processes such as convection, mass-loss, overshooting or semi-convection and so we will not discuss these here.

C.1.1 The Architecture of MESA

MESA is a one-dimensional code (meaning that it assumes spherical symmetry) that solves the stellar structure equations in a fully consistent manner. A stellar model is defined as a star

at any specific time-step. MESA divides the star into N cells of variable width labelled by an integer k that varies from 1 at the stellar surface to N at the centre ($r = 0$). The number of cells is determined by MESA according to the complexity of the phase of stellar evolution and can vary from $\mathcal{O}(10^2)$ on the main-sequence to $\mathcal{O}(10^5)$ for more complicated post-main-sequence stars. Note that MESA defines the stellar surface as the radius at which the pressure falls to zero. When observing real stars, one actually observes light emitted from the radius at which the optical depth falls to 2/3 — the so-called *photosphere* — and so the surface temperature is not equal to the effective temperature (or $B - V$ if one is dealing with magnitudes). MESA keeps track of the location of the photosphere and so it is possible to output data on any variables if one so desires. In particular, when one refers to the stellar luminosity, one is in fact referring to the luminosity at the location of the photosphere and it is this that MESA outputs.

MESA works with a variety of different variables such as pressure, temperature, density etc., which may be defined either at the cell centres or the cell boundaries. As a rule of thumb, extensive variables such as the mass enclosed within the cell or the luminosity in the cell are defined at the cell boundary whereas intensive variables such as the density and temperature are defined at the cell centre. A schematic diagram of this is shown in figure C.1 which includes some examples of the cell assignments of some stellar quantities. Different quantities are defined at different locations for reasons of numerical stability and efficiency [170], however one can always interpolate from cell centres to cell boundaries and vice versa if necessary. MESA uses $q \equiv M(r)/M(R)$ as the radial variable and not r and so we must interpolate in m. As an example, we will interpolate the pressure — which is cell-centred and whose value in cell k is P_k — from the centre of cell k to its boundary. We start by defining $\mathrm{d}q_k$ as the ratio of the mass enclosed inside the cell to the stellar mass so that in the notation of figure C.1 (see the caption) we have $\mathrm{d}q_k = \mathrm{d}m_k/M(R)$. Next, we define the interpolation variable δ_k for cell k via

$$\delta_k = \frac{\mathrm{d}q_{k-1}}{\mathrm{d}q_k + \mathrm{d}q_{k-1}}. \tag{C.1}$$

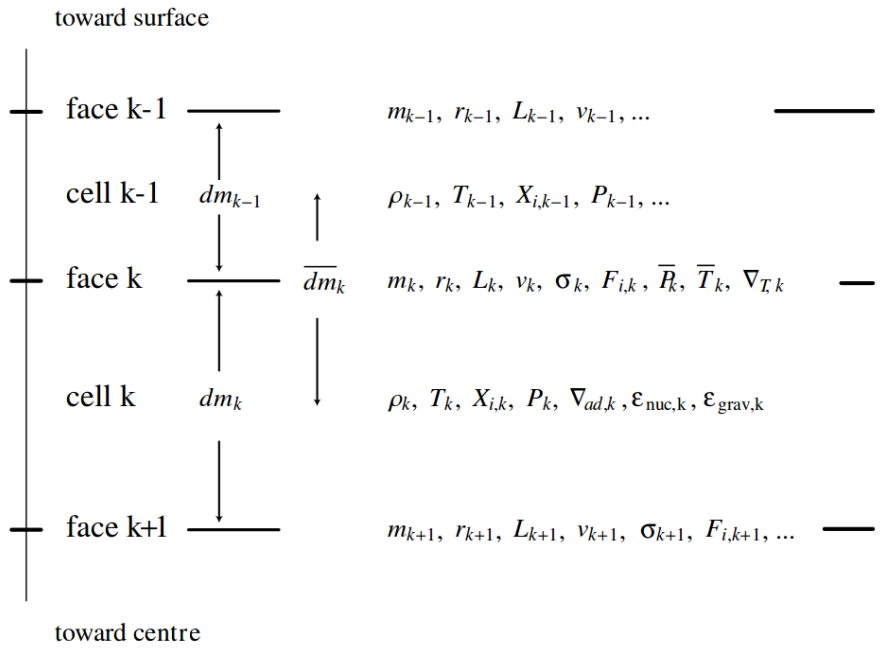


Figure C.1: The cell structure of stars in MESA and the cell assignments of various stellar quantities. Figure reproduced from [108]. The variables shown that are relevant for this thesis are the temperature T, the density ρ the mass m enclosed by radius r and the luminosity L. $\mathrm{d}m_k$ refers to the mass enclosed within cell k and $\bar{\mathrm{d}}m_k$ is the average mass enclosed in cells k and $k-1$. The reader is referred to [108] for the details of the other quantities shown.

The pressure at the cell boundary $\bar{P}_k$ is then

$$\bar{P}_k = \delta_k P_k + (1-\delta_k) P_{k-1}. \tag{C.2}$$

If one wishes to interpolate from cell boundaries to cell centres one simply replaces $\mathrm{d}m_k$ by $\overline{\mathrm{d}m_k}$ in the definition of $\mathrm{d}q_k$ (see the caption in figure C.1).

Given some initial stellar model, MESA uses the values of the various quantities defined at the cell boundaries or centres to solve the stellar structure equations using the Newton-Raphson method. The initial stellar model is used as the trial solution and the system is iterated until convergence is achieved. Where necessary, MESA uses opacity tables and reaction networks (including reaction rates) to close the system. At no point is any equation of

state assumed. MESA uses a variable time-step that is chosen in order to be short enough to give a fast convergence but long enough that the stellar evolution is efficient. The details of the algorithm are very complicated and are presented in [108] section 6.4.

C.1.2 Implementation of Modified Gravity

Modified gravity is implemented into MESA by including the radial variation of G according to equation (3.48). This is done in two stages: first, the screening radius is found and second, the value of G in each cell exterior to this is updated according to (3.48). Given input values of χ_0 and α, this is achieved numerically using the following algorithm:

1. Starting from an initial stellar model, the cell-centred density is interpolated to the cell boundary, where the radial coordinate is defined.

2. Using the trapezium rule, the integral (2.75) is performed using the density at the cell boundary and the cell width as the discretised radial coordinate[1]. The integral is performed inwards from the outer cell ($k = 1$) to successively deeper cells until (2.75) is satisfied. This cell is designated as the screening cell k_s.

3. The total mass of the cells with $k \geq k_s$ ($M(r_s)$) is calculated, which is all that is needed to find $G(r)$ according to (3.48).

4. The value of G in the cells with $k \geq k_s$ is left unaltered but the value in each cell with $k < k_s$ is updated according to (3.48).

5. The code is evolved to the next time-step i.e. the stellar structure equations with $G \rightarrow G(r)$ are solved.

6. The above steps are repeated using the new stellar model.

[110] have used a different method of implementing modified gravity into MESA using an ansatz for the field profile and interpolating the screening radius to a cell-centred value.

[1] MESA uses CGS units and so the appropriate factors of c are included.

We have compared the output of our code with theirs and the results are indistinguishable. One may still worry that this method is not self-consistent, i.e. we use a given stellar model to find $G(r)$ and then evolve the system rather than calculating $G(r)$ at the same time using the Newton-Raphson solver. This is what [110] do and since our results match theirs to a high accuracy we conclude that our method does not introduce any errors due to our numerical procedure[2]. This is because of the time-step selection mentioned above. If any large error is introduced by our procedure, the stellar structure equations are not satisfied and MESA reduces the time-step accordingly until convergence is achieved[3].

C.2 Numerical Methods for Solving the MLAWE

In this section we describe the numerical procedure used to solve the MLAWE and obtain the results in chapter 5.

C.2.1 First-Order form of the MLAWE

Whereas the form presented in equation (5.22) is useful for extracting the new physical features, numerically, it is more convenient to work with a first order system. One may re-write the homogeneous MLAWE in the form

$$\frac{\mathrm{d}}{\mathrm{d}r}\left[\frac{\Gamma_{1,0}P_0}{r^2}\frac{\mathrm{d}}{\mathrm{d}r}\left(r^3\xi\right)\right]-4\frac{\mathrm{d}P_0}{\mathrm{d}r}-4\pi\alpha G\rho_0^2 r\xi+\omega^2 r\rho_0\xi=0. \tag{C.3}$$

In order to cast this into first order form we introduce the new variable η, defined by

$$\eta(r)=\frac{1}{r^2}\frac{\mathrm{d}}{\mathrm{d}r}\left(r^3\xi\right), \tag{C.4}$$

[2]The advantage of our method is that MESA is constantly developing and changing. Our implementation can easily be incorporated into successive versions of MESA whereas including $G(r)$ as another variable found using the Newton-Raphson solver requires a complete re-writing of the code with every new release.

[3]The disadvantage of this is that the run-time for a given star is longer than if one had included $G(r)$ as a dynamical variable. In fact, the run-time for most modified gravity simulations using our method is of order minutes and so this trade-off against compatibility with future releases is perfectly reasonable.

which, using equation (5.8), is nothing but $-\delta\rho/\rho_0$. Using this definition, we can cast (C.3) into a convenient first-order from for both Lane-Emden and MESA models.

C.2.2 Lane-Emden Form

When solving for Lane-Emden profile, we replace r with y using (1.57) and the pressure and density with θ to obtain

$$\frac{\mathrm{d}\eta}{\mathrm{d}y} = \frac{1}{\Gamma_{1,0}\theta}\left[4(n+1)\frac{\mathrm{d}\theta}{\mathrm{d}y}\xi + \alpha(n+1)y\theta^n\xi - (n+1)\Gamma_{1,0}\frac{\mathrm{d}\theta}{\mathrm{d}y}\eta - \tilde{\omega}^2 y\xi\right] \tag{C.5}$$

$$\frac{\mathrm{d}\xi}{\mathrm{d}y} = \frac{\eta - 3\xi}{y}, \tag{C.6}$$

where $\Gamma_{1,0}$ is treated as constant in Lane-Emden models, $\tilde{\omega}$ is defined in (5.48) and the term proportional to α is present only when $r > r_s$. The value of $\Gamma_{1,0}$ may be chosen at will. These are supplemented by the boundary conditions

$$\eta(0) = 3\xi(0) \tag{C.7}$$

$$\eta(y_R) = \frac{\xi(y_R)}{\Gamma_{1,0}}\left(4 + \frac{\tilde{\omega}^2 y_R}{(n+1)\,\mathrm{d}\theta/\mathrm{d}y}\right)\Bigg|_{y=y_R}, \tag{C.8}$$

which are the Lane-Emden equivalents of (5.24) and (5.25). We solve this equation using the shooting technique. Using the fourth-order Runge-Kutta method, we solve equations (C.5) and (C.6) in conjunction with the modified Lane-Emden equation (3.13) using a trial value of $\tilde{\omega}^2$ and the centre boundary condition (C.7). We then test the surface condition (C.8) against our solution, iterating over different values of $\tilde{\omega}^2$ until the difference between our solution and the boundary condition is less than some predefined tolerance (exactly how much depends on the accuracy required for the eigenvalue). Using this method, one can obtain $\tilde{\omega}^2$ and the corresponding eigenfunction to the desired accuracy.

C.2.3 MESA form

MESA produces pressure, density, temperature etc. profiles in physical units, and so it is convenient to use the dimensionless quantities defined in (5.29), (5.30) and (5.31) so that the MLAWE is

$$\frac{\mathrm{d}\eta}{\mathrm{d}x} = \left(\Gamma_{1,0}(x)\bar{P}_0(x)\right)^{-1}\left[-\eta\left(\bar{P}_0\frac{\mathrm{d}\Gamma_{1,0}}{\mathrm{d}x} + \Gamma_{1,0}\frac{\mathrm{d}\bar{P}_0}{\mathrm{d}x}\right)\right. \tag{C.9}$$

$$\left. + 4\frac{\mathrm{d}\bar{P}_0}{\mathrm{d}x} + 4\pi\alpha x\bar{\rho}_0^2\xi - \Omega^2 x\bar{\rho}_0\xi\right], \tag{C.10}$$

$$\frac{\mathrm{d}\xi}{\mathrm{d}x} = \frac{\eta - 3\xi}{x}, \tag{C.11}$$

where, again, the term proportional to α is only present when $x > x_\mathrm{s} \equiv r_\mathrm{s}/R$ and Ω^2 is the dimensionless eigenfrequency defined in (5.34).

The eigenvalue problem is solved in a similar manner to the Lane-Emden models. Using profiles for $\bar{P}_0$ and $\bar{\rho}_0$ at both the cell boundaries and centres as well as the screening radius from MESA, these equations are integrated from the stellar centre using the fourth order Runge-Kutta scheme for a test value of Ω^2. Ω^2 is then iterated until the boundary condition at the stellar surface,

$$\eta(1) = \frac{1}{\Gamma_{1,0}(1)}\left(\Omega^2 + 4\right)\xi(1), \tag{C.12}$$

is satisfied up to some pre-set tolerance. In this manner, Ω^2 and the corresponding eigenfunction can be found for any given model and the period found by inverting (5.34).

D

Modified Bessel Equations

This appendix details some important properties of modified Bessel functions that appear in the solution of the equations governing linear perturbations in the CDM power spectrum studied in chapter 7.

D.1 Generalised Modified Bessel Equations

We have seen in section 7.3 that the linearised perturbation equations are all of the form

$$t^2\ddot{\delta}_c + at\dot{\delta}_c - \left(b^2 + c^2t^{2r}\right)\delta_c = 0, \tag{D.1}$$

with $a = 4/3$. The substitution $\delta_c = t^n\delta_c(t)$ with $n = (1-a)/2$ may be used to find the following equation for δ_c:

$$t^2\ddot{\delta}_c + t\dot{\delta}_c - \left(\frac{(a-1)^2}{4} + b^2 + c^2t^{2r}\right)\delta_c = 0, \tag{D.2}$$

which may further be transformed into the form

$$u^2\delta_{\rm c}'' + u\delta_{\rm c}' - \left(\nu^2 + u^2\right)\delta_{\rm c}; \quad \nu^2 \equiv \frac{(a-1)^2}{4r^2} + \frac{b^2}{r^2} \tag{D.3}$$

using the substitution $u = ct^r/r$ and the notation $' \equiv \mathrm{d}/\mathrm{d}u$. Equation (D.3) is a *modified Bessel equation*, the solutions of which are *modified Bessel functions* of the first and second kind, $I_\nu(u)$ and $K_\nu(u)$. Unlike regular Bessel functions, which are oscillatory in nature, these functions either grow (I_ν) or decay (K_ν) with increasing u. The general solution is then

$$\delta_{\rm c}(t) = t^{\frac{1-a}{2}}\left[C_1 I_\nu\left(\frac{c}{r}t^r\right) + C_2 K_\nu\left(\frac{c}{r}t^r\right)\right], \tag{D.4}$$

where $C_{1,2}$ are arbitrary integration constants. In chapter 7 we shall only be interested in whichever function is the growing mode (this depends on the sign of r). The modified Bessel function of the first kind has the power series expansion

$$I_\nu(x) = \sum_{k=0}^{\infty}\frac{1}{k!\Gamma(\nu+k+1)}\left(\frac{x}{2}\right)^{\nu+2k} = \frac{1}{\Gamma(1+\nu)}\left(\frac{x}{2}\right)^{\nu}\left(1+\mathcal{O}(x^2)+\ldots\right), \tag{D.5}$$

where $\Gamma(m)$ is the gamma function. The modified Bessel function of the second kind is defined via

$$K_\nu(x) = \lim_{n\to\nu}\frac{\pi\left[I_{-n}(x) - I_n(x)\right]}{2\sin(n\pi)}. \tag{D.6}$$

Its power series expansion for $\nu \notin \mathbb{Z}$ is as follows:

$$K_\nu(x) = \frac{\pi\csc(\pi\nu)}{2}\left[\sum_{k=0}^{\infty}\frac{1}{\Gamma(k-\nu+1)k!}\left(\frac{x}{2}\right)^{2k-\nu} - \sum_{k=0}^{\infty}\frac{1}{\Gamma(k+\nu+1)k!}\left(\frac{x}{2}\right)^{2k+\nu}\right]. \tag{D.7}$$

D.2 Second Kind Power Series Expansions for the Power Spectra

In this section we briefly outline the steps that lead to the factor $F(\omega)$ given in (7.57) and appearing in the deviation from the ΛCDM spectra (7.56). The expansion of the first kind modified Bessel functions (D.5) is a trivial exercise in algebra, however the second kind expansion (D.7) requires more thought. The three leading terms are:

$$K_\nu(x) = \frac{\pi \csc(\pi\nu)}{2\Gamma(1-\nu)}\left(\frac{2}{x}\right)^\nu \left[1 + \frac{\Gamma(1-\nu)}{\Gamma(2-\nu)}\left(\frac{x}{2}\right)^2 - \frac{\Gamma(1-\nu)}{\Gamma(1+\nu)}\left(\frac{x}{2}\right)^{2\nu}\right], \tag{D.8}$$

which correspond to the first two terms in the first sum in (D.7) and the first term in the second sum. The next-to-leading order correction to the leading order term ($\propto x^{-\nu}$) depends on whether $\nu > 1$ or the converse, which gives rise to the factor $F(\omega)$ in (7.56). When $\nu = 1$ a different power series is needed, which we do not give here since it corresponds to an uninteresting cosmological scenario. When $\nu < 1$, the final factor can be evaluated using the relation

$$\Gamma(1-m)\Gamma(m) = \frac{\pi}{\sin(\pi m)}. \tag{D.9}$$

E

The Global Potential for Supersymmetric Chameleon Models

In this appendix we show how the global F-term scalar potential for supersymmetric chameleons coupled to charged scalar fields studied in chapter 7 can be minimised to recover the simple form given in equation (7.4).

E.1 Minimisation of the Global Potential

Ignoring the contribution from the Kähler potential for now (it depends on $|\phi|$ only) and setting $\langle\phi_\pm\rangle = 0$, which is always a minimum, we have:

$$\left|\frac{\mathrm{d}W}{\mathrm{d}\phi}\right|^2 = g'^2|\pi_+|^2|\pi_-|^2 + \frac{\gamma^2}{2}\left(\frac{|\phi|^{2\alpha-2}}{\Lambda_0^{2\alpha-6}} + \frac{|\phi|^{2\gamma-2}}{\Lambda_2^{2\gamma-6}}\right) + \gamma\,\mathrm{Re}\left(\frac{\phi^{\alpha-1}\phi^{*\gamma-1}}{\Lambda_0^{\alpha-3}\Lambda_2^{\gamma-3}}\right) + \sqrt{2}g'\gamma\,\mathrm{Re}\left[\pi_+\pi_-\left(\frac{\phi^{*\alpha-1}}{\Lambda_0^{\alpha-3}} + \frac{\phi^{*\gamma-1}}{\Lambda_2^{\gamma-3}}\right)\right], \tag{E.1}$$

which, as can be seen, simplifies greatly when the negatively charged field has zero VEV. We shall see now that this VEV does indeed minimise the potential. We begin by writing the

charged fields in polar form $\pi_\pm \equiv \pi_\pm e^{i\theta_\pm}$. Ideally, one would hope to set the three angular fields $\{\theta, \theta_\pm\}$ to constant values in order to give negative signs in front of the final three terms in (E.1)[1], however, this is not possible and instead one must eliminate them in terms of the other fields. In order to do this, we exploit the local U(1) symmetry, which acts as $\theta_\pm(x) \to \pm q\alpha(x)$, to set $\theta_+(x) = \theta_-(x) = \chi(x)/2$, which reduces the angular fields to the set $\{\theta, \chi\}$. With this in mind, the scalar potential, including the contribution from the Kähler potential is

$$\begin{aligned} V(\phi,\theta,\pi_+,\pi_-,\chi) = {} & \frac{2g'^2\pi_+^2\pi_-^2}{\gamma^2}\left(\frac{\Lambda_1}{\phi}\right)^{2\gamma-2} + \left(\frac{\Lambda_1}{\phi}\right)^{2\gamma-2}\left(\frac{\phi^{2\alpha-2}}{\Lambda_0^{2\alpha-6}} + \frac{\phi^{2\gamma-2}}{\Lambda_2^{2\gamma-6}}\right) \\ & + \frac{2}{\gamma}\left(\frac{\Lambda_1}{\phi}\right)^{2\gamma-2}\frac{\phi^{\alpha+\gamma-2}}{\Lambda_0^{\alpha-3}\Lambda_2^{\gamma-3}}\cos[(\alpha-\gamma)\theta] \\ & + \frac{g'}{\sqrt{2}\gamma}\left(\frac{\Lambda_1}{\phi}\right)^{2\gamma-2}\pi_+\pi_-\left[\frac{\phi^{\alpha-1}}{\Lambda_0^{\alpha-3}}\cos[\chi-(\alpha-1)\theta] + \frac{\phi^{\gamma-1}}{\Lambda_2^{\gamma-3}}\cos[\chi-(\gamma-1)\theta]\right]. \end{aligned} \tag{E.2}$$

Minimising this with respect to χ one finds

$$\frac{\phi^{\alpha-\gamma}}{\Lambda_0^{\alpha-3}}\sin[\chi-(\alpha-1)\theta] + \frac{1}{\Lambda_2^{\gamma-3}}\sin[\chi-(\gamma-1)\theta] = 0, \tag{E.3}$$

which may be used in the equation found by minimising equation (E.2) with respect to θ to find a relation between $\sin[(\alpha-\gamma)\theta]$ and $\sin[\chi-(\gamma-1)\theta)]$ (or equivalently $\sin[\chi-(\alpha-1)\theta]$):

$$\frac{2\phi^{\alpha-1}}{\Lambda_0^{\alpha-3}}\sin[(\alpha-\gamma)\theta] = \frac{g'}{2}\pi_+\pi_-\sin[\chi-(\gamma-1)\theta]. \tag{E.4}$$

[1] This is the approach taken when the charged fields are absent [98].

This may be used to eliminate χ from the potential to find:

$$\begin{aligned} V(\phi,\theta,\pi_+,\pi_-) = &\frac{2g'^2\pi_+^2\pi_-^2}{\gamma^2}\left(\frac{\Lambda_1}{\phi}\right)^{2\gamma-2} + \left(\frac{\Lambda_1}{\phi}\right)^{2\gamma-2}\left(\frac{\phi^{2\alpha-2}}{\Lambda_0^{2\alpha-6}} + \frac{\phi^{2\gamma-2}}{\Lambda_2^{2\gamma-6}}\right) \\ &+ \frac{2}{\gamma}\left(\frac{\Lambda_1}{\phi}\right)^{2\gamma-2}\frac{\phi^{\alpha+\gamma-2}}{\Lambda_0^{\alpha-3}\Lambda_2^{\gamma-3}}\cos[(\alpha-\gamma)\theta] \\ &+ \frac{g'}{\sqrt{2}\gamma\Lambda_0^{\alpha-3}}\phi^{\alpha-1}\left(\frac{\Lambda_1}{\phi}\right)^{2\gamma-2}\sqrt{\pi_+^2\pi_-^2 - \frac{8\phi^{2\gamma-2}}{g'^2\Lambda_2^{2\gamma-6}}\sin^2[(\alpha-\gamma)\theta]} \\ &+ \frac{g'}{\sqrt{2}\gamma\Lambda_2^{\gamma-3}}\phi^{\gamma-1}\left(\frac{\Lambda_1}{\phi}\right)^{2\gamma-2}\sqrt{\pi_+^2\pi_-^2 - \frac{8\phi^{2\alpha-2}}{g'^2\Lambda_0^{2\alpha-6}}\sin^2[(\alpha-\gamma)\theta]}\,. \end{aligned} \tag{E.5}$$

At first glance, one may worry about the square roots. In fact, these are somewhat spurious since the above expression is only true when χ is fixed to its minimum. Furthermore, if one examines equation (E.4) then it is evident that as $\pi_+, \pi_- \to 0$ the second term in the square root has exactly the same behaviour and so there is never a region in configuration space where the argument is negative. Minimising (E.5) together with the potential coming from the D-term and the $\pi_\pm$ terms in the superpotential,

$$V_D + \left|\frac{dW}{d\pi_+}\right| + \left|\frac{dW}{d\pi_-}\right| = \frac{1}{2}\left(q\pi_+^2 + -q\pi_-^2 - \xi^2\right)^2 + g'^2\phi^2\left(\pi_+^2 + \pi_-^2\right), \tag{E.6}$$

with respect to π_- one indeed finds that $\langle\pi_-\rangle = 0$ is a solution. If one expands the global potential around this minimum by setting $\pi_- \to \langle\pi_-\rangle + \delta\pi_-$ then the coefficient of the $\delta\pi_-^2$ term is

$$q\left(\xi^2 - q\pi_+^2\right) + g'^2|\phi|^2. \tag{E.7}$$

In theory, this can be negative, however we have not yet finished minimising the potential. In section 7.2.2 we learnt that there are two possible solutions for π_+ given by equation (7.32) when $\pi_- = 0$ and so we should check that these are indeed stable minima of the global potential. The case where $\pi_+ = 0$ is clearly a minimum since the negative term vanishes. The second case gives the coefficient as $2g'^2|\phi|^2$ and so in either case the coefficient is positive and

the stationary point is a stable minimum. When $\langle \pi_- \rangle = 0$ equation (E.4) gives $\sin[(\alpha-\gamma)\theta] = 0$ and hence $\cos[(\alpha-\gamma)\theta] = -1$. Making this substitution in (E.5) yields the far simpler form of the potential given in (7.4).

F

Corrections to the Effective Potential for Supersymmetric Chameleon Models

In this appendix we show how one can explore the importance of the corrections to the effective potential for the supersymmetric chameleon studied in chapter 7 at early times when the $\mathbb{Z}_2$ symmetry of the potential for the charged scalars is broken and they acquire non-zero VEVs.

F.1 Late Time Importance of the Corrections

The corrections to the effective potential are of the form

$$V_{\text{corr}} = \frac{g'^2\xi^2}{q}\phi^2 - \frac{g'^4}{2q^2}\phi^4 \tag{F.1}$$

and we shall make use of the definition (7.36) and for brevity define $Z \equiv (1+z_\infty)^3$.

We can estimate the density at which each correction becomes important and we can no longer neglect them by equating each one with the magnitude of the density dependent term in turn. In this case, one finds that the field values ϕ_i at which the order i corrections are

important are

$$\phi_2 = \left(\frac{\mathscr{G}^2\xi^2}{x\rho_c}\right)^{\frac{1}{\delta-2}} \phi_{\min}^{\frac{\delta}{\delta-4}} \quad \text{and} \tag{F.2}$$

$$\phi_4 = \left(\frac{\mathscr{G}^4}{x\rho_c}\right)^{\frac{1}{\delta-4}} \phi_{\min}^{\frac{\delta}{\delta-4}} \tag{F.3}$$

respectively. Now we can always begin the cosmic evolution far enough in the past such that the density is large enough that the corrections are negligible, in which case the field evolves according to the background cosmology detailed in section 7.2.1. As the field evolves, the coefficient of the density dependent term becomes smaller and the corrections will eventually become important. If this occurs before the field rolls past Δ then we must correct the dynamics appropriately. If, on the other hand, this occurs after the field has passed Δ then these corrections will no longer be present and we can neglect them completely. Using equations (7.23) and (7.10), we can estimate the densities ρ_i at which $\phi = \phi_i$ and the density ρ_Δ at which $\phi = \Delta$:

$$\begin{aligned}
\rho_2^{\frac{n+2}{n+\delta}} &= \frac{M^2\mathscr{G}^2\xi^2}{x}\left(\frac{M}{\Lambda}\right)^{\frac{4}{n}} \rho_\infty^{-\frac{\delta-2}{n+\delta}} \\
\rho_4^{\frac{n+4}{n+\delta}} &= \frac{M^4\mathscr{G}^4}{2x}\left(\frac{M}{\Lambda}\right)^{\frac{16}{n}} \rho_\infty^{-\frac{\delta-4}{n+4}} \\
\rho_\Delta^{\frac{1}{n+\delta}} &= \frac{GM}{\xi}\left(\frac{M}{\Lambda}\right)^{\frac{4}{n}} \rho_\infty^{\frac{1}{n+\delta}}
\end{aligned} \tag{F.4}$$

The condition that the corrections can be neglected is then $\rho_\Delta \gg \rho_i$. In this analysis we shall take "much greater than" to mean an order of magnitude i.e. $\rho_\Delta \geq 10\rho_i$.

F.1.1 Mass Scales

One must be careful that the model parameters are inter-dependent and it is important to keep track of which are fixed by specific choices of others. In the analysis of section 7.2.2 we consider the low-energy model parameters $\{n, \delta, x, m, \mathscr{G}, z_\infty\}$ independent, which completely

fixes the derived scales M and Λ via equation (7.3). We start by writing equations (7.11) and (7.15) in the form

$$\left(\frac{\Lambda}{10^{-3}\text{eV}}\right)^4 = \frac{\delta x}{n} Z \tag{F.5}$$

$$\phi_{\text{min}} = x^{\frac{1}{\delta}} \mu, \tag{F.6}$$

which can be combined using equation (7.3) to find

$$M^{4+n} = 10^{-12} \frac{\delta}{n} Z x^{\frac{n+\delta}{\delta}} \mu^n \text{eV}^4. \tag{F.7}$$

These relations can then be used to eliminate the quantities M and Λ in equation (F.4) in favour of the low-energy parameters.

F.2 The Quadratic Correction

When $\rho_2 \gg \rho_\Delta, \rho_4, \rho_c$ the effective potential is

$$V_{\text{eff}}(\phi) \approx \Lambda^4 \left[1 - \left(\frac{\phi_{\text{min}}}{\phi}\right)^{\frac{n}{2}}\right]^2 + \mathscr{G}^2 \xi^2 \phi^2. \tag{F.8}$$

This is minimised at field values satisfying

$$\left(\frac{\phi_{\text{min}}}{\phi}\right)^{n+2} - \left(\frac{\phi_{\text{min}}}{\phi}\right)^{\frac{n}{2}+2} = \frac{\mathscr{G}^2 \xi^2 x^{\frac{2}{\delta}} \mu^2}{n \Lambda^4}. \tag{F.9}$$

When $\mathscr{G} \xi x^{1/\delta} \mu \ll \Lambda^2$ we have $\phi \approx \phi_{\text{min}}$ and so this case is still viable provided that $\phi_{\text{min}} > \Delta$. If the converse is true then the minimum lies at field values

$$\phi = \phi_{\text{min}} \left(\frac{n \Lambda^4}{\mathscr{G}^2 \xi^2 x^{\frac{2}{\delta}} \mu^2}\right)^{\frac{1}{n+2}} \tag{F.10}$$

and demanding that this is larger than Δ we find that the parameters must satisfy

$$\xi^{n+4}\mathscr{G}^n x^{\frac{n}{\delta}}\mu^n > n\Lambda^4 \tag{F.11}$$

in order for the cosmological constant to be generated.

F.3 The Quartic Correction

When the quartic correction is important the potential takes the following form:

$$V(\phi) = \Lambda^4\left(1 - \left(\frac{\phi_{\min}}{\phi}\right)^{\frac{n}{2}}\right)^2 - \frac{\mathscr{G}^4}{2}\phi^4. \tag{F.12}$$

The minimum, if it exists, is given by the solution of

$$\left(\frac{\phi_{\min}}{\phi}\right)^{\frac{n}{2}+4} - \left(\frac{\phi_{\min}}{\phi}\right)^{n+4} = \frac{2}{n}\mathscr{G}^4\left(\frac{\phi_{\min}}{\Lambda}\right)^4 \tag{F.13}$$

and so the only possible solutions have $\phi > \phi_{\min}$. This means that when this correction only is important the field will always pass Δ at some time and generate a cosmological constant. With this in mind, one may wonder if the case $\phi_{\min} < \Delta$ is allowed since in this case the field can still pass Δ if the minimum lies at large enough field values. This situation is highly unnatural since once the corrections vanish the field lies at values greater than $\phi_{\min}$ and will subsequently roll backwards, reintroducing the corrections. Hubble friction will eventually reduce the amplitude of the oscillations, however this leads to a situation that is highly fine-tuned and sensitive to the initial conditions and so we exclude it.

F.4 Simultaneous Corrections

When both corrections are simultaneously important the effective potential, including the matter coupling, is

$$V(\phi) = \Lambda^4 \left(1 - \left(\frac{\phi_{\rm min}}{\phi}\right)^{\frac{n}{2}}\right)^2 + x\rho_{\rm c}\left(\frac{\phi}{\phi_{\rm min}}\right)^{\delta} - \frac{\mathscr{G}^4}{2}\phi^4 + \mathscr{G}^2\xi^2\phi^2. \tag{F.14}$$

When including the density term one should technically solve the entire dynamical system in terms of φ and $\rho_{\rm c}(t)$, however we can glean all the information we need if we simply set $\rho_{\rm c} = 1$ eV^4. As mentioned above, we require that the field rolls past Δ before $\rho_{\rm c} = 1$ eV^4 so that the cosmological constant is generated before last scattering and this will be the case if the minimum is located at field values greater than this by last scattering. Technically, this condition is not sufficient since it only guarantees that the minimum is located at values greater than Δ by last scattering, not that the field passes Δ by this time, however the large mass of the field ensures that this approximation is sensible. Far enough in the past the corrections are unimportant and field tracks its minimum owing to this large mass. Eventually we reach the epoch where all three terms become important and pass to the regime where the density-dependent term is negligible. This transition is smooth and so given the large mass we expect that the field should simply remain fixed at the new, density-independent minimum and therefore the dynamics should not differ largely from the static analysis we will employ here.

The field value at the minimum satisfies

$$\frac{n\Lambda^4}{\phi_{\rm min}^2}\left[\left(\frac{\phi_{\rm min}}{\phi}\right)^{\frac{n}{2}+2} - \left(\frac{\phi_{\rm min}}{\phi}\right)^{n+2}\right] + \frac{x\delta\rho_{\rm c}}{\phi_{\rm min}^2}\left(\frac{\phi_{\rm min}}{\phi}\right)^{2-\delta} + 2G^2\xi^2 - 2G^4\phi^2 = 0, \tag{F.15}$$

which must be solved numerically for the minimum given a specific set of parameters and for the same reasons given in section F.3, we will impose $\phi_{\rm min} > \Delta$. If this has no solutions then the potential is runaway near $\rho_{\rm c} = 1$ eV^4 and the field will be able to pass Δ. When solutions

exist the parameters where the minimum occurs at field values larger than Δ are viable and those where the converse is true are not.